TECTONIC EVOLUTION OF THE RHODOPE METAMORPHIC CORE COMPLEX, NORTHEASTERN GREECE

by

DAVID ANTON DINTER

B.S., Geology, Stanford University, 1982

M.S., Geophysics, Stanford University, 1982

Submitted to the Department of Earth, Atmospheric, and Planetary Sciences in Partial Fulfillment of the Requirements for the Degree of

DOCTOR OF PHILOSOPHY

at the MASSACHUSETTS INSTITUTE OF TECHNOLOGY

February, 1994

Signature of Author _____
Department of Earth, Atmospheric, and Planetary Sciences
February, 1994

Certified by _____
Leigh H. Royden
Thesis Advisor

Accepted by _____
Thomas H. Jordan
Department Chairman

TECTONIC EVOLUTION OF THE RHODOPE METAMORPHIC CORE COMPLEX, NORTHEASTERN GREECE

by

David Anton Dinter

Submitted to the Department of Earth, Atmospheric, and Planetary Sciences at the Massachusetts Institute of Technology on February 7, 1994, in Partial Fulfillment of the Requirements for the Degree of Doctor of Philosophy in Geology

ABSTRACT

In the eastern Mediterranean region, a number of continental fragments that were isolated by rifting during the early Mesozoic breakup of Pangaea have been juxtaposed and deformed since early Jurassic time in the overall plate-tectonic context of convergence between Africa and Europe. The Alpine orogen was created by the collision of the "Apulian fragment" with the European continental platform. On the Balkan Peninsula, a strongly deformed, mixed high- and low-grade metamorphic province broken up by Tertiary basins intervenes between the thrust-shortened remnant of Apulia exposed in the Hellenic and Dinaric Alps and the southern (Balkan) margin of the European platform. The Tertiary tectonic evolution of this intervening metamorphic province, conventionally referred to as the "Rhodope continental fragment" is the subject of this study.

The Rhodope metamorphic province and the adjacent north Aegean Sea lie in a back-arc position relative to the Hellenic subduction system, which accommodates northeasterly subduction of Ionian and Adriatic lithosphere beneath the southwestern margin of the Balkan Peninsula. Continental lithosphere appears to have been extended on the order of 100% in this setting, because the 22- to 32-km thickness of Aegean crust is only about half that of western mainland Greece and Turkey. It is commonly assumed that much of this extension is accounted for in northern Greece and Bulgaria by the subsidence of Neogene basins that are conventionally interpreted as simple grabens. The results of geologic mapping conducted by the author in the Strymon Valley region of northeastern Greece from 1989 to 1991 imply instead that most of this extension was accommodated by regionally developed low-angle normal fault systems similar to those widely exposed in the Basin-and-Range Province of the western U.S.

The gross structural geometry of the Rhodope province in northeastern Greece is quite simple: The Falakron marble series, an enormously thick, highly strained, platform carbonate unit of unknown age exposed between the Strymon and Nestos Rivers, is overlain at its northeastern margin on a mylonitic, southwest-vergent thrust fault by the "West Thracian gneiss complex", and at its southwestern margin on a brittle, low-angle, southwest-dipping shear zone by the "Serbo-Macedonian gneiss complex" and a veneer of strongly deformed, unmetamorphosed Neogene sediments. This shear zone has previously been interpreted as a northeast-vergent Neogene thrust, but is reinterpreted here as a southwest-vergent low-angle normal fault, the Strymon Valley detachment. The recognition that this structure facilitated the unroofing of the Falakron marble series in its footwall in Neogene time necessitates a comprehensive revision of the tectonic evolution of the Rhodope metamorphic province.

Based on geologic field mapping augmented by $^{40}Ar/^{39}Ar$ and U-Pb studies, I rationalize the Tertiary tectonic evolution of the southwestern Rhodope region as a

succession of four deformational events: D_1 comprises the middle - late Eocene ductile folding, penetrative deformation, and dynamic metamorphism of the Falakron series as it was subducted northeastward in the footwall of the Nestos thrust. In mid-Oligocene time, a number of granodiorite plutons were emplaced within the Falakron series and correlative arc-type andesitic lavas blanketed a large region above the overlying gneiss complex. The northeast-southwest extensional collapse of the Alpine nappe pile began ~15 m.y. after the cessation of continental subduction and appears to have been accommodated by three successive shear systems that alternated in polarity. Early Miocene extension (D_2) is recorded by the emplacement and mylonitization of the Symvolon granodiorite beginning ~22 Ma within a northeast-dipping coaxial shear zone that may represent an extensional rupture of the Falakron carbonate slab. The Symvolon shear zone was succeeded by the southwest-dipping Strymon Valley detachment system (D_3), which facilitated the southwestward-progressive tectonic unroofing of the Rhodope metamorphic core complex and a consequent transition from ductile to brittle deformation from ~16 to 3.5 Ma. Continuing extension from ~3.5 Ma to the present (D_4) is principally expressed by the subsidence of the Strymon and Drama basins, whose northwest-striking bounding faults may sole into an active northeast-dipping detachment that terminates to the southeast at the North Aegean trough.

The recognition that tectonostratigraphic units in the southern Rhodope province have experienced large lateral displacements on extensional detachments in Neogene time profoundly influences the interpretation of pre-Neogene deformation in this region. In the conventional view, the Rhodope province is a continental fragment of the sort described above that was caught between Apulia and Europe and deformed by folding and thrusting in the hinterland of an Alpine collisional orogen along its southwestern margin. The contrasting interpretation emerging from the present study is that the Rhodope province in northeastern Greeece represents an A-type (continental) Alpine subduction zone that was unroofed by Neogene extension accommodated by a succession of low-angle normal fault systems that appear to have alternated in polarity. I suggest that large lateral displacements on extensional detachments may have played a much greater role in the Tertiary structural evolution of the Balkan Peninsula than has previously been imagined.

Thesis advisor: Leigh H. Royden, Professor of Geophysics

ACKNOWLEDGMENTS

I am indebted to my thesis advisor, Professor Leigh Royden, for suggesting northern Greece as a field area and for continuing her support as the focus of my project changed and its scope widened with each passing field season. Profs. Royden and Burchfiel provided valuable advice and direction during early phases of my field research, and Profs. Kip Hodges and Sam Bowring were generous with their time, insights, and laboratory facilities, making possible the $^{40}Ar/^{39}Ar$ and U-Pb geochronological analyses of the Symvolon pluton that are integral to the conclusions reached in this study. Profs. Royden, Burchfiel, Hodges, Bowring, and Elizabeth Schermer served on my thesis committee; their advice and criticism resulted in a clearer and more tightly reasoned presentation of my results.

I was fortunate in the company and support of my fellow graduate students and others associated with the Department of Earth, Atmospheric, and Planetary Sciences. Their expertise and creativity were integral to every aspect of my education and research, their friendship is generous, and their bad jokes are unrelenting. Special thanks are due to my officemates, Allison Macfarlane and David Applegate, who stared at maps of Greece with me late into many nights and suffered through early drafts of every manuscript I churned out. I look forward to more scientific collaborations and long friendships with these characters. Bill Hames walked me and many others through the process of acquiring $^{40}Ar/^{39}Ar$ data, from picking the grains to the final laser blast. Clark Isachsen and Dave Hawkins taught me to pick zircons and sphenes and performed the U-Pb laboratory work. Professor Fritz Steininger of the University of Vienna identified fossils from the Strymon Valley supradetachment basin complex. Karen Campbell helped me find obscure Balkan publications in seven languages, Catherine Burger, Susanne Ehlert, and Ewa Ostrowski assisted with German translations, and Radoslav Nakov provided many insights on Bulgarian geology and assisted with Russian and Bulgarian translations. I also thank Meg Coleman, Roy Adams, C.J. "Mylonite" Northrup, David Silverberg, Cathy Summa, and the rest of the gang on the 8th through 11th floors for many intriguing discussions, good times, and kindnesses too numerous to mention.

Finally, I thank my partner, Peggy Collier, our daughter Cory, and my parents, Hank and Vonnie Dinter, for their patience, support, and love.

To my partner, Peggy Collier, and our daughter, Cory Dinter

and to my parents, Henry and LeVon Dinter

TABLE OF CONTENTS

CHAPTER 1

INTRODUCTION

Since Late Jurassic time, the deformation and metamorphism of rocks in the eastern Mediterranean region has occurred in the overall plate-tectonic context of convergence between Africa and Europe. Between these continents, a number of continental fragments that were isolated by rifting during the early Mesozoic breakup of Pangaea have been juxtaposed in a complicated manner. The Alpine orogen was created by the collision of one such fragment, "Apulia", with the southeastern margin of the European continental platform. On the Balkan Peninsula, the locus of the Alpine suture is generally identified with the ophiolitic "Vardar zone" (Fig. 1). The Hellenic and Dinaric Alps comprise the deformed remnant of the Apulian fragment southwest of this zone. To the northeast, a strongly deformed province of mixed high- and low-grade metamorphic rocks broken up by Tertiary basins intervenes between the Vardar suture and the European platform. The Tertiary tectonic evolution of this province, which has been termed the "Rhodope continental fragment" (Burchfiel, 1980), is the subject of this study.

The Rhodope fragment widens southward from ~200 km in eastern Serbia and northwestern Bulgaria to >500 km along the north Aegean coastline (Fig. 1). The number, width, and thickness of Neogene basins increase markedly to the south in this region, suggesting that much of this widening is attributable to Neogene extension. The magnitude of Neogene extension may be on the order of 100%, because seismic refraction and gravity data imply that crustal thickness beneath the Aegean Sea varies from about 22 to 32 km, compared with 40 to 50 km beneath mainland Greece and Turkey (Jongsma et al., 1977; Makris, 1976; Makris and Vees, 1977).

Neogene basins in northern Greece and Bulgaria have traditionally been interpreted as simple grabens. However, it has long been realized that horst-and-graben geometries can account for extension of only 10 - 20%, whereas low-angle normal fault systems such as those that are widely documented in the Basin-and-Range province of the western U.S. can accommodate extensional magnitudes of 100% and greater. The recognition, early in the present study, of a major low-angle normal fault with up to 80 km of displacement necessitated a complete reevaluation of the extensional evolution of northern Greece. Much of this thesis reflects an effort to characterize the geometry and timing of the Strymon Valley detachment system. Chapter 2 summarizes its general kinematic character and discusses timing constraints based on earlier studies. Chapter 3 presents middle Miocene $^{40}Ar/^{39}Ar$ biotite and K-feldspar dates that constrain the cooling history of the Rhodope metamorphic core complex during its unroofing in the footwall of the Strymon Valley detachment. Early Miocene $^{40}Ar/^{39}Ar$ hornblende dates and U-Pb zircon and sphene dates from the Symvolon pluton are related in Chapter 3 to a pre-Strymon Valley episode of extensional deformation in the core complex. Chapter 4 details the Tertiary structural evolution of the southwestern Rhodope province and explores the implications of Neogene detachment geometries for the origin of Neogene basins and for paleogeographic reconstructions of earlier deformation in northeastern Greece.

Chapter 5 expands upon Chapter 4, providing detailed descriptions of the units displaced in the Strymon Valley detachment system and of the structures that accommodated these displacements, and concludes with a speculative discussion of the how the Tertiary deformational history of the southern Rhodope province may fit into the larger context of Alpine tectonic events on the Balkan Peninsula. The recognition that tectonostratigraphic units in the southern Rhodope province have experienced large lateral displacements on extensional detachments in Neogene time profoundly influences the interpretation of pre-Neogene deformation in this region. In the conventional view, the

Rhodope province is a continental fragment of the sort described above that was caught between Apulia and Europe and deformed by folding and thrusting in the hinterland of an Alpine collisional orogen along its southwestern margin (e.g., Jacobshagen et al., 1978). The contrasting interpretation that emerges from the present study is that Rhodope province in northeastern Greeece represents an A-type (continental) Alpine subduction zone that was unroofed by Neogene extension accommodated by a succession of low-angle normal fault systems that appear to have alternated in polarity. I suggest that large lateral displacements on extensional detachments may have played a much greater role in the Tertiary structural evolution of the Balkan Peninsula than has previously been imagined.

REFERENCES

Burchfiel, B. C., 1980, Eastern European Alpine system and the Carpathian orocline as an example of collision tectonics: Tectonophysics, v. 63, p. 31-61.

Dinter, D. A. and Royden, L., 1993, Late Cenozoic extension in northeastern Greece: Strymon Valley detachment and Rhodope metammorphic core complex: Geology, v. 21, p. 45-48.

Jacobshagen, V., Dürr, S., Kockel, F., Kopp, K.-O., Kowalczyk, G., Berckhemer, H. and Büttner, D., 1978, Structure and geodynamic evolution of the Aegean region, in Closs, H., Roeder, D. and Schmidt, K., ed., Alps, Apennines, Hellenides, Inter-Union Commission on Geodynamics Scientific Report No. 38, Stuttgart, E. Schweizerbart'sche Verlagsbuchhandlung, p. 537-564.

Jongsma, D., Wissman, G., Hinz, K., and Garde, S., 1977. Seismic studies in the Cretan Sea, 2, The southern Aegean Sea: an extensional marginal basin without seafloor spreading?, "Meteor" Forschungsergeb. Reihe C, p. 27.

Makris, J., 1976. Crustal structure of the Aegean Sea and the Hellenides obtained from geophysical surveys: Journal of Geophysics, v. 41, 441.

Makris, J., and Vees, R., 1977. Crustal structure of the central Aegean Sea and the islands of Evvia and Crete, Greece, obtained by refraction seismic experiments: Journal of Geophysics, v. 42, p. 329.

Royden, L. H., 1988, Late Cenozoic tectonics of the Pannonian basin system, in Royden, L. H. and Horvath, F., ed., Pannonian Basin: A Study in Basin Evolution, AAPG Memoir 45, p. 27-48.

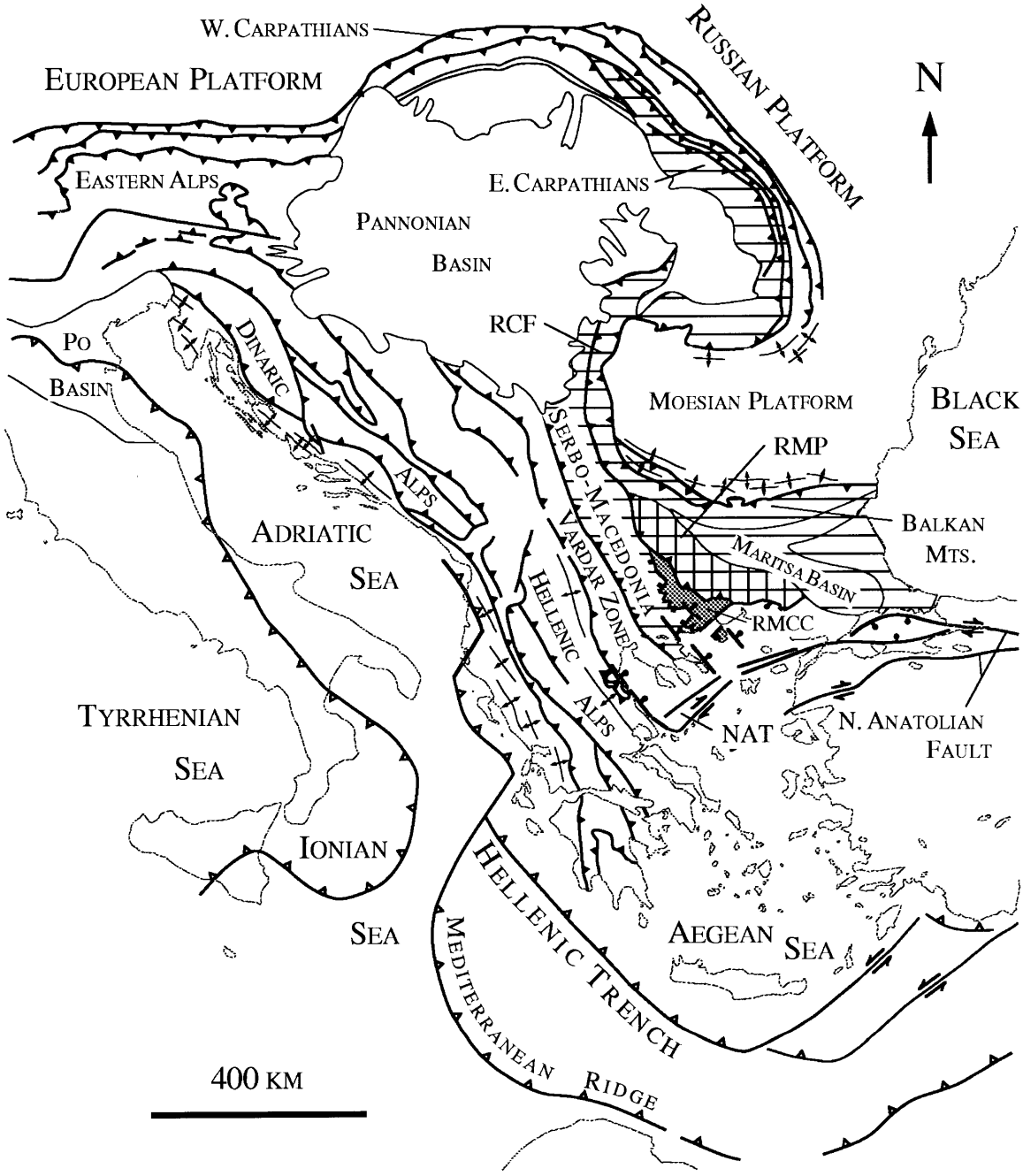

Figure 1. Sketch map of major tectonic elements in southeastern Europe and the northeastern Mediterranean region. RCF – Rhodope continental fragment (horizontal lines), RMP – Rhodope metamorphic province (vertical lines), RMCC – Rhodope metamorphic core complex (gray pattern). NAT – North Aegean Trough. Modified from Burchfiel (1980), Royden (1988), and Dinter and Royden (1993).

CHAPTER 2

LATE CENOZOIC EXTENSION IN NORTHEASTERN GREECE: STRYMON VALLEY DETACHMENT SYSTEM AND RHODOPE METAMORPHIC CORE COMPLEX

David A. Dinter and Leigh Royden
Department of Earth, Atmospheric and Planetary Sciences
Massachusetts Institute of Technology
Cambridge, Massachusetts 02139

ABSTRACT

The Strymon Valley detachment system accommodated at least 25 km of extension at the northern margin of the Aegean extensional province from middle Miocene through early Pliocene time. The primary detachment surface is exposed as a gently southwest-dipping low-angle normal fault – similar to those widely known in core complex settings of the U.S. Basin and Range province – for more than 150 km along strike, from the Aegean Sea coast in northeastern Greece northward into the Struma Valley of southern Bulgaria. Hanging wall rocks in the Strymon Valley detachment system moved in a S53°W direction with respect to the footwall, resulting ultimately in the tectonic unroofing of the Rhodope metamorphic core complex. Several segments of the Strymon Valley detachment have previously been interpreted as thrust faults formed during a Miocene compressional event. Our results negate the principal evidence for this event, and imply instead that extensional deformation has characterized the north Aegean region since at least middle Miocene time.

Displacement ceased on the Strymon Valley detachment with the late Pliocene development of the Strymon and Drama basins. We propose that those basins, together with the other principal basins of the north Aegean region, are subsiding above an active northeast-dipping extensional detachment zone that forms a unified kinematic system with the western offshore continuation of

the dextral North Anatolian strike-slip fault, the North Aegean trough. If this hypothesis is correct, then the North Aegean trough, the western strands of the North Anatolian fault, and the principal modern depocenters of the north Aegean region may all have originated no earlier than late Pliocene time.

INTRODUCTION

Northeastward subduction of Ionian and Adriatic sea floor beneath Greece and Anatolia has accommodated convergence between Europe and Africa in the eastern Mediterranean region throughout much of late Cenozoic time (e.g., Le Pichon and Angelier, 1979). In the back-arc setting above the descending slab, the overriding plate has been thinned and broadened over a wide area including the Aegean Sea and surrounding territories onshore (Fig. 1). Structural elements characteristic of this regional Neogene extension are spectacularly exposed in northeastern Greece, where they have disrupted and overprinted older compressional structures. Our geologic mapping in this area between 1987 and 1991 implies that much of the extension was accomplished by large normal displacements on low-angle detachment faults similar to those widely documented in the Basin and Range province of western North America (e.g., Davis and Lister, 1988).

GEOLOGIC SETTING

The Aegean Sea and adjacent areas onshore are referred to below as the Aegean extensional province. The Neogene extension of this region is conventionally considered to have begun in late Miocene time based on ages of fill in extensional basins (e.g., Büttner and Kowalczyk, 1978). However, extension-related metamorphism and mylonitization in the southern Aegean Cycladic islands have recently been dated at ~25 Ma (Lister et al., 1984), and 16-23 Ma ^{40}Ar-^{39}Ar dates on K-feldspars from the footwalls of low-angle normal faults near Mount Olympos have been interpreted as

cooling ages related to extensional unroofing (Schermer et al., 1990). These studies imply that extension of the Aegean region began by at least early Miocene time.

In its present configuration, the Aegean extensional province comprises two structurally distinct domains separated by the normal and right-slip fault system of the North Aegean trough, which appears to be the westward offshore continuation of the North Anatolian fault in Turkey (Fig. 1). We focus here on the region north of the trough. The latest Neogene extensional morphology of the northern domain is dominated by a series of elongate, north-northwest-trending depocenters, the Thermaikos, Strymon, and Drama basins, which contain up to several kilometers of Pliocene to Quaternary fill (Lalechos and Savoyat, 1977; Erki et al., 1984). Evidence of extensional deformation predating the formation of these basins is preserved both within the basins and on their flanks in syntectonic sediments as old as ~15 Ma, as well as in underlying igneous and metamorphic rocks.

STRYMON VALLEY DETACHMENT SYSTEM

Along the northeast margin of the Strymon River Valley in northeastern Greece the primary contact between poorly consolidated Neogene sedimentary strata and underlying metamorphic and igneous rocks is a regionally developed low-angle normal fault, the Strymon Valley detachment, which can be traced along strike for more than 150 km from the Aegean coast near Kavala northwestward into the Struma Valley of Bulgaria (Fig. 2). The exposed width of this fault is typically ~25 km in a northeast-southwest direction, and its regional dip is approximately 3° to the southwest. A similar and probably correlative structure, the Thasos detachment, crops out discontinuously along the southwest coast of the island of Thasos.

The hanging-wall suite of the Strymon Valley detachment northeast of the Strymon basin comprises mainly Neogene terrigenous and nearshore sediments. Clasts in coarse alluvial conglomerates and in angular, sedimentary breccias are mixtures of granodiorite, gneiss, schist, and

marble, derived primarily from the footwall. Predominantly northwest-trending intrahanging-wall normal faults have rotated hanging-wall strata into angular discordance with the main detachment surface. Beds typically dip 10°-30° and are commonly truncated by the detachment fault (Fig. 2).

The footwall of the Strymon Valley detachment comprises tectonically intercalated marbles, granodiorites, gneisses, and schists of the Rhodope metamorphic core complex (Dinter, 1991). Regionally pervasive, gently to moderately northeast-plunging intersection lineations and cm- to m-scale isoclinal shear folds developed in these rocks have been interpreted as Alpine compressional structures (e.g., Meyer, 1969). These are overprinted in zones adjacent to the brittle detachment surface by a regionally southwest-dipping mylonitic fabric. Although each of the footwall lithologies in the Greek portion of the Rhodope province is locally imprinted by this fabric, the material most commonly observed immediately beneath the detachment surface, even where gneiss or granitoid constitutes the dominant footwall lithology, is a highly sheared carapace of marble ranging in thickness from a few cm to several m. Metamorphic foliations within this layer are subparallel to the overlying detachment surface, and common cm- to m-scale, tight to isoclinal folds are defined by coarse-grained, recrystallized, white marble bands a few mm thick. An axial planar foliation associated with these folds intersects the earlier mylonitic foliation at a very low angle to form a prominent intersection lineation that plunges gently to moderately southwest or northeast, subparallel to the isoclinal fold axes. This lineation is parallel to a strongly developed calcite stretching lineation that records a roughly northeast-southwest shear direction (Fig. 2). Similar mylonitic fabrics are developed in the Symvolon and Vrondou plutons beneath the Strymon Valley detachment. In these granitoids, flattened, recrytallized quartz and aligned mica grains define mylonitic foliations, and elongate quartz aggregates and recrystallized feldspar grain tails define gently southwest- or northeast-plunging stretching lineations. S-C geometries, asymmetric feldspar porphyroclast tails, and oblique, strain-insensitive quartz grain shape fabrics within these mylonites record a regionally consistent top-to-the-southwest sense of shear. Kolocotroni and Dixon (1991) also describe extensional mylonites with a top-to-the-southwest sense of shear at the southern margin of the Vrondou pluton.

The Strymon Valley detachment surface itself is a brittle structure, commonly polished and streaked with dark brown, chloritic microbreccia. Regionally, the microbreccia streaks trend within a few degrees of S53°W, parallel to sparsely developed slickensides and subparallel to stretching lineations in the underlying mylonite. Where the footwall beneath poorly consolidated clastic hanging wall deposits is marble, the detachment surface locally bears small duplex structures consisting of marble slivers 1-4 cm thick nested in an imbricate stack 5-15 cm high and ~1 meter wide. The duplexes uniformly verge to the southwest and typically terminate at a roughly concave, southwest-facing fracture that may have an accumulation of chloritic microbreccia at its base, in the structural shadow of the stacked slivers.

In map view, the Strymon Valley detachment traces out a series of southwest-facing scallops (Fig. 2). This pattern results from large, primary, southwest-plunging corrugations in the fault surface that appear to be primary mullion structures (cf. John, 1987). The largest corrugations have 10-35 km wavelengths and apparent amplitudes as great as 1 km, possibly augmented by isostatic footwall uplift. Morphologic highs in the detachment surface expose metamorphic basement domes elongate parallel to corrugation axes, and intervening hollows form tectonically eroded valleys partially occupied by Neogene hanging-wall strata. Smaller scale corrugations are also common, from parasitic undulations with 50-300 m wavelengths and 10-50 m amplitudes on the limbs of larger corrugations, to outcrop-scale fluting with 1-5 m wavelengths and 0.2-1.0 m amplitudes. Corrugation and fluting axes have remarkably consistent orientations at all scales, plunging roughly 3° to S53°W (Fig.2).

We infer from the regional southwest dip of the fault surface, the uniform southwest vergence of fault plane duplexes, and the parallelism of slickensides, microbreccia streaks, and corrugation axes on the fault plane with stretching lineations in the immediately underlying mylonites that the hanging wall of the Strymon Valley detachment fault moved in a S53°W direction with respect to its

footwall. Although the total magnitude of displacement on the Strymon Valley detachment system is unclear, the minimum displacement on the main detachment fault is defined by the displacement-parallel width of its exposure over which bedding in syntectonic basinal sediments is observed to be rotated and truncated at the fault surface, approximately 25 km.

The timing of brittle-regime motion on the detachment system is presently constrained only by fossil dates from syndetachment deposits in the hanging wall suite. The oldest known fauna from such deposits in the Strymon Valley area are rodent remains dated at ~9.8 Ma, preserved in nonmarine clastic sediments north of Serres (Fig. 2; Armour-Brown et al., 1977). Older syndetachment sediments crop out in that area, but have not yielded fossils. A borehole through probably correlative, early syndetachment deposits in the Struma Valley to the north yielded middle Miocene mammal fauna (Kojumdgieva et al., 1982), implying that syntectonic basins related to activity on the Strymon Valley detachment system were forming by ~15 Ma. Deposits from the Serres area contain monolithic granitic megabreccias that record subaerial exposure of the nearby Vrondou pluton in the footwall of the detachment by ~6 Ma and continuing detachment activity as late as 3.5 Ma (Armour-Brown et al., 1977). In Greece, motion on the Strymon Valley detachment fault ceased when it was displaced by NW-trending normal faults bounding the Strymon and Drama basins. The inception age of these younger depocenters must be at least earliest Pleistocene, based on their mature morphology and sediment accumulations in excess of 1000 m (Erki et al, 1984).

Timing constraints on the ductile shearing and unroofing of footwall rocks are presently limited to scattered K-Ar dates from various plutonic bodies of the Rhodope metamorphic core complex. We consider four biotite dates ranging between 13.8 and 17.8 Ma from the Symvolon pluton as cooling ages acquired during its tectonic unroofing in the footwall of the Strymon Valley detachment system (Harre et al., 1968; Kokkinakis, 1980).

We interpret the Strymon Valley detachment system as an evolving extensional shear zone similar to those widely recognized in core complex settings of the North American Basin and Range province. Evidence in support of kinematic coordination between the ductile and brittle phases of shearing includes (1) a spatial association of the youngest footwall mylonites with the detachment surface, (2) an increase in the intensity of mylonitization structurally upward toward the detachment surface, (3) a regional consistency in direction and sense of shear indicators common to ductile and brittle fabrics (mylonitic stretching lineations, S-C relations, microbreccia streaks, slickensides, fault plane corrugation axes, and small-scale fault plane duplexes), and (4) overlapping and partly sequential age ranges for the formation of ductile and brittle fabrics: K-Ar ages ranging from 17.8-13.8 Ma that date the cooling of footwall mylonites are succeeded by fossil ages of ~15-3.5 Ma from syntectonic hanging wall deposits that record brittle, surficial, low-angle normal faulting.

The Strymon Valley detachment fault has not formerly been recognized as a single tectonic contact. Disparate segments have previously been mapped as thrust faults (Kockel and Walther, 1965), strike-slip faults (e.g., Lybéris, 1984), normal faults (Armour-Brown et al., 1977), or as depositional contacts (Bornovas and Rondogianni-Tsiambaou, 1983). Our reinterpretation of supposed thrust contacts as segments of a low-angle normal fault has particularly important regional tectonic implications. At the southeast margin of the Strymon basin a gneiss body similar in lithology to gneisses of the Serbo-Macedonian metamorphic province west of the Strymon basin overlies granitic rocks of the Rhodope metamorphic core complex on a gently west-dipping fault designated by Kockel and Walther (1965) as the "Strimon overthrust" (Fig. 2). This contact is conventionally interpreted as evidence of a Miocene compressional event during which Serbo-Macedonia was thrust eastward over the Rhodope province (e.g., Jacobshagen et al., 1978). Our mapping shows that the "Strimon overthrust" is actually a segment of the Strymon Valley detachment fault, and implies that (1) Serbo-Macedonia was not thrust northeastward over the Rhodope province in early Neogene time, but was instead translated southwestward to its present position in the hanging wall of the Strymon Valley detachment system (Fig. 2), and (2) there was

no middle Miocene compressional event in the north Aegean region; rather, the entire period from at least 18 Ma to the present was characterized by extensional deformation (see below).

POST-STRYMON VALLEY EXTENSIONAL DEFORMATION

Tilted, highly disrupted, Neogene strata preserved between the Strymon and Drama basins were deposited in syndetachment basins between the breakaway zone of the Strymon Valley detachment fault (possibly near the northeast margin of present-day Drama basin) and the trailing edge of its hanging wall block (northeast margin of Serbo-Macedonia). These deposits were translated southwestward as part of the hanging wall suite and overlie the mylonitic footwall rocks of the Rhodope metamorphic core complex at a low-angle normal fault (Figs. 2, 3). The youngest syndetachment sediments are early Pliocene in age, and must have been deposited prior to the formation of the Strymon and Drama basins, because the normal faults bounding those basins cut the Strymon Valley detachment surface. This geometry implies that the Strymon and Drama basins, although they preserve middle Miocene through early Pliocene syndetachment deposits as thick as 2 km within their margins (Erki et al., 1984), began to form no earlier than late Pliocene time.

The Strymon and Drama basins are members of a North Aegean basin system that appears to have succeeded the Strymon Valley detachment system in late Pliocene time as the major structural network accommodating regional extension. Other members include the Vardar-Thermaikos and West and East Thasos basins (Fig. 1). These depressions are in general elongate and parallel, with long axes trending about N35°W, and all persist as modern depocenters. They also share a common asymmetry: southwest margins are bounded by relatively steep normal faults that set modern basin fill against bedrock, whereas more gently dipping northeast margins locally preserve a thin cover of syndetachment Neogene deposits older than the present depocenters. In the central parts of these basins, 1-2 km of late Pliocene to Recent basin fill overlies strata that we interpret as thicker remnants of the syndetachment deposits exposed on the basin margins, presumably at an unconformity that has

gone unrecognized in cores and seismic profiles (Fig. 3; Lalechos and Savoyat, 1977; Erki et al., 1984).

The North Aegean basin system terminates to the south at the northeast-trending North Aegean trough, implying that right-slip motion along the trough and extensional deformation to the north are kinematically linked. We suggest that the present basin configuration has resulted from a transfer of right-slip displacement along the trough into northeast-southwest extension in the Thermaikos, Strymon, Drama, and West and East Thasos basins.(Figs. 1, 3). The North Aegean trough terminates to the west at the western margin of the Thermaikos basin, and no significant strike-slip offset can be traced westward through central mainland Greece (Bornovas and Rondogianni-Tsiambaou, 1983). From this geometry we infer that the final increment of right-slip along the trough axis is absorbed by extensional deformation on the active normal fault system along the western margin of the Thermaikos basin (Figs. 3, 4).

The Strymon Valley detachment system, together with a system of brittle, low-angle normal faults in the Mount Olympos vicinity (Schermer et al., 1990), show that the late Neogene extension of northern Greece was largely accommodated by normal displacements along gently-dipping, regionally developed detachment zones. We suggest that the late Pliocene to Holocene basins described above may be forming in the hanging wall of an active detachment zone analogous to the Strymon Valley system, but of opposite polarity. If this interpretation is correct, then the normal faults bounding these basins and the strike-slip faults of the North Aegean trough must all merge with the proposed North Aegean detachment zone at depth (Figs. 3, 4). The basins, strike-slip faults, and detachment zone form a single extensional system, of which no structural component penetrates to lithospheric levels deeper than the basal detachment.

Previous authors have concluded that the modern north Aegean basins and the North Aegean trough began to subside in late Miocene time (e.g., Lybéris, 1984). However, if the formation of the

North Aegean basin system is kinematically linked to right-slip displacement along the North Aegean trough, and the basin system originated in late Pliocene time as we have suggested here, then the North Aegean trough and perhaps the western strands of the North Anatolian fault, as well, are also no older than late Pliocene.

ACKNOWLEDGMENTS

Supported by NASA Geodynamics Grant NAGW-1951. We are grateful to John Oldow and Elizabeth Schermer for careful and constructive reviews.

REFERENCES CITED

Armour-Brown, A., de Bruijn, H., Maniati, C., Siatos, G. and Neisen, P., 1977, The geology of the Neogene sediments north of Serrai and the use of rodent faunas for biostratigraphic control, in Kallergis, G., ed., Colloquium on the geology of the Aegean region, VI, Proceedings: Athens, Institute of Geological and Mining Research, v. 2, p. 615-622.

Bornovas, J., and Rondogianni-Tsiambaou, T., 1983, Geological map of Greece, second edition: Athens, Institute of Geology and Mineral Exploration, scale 1:500,000.

Büttner, D., and Kowalczyk, G., 1978, Late Cenozoic stratigraphy and paleogeography of Greece–A review, in Closs, H., et al., eds., Alps, Apennines, Hellenides: Stuttgart, E. Schweizerbart'sche, p. 494-500.

Davis, G.A., and Lister, G.S., 1988, Detachment faulting in continental extension; perspectives from the Southwestern U.S. Cordillera, in Clark, S.P., et al., eds., Processes in continental lithospheric deformation: Geological Society of America Special Paper 218, p. 133-159.

Dinter, D.A., 1991, Neogene detachment faulting and the Rhodope metamorphic core complexes, northern Greece [abs.]: Eos (Transactions, American Geophysical Union), v. 72, p. 460.

Erki, I., Kolios, N., and Stegena, L., 1984, Heat flow density determination in the Strymon basin, northeast Greece: Journal of Geophysics, v. 54, p. 106-109.

Harre, W., Kockel, F., Kreuzer, H., Lenz, H., Müller, P., and Walther, H.W., 1968, Über Rejuvenationen im Serbo-Madzedonischen Massiv (Deutung radiometrischer Alterbestimmungen), in Proceedings of the XXIII international geological congress: Prague, v. 6, p. 223-236.

Jacobshagen, V., Dürr, S., Kockel, F., Kopp, K.-O., Kowalczyk, G., Berckhemer, H., and Büttner, D., 1978, Structure and geodynamic evolution of the Aegean region, in Closs, H., et al., eds., Alps, Apennines, Hellenides: Stuttgart, E. Schweizerbart'sche, p. 537-564.

John, B.E., 1987, Geometry and evolution of a mid-crustal extensional fault system: Chemehuevi Mountains, southeastern California, in Coward, M.P., et al., eds., Continental extensional tectonics, Geological Society of London Special Publication 28, p. 313-335.

Kockel, F., and Walther, H.W., 1965, Die Strimonlinie als Grenze zwischen Serbo-Mazedonischem und Rila-Rhodope-Massiv in Ost-Mazedonien: Geologisches Jahrbuch, v. 83, p. 575-602.

Kolocotroni, C., and Dixon, J.E., 1991, The origin and emplacement of the Vrondou granite, Serres, N.E. Greece: Bulletin of the Geological Society of Greece, v. 25, p. 469-483.

Kojumdgieva, E., Nikolov, I., Nedjalkov, P., and Busev, A., 1982, Stratigraphy of the Neogene in Sandanski graben: Geologica Balcanica, v. 12, p. 69-81.

Kokkinakis, A., 1980, Geologie und petrographie des Kavala-Gebietes und des Symvolon-gebirges in Griechisch-Ostmakedonien: Zeitschrift der Deutschen Geologischen Gesellschaft, v. 131, p. 903-925.

Kronberg, P., 1969, Gliederung, Petrographie und Tectogenese des Rhodopen-Kristallins im Tsal-Dag, Simvolon und Ost-Pangäon (Griechisch-Makedonien): Geotektonische Forschungen, v. 31, p. 1-49.

Lalechos, N., and Savoyat, E., 1977, La sédimentation Néogène dans le Fossé Nord Egéen, in Kallergis, G., ed., Colloquium on the geology of the Aegean region, VI, Proceedings: Athens, Institute of Geological and Mining Research, v. 2, p. 591-603.

Le Pichon, X., and Angelier, J., 1979, The Hellenic arc and trench system: A key to the neotectonic evolution of the eastern Mediterranean area: Tectonophysics, v. 60, p. 1-42.

Lister, G.S., Banga, G., and Feenstra, A., 1984, Metamorphic core complexes of Cordilleran type in the Cyclades, Aegean Sea, Greece: Geology, v. 12, p. 221-225.

Lybéris, N., 1984, Tectonic evolution of the North Aegean trough, in Dixon, J.E., and Robertson, A. H. F., eds., The geological evolution of the eastern Mediterranean, Geological Society of London Special Publication 17, p. 709-725.

Meyer, W., 1969, Die Faltenachsen im Rhodopen-Kristallin östlich des Strimon (Nordost-Griechenland): Geotektonische Forschungen, v. 31, p. 86-96.

Schermer, E.R., Lux, D.R., and Burchfiel, B.C., 1990, Temperature-time history of subducted continental crust, Mount Olympos region, Greece: Tectonics, v. 9, p. 1165-1195.

FIGURE CAPTIONS

Figure 1. Tectonic elements of northeast Mediterranean region. Subduction-related thrust contacts have barbs on hanging wall. High-angle faults bounding modern basins have balls on downthrown side. Offshore geometry of modern depocenters shaded north of North Aegean trough is from Lalechos and Savoyat (1977).

Figure 2. Generalized geologic map of Strymon Valley area, northeastern Greece. Strymon Valley (SVDF) and Thasos detachment faults and adjacent areas in Greece were mapped by the authors. SVDF is locally offset by post-detachment, high-angle faults. Areal distribution of map units northeast of Drama basin and southwest of Strymon basin is based on 1:500,000 Geological Map of Greece (Bornovas and Rondogianni-Tsiambaou, 1983). Detachments have barbs on hanging wall. High-angle normal faults bounding modern basins have balls on downthrown side. Attitudes: foliations in gneiss, marble, and granodiorite designated with open, triangular barbs, detachment planes with solid, square barbs, bedding in hanging-wall deposits with tick marks, stretching lineations in extensional mylonites with arrows. All contacts shown between units of Rhodope metamorphic core complex are ductile or brittle-ductile detachments. See inset for location. Gr – Greece, Al – Albania, Yg – Yugoslavia (at submittal), Bg – Bulgaria, T – Turkey. Stereonet: filled circles – poles to SVDF (n = 74), filled square – corrugation axis of SVDF = transport direction of hanging wall, plus signs – slickenside striations and microbreccia streaks on SVDF (n = 6), open squares – mineral stretching lineations in extensional mylonites below SVDF (n = 19).

Figure 3. Schematic cross section showing major late Cenozoic extensional structures of northeastern Greece. Plane of section is parallel to slip on Strymon Valley detachment fault and subparallel to slip on the North Aegean detachment system proposed in this paper. No vertical exaggeration. See Figure 1 for location.

Figure 4. Block diagram showing proposed geometry of North Aegean trough-basin-detachment system (see text).

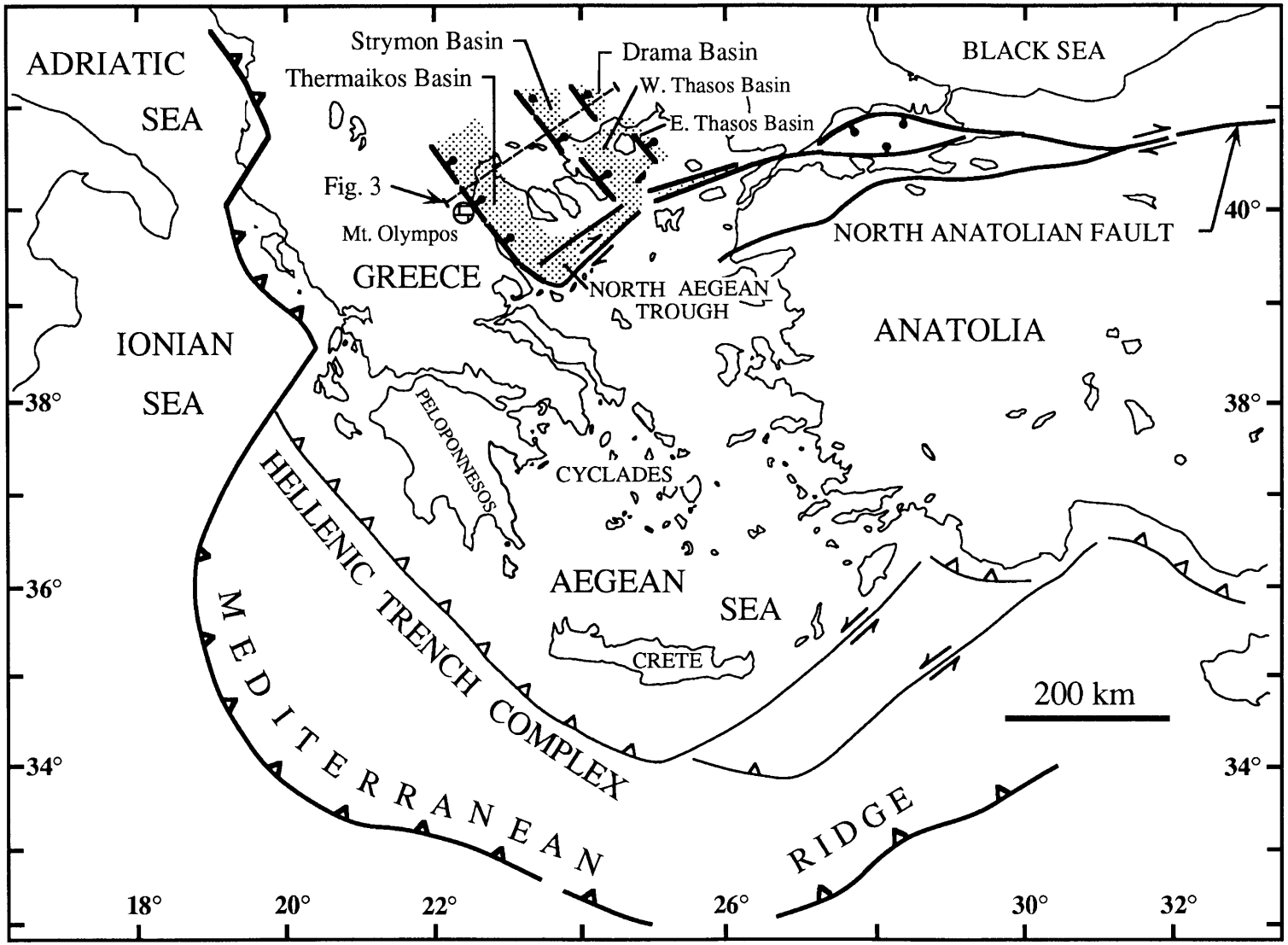

Fig. 1. Active tectonic elements of the northeast Mediterranean region. Subduction-related thrust contacts have barbs on hanging wall. High-angle normal faults bounding modern basins have balls on downthrown side. Offshore geometry of modern depocenters (shaded) north of North Aegean Trough is modified from Lalechos and Savoyat (1977).

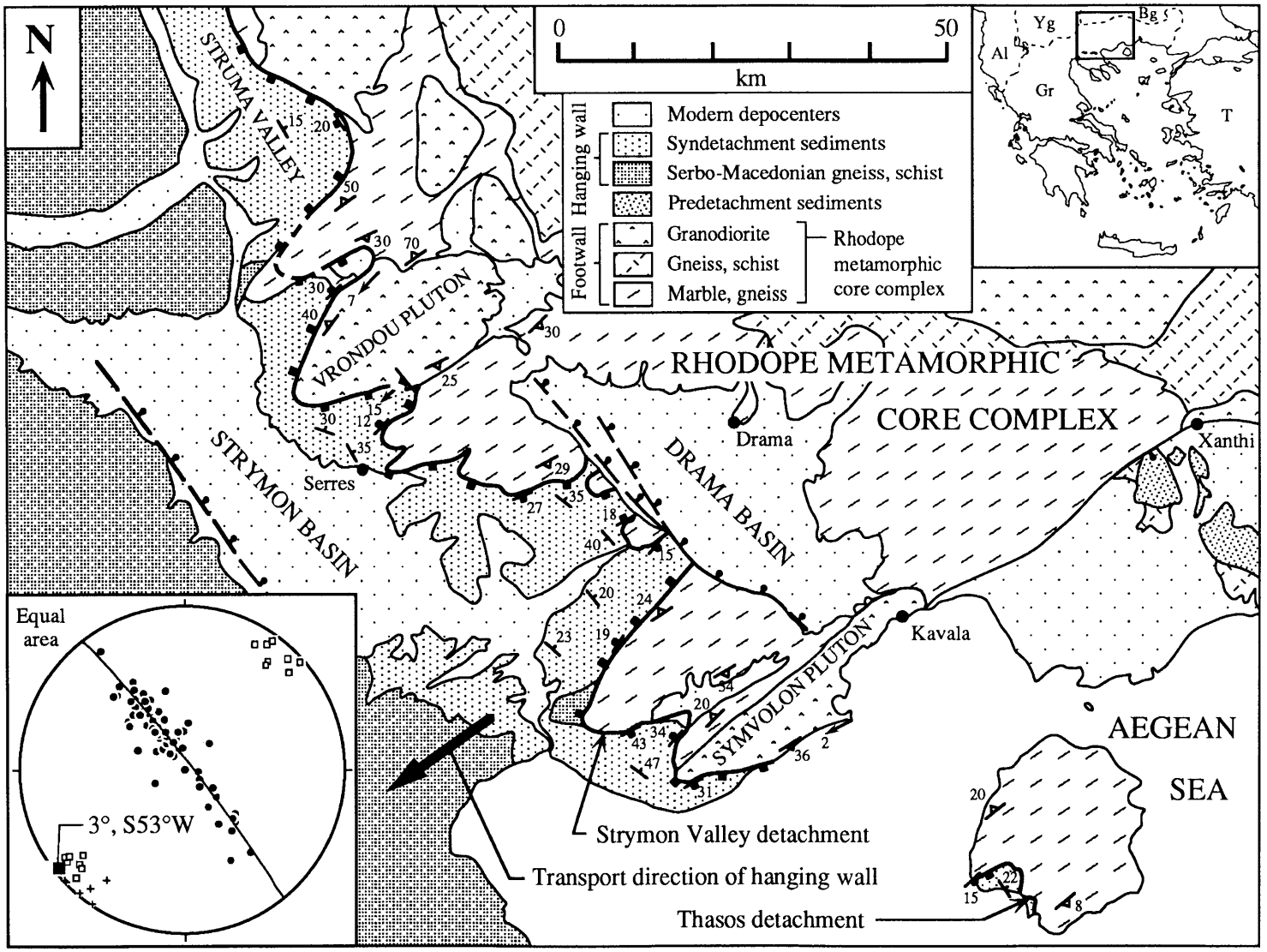

Fig. 2. Generalized geologic map of the Strymon Valley area, northeastern Greece. Stereonet: filled circles – poles to Strymon Valley detachment (SVDF; n = 74); filled square – corrugation axis of SVDF = transport direction of hanging wall; plus signs – slickenside striations and microbreccia streaks on SVDF (n = 6); open squares – mineral stretching lineations in extensional mylonites below SVDF (n = 19).

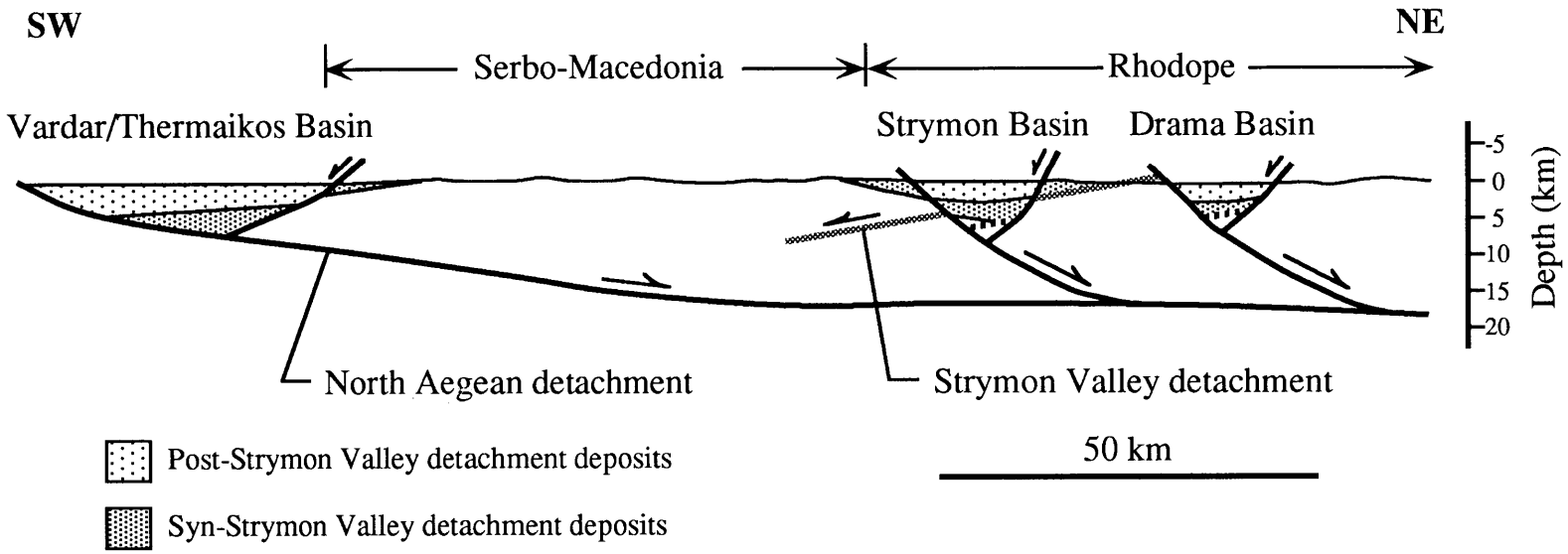

Fig. 3. Schematic cross section showing major middle Miocene - Holocene extensional structures in northeastern Greece. Strymon Valley detachment was active ~16 - 3.5 Ma; North Aegean detachment is inferred to have initiated ~3.5 Ma and to be presently active.

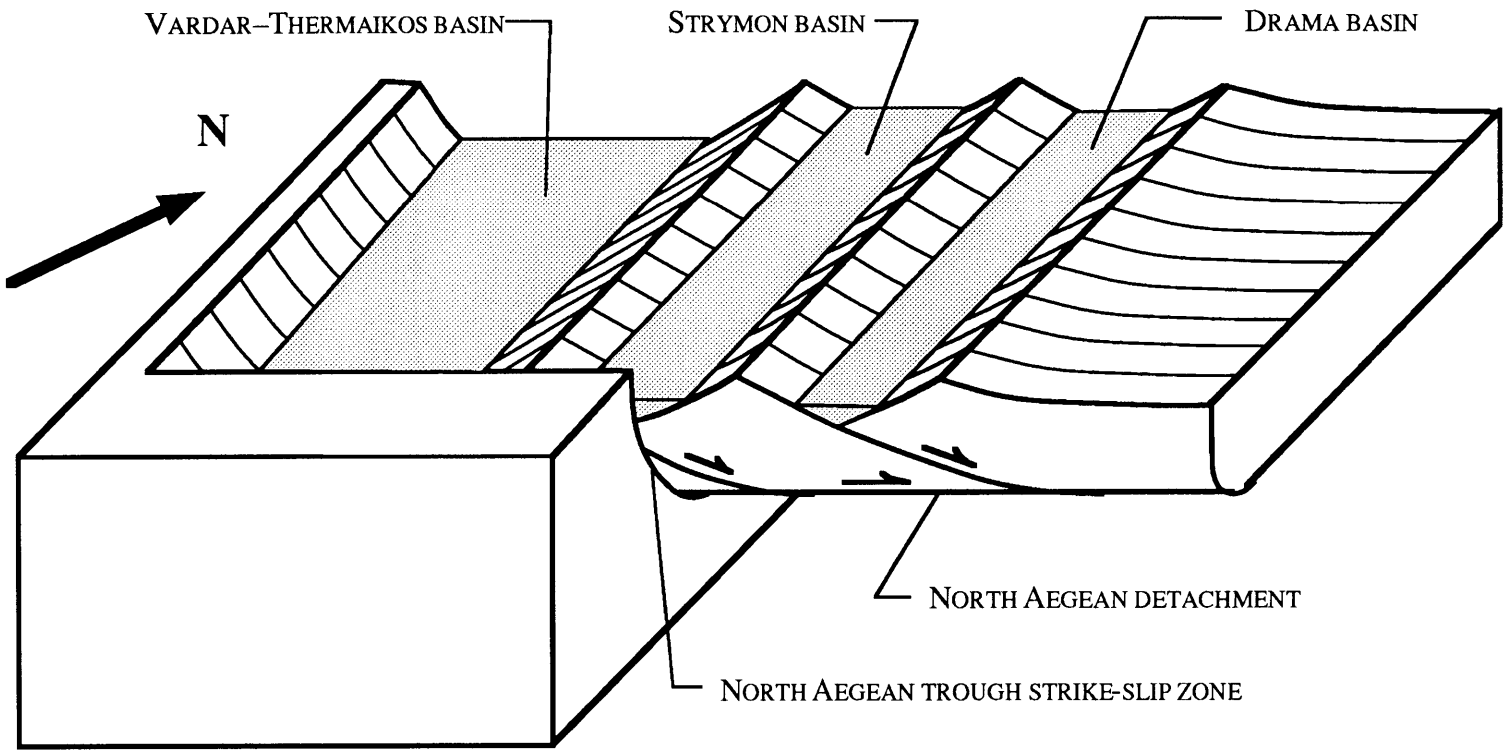

Fig. 4. Block diagram showing proposed geometry of Late Pliocene (?) - Holocene North Aegean detachment system

CHAPTER 3

U-Pb AND $^{40}Ar/^{39}Ar$ GEOCHRONOLOGY OF THE SYMVOLON GRANODIORITE:

IMPLICATIONS FOR THE THERMAL AND STRUCTURAL EVOLUTION OF THE RHODOPE METAMORPHIC CORE COMPLEX, NORTHEASTERN GREECE

David A. Dinter
Department of Earth, Atmospheric and Planetary Sciences
Massachusetts Institute of Technology
Cambridge, MA 02139

ABSTRACT

Northeast Aegean continental crust that was thickened due to thrusting within the Alpine collisional orogen has subsequently been greatly thinned in the back-arc of the Hellenic subduction system. The extension of the Alpine nappe pile in northeastern Greece was principally accommodated by large lateral displacements on a succession of low-angle normal faults. The Rhodope metamorphic core complex, exposed between the Strymon and Nestos Rivers, was unroofed beginning in middle Miocene time in the footwall of one such normal fault, the gently southwest-dipping Strymon Valley detachment. Alpine convergent structures preserved in the Rhodope core complex are constrained to be pre-mid-Oligocene in age by crosscutting relationships with two relatively undeformed granodiorite bodies emplaced ~31 - 33 Ma, the Xanthi and eastern Vrondou plutons. The onset of northeast-southwest extension, manifested by the intrusion and incipient mylonitization of the Symvolon pluton within a northeast-dipping extensional rupture at the southwestern margin of the core complex, the "Symvolon shear zone", is constrained at ~21 - 22 Ma by U-Pb zircon and titanite dates and $^{40}Ar/^{39}Ar$ hornblende dates obtained in this study. The Symvolon shear zone may have continued active for 4 - 5 m.y. while temperatures in the pluton remained between 300°C and 500°C. Beginning no later than

15.5 Ma, however, rapid cooling from > 300°C to < 150°C is documented by $^{40}Ar/^{39}Ar$ biotite and K-feldspar dates, respectively. Increasingly youthful to the southwest, these dates appear to record the progressive southwestward unroofing of the Rhodope metamorphic core complex in the footwall of the Strymon Valley detachment.

INTRODUCTION

The Rhodope/Serbo-Macedonian province is a mountainous, structurally complex domain of tectonically intercalated high- and low-grade metamorphic rocks and igneous bodies whose role in the evolution of the Alpine orogen remains poorly understood. It lies between two branches of the Alpine chain, the Carpathian-Balkan branch to the northeast and the Dinaric-Hellenic branch to the southwest (Fig. 1). The Carpathians and Balkans form a Z-shaped, north- to northeast-vergent thrust belt buttressed to the north by the Russian and Moesian (Romanian) platforms. The Dinaric and Hellenic Alps comprise a predominantly southwest-vergent thrust belt; they parallel the eastern coastline of the Adriatic Sea and lie at the leading edge of the overriding plate in the west- to southwest-vergent Hellenic subduction system, which has been active in roughly its present position throughout much of Neogene time (e.g., Le Pichon and Angelier, 1979). The eastern margin of the Hellenic Alps coincides approximately with the western boundary of the ophiolitic Vardar zone, a major mid- to late Mesozoic continental suture along which the western Tethyan "Apulian continental fragment", represented in the Hellenic nappes by granitic and gneissic basement rocks of the Pelagonian zone, collided with southeastern Europe early in the Alpine orogeny (Fig. 2; Jacobshagen et al., 1978; Burchfiel, 1980).

Structural and geochronologic studies in the Mt. Olympos region west of the Vardar suture have established that Alpine convergence, principally expressed by major east- to northeast-dipping thrust faults, persisted through at least late Eocene time in that area and

was succeeded by extension on northeast-dipping low-angle normal faults beginning no later than early Miocene time (Fig. 2; Schermer, 1989, 1990, 1993; Schermer et al., 1990). East- to northeast-dipping Alpine thrusting followed by extensional deformation also characterizes the region east of the Vardar suture in the Rhodope/Serbo-Macedonian province (Kockel et al., 1977; Jacobshagen et al., 1978; Ivanov, 1981; Papanikolaou and Panagopoulos, 1981; Zachos and Dimadis, 1983; Dixon and Dimitriades, 1984; Burg et al., 1990; Koukouvelas and Doutsos, 1990). In general, however, the chronology of deformation is poorly established in this region owing to a paucity of information on the relevant ages of the igneous and metamorphic units juxtaposed there.

Within the Rhodope/Serbo-Macedonian province, along the northeast margin of the Strymon/Struma Valleys in northeastern Greece and southwestern Bulgaria, a high-grade gneiss complex to the west overlies a thick, low-grade marble unit and several granodiorite intrusives to the east on a low-angle, *southwest*-dipping fault that has conventionally been regarded as an Alpine thrust, the "Strimonüberschiebung" (Kockel and Walther, 1965; Schenk, 1970; Koukouzas, 1972). The presence of Neogene sediments sheared within this fault zone has long been taken to imply that a Neogene compressional event affected northeastern Greece (e.g., Schenk, 1970). Based on detailed geologic mapping, Dinter and Royden (1993) reinterpreted the "Strimonüberschiebung" as a major Neogene low-angle normal fault, the Strymon Valley detachment, thus negating the principal evidence for Neogene convergent deformation in this region (Figs. 2 and 3). The present study addresses the thermal and structural history of the Rhodope metamorphic core complex – exposed in the footwall of the Strymon Valley detachment – through a series of geochronologic analyses of the Symvolon pluton, a highly strained granodiorite body that immediately underlies the detachment surface (Fig. 3). U-Pb analyses of titanite and zircon fractions and $^{40}Ar/^{39}Ar$ furnace step-heating and laser fusion analyses of hornblende, biotite, and K-feldspar separates yield robust age constraints on the emplacement,

mylonitization, and cooling of the pluton. Combined with newly acquired structural data, these ages also provide crucial information on the geometry, timing, and magnitude of Neogene extension in northeastern Greece.

Regional Geologic Framework and Previous Studies

Southwestward translation of the Serbo-Macedonian gneiss complex in the hanging wall of the Strymon Valley detachment system from > 15 to ~3.5 Ma resulted in the unroofing and subaerial exposure of the Rhodope metamorphic core complex (Dinter and Royden, 1993). The Falakron marble series, composed of massive marble intercalated with relatively minor amphibolite and metapelite layers bearing upper greenschist-facies mineral assemblages, is the principal tectonostratigraphic unit exposed in the Rhodope complex (Fig. 4). Its effective thickness increases northeastward from a few hundred meters in the Strymon Valley vicinity to >5000 m along the Nestos River, where the marble series is overlain on the southwest-vergent Nestos thrust by the West Thracian gneiss complex (Figs. 2 and 3; Kronberg, 1969; Schenk, 1970). The Serbo-Macedonian and West Thracian gneiss complexes both bear upper amphibolite-facies mineral assemblages with relict eclogite intervals in places (Dixon and Dimitriades, 1984; Liati, 1986; Mposkos et al., 1988) and appear to represent segments of a formerly continuous Mesozoic(?) metamorphic complex that were separated by as much as 80 km subhorizontally as a consequence of Neogene normal displacement on the Strymon Valley detachment system.

The Vrondou, Xanthi, and Symvolon plutons, three Tertiary granitic to dioritic bodies that intrude the Falakron marble series, provide constraints on the sequence and timing of deformational events in the Rhodope metamorphic core complex (Fig. 3). An early ductile deformation associated with the formation of the Nestos thrust produced gently to moderately northeast-plunging mineral stretching lineations and m- to km-scale,

open to tight folds throughout the Falakron series (Kronberg, 1969; Meyer, 1969; de Boer, 1970; Schenk, 1970). These structures are crosscut by the eastern intrusive boundary of the Vrondou pluton and by the Xanthi pluton, which also cuts the Nestos thrust (Fig. 3; Kronberg and Eltgen, 1973). A hornblende separate from the Xanthi pluton gave a K-Ar date of 30.4 ± 0.6 Ma (Liati, 1986) and hornblende phenocrysts from a cluster of andesite dikes intruded by the Xanthi pluton at its eastern margin yielded a K-Ar date of 33.5 ± 1.2 Ma (Eleftheriadis et al., 1984), constraining the emplacement age to be between those values (mid-Oligocene), assuming that the Ar system in the dike phenocrysts was not reopened during the intrusion of the pluton. This assumption is probably valid, because the dikes appear to be part of a large volcanic arc suite exposed immediately to the north, the Paranestion andesites, which have yielded K-Ar biotite, sanidine, and whole rock dates ranging from 28.7 ± 1.1 Ma to 35.0 ± 1.2 Ma (Fig. 3; Eleftheriadis and Lippolt, 1984).

The Vrondou pluton, composed predominantly of quartz monzonite (e.g., Kotopouli and Pe-Piper, 1989), is similar to the Xanthi pluton compositionally and has yielded K-Ar hornblende dates ranging from 29 ± 1 Ma to 33 ± 2 Ma (Marakis, 1969). These values must be interpreted *sensu strictu* as minimum ages for the emplacement of the Vrondou body; however, given the chemical similarities between the Vrondou and Xanthi plutons and the fact that the eastern Vrondou intrusive margin truncates deformational structures in the country rock inferred to have been active as late as 36 Ma (Chap. 3), it seems likely that the Vrondou pluton was emplaced during the same mid-Oligocene magmatic event represented by the Xanthi granodiorite (cf. Kotopouli and Pe-Piper, 1989).

The Symvolon (or "Kavala") granodiorite crops out in the southwest corner of the Rhodope metamorphic core complex beneath the Strymon Valley detachment as a northeast-elongate dome some 40 km long and 10 - 15 km wide (Fig. 3). It is markedly different from the Vrondou and Xanthi plutons in significant chemical, structural, and

textural aspects and appears to represent a distinct episode of magmatism, the age of which has long been disputed. Harre et al. (1968) reported K-Ar biotite dates of 13.8 ± 0.2 Ma and 15.0 ± 0.3 Ma from the Mesolakkia granodiorite, which intrudes the Falakron marble series beneath Mt. Pangaion and appears to be continuous with the Symvolon body. Meyer (1968) interpreted these dates as "rejuvenation" ages; he considered the emplacement of the pluton to be syntectonic with the Nestos thrust-related ductile deformation of the host rock because, like the Falakron marble series it intrudes, the Symvolon granodiorite bears pervasive, gently northeast-plunging folds and stretching lineations (Kokkinakis, 1980a). Based on stratigraphic and structural relationships in eastern Thrace, where northeast-trending folds in metamorphic rocks that are possibly correlative with those in the Rhodope core complex are overlapped by middle Eocene sedimentary strata (Kopp, 1961), Meyer (1968) proposed that the ductile folding of the Falakron series and the emplacement and mylonitization of the Symvolon pluton occurred prior to middle Eocene time.

Kokkinakis (1980b) obtained K-Ar biotite ages of 15.5 ± 0.5 Ma and 17.8 ± 0.8 Ma from the Symvolon pluton, which he also considered to represent a Miocene resetting of the biotite Ar system. From the results of a single U-Pb zircon analysis that gave discordant $^{206}Pb/^{238}U$ and $^{207}Pb/^{235}U$ model ages of 95 ± 5 Ma and 101 ± 8 Ma, respectively, and a $^{207}Pb/^{206}Pb$ age of 335 ± 40 Ma, Kokkinakis (ibid.) interpreted a minimum Carboniferous emplacement age for the pluton.

The 13.8 - 17.8 Ma K-Ar biotite dates of Harre et al. (1968) and Kokkinakis (1980b) were reinterpreted by Dinter and Royden (1993) as cooling ages related to the tectonic unroofing of the Symvolon pluton in the footwall of the Strymon Valley detachment. This interpretation is consistent with the occurrence of fossils as old as 15 - 18 Ma in the basal deposits of a syndetachment hanging-wall basin complex (Kojumdgieva et al., 1982). Rb-Sr biotite model ages of 12.2 ± 0.4 Ma and 12.6 ± 0.4 Ma obtained by

Del Moro et al. (1990) from paragneisses on the flanks of the Marmara Valley immediately adjacent to the Mesolakkia and Symvolon granodiorite bodies also probably appertain to the unroofing of the Rhodope core complex. These low-grade metamorphic rocks are structurally intercalated and mylonitized concordantly with the margins of those intrusives and clearly experienced a syn- and post-intrusional deformational and thermal evolution similar to that of the plutons themselves.

STRUCTURAL AND TEXTURAL ASPECTS OF THE SYMVOLON GRANODIORITE

The Xanthi pluton and the eastern part of the Vrondou pluton are essentially nonmylonitic and are associated with well-developed contact aureoles (Fig. 3; Meyer, 1968; Marakis, 1969; de Boer, 1970; Kronberg and Eltgen, 1973; Liati, 1986; Kolocotroni and Dixon, 1991; Koukouvelas and Pe-Piper, 1991; Dinter and Royden, 1993). The Symvolon pluton, by contrast, is pervasively mylonitic (Fischer, 1963; Meyer, 1968; Kokkinakis, 1980a). Its margins are zones as wide as ~100 m within which strongly mylonitized granitic material and Falakron country rocks are intercalated in structurally concordant sheets and tabular masses ranging from a few millimeters to tens of meters in thickness, and no contact aureole is preserved.

Mineral stretching lineations in the Symvolon granodiorite are defined by the alignment of fine-grained biotite and dynamically recrystallized quartz on mylonitic C-planes and by asymmetric "tails" or "wings" developed around K-feldspar phenocrysts and porphyroclasts and hornblende porphyroblasts (Figs. 5a, 5b, and 5c). C-planes in the south central part of the pluton typically dip gently to moderately northeast, and associated stretching lineations have orientations in the range 10°-25°, N45°-85°E, with a well-defined mean value of 18°, N58°E (Fig. 6). Similar results also obtain for the remainder of the pluton (Kokkinakis, 1980a). Fifty-seven field measurements of macroscopic S-C

mylonitic fabrics show an approximate 5:3 ratio of top-to-the-southwest transport over top-to-the-northeast, which must be considered indeterminate owing to ambiguities inherent in distinguishing S- and C-planes in outcrop, particularly in quartz-rich granitic rocks. Better-constrained determinations of shear sense in ten oriented thin sections yielded a 1:1 ratio of southwest to northeast vergence, interpreted here as evidence that the mylonitization process involved a large component of pure shear (Fig. 6).

Structural and textural data preclude an association between the northeast-dipping Symvolon mylonitic fabrics and the southwest-dipping Strymon Valley detachment system. Mylonitic foliations dipping oppositely to the main detachment in extensional settings are commonly observed in a relatively narrow back-rotated zone of the footwall up-dip of the detachment outcrop (the "mylonitic front" of Davis and Lister, 1988). By contrast, the Symvolon mylonites dip uniformly northeast throughout most of the 40-km length of the pluton's northeast-elongate dome-shaped exposure (Fig. 6; see also Kokkinakis, 1980a). The northeast-dipping fabric elements are truncated in places by the Strymon Valley detachment and may also be overprinted locally by weakly developed southwest-dipping mylonites that represent ductile levels of the Strymon Valley shear zone (Dinter and Royden, 1993). Moreover, as the Strymon Valley detachment is characterized predominantly by *simple* shear (ibid.), associated mylonites might be anticipated to show a marked bias toward top-to-the-southwest vergence that clearly is not characteristic of the Symvolon shear fabrics.

SAMPLE SELECTION AND PREPARATION / ANALYTICAL PROCEDURES AND DATA REDUCTION

From a pool of 24 medium- to coarse- grained granitic S-C mylonite samples of the central Symvolon pluton, the five from which various mineral separates were analyzed in

this study were chosen based on thin-section examinations to maximize the volume and freshness of the desired mineral phases. Hand specimens were crushed, milled, and sieved using standard equipment at the geochronologic facilities of the Massachusetts Institute of Technology. Hornblende, biotite, and K-feldspar separates from the 60-80, 80-100, or 100-150 mesh sieve fractions were obtained using heavy liquids and a Frantz magnetic separator and purified further by hand-removal of chlorite, epidote, and other remaining impurities. Grain aggregates with quartz and feldspar were especially problematic in hornblende fractions. Rims of these materials were removed by vigorous saltation of the separates for 5 to 10 minutes in distilled water, sonically induced by a Cole-Farmer series 4710 ultrasonic homogenizer. Hornblendes and biotites for $^{40}Ar/^{39}Ar$ laser fusion analysis and zircons and titanites from the 80-100, 100-140, or 140-200 mesh sieve fractions for U-Pb analysis were hand-picked grain-by-grain, resulting in at least 99.9% purity. The minimum purity of the larger hornblende, biotite, and K-feldspar separates for $^{40}Ar/^{39}Ar$ furnace step-heating analyses is estimated at 99%. Principal visible impurities in biotite and hornblende fractions were small intergrowths of chlorite, and in K-feldspar fractions, minor quartz and plagioclase.

U-Pb analyses

Zircon and titanite (sphene) grains for U-Pb analysis were individually hand-picked in ethanol under a 60x picking scope from the nonmagnetic heavy fractions ($\rho \geq 3.3$ gm/cm^3) of samples M90-K71 and M90-K73. Grains were segregated into groups or "picks" so as to maximize similarities in crystal size, habit, color, and clarity, and to minimize visible inclusions. Exceptionally low analytical blanks attained during the tenure of this study (~5 pg total Pb) allowed for relatively small and homogeneous zircon picks, even given the possible Tertiary emplacement age anticipated for the Symvolon pluton based on structural and $^{40}Ar/^{39}Ar$ data. In one case a single coarse zircon grain was

analyzed; more typical pick sizes were 20 - 50 grains, depending on the size fraction (Table 1). Estimated Pb concentrations as low as 1 ppm in titanite required picks as large as 3 - 4 mg, comprising several hundred grains.

Most zircon picks were air-abraded with pyrite for 18 - 24 hours following the technique developed by Krogh (1982) in an effort to reduce the effects of surficial lead loss. Pyrite and other surficial contaminants were removed from the abraded grains by leaching for 10 - 30 minutes in 30% HNO_3 at ~60°C. After leaching, each pick was washed in distilled water, dried in acetone, weighed, spiked with a mixture of ^{205}Pb, ^{235}U, and ^{233}U, and then dissolved at 230°C in a mixture of HF and HNO_3 in a TFE teflon microcapsule following the method of Parrish (1987). Titanites, which are considerably more friable at room temperature than zircons, were neither abraded nor leached. Picks were weighed and spiked as above and dissolved at 230°C in a mixture of HF and HCl in TFE teflon bombs similar to those described in Mattinson (1978). Solutions derived from both zircon and titanite picks were dried to fluoride salts and converted to chlorides in 6N HCl at 180°C, and Pb and U were separated on standard anion columns using HCl chemistry in the case of zircons and HCl and HBr chemistry for titanite solutions, using a procedure modified from Krogh (1973). Pb fractions were affixed to rhenium filaments employing silica gel and phosphoric acid; U fractions were fixed with graphite.

All isotopic measurements were performed in a static multicollector mode using a Daly electron multiplier for ^{204}Pb data on the VG Sector 54 solid source mass spectrometer at the Mass Spectrometry Laboratory in the Department of Earth, Atmospheric, and Planetary Sciences, Massachusetts Institute of Technology. A mass fractionation correction factor for Pb of 0.123% ± 0.03 per atomic mass unit was determined by replicate analyses of the NBS standards SRM 981 (common Pb) and SRM 983 (radiogenic Pb) and applied to all analyses. Following Ludwig (1980), Pb concentrations and Pb/U

ratios were calculated from the fractionation-corrected spectrometer data using the PBDAT program for MS-DOS, v. 1.03 (Ludwig, 1988a). Initial Pb composition estimates are based on the two-stage evolutionary model of Stacey and Kramers (1975), and age calculations were made using the decay constants 0.155125 x 10^{-9}/yr for ^{238}U and 0.98485 x 10^{-9}/yr for ^{235}U (Steiger and Jäger, 1977). Linear regressions and calculations of intercepts and uncertainties were attempted using the ISOPLOT program for MS-DOS, v. 1.01 (Ludwig, 1988b). Uncertainties in ages are reported at the 2σ confidence level.

$^{40}Ar/^{39}Ar$ analyses

Mineral separates for $^{40}Ar/^{39}Ar$ laser fusion and furnace step-heating analyses were irradiated in two separate layered aluminum canisters for seven hours each in the core facility of the Omega West reactor at the Los Alamos National Laboratory in New Mexico. Biotite and hornblende separates for laser analysis averaged 50 - 60 grains in size, and furnace samples, which were encased in aluminum foil prior to loading in the irradiation canister, averaged 30 mg for biotite and K-feldspar and 80 mg for hornblende. Interlaboratory standards MMhb-1 hornblende (520.4 Ma; Samson and Alexander, 1987) and Fish Canyon tuff sanidine (27.8 Ma; Cebula et al., 1986) were included in alternate layers as neutron flux monitors. J-values vary linearly from layer to layer, ranging from 0.00575 to 0.00584 across 6 layers in the laser package, CLAIR 8, and from 0.00566 to 0.00576 across 8 layers in the furnace package, CLAIR 9, with a minimum precision in any given layer of 1% at the 2σ confidence level.

All samples were analyzed at the CLAIR $^{40}Ar/^{39}Ar$ facility at the Massachusetts Institute of Technology. The CLAIR apparatus includes two automatically driven laser sample chambers, each with a maximum capacity of 100 samples loaded in a 1-inch square 10 x 10 grid of shallow borings in a copper planchet, a double vacuum resistance furnace,

a stainless steel extraction line, and an MAP 215-50 mass spectrometer. 1- to 5-grain laser subsamples were fused by exposure for 10 seconds to the continuous emission of an argon-ion laser operating at approximately 4 watts. Furnace samples were baked at each successive temperature increment for 5 minutes and cooled to 200°C - 250°C between heating intervals. Gas extracted by either laser fusion or furnace heating was cleansed of reactive gasses by exposure for 10 minutes to SAES AP-10 Al-Zr and SAES 172 FE-V-Zr getters, and then admitted to the spectrometer. ^{40}Ar, ^{39}Ar, ^{38}Ar, ^{37}Ar, and ^{36}Ar values for laser fusion release increments were measured using a Johnston electron multiplier with a 10^9 ohm resistor, and for resistance furnace temperature steps, a faraday detector with a 10^{11} ohm resistor. Linear regressions were performed on the results of five successive counting cycles for each increment to estimate the isotope composition at the time of admittance. Line blanks were measured at the beginning and end of each block of 10 to 20 laser analyses and at the end of each 10- to 14-step furnace analysis. Typical blank values obtained during laser analyses were: ^{40}Ar – 8.4 x 10^{-16} moles, ^{39}Ar – 3.9 x 10^{-17} moles, ^{38}Ar – 1.5 x 10^{-17} moles, ^{37}Ar – 2.3 x 10^{-17} moles, and ^{36}Ar – 1.6 x 10^{-17} moles, and during furnace analyses: ^{40}Ar – 7.4 x 10^{-15} moles, ^{39}Ar – 7.6 x 10^{-17} moles, ^{38}Ar – 2.4 x 10^{-17} moles, ^{37}Ar – 3.9 x 10^{-17} moles, and ^{36}Ar – 7.2 x 10^{-17} moles. Spectrometer mass discrimination characteristics are determined by regular measurements of atmospheric Ar. After applying blank and mass discrimination corrections to the raw data, model ages were calculated from the derived isotopic ratios assuming a decay constant of 5.543 x 10^{-10}/yr ± 0.010 x 10^{-10} for the production of radiogenic ^{40}Ar from ^{40}K (Steiger and Jäger, 1977).

SAMPLE DESCRIPTIONS AND ANALYTICAL RESULTS

Primary goals of this radiometric study were to establish the emplacement age, mylonitization age, and cooling history of the Symvolon granodiorite as fully and robustly as possible from the samples in hand. To that end, as many as five coexisting mineral

phases, including zircon, titanite, hornblende, biotite, and K-feldspar, were dated from a single hand specimen (M90-K73), and $^{40}Ar/^{39}Ar$ ages of hornblende and biotite separates were obtained by both laser fusion and furnace step-heating gas extraction methods whenever sufficient material was available. U-Pb analyses were performed on 7 zircon picks from a single sample (M90-K73) and on 3 titanite picks from 2 samples (M90-K71 and M90-K73). $^{40}Ar/^{39}Ar$ methods were employed to analyze 17 hornblende, biotite, and K-feldspar separates representing 5 samples (M90-K5, -K12, -K71, -K73, and -K79). The results of these analyses are summarized in Tables 1 and 4 and on Figures 6 and 12.

U-Pb analyses

Wedge-shaped, euhedral to subhedral, honey-colored titanites are abundant accessories in nearly all of the mylonitic Symvolon granodiorite samples analyzed in this study (Fig. 7a). They typically occur as discrete grains with long axes oriented along S- or C-planes, surrounded by finer biotite and dynamically recrystallized quartz, and may have crystallized either prior to or relatively early in the tenure of the mylonitic shear environment, or both (Fig. 7b). Some grains clearly record two growth periods; cloudy, euhedral, honey-colored cores are surrounded by nearly clear euhedral overgrowths (Fig. 7c). Titanites are also found as rare, marginal inclusions in K-feldspar phenocrysts or as inclusions in hornblende (Fig. 7d). Euhedral zircons (Fig. 8a), which are commonly observed as inclusions in feldspar phenocrysts, were sectioned and imaged with a scanning electron microscope, revealing chemically (?) eroded cores in nearly all grains (Fig. 8b).

$^{206}Pb/^{238}U$, $^{207}Pb/^{235}U$, and $^{207}Pb/^{206}Pb$ ages obtained in 3 titanite and 7 zircon analyses are summarized in Table 1, and $^{206}Pb/^{238}U$ and $^{207}Pb/^{235}U$ ages are also plotted on a concordia diagram (Fig. 9). Raw and corrected data for each U-Pb analysis are reported in Tables 2 and 3.1 - 3.10. $^{207}Pb/^{235}U$ and $^{207}Pb/^{206}Pb$ ages of both titanite and

zircon fractions from the Symvolon pluton are poorly constrained owing to the paucity of original ^{235}U typically incorporated in Tertiary magmas; $^{206}Pb/^{238}U$ ratios are less sensitive to the choice of common lead composition and provide more robust age estimates for young intrusives. $^{206}Pb/^{238}U$ ages of 19.7 ± 0.3 Ma, 20.0 ± 0.5 Ma, and 21.1 ± 0.8 Ma were obtained in analyses of a single titanite fraction from sample M90-K71 and of two size fractions from M90-K73, respectively (Table 1; Fig. 9). The larger size fraction from M90-K73 yielded the older age, which may indicate an earlier crystallization of the larger grains. Alternatively, larger titanite grains may have retained their radiogenic Pb more completely than smaller ones.

Seven zircon picks from sample M90-K73 yielded discordant $^{206}Pb/^{238}U$ and $^{207}Pb/^{235}U$ age pairs ranging from 24.4 ± 0.7 Ma and 27.1 ± 1.3 Ma to 97.0 ± 0.1 Ma and 102.4 ± 1.0 Ma (Tables 1, 2, and 3.4 - 3.10). These pairs are not strictly colinear within accepted statistical confidence levels (Ludwig, 1988b); nonetheless, they clearly define a linear trend on a concordia plot, implying that the derived ages are mixing ages representing at least two periods of crystal growth. Subhedral to anhedral zircon cores obvious in scanning electron microscopic images probably survive from the earliest crystallization period, which is unlikely to be older than ~325 Ma based on a qualitative graphical estimate of the maximum upper intercept with concordia (Fig. 9a). A minimum earliest Permian age for these cores is implied by the maximum $^{207}Pb/^{206}Pb$ age obtained, 281.8 ± 9.3 Ma (Table 1).

A graphical estimate of the maximum lower intercept with concordia suggests that the crystallization age of euhedral overgrowths surrounding the eroded cores must be Oligocene or younger (Fig. 9b). A closer constraint on this later period of zircon growth is provided by the analysis of a single, euhedral, hyacinth-colored grain that was approximately three times larger than any included in the multigrain picks; this grain yielded

the minimum $^{206}Pb/^{238}U$ age obtained in the present study, 24.4 ± 0.7 Ma (Tables 1, 2, and 3.10). A component of Pb inheritance is indicated by the $^{207}Pb/^{206}Pb$ age of this grain, 281.8 ± 9.3 Ma, so that 24.4 ± 0.7 Ma must be interpreted as a maximum age for the later crystallization period. It appears likely that this period is identical to that during which the titanites formed, and occurred ~20 - 22 Ma.

$^{40}Ar/^{39}Ar$ analyses

The results of nine $^{40}Ar/^{39}Ar$ furnace step-heating experiments are presented graphically both as conventional age spectra (Figs. 10.1a - 10.9a) and on inverse isotope correlation plots (Figs. 10.1b - 10.9b; Roddick, 1980; Heizler and Harrison, 1988), showing either York 2 isochrons (York, 1969) or York 1 "errochrons" (York, 1966). The York 1 regression was employed only when the mean squared weighted deviation (MSWD) associated with the York 2 regression was unacceptably high (usually >2.5; see McDougall and Harrison, 1988; Wendt and Carl, 1991). Ages quoted in Table 4 and in Figs. 10.1 - 10.9 are exclusively York 2 or York 1 regression ages, which do not assume an atmospheric value for $[^{40}Ar/^{36}Ar]_0$. Values for one or two heating increments, typically the initial or final ones or those associated with extremely small gas releases, were omitted from some regressions when they clearly fell outside the envelope defined by the remaining increments. Heating schedules with pertinent isotopic ratios and model ages associated with each temperature step are presented in Tables 5.1 - 5.9.

Each of eight biotite and hornblende separates selected for $^{40}Ar/^{39}Ar$ laser fusion analysis was divided into a set of 10 to 20 subsamples. Each subsample, comprising 1 - 5 grains, was fused separately, yielding a model age (assuming an atmospheric value for $[^{40}Ar/^{36}Ar]_0$) directly analogous to a conventional K-Ar age (Tables 6.1 - 6.8). Thus, an average age with uncertainties could be calculated for each mineral separate from the 10 to

20 replicate analyses. An alternate method of interpretation preferred in this study is to plot the analytical results on an inverse isotope correlation diagram and calculate a York 2 or York 1 regression line for the points in exactly the same manner as for incremental heating experiments. The philosophical justification for this approach is somewhat different than for furnace step-heating data. In both cases the Ar present in a given crystal is assumed ideally to represent two end-member reservoirs in some proportion: initial or "trapped" Ar from meteoric or other sources that was incorporated in the sample during crystallization or metamorphism, and radiogenic ^{40}Ar produced by the decay of ^{40}K (e.g., McDougall and Harrison, 1988). (The presence of "excess" ^{40}Ar, typically derived from metamorphic fluids or gas phases at some time subsequent to crystallization and concentrated within crystal margins during relatively low-temperature diffusion, commonly results in an inability to fit a straight line on a plot of $^{39}Ar/^{40}Ar$ vs. $^{36}Ar/^{40}Ar$). In applying the inverse isotope correlation method to furnace experiments it is assumed that each successive heating increment will sample Ar from "trapped" and radiogenic sources in a slightly different proportion, thus yielding a linear spread of points on an inverse isotope correlation plot. By contrast, the inverse isotope correlation approach as applied to laser fusion data assumes that each crystal in a rock is to some extent an independent system and will incorporate or "sample" Ar from the two ideal end-member sources in proportions quantifiably distinct from those in nearby crystals, thus also yielding a linear spread on an inverse isotope correlation plot. In the absence of significant excess ^{40}Ar, the application of this method to both types of data appears to be justified on empirical grounds.

In addition to inverse isotope correlation plots (Figs. 11.1a - 11.8a) and data tables (Tables 6.1 - 6.8), laser fusion data are presented in model-age distribution diagrams (Figs. 11.1b - 11.8b) analogous in some respects to "age spectra" conventionally drawn for step-heating experiments. These plots are useful in that they graphically portray the relative amounts of gas released during the fusion of each subsample and the scatter of model total-

fusion $^{40}Ar/^{39}Ar$ ages obtained in replicate analyses of crystals from a single separate. It should be emphasized, however, that each laser-fusion analysis is independent, so that the concept of an "age plateau" as defined for successive temperature increments in a step-heating analysis cannot be meaningfully applied to laser-fusion data.

Sample M90-K5

M90-K5, a coarse, granodioritic S-C mylonite collected near the northeast limit of the study area (Fig. 6), is composed of ~60% plagioclase and K-feldspar, 30% quartz, 5% biotite, 3% hornblende, and 2% titanite and other accessory minerals. K-feldspar phenocrysts as large as 1 cm in diameter commonly have sigmoid tails indicative of top-to-the-northeast mylonitic strain and invariably exhibit undulose extinction. Hornblende, biotite, and titanite, which generally occur along S-planes, less commonly along C-planes, and are not typically mechanically deformed, may have crystallized in the mylonitic shear environment (Fig. 5c). Most of the quartz is dynamically recrystallized and appears to have accommodated much of the C-plane shear strain (Fig. 5a).

Four mineral separates from sample M90-K5 were dated by $^{40}Ar/^{39}Ar$ methods: K-feldspar and biotite by incremental heating, and biotite and hornblende by laser fusion. The step-heating release spectrum for M90-K5 K-feldspar is relatively flat, with model ages for all save the final (total-fusion) step falling in the range 14.6 ± 0.3 Ma to 16.4 ± 0.3 Ma (Table 5.1) and higher temperatures yielding slightly older model ages (Fig. 10.1a). The inverse isotope correlation plot shows low proportions of trapped Ar in the gas released. A York 1 age of 15.0 ± 0.1 Ma is well-constrained by points close to the $^{39}Ar/^{40}Ar$ axis; an initial $^{40}Ar/^{36}Ar$ ratio of 400 ± 90 is poorly constrained (Fig. 10.1b).

Steps 2 - 9 in the M90-K5 biotite step-heating release spectrum yielded model ages in the range 13.7 ± 0.3 Ma to 16.2 ± 0.3 Ma (Fig. 10.2a; Table 5.2). The initial heating step, which released >28% of the total gas and gave a model age of 11.7 ± 0.4 Ma, plots close to the y-axis in the correlation diagram, closely constraining a near atmospheric initial $^{40}Ar/^{36}Ar$ ratio of 280 ± 10 (Fig. 10.2b). The remaining steps also released significant proportions of trapped Ar; nonetheless, the York 2 isochron age of 15.5 ± 0.3 Ma is well-constrained. Laser-fusion analyses of the same biotite separate show a greater range of model ages, from 7.7 ± 0.1 Ma to 16.0 ± 0.2 Ma (Table 6.1; Fig. 11.1); however, the York 2 isochron age derived from the laser data, 15.4 ± 0.3 Ma, closely agrees with the analogous furnace age.

M90-K5 hornblende was not analyzed by incremental heating owing to insufficient sample size. 10 hornblende subsamples fused by the laser yielded model ages ranging from 8.9 ± 0.2 Ma to 20.0 ± 0.2 Ma, and a York 2 isochron age of 21.7 ± 0.4 Ma (Tables 4 and 6.2; Fig. 11.2). A single analysis plotting below the $^{39}Ar/^{40}Ar$ axis (implying overcorrection for the blank) was excluded from the regression.

Sample M90-K12

Sample M90-K12, a porphyritic, mylonitic granodiorite collected on the peninsula south of Nea Peramos, contains ~60% K-feldspar and plagioclase, 30% quartz, 9% biotite, and 1% minor hornblende and accessories (Fig. 6). K-feldspar phenocrysts up to 1 cm in diameter commonly exhibit undulose extinction and mechanical twinning, and have sigmoid tails consistent with top-to-the-southwest mylonitic strain, which is also indicated by a poorly developed S-C fabric. There appear to be two generations of biotite. Larger grains occur principally within cracks in K-feldspar phenocrysts and so may be inferred to have grown within the brittle regime for K-feldspar deformation, at temperatures < ~500°C.

Fine-grained biotite in long, narrow laths aligned subparallel to S- and C-planes is intimately intergrown with dynamically recrystallized quartz and appears to have grown in the mylonitic shear environment.

Laser-fusion methods were used to analyze a coarse-grained (60 - 80 mesh) biotite separate from sample M90-K12. Model ages for 10 subsamples range from 3.3 ± 1.1 Ma to 7.9 ± 0.2 Ma (Table 6.3; Fig. 11.3). Proportions of trapped ^{40}Ar were generally high, but the spread and linearity of the measured gas compositions were sufficient to yield a York 2 isochron age of 11.1 ± 0.2 Ma and an initial $^{40}Ar/^{36}Ar$ ratio of 260 ± 10.

Sample M90-K71

Sample M90-K71, a medium-grained, nonporphyritic, mylonitic granodiorite collected 2.5 km SSW of Nea Peramos (Fig. 6), consists of ~60% K-feldspar and plagioclase, 20% quartz, 10% hornblende, 9% biotite, and 1% titanite and other accessories. K-feldspar and hornblende grains are coarse, cracked, and commonly have sigmoidal tails composed largely of intimately intergrown, fine-grained, lath-shaped biotite and dynamically recrystallized quartz, which also define mylonitic shear and schistosity planes. K-feldspar and hornblende also both display undulose extinction and are interpreted to represent relatively early phases that were plastically deformed at high temperatures and subsequently cracked and rotated at lower temperatures. Biotite and quartz appear to have crystallized or recrystallized within the mylonitic shear environment and show little evidence of subsequent brittle deformation.

Model ages obtained in laser-fusion analyses of eleven M90-K71 hornblende subsamples range from 13.4 ± 0.2 Ma to 21.2 ± 0.2 Ma (Table 6.4, Fig. 11.4), and from a hornblende step-heating analysis, 16.3 ± 0.3 Ma to 20.6 ± 0.4 Ma, with a clear correlation

between higher temperature steps and older model ages (Table 5.3, Fig. 10.3a). Inverse isotope correlation plots for the laser and furnace data are similar, each showing a cluster of points with low trapped ^{40}Ar. A York 1 step-heating age of 20.1 ± 0.3 Ma and a York 2 isochron age of 20.8 ± 0.4 Ma obtained for laser and furnace analyses, respectively, agree within errors. Corresponding initial $^{40}Ar/^{36}Ar$ ratios of 140 ± 80 and 110 ± 50 are poorly constrained and probably meaningless.

Sample M90-K73

Sample M90-K73, a granodioritic S-C mylonite collected 200 m south-southeast of M90-K71 (Fig. 6), contains ~50% K-feldspar and plagioclase, 30% quartz, 12% biotite, and 8% zoisite, epidote with cores of allanite, hornblende, and chlorite, with accessory titanite, zircon, and opaques. A top-to-the-northeast S-C mylonitic fabric is strongly developed, with S-planes defined principally by coarse biotite and C-planes by fine lath-shaped biotite and dynamically recrystallized quartz. Coarse feldspar grains exhibit undulose extinction and are commonly cracked nearly perpendicular to C-planes. Quartz and fine biotite typically anneal such cracks and also compose well-developed sigmoidal tails. Rare hornblende grains are generally surrounded by biotite.

Model ages obtained in a 10-step incremental heating analysis of M90-K73 K-feldspar range from 11.0 ± 0.2 Ma to 14.4 ± 0.3 Ma (Table 5.4). Older model ages correspond to higher temperatures; the final five increments yield a relatively flat release spectrum and increments 6 - 8, comprising 55.5% of the total gas released, define an age "plateau" of 13.8 ± 0.2 Ma that is indistinguishable from the York 2 isochron age of 13.8 ± 0.3 Ma (Fig. 10.4a). The York 2 regression, tightly constrained by the higher temperature increments, yields an initial $^{40}Ar/^{36}Ar$ ratio of 300 ± 10, close to atmospheric (Fig. 10.4b).

Two size fractions of biotite were analyzed from sample M90-K73. Incremental heating of the 80 - 150 mesh fraction yielded model ages ranging from 13.2 ± 0.3 Ma to 14.3 ± 0.3 Ma, excluding the final (total-fusion) step (Table 5.5, Fig. 10.5a), a York 2 isochron age of 13.9 ± 0.3 Ma, and a nearly atmospheric initial $^{40}Ar/^{36}Ar$ ratio of 290 ± 20 (Fig. 10.5b). Incremental heating of the 60 - 80 mesh biotite fraction gave similar results: a York 1 age of 14.1 ± 0.5 Ma and an identical initial $^{40}Ar/^{36}Ar$ ratio of 290 ± 20 (Table 5.6, Figs. 10.6a and 10.6b). Laser fusion analyses of the 60 - 80 mesh separate gave remarkably different results, however: a York 2 isochron age of 12.8 ± 0.3 Ma and an initial $^{40}Ar/^{36}Ar$ ratio of 350 ± 30 (Fig. 11.5b). The York 2 regression is dominated by three subsamples that yielded anomalously young model ages (Table 6.5, Fig. 11.5). Given the relatively robust regressions of the biotite furnace data for this sample and the fact that all other biotite separates analysed from the Symvolon pluton yielded close to atmospheric values of $[^{40}Ar/^{36}Ar]_0$, I question the results of the laser-fusion analysis and suggest that too few subsamples were analyzed to robustly constrain an isochron age.

Ten subsamples of M90-K73 hornblende analyzed by laser fusion yielded model ages from 12.8 ± 0.4 Ma to 20.7 ± 0.2 Ma (Table 6.6), and a York 2 isochron age of 21.4 ± 0.4 Ma (Fig. 11.6). An initial $^{40}Ar/^{36}Ar$ ratio of 150 ± 60 is poorly constrained.

Sample M90-K79

M90-K79, a coarse, porphyritic, hornblende-rich, S-C mylonitic granodiorite collected 1.5 km west of M90-K71 (Fig. 6), is composed of ~55% K-feldspar and plagioclase, 30% quartz, 10% hornblende, 3% biotite, and 2% titanite, zircon, opaques, and other accessories. Phenocrysts of K-feldspar as large as 1.5 cm in diameter exhibit strongly undulose extinction, have sigmoidal tails of dynamically recrystallized quartz and minor fine-grained biotite, and contain inclusions of titanite, zircon, and earlier grown K-

feldspar. S-planes are defined principally by the orientations of coarse hornblendes that may have crystallized in the mylonitic environment (Fig. 5c). Owing to the paucity of biotite, C-planes are defined mainly by dynamically recrystallized quartz.

An incremental heating analysis of M90-K79 K-feldspar yielded model ages from 11.4 ± 0.2 Ma to 16.7 ± 0.3 Ma (Table 5.7, Fig. 10.7a). No York 2 isochron is defined; a measure of confidence is accorded to the poorly constrained York 1 age of 13.4 ± 1.7 Ma (Fig. 10.7b) only because it is consistent with well-constrained biotite ages for this sample. Incremental heating and laser-fusion biotite analyses yielded York 2 isochron ages of 13.4 ± 0.3 Ma and 13.7 ± 0.3 Ma, respectively (Tables 5.8 and 6.7, Figs. 10.8 and 11.7). A near-atmospheric initial $^{40}Ar/^{36}Ar$ ratio of 300 ± 20 is tightly constrained by the initial furnace step, which released a large component of trapped Ar (Fig. 10.8b); the value for $[^{40}Ar/^{36}Ar]_0$ derived from the laser analyses, 330 ± 150, is poorly defined because none of the subsamples contained significant trapped Ar (Fig. 11.7a).

Incremental heating of M90-K79 hornblende yielded a complex release spectrum with model ages from 13.4 ± 0.3 Ma to 24.2 ± 0.5 Ma, and a York 2 isochron age of 20.1 ± 0.4 Ma (Table 5.9, Fig. 10.9). 20 subsamples fused by the laser yielded even more widely scattered model ages ranging from 9.5 ± 0.1 Ma to 24.9 ± 0.2 Ma (Table 6.8, Fig. 11.8). A poorly constrained York 1 age of 21.3 ± 3.1 Ma regressed from these data is consistent within error limits with the furnace age.

Summary and Discussion

$^{206}Pb/^{238}U$ titanite ages of 19.7 ± 0.3 Ma, 20.0 ± 0.5 Ma, and 21.1 ± 0.8 Ma representing two Symvolon mylonite samples are indistinguishable within errors from five $^{40}Ar/^{39}Ar$ York 2 or York 1 hornblende ages ranging from 20.1 ± 0.4 Ma to 21.7 ± 0.4

Ma, representing four samples (Tables 1 and 4). Assuming a nominal 600°C closure temperature of titanite to the U-Pb system (Ghent et al., 1988) and a 500°C closure of hornblende to Ar (Harrison, 1981), these values record rapid cooling of the Symvolon granodiorite between ~22 Ma and 20 Ma (~100°C/10^6 yr). The country rock intruded by the Symvolon body, the Falakron marble series, bears mineral assemblages indicative of metamorphic conditions no higher than upper greenschist facies. In particular, the stable occurrence of actinolite as the sole amphibole in metabasite layers (e.g., Kronberg, 1969) suggests an ambient temperature at or below ~500°C. As there is no evidence for a higher-grade, post-intrusive, regional metamorphic event that might have reset the granitic hornblende and titanite isotope clocks, it must be the pluton's emplacement that is recorded by its abrupt cooling from temperatures >600°C in early Miocene time. The maximum $^{206}Pb/^{238}U$ titanite date obtained in this study, 21.1 ± 0.8 Ma, is interpreted here as a close minimum estimate of the emplacement age. Rb-Sr muscovite model ages of 22.3 ± 0.7 Ma and 22.6 ± 0.7 Ma obtained by Del Moro et al. (1990) from Falakron-series paragneisses in the Marmara Valley that were mylonitized concordantly with the Symvolon pluton may indicate a slightly earlier emplacement age; alternatively, the Rb-Sr system of these rocks may have been incompletely reset during the early Miocene intrusive event.

$^{207}Pb/^{206}Pb$ zircon ages ranging from 116.3 ± 0.5 Ma to 281.8 ± 9.3 Ma record radiogenic Pb inheritance from a pre-Symvolon pluton igneous or high-temperature metamorphic event at least early Permian in age. Given this legacy of Paleozoic isotopic compositions from the source material of the Symvolon magma, and the linear trend defined by discordant $^{206}Pb/^{238}U$ and $^{207}Pb/^{235}U$ zircon age pairs on a concordia plot (Fig. 9), $^{206}Pb/^{238}U$ zircon ages ranging from 24.4 ± 0.7 Ma to 96.9 ± 0.1 Ma must be interpreted as mixing ages representing at least two periods of zircon growth. The latest closure of the U-Pb system in the Symvolon zircons occurred later than ~24.4 Ma and is almost certainly associated with the emplacement and cooling of the pluton. If euhedral

zircon overgrowths surrounding the subhedral Paleozoic cores crystallized ~21 - 22 Ma at roughly the same time as titanites and hornblendes, then the cooling associated with the pluton's emplacement may have been even more precipitous than implied above, as great as ~250°C/10^6 yr, assuming a 750°C closure of zircon to the U-Pb system (Fig. 12; Ghent et al., 1988). Note, however, that zircon overgrowths could have crystallized at temperatures lower than 750°C, so that this cooling gradient must be interpreted as a maximum.

Combined with thin-section textural data, ages obtained in this study also yield information pertaining to when the Symvolon pluton was mylonitized. K-feldspar phenocrysts as long as 4 cm uniformly exhibit undulose extinction, indicative of crystal plastic deformation at temperatures in excess of ~500°C (e.g., Simpson and de Paor, 1991). Given that the Symvolon body cooled rapidly below ~500°C soon after its emplacement as recorded by $^{40}Ar/^{39}Ar$ hornblende ages, these high-temperature shear textures suggest that the intrusion and mylonitization of the Symvolon body may have been essentially simultaneous. Textural evidence that relatively coarse, undeformed hornblende and possibly some titanite grains with radiometric ages clustering near 21 Ma crystallized along mylonitic S-planes supports this interpretation, because younger ages would be expected if these minerals had recrystallized in a post-emplacement shear zone.

Undeformed fine-grained biotite typically defines S- and C-planes and clearly grew in a mylonitic environment, but did not cool below its closure temperature to Ar, ~300°C (Harrison et al., 1985), for at least 4 - 5 m.y. subsequent to the emplacement of the pluton, as indicated by $^{40}Ar/^{39}Ar$ biotite ages $\leq 15.5 \pm 0.3$ Ma. Cooling of the pluton from ~500°C to 300°C may have occurred abruptly at $\leq$ 15.5 Ma after a period of slow cooling as implied by path segment 2 on Fig. 12, or more gradually between ~20 and 15 Ma as implied by segment 2'; in the absence of $^{40}Ar/^{39}Ar$ muscovite ages the shape of the T-t curve in this interval is poorly defined. $^{40}Ar/^{39}Ar$ K-feldspar ages are only 0.3 - 0.5 m.y.

younger than $^{40}Ar/^{39}Ar$ biotite ages in any given sample and document renewed rapid cooling in early middle Miocene time from 300°C to 150°C, assuming the latter value as the Ar closure temperature of K-feldspar (McDougall and Harrison, 1988).

IMPLICATIONS FOR THE TECTONIC EVOLUTION OF THE RHODOPE METAMORPHIC CORE COMPLEX

U-Pb and $^{40}Ar/^{39}Ar$ dates from the Symvolon granodiorite directly constrain the timing of three major thermal and deformational events in the Rhodope metamorphic core complex: (1) cooling in the source terrane of the Symvolon magma after an intrusive or high-grade metamorphic event in late Paleozoic time ($^{207}Pb/^{206}Pb$ zircon ages as old 281.8 ± 9.3 Ma); (2) the intrusion, mylonitization, and cooling of the Symvolon pluton to below 500°C approximately 20 - 21 Ma (U-Pb zircon and titanite ages and $^{40}Ar/^{39}Ar$ hornblende ages); and (3) a second episode of cooling to temperatures < ~150°C - 300°C from ~11 - 15.5 Ma ($^{40}Ar/^{39}Ar$ biotite and K-feldspar ages). The Tertiary part of the cooling history beginning with the intrusion of the pluton is summarized in Fig. 12.

Late Paleozoic zircon cores: Derived from Hercynian crystalline basement?

The age of the Falakron marble series is unknown because the unit is highly strained and no dateable fossils have yet been recovered. A single, poorly preserved coral specimen implies only that the marbles are Ordovician or younger (e.g., Meyer and Pilger, 1963; Kronberg, 1969), and K-Ar hornblende dates in the range 30 - 33 Ma from the oldest plutons known to intrude the Falakron series, the Vrondou and Xanthi granodiorites (Marakis, 1969; Liati, 1986), constrain its deposition to be pre-mid-Oligocene.

Basement rocks underlying the Falakron series between the Strymon and Nestos Rivers are not exposed, but a clue to their age may be derived from the radiogenic Pb inheritance attributable to subhedral cores in zircons from the Symvolon pluton. These cores either crystallized or cooled from extremely high temperatures (>750°C) between approximately 280 Ma and 325 Ma. As noted above, the lower bound is constrained by the maximum $^{207}Pb/^{206}Pb$ zircon age obtained in this study, 281.8 ± 9.3 Ma, and the upper bound by the maximum upper intercept with concordia of the linear trend defined by discordant $^{206}Pb/^{238}U$ and $^{207}Pb/^{235}U$ zircon age pairs (Fig. 9). A single $^{207}Pb/^{206}Pb$ zircon age of 335 ± 40 Ma reported from the Symvolon body by Kokkinakis (1980b) and an upper intercept U-Pb zircon age of 299 ± 1 Ma obtained from a granodiorite body exposed beneath thick Falakron marbles on the island of Thasos by Wawrzenitz et al. (1992) also attest to Late Carboniferous cooling in the magma provenance of Tertiary granitic bodies within the Rhodope metamorphic core complex. Assuming that Symvolon zircon cores derive from a crystalline basement underlying the Falakron series, then the Falakron marbles are unlikely to be older than Late Permian. Late Carboniferous cooling ages in the unexposed Rhodope basement suggest that it may have originated within the European Hercynian (Variscan) orogen during the assembly of Pangaea.

Early Miocene intrusion and mylonitization: Symvolon shear zone

It is conventionally assumed that gently to moderately northeast-dipping foliations and northeast-plunging folds and stretching lineations formed essentially simultaneously throughout the Rhodope metamorphic core complex during a single, Paleogene (?) episode of ductile shear (e.g., Kronberg, 1969; Jordan, 1969; Meyer, 1968, 1969). Results presented here directly contradict this interpretation, implying instead that such structural elements must represent at least two distinct shear zones that were similar in orientation and textural expression but entirely different in age and tectonic origin. Northeast-plunging

folds and calcite stretching lineations that are pervasively developed in the Falakron marble series in the Falakron and Lekanis Mountains formed in an Alpine convergent setting in the footwall of the Nestos thrust; they are crosscut by the undeformed, nonmylonitic, mid-Oligocene Xanthi and eastern Vrondou plutons and must, therefore, be older than mid-Oligocene. By contrast, northeast-dipping shear elements that characterize the Symvolon pluton and its cover rocks at the southwest margin of the Rhodope core complex must represent a second shear zone, designated here the "Symvolon shear zone", because $^{206}Pb/^{238}U$ zircon and titanite ages and $^{40}Ar/^{39}Ar$ hornblende ages reported above establish unequivocally that the Symvolon pluton was emplaced and penecontemporaneously mylonitized in early Miocene time.

The Symvolon shear zone coincides areally with a dramatically thinned Falakron marble section. Marble thicknesses in excess of 5000 meters in the Falakron and Lekanis Mountains are reduced to a few hundred meters at most to the southwest in the Menoikion Mtns. and at Mt. Pangaion (Kronberg, 1969; Kronberg et al., 1970; de Boer, 1970; Schenk, 1970). There is no field evidence that this thinning is an original stratigraphic attribute; rather, the marble appears to be thinnest where it has been mylonitized concordantly with the Symvolon and Messolakia plutons at their margins. We suggest that the Symvolon shear zone may represent a mid-crustal extensional rupture that was created in early Miocene time by a taffy-like stretching and thinning of the Falakron carbonate slab along a ~NNW-trending zone localized at the southwest margin of the Rhodope core complex. This interpretation is supported by the roughly equal numbers of northeast- and southwest-vergent mylonitic shear indicators within the Symvolon body, implying a predominance of pure shear (flattening) over simple shear in the mylonitic environment (Fig. 6), and by the common boudinage of aplitic dikes in the pluton and of relatively competent layers in the Falakron series cover rocks (Kokkinakis, 1980a). While the Symvolon shear zone appears to represent a widening extensional space characterized by

predominantly pure shear, it is likely to have been kinematically linked to one or more simple shear zones during its period of activity. Such a rupture at mid-crustal depths within the Falakron series might have facilitated the ramping of a northeast-dipping detachment to a deeper structural level; alternatively, it might have accommodated the downdip termination of a northeast-dipping detachment system.

$^{40}Ar/^{39}Ar$ biotite ages obtained in this study are all ≤15.5 Ma, which indicates that temperatures within the Symvolon body remained higher than ~300°C for at least 5.5 m.y. after its intrusion at ~21 - 22 Ma. Although neither hornblende nor titanite recrystallized later than ~20 Ma as attested by their radiometric ages, it is possible that ductile shear continued within the Symvolon shear zone during this post-emplacement interval of relatively slow cooling, accommodated within the pluton principally by recrystallization of fine-grained biotite and quartz along mylonitic S- and C-planes and by fracturing and rotation of K-feldspar phenocrysts, and within adjacent Falakron cover rocks by plastic deformation of marbles (Fig. 12). Pervasive mineral stretching lineations and minor fold axes in the Symvolon pluton uniformly plunge gently to moderately northeast, defining a mean stretching axis for the Symvolon shear zone of 18°, N58°E (Fig. 6). In the absence of evidence for large-scale block rotations during subsequent deformational events, this figure may be taken as the approximate principal extensional axis associated with the early Miocene rupturing of the Falakron series in the Strymon Valley region.

The intrusion and mylonitization of the Symvolon pluton at ~21 - 22 Ma within the Symvolon shear zone is the earliest known manifestation of extension in the Rhodope metamorphic core complex. On the flanks of Mt. Olympos ~170 km southwest of the Symvolon pluton, the east- to northeast-dipping Kallipevki-Lizadiko Ridge low-angle normal fault system was active from ~23 - 16 Ma based on $^{40}Ar/^{39}Ar$ cooling ages of sanidines in its footwall, and represents the earliest post-Alpine extensional deformation in

the area west of the Vardar suture (Fig. 2; Schermer, 1990, 1993). The coincidence in age and orientation between these widely separated shear zones may suggest that the onset of east-northeasterly extension in earliest Miocene time is broadly characteristic of the north Aegean region.

Middle Miocene cooling: Strymon Valley detachment system

The Strymon Valley detachment represents the brittle, upper crustal portion of yet a third low-angle shear zone that is associated with northeast-trending structural elements in the Rhodope metamorphic core complex. Weakly developed, gently southwest-dipping Strymon Valley mylonitic fabrics overprint ductile shear elements that formed during the two previous shear episodes and are themselves overprinted by the brittle detachment surface, which accommodated extensional southwesterly transport of its hanging wall (3°, S53°W) from >15 Ma to ~3.5 Ma (Dinter and Royden, 1993). As noted above, four K-Ar biotite dates ranging from 13.8 ± 0.2 Ma to 17.8 ± 0.8 Ma from the Messolakia and Symvolon plutons (Harre et al.,1968; Kokkinakis, 1980b) were considered by Dinter and Royden (1993) to be cooling ages that date the unroofing of the Rhodope core complex in the footwall of the Strymon Valley detachment system. $^{40}Ar/^{39}Ar$ biotite and K-feldspar dates ranging from 11.1 ± 0.2 Ma to 15.5 ± 0.3 Ma reported above are in accord with that interpretation and, in addition, appear to define a lateral cooling gradient that can be related to the progressive southwestward unroofing of the Symvolon pluton (Figs. 6 and 12).

The five samples analyzed in this study represent a 12-km transect parallel to the displacement axis of the Strymon Valley detachment system. The northeasternmost sample analyzed, M90-K5, yielded three $^{40}Ar/^{39}Ar$ K-feldspar and biotite dates ranging from 15.0 ± 0.1 Ma to 15.5 ± 0.3 Ma, whereas the four remaining samples, clustered 10 - 12 km SSW of M90-K5, yielded analogous dates in the range 11.1 ± 0.3 Ma to 14.1 ± 0.5 Ma

(Table 4; Fig. 6). In general, the furnace analyses from the latter group gave better constrained dates that cluster in a smaller range, 13.4 ± 0.3 Ma to 14.1 ± 0.5 Ma. Taking nominal mean biotite ages of 15.4 Ma for sample M90-K5 and 13.4 Ma for the southwestern sample group, a rough estimate of 6.0 km/10^6 yr (= 6.0 mm/yr) can be calculated for the average middle Miocene lateral displacement rate on the Strymon Valley detachment, assuming a linear relationship between displacement on the fault and biotite cooling ages in its footwall. Poorly constrained though it is, this value compares favorably with an estimated 6.4 mm/yr average displacement rate on the detachment system at the latitude of the Symvolon pluton over the entire middle Miocene (~16 Ma) through early Pliocene (~3.5 Ma) period of its activity. The latter estimate assumes a cumulative lateral offset on the Strymon Valley detachment near the north Aegean coastline of ~80 km based on the apparent structural separation there between the Serbo-Macedonian and West Thracian gneiss complexes.

CONCLUSIONS

U-Pb and $^{40}Ar/^{39}Ar$ radiometric analyses of five coexisting mineral phases from the Symvolon pluton in northeastern Greece define a late Paleozoic high-T thermal event in the magmatic provenance, an early Miocene age for the emplacement and mylonitization of the pluton, and a middle Miocene period of cooling related to its tectonic unroofing. Late Paleozoic $^{207}Pb/^{206}Pb$ zircon dates are interpreted as inheritance ages and may indicate that the Falakron marble series, which serves as the host rock to the Symvolon body, is underlain by granitic or metamorphic basement rocks that cooled or crystallized in Late Carboniferous time during the Hercynian orogeny. $^{206}Pb/^{238}U$ titanite ages and $^{40}Ar/^{39}Ar$ mylonitic hornblende ages ranging from 19.7 Ma to 21.7 Ma bracket the emplacement and incipient mylonitization of the Symvolon pluton in early Miocene time. Discordant $^{206}Pb/^{238}U$ and $^{207}Pb/^{235}U$ zircon age pairs are strongly affected by late Paleozoic Pb

inheritance, but define a linear trend on a concordia plot that is consistent with a crystallization event at ~21 - 22 Ma. $^{40}Ar/^{39}Ar$ biotite and K-feldspar dates decrease from 15.5 ± 0.3 Ma at the northeast margin of the study area to a minimum of 11.1 ± 0.2 Ma some 12 km to the southwest, and appear to record the progressive southwestward unroofing and cooling of the Rhodope metamorphic core complex in the footwall of the gently southwest-dipping Strymon Valley detachment system.

The Symvolon pluton was emplaced in a gently northeast-dipping shear zone that coincides areally with a dramatic structural thinning of the Falakron marble series. S-C mylonitic sense-of-shear indicators are roughly equally divided between southwest and northeast vergence in the pluton, indicating a large component of pure shear in the mylonitic environment. On this basis, the Symvolon shear zone is interpreted as a mid-crustal extensional rupture in the Falakron series. The intrusion of the Symvolon pluton within this rupture at ~21 - 22 Ma appears to be the earliest expression of post-Alpine extension in the Rhodope metamorphic core complex.

REFERENCES

Bornovas, J., and Rondogianni-Tsiambaou, T., 1983, Geological map of Greece, second edition: Institute of Geology and Mineral Exploration, Athens, scale 1:500,000.

Burchfiel, B. C., 1980, Eastern European Alpine system and the Carpathian orocline as an example of collision tectonics: Tectonophysics, v. 63, p. 31-61.

Burg, J.-P., Ivanov, Z., Ricou, L.-E., Dimor, D. and Klain, L., 1990, Implications of shear-sense criteria for the tectonic evolution of the Central Rhodope massif, southern Bulgaria: Geology, v. 18, p. 451-454.

Cebula, G. T., Kunk, M. J., Mehnert, H. H., Naeser, C. W., Obradovich, J. D. and Sutter, J. F., 1986, The Fish Canyon tuff, a potential standard for the $^{40}Ar/^{39}Ar$ and fission track methods: Terra Cognita, v. 6, p. 139-140.

Cheshitev, G., and Kancev, I., 1989, Geological Map of the People's Republic of Bulgaria: Sofia, Committee of Geology, Department of Geophysical Prospecting and Geological Mapping, scale 1:500,000.

Davis, G. A. and Lister, G. S., 1988, Detachment faulting in continental extension: Perspectives from the southwestern U.S. Cordillera, in S.P. Clark, B.C. Burchfiel, and J. Suppe, eds., Processes in Continental Lithospheric Deformation, Geological Society of America Memoir 218, Boulder, CO, p. 133-159.

de Boer, H. U., 1970, Geologisch-petrographische Untersuchungen im Rhodope-Massiv Griechisch-Ostmazedoniens: Der Menikion-Bergzug nordöstlich Serrai, in Birk, F., de Boer, H. U., Kronberg, P., Meyer, W., Pilger, A. and Schenck, P., eds., Zur Geologie des Rhodopen-Kristallins im Gebiet zwischen Strimon und Nestos (Griechisch-Ostmazedonien), Beihefte zum Geologischen Jahrbuch, Heft 88, Hannover, p. 43-79.

Del Moro, A., Kyriakopoulos, K., Pezzino, A., Atzori, P. and Lo Giudice, A., 1990, The metamorphic complex associated to the Kavala plutonites: an Rb-Sr geochronological, petrological and structural study: Proceedings of the 2nd Hellenic-Bulgarian Symposium, Thessaloniki, 1989, Geologica Rhodopica, v. 2, p. 143-152.

Dinter, D. A. and Royden, L., 1993, Late Cenozoic extension in northeastern Greece: Strymon Valley detachment and Rhodope metammorphic core complex: Geology, v. 21, p. 45-48.

Dixon, J. E. and Dimitriades, S., 1984, Metamorphosed ophiolitic rocks from the Serbo-Macedonian Massif, near Lake Volvi, North-east Greece, in Dixon, J. E. and Robertson, A. H. F., eds., The Geological Evolution of the Eastern Mediterranean, Geological Society Special Publication No. 17, Oxford, Blackwell Scientific Publications, p. 603-618.

Eleftheriadis, G., Christofides, G. and Kassoli-Fournaraki, A., 1984, Geochemistry of the high-K calc-alkaline basaltic sills and dykes in the south Rhodope massif (N. Greece): Bulletin Volcanologique, v. 47, p. 569-579.

Eleftheriadis, G. and Lippolt, H. J., 1984, Altersbestimmungen zum oligozänen vulkanismus der Süd-Rhodopen/Nord Griechenland: Neues Jahrbuch für Geologie und Paläontologie, Monatshefte, v. 3, p. 179-191.

Fischer, G., 1963, Über das Granitmassiv des Symvolon-Gebirges bei Kavala: Geologische Rundschau, v. 53, p. 390-392.

Ghent, E. D., Stout, M. Z. and Parrish, R. R., 1988, Determination of metamorphic pressure-temperature-time (PTt) paths, in Nisbet, E. G. and Fowler, C. M. R., eds., Short Course on Heat, Metamorphism, and Tectonics, St. John's, Mineralogical Association of Canada, p. 155-188.

Hanmer, S., and Passchier, C., 1991, Shear-sense indicators: a review: Geological Survey of Canada Paper 90-17, 72 p.

Harre, W., Kockel, F., Kreuzer, H., Lenz, H., Müller, P. and Walther, H. W., 1968, Über Rejuvenationen im Serbo-Madzedonischen Massiv (Deutung radiometrischer Altersbestimmungen) [abs.]: Proceedings of the 23rd International Geological Congress, Prague, p. 223-236.

Harrison, T. M., 1981, Diffusion of ^{40}Ar in hornblende: Contributions in Mineralogy and Petrology, v. 78, p. 324-331.

Harrison, T. M., Duncan, I. and McDougall, I., 1985, Diffusion of ^{40}Ar in biotite: temperature, pressure, and compositional effects: Geochimica et Cosmochimica Acta, v. 49, p. 2461-2468.

Heizler, M. T. and Harrison, T. M., 1988, Multiple trapped argon isotope components revealed by $^{40}Ar/^{39}Ar$ isochron analysis: Geochimica et Cosmochimica Acta, v. 52, p. 1295-1303.

Ivanov, R., 1981, The deep-seated central Rhodope nappe and interference tectonics of the Rhodope crystalline basement: Geologica Balcanica, v. 11, p. 47-66.

Jacobshagen, V., Dürr, S., Kockel, F., Kopp, K.-O., Kowalczyk, G., Berckhemer, H. and Büttner, D., 1978, Structure and geodynamic evolution of the Aegean region, in Closs, H., Roeder, D. and Schmidt, K., ed., Alps, Apennines, Hellenides, Inter-Union Commission on Geodynamics Scientific Report No. 38, Stuttgart, E. Schweizerbart'sche Verlagsbuchhandlung, p. 537-564.

Jordan, H., 1969, Geologie und Petrographie im Zentralteil des Bos Dag (Drama, Griechisch-Makedonien): Geotectonische Forschungen, v. 31, p. 50-85.

Kockel, F. and Walther, H. W., 1965, Die Strimonlinie als Grenze zwischen Serbo-Mazedonischem und Ril-Rhodope-Massiv in Ost-Mazedonien: Geologisches Jahrbuch, v. 83, p. 575-602.

Kockel, F., Mollat, H. and Walther, H. W., 1977, Erläuterungen zur Geologischen Karte der Chalkidhiki und angrenzender Gebiete 1:100,000 (Nord-Griechenland), Hannover, Bundesanstalt für Geowissenschaften und Rohstoffe, 119 p.

Kojumdgieva, E., Nikolov, I., Nedjalkov, P. and Busev, A., 1982, Stratigraphy of the Neogene in Sandanski graben: Geologica Balcanica, v. 12, p. 69-81.

Kokkinakis, A., 1980a, Zum faltenbau des Symvolongebirges und des gebietes von Kavala (Griechisch-Ostmakedonien): Annales Géologiques des Pays Helléniques, v. 30, p. 398-420.

Kokkinakis, A., 1980b, Altersbeziehungen zwischen Metamorphosen, mechanischen Deformationen und Intrusionen am Südrand des Rhodope-Massivs (Makedonien, Grieschenland): Geologische Rundschau, v. 69, p. 726-744.

Kolocotroni, C. and Dixon, J. E., 1991, The origin and emplacement of the Vrondou granite, Serres, N.E. Greece: Bulletin of the Geological Society of Greece, v. 25, p. 469-483.

Kopp, K. O., 1961, Geologie Thrakiens I. Beschreibung und Vergleich intramontaner Tertiärsenken beiderseits des Marmara-Meeres: Neues Jahrbuch für Geologie und Paläontologie, Abhandlungen, v. 112, p. 325-382.

Kotopouli, C. N. and Pe-Piper, G., 1989, Geochemical characteristics of felsic intrusive rocks within the Hellenic Rhodope: A comparative study and petrogenetic implications: Neues Jahrbuch für Mineralogie, Abhandlungen, v. 161, p. 141-169.

Koukouvelas, I. and Doutsos, T., 1990, Tectonic stages along a traverse cross cutting the Rhodopian zone (Greece): Geologische Rundschau, v. 79, p. 753-776.

Koukouvelas, I. and Pe-Piper, G., 1991, The Oligocene Xanthi pluton, northern Greece: a granodiorite emplaced during regional extension: Journal of the Geological Society, London, v. 148, p. 749-758.

Koukouzas, C., 1972, Le chévauchement de Strymon dans la région Strymon dans la région de la frontiére Gréco-Bulgare: Zeitung der deutsche geologische Gesellschaft, v. 123, p. 343-347.

Krogh, T. E., 1973, A low-contamination method of hydrothermal decomposition of zircon and extraction of U and Pb for isotopic age determinations: Geochimica et Cosmochimica Acta, v. 37, p. 485-494.

Krogh, T. E., 1982, Improved accuracy of U-Pb ages by the creation of more concordant systems using an air abrasion technique: Geochimica et Cosmochimica Acta, v. 46, p. 637-649.

Kronberg, P., 1969, Gliederung, Petrographie und Tectogenese des Rhodopen-Kristallins im Tsal-Dag, Simvolon und Ost-Pangäon (Griechisch-Makedonien): Geotektonische Forschungen, v. 31, p. 1-49.

Kronberg, P. and Eltgen, H., 1973, Geological Map of Greece, Xanthi sheet: Athens, Institute of Geology and Mineral Exploration, scale 1:50,000.

Kronberg, P., Meyer, W. and Pilger, A., 1970, Geologie der Rila-Rhodope-Masse zwischen Strimon und Nestos (Nordgriechenland), in Birk, F., de Boer, H. U., Kronberg, P., Meyer, W., Pilger, A. and Schenck, P., eds., Zur Geologie des Rhodopen-Kristallins im Gebiet zwischen Strimon und Nestos (Griechisch-Ostmazedonien), Beihefte zum Geologischen Jahrbuch, Heft 88, Hannover, p. 133-180.

Le Pichon, X. and Angelier, J., 1979, The Hellenic Arc and Trench system: A key to the neotectonic evolution of the eastern Mediterranean area: Tectonophysics, v. 60, p. 1-42.

Liati, A., 1986, Regional metamorphism and overprinting contact metamorphism of the Rhodope zone, near Xanthi (N. Greece). Petrology, geochemistry, geochronology [Ph.D. thesis]: Techn. Univ. Braunschweig, 186 p.

Ludwig, K. R., 1980, Calculation of uncertainties of U-Pb isotopic data: Earth and Planetary Science Letters, v. 46, p. 212-220.

Ludwig, K. R., 1988a, PBDAT for MS-DOS: a computer program for IBM-PC compatibles for processing raw Pb-U-Th isotope data: U.S. Geological Survey Open File Report 88-542.

Ludwig, K. R., 1988b, ISOPLOT for MS-DOS: a plotting and regression program for radiogenic-isotope data, for IBM-PC compatible computers: U.S. Geological Survey Open File Report 88-557.

Marakis, G. I., 1969, Geochronologic studies of some granites from Macedonia: Annales Géologiques des Pays Helléniques, v. 21, p. 121-152.

Mattinson, J. M., 1978, Age, origin, and thermal histories of some plutonic rocks from the Salinian block of California: Contributions to Mineralogy and Petrology, v. 67, p. 233-245.

McDougall, I. and Harrison, T. M., 1988, Geochronology and Thermochronology by the $^{40}Ar/^{39}Ar$ method, New York, Oxford University Press, 212 p.

Meyer, N. and Pilger, A., 1963, Zur Geologie des Gebietes zwischen Strimon und Nestos (Rhodopen-Massiv) in Griechisch-Makedonien: Neues Jahrbuch für Geologie und Paläontologie, Abhandlungen, v. 118, p. 272-280.

Meyer, W., 1968, Zur Alterstellung des Plutonismus im Südteil der Rila-Rhodope-Masse (Nordgriechenland): Geologica et Paleontologica, v. 2, p. 173-192.

Meyer, W., 1969, Die Faltenachsen im Rhodopen-Kristallin östlich des Strimon (Nordost-Griechenland): Geotektonische Forschungen, v. 31, p. 86-96.

Mposkos, E., Perdikatsis, V. and Liati, A., 1988, Geochemical investigation of amphibolites from eastern and central Rhodope: Bulletin of the Geological Society of Greece, v. 22, p. 413-427.

Papanikolaou, D. and Panagopoulos, A., 1981, On the structural style of southern Rhodope, Greece: Geologica Balcanica, v. 11, p. 13-22.

Parrish, R. R., 1987, An improved micro-capsule for zircon dissolution in U-Pb geochronology: Chemical Geology (Isotope Geoscience Section), v. 66, p. 99-102.

Roddick, J. C., Cliff, R. A. and Rex, D. C., 1980, The evolution of excess argon in alpine biotites – a $^{40}Ar/^{39}Ar$ analysis: Earth and Planetary Science Letters, v. 48, p. 185-208.

Royden, L. H., 1988, Late Cenozoic tectonics of the Pannonian basin system, in Royden, L. H. and Horvath, F., ed., Pannonian Basin: A Study in Basin Evolution, AAPG Memoir 45, p. 27-48.

Samson, S. D. and Alexander, E. C., 1987, Calibration of the interlaboratory $^{40}Ar/^{39}Ar$ dating standard, MMhb-1: Geochimica et Cosmochimica Acta, v. 66, p. 27-34.

Schenk, P.-F., 1970, Geologie des westlichen Pangaion in Griechisch-Ostmakedonien, in Birk, F., de Boer, H. U., Kronberg, P., Meyer, W., Pilger, A. and Schenck, P., ed., Zur Geologie des Rhodopen-Kristallins im Gebiet zwischen Strimon und Nestos (Griechisch-Ostmazedonien), Beihefte zum Geologischen Jahrbuch, Heft 88, Hannover, p. 81-132.

Schermer, E. R., 1989, Tectonic Evolution of the Mt. Olympos Region, Greece [Ph.D. Thesis]: Cambridge, Massachusetts Institute of Technology, 272 p.

Schermer, E. R., 1990, Mechanisms of blueschist creation and preservation in an A-type subduction zone, Mount Olympos region, Greece: Geology, v. 18, p. 1130-1133.

Schermer, E. R., 1993, Geometry and kinematics of continental basement deformation during the Alpine orogeny, Mt. Olympos region, Greece: Journal of Structural Geology, v. 15, p. 571-591.

Schermer, E. R., Lux, D. R. and Burchfiel, B. C., 1990, Temerature-time history of subducted continental crust, Mount Olympos region, Greece: Tectonics, v. 9, p. 1165-1195.

Simpson, C. and De Paor, D., 1991, Deformation and Kinematics of High Strain Zones, Short Course Notes, Annual Meeting, San Diego, Geological Society of America, 116 p.

Stacey, J. S. and Kramers, J. D., 1975, Approximation of terrestrial lead isotope evolution by a two-stage model: Earth and Planetary Science Letters, v. 26, p. 207-221.

Steiger, R. H. and Jäger, E., 1977, Subcommission on geochronology: convention on the use of decay constants in geo- and cosmochronology: Earth and Planetary Science Letters, v. 36, p. 359-362.

Wawrzenitz, N., Baumann, A. and Nollau, G., 1992, Preliminary results of U-Pb- and Rb-Sr-investigations on metamorphic rocks of Thassos, Pangaeon complex, northern Greece [abs.]: 6th Congress of the Geological Society of Greece, with emphasis on the geology of the Aegean, Athens, May 25 - 27, 1992, abstracts, p. 37.

Wendt, I. and Carl, C., 1991, The statistical distribution of the mean squared weighted deviation: Chemical Geology (Isotope Geoscience Section), v. 86, p. 275-285.

York, D., 1966, Least-squares fitting of a straight line: Canadian Journal of Physics, v. 44, p. 1079-1086.

York, D., 1969, Least squares fitting of a straight line with correlated errors: Earth and Planetary Science Letters, v. 5, p. 320-324.

Zachos, S. and Dimadis, E., 1983, The geotectonic position of the Skaloti-Echinos granite and its relationship to the metamorphic formations of Greek Western and Central Rhodope: Geologica Balcanica, v. 13, p. 17-24.

FIGURE CAPTIONS

Figure 1. Sketch map of major tectonic elements in southeastern Europe and the northeastern Mediterranean region. RMCC - Rhodope metamorphic core complex (stipple pattern). Modified from Royden (1984) and Dinter and Royden (1993).

Figure 2. Generalized tectonic map of the north Aegean region. See text for discussion, Fig. 3 for explanation of contact symbols. Data compiled from Bornovas and Rondogianni-Tsiambaou (1983), Cheshitev and Kancev (1989), Schermer (1989, 1993), Dinter and Royden (1993), and unpublished mapping by the authors.

Figure 3. Generalized geology of the Strymon Valley region. Heavy lines are faults, dashed where inferred: with barbs - thrust fault (barbs on hanging wall), with boxes - low-angle normal fault (boxes on hanging wall), with balls - high-angle normal fault (balls on hanging wall), with arrows parallel to fault trace - strike-slip fault with inferred sense of displacement as shown by arrows, unadorned - fault of uncertain tectonic identity. Attitude symbols: open triangles - metamorphic foliations, solid boxes - fault planes, short lines - bedding. Light solid lines - depositional or intrusive contacts. Light dashed line in West Thracian gneiss complex - contact between migmatic granite and host rock. See Fig. 2 for location, Fig. 4 for explanation of tectonostratigraphic units.

Figure 4. Generalized tectonostratigraphy of the Strymon - Nestos region, northeastern Greece.

Figure 5. Photomicrographs of dextral mylonitic fabrics in the Symvolon pluton, northeastern Greece. (a) Asymmetric shape fabric defined by dynamically recrystallized quartz in S-C mylonite (e.g., Hanmer and Passchier, 1991). (b) K-feldspar porphyroclast showing well-developed tails of fine-grained biotite and dynamically recrystallized quartz in granitic ultramylonite. (c) Asymmetric hornblende porphyroblast in granitic S-C mylonite.

Figure 6. Structural and geochronological data, central Symvolon pluton. Attitudes with boxes are on brittle shear surfaces; attitudes with triangles are on mylonitic C-planes. Arrows represent stretching lineations. Single barb or outer barb of double-barbed arrows gives plunge of lineation. Inner barb gives sense of shear based on mylonitic fabric indicators. (Barb points in transport direction of material *above* shear plane.) In data boxes, (f) indicates furnace step-heating analysis, (l) indicates laser-fusion analysis. Inset: Stretching lineations plotted with mylonitic sense of shear on equal area net. (Arrows point in transport direction of material *above* shear plane.) Bar graph tabulates SW vs. NE sense-of-shear indicators based on field determinations of S-C asymmetries. See Fig. 3 for location.

Figure 7. Photomicrographs of titanites from the Symvolon pluton, representative of those analyzed by U-Pb methods in the present study. Plane polarized light. See Fig. 6 for sample locations. (a) Cracked, euhedral titanite with minor needle-shaped inclusions from sample M90-K73. (b) Cracked, subhedral titanites with long axes oriented parallel to S-planes defined by fine-grained biotite in dextral S-C mylonite sample M90-K79; interpreted as evidence that titanite crystallized prior to or early in the Symvolon mylonitic environment. (c) Euhedral titanite from sample M90-K79 showing two distinct growth periods. (d) Euhedral titanite inclusions in an M90-K79 hornblende porphyroblast that crystallized within the mylonitic environment; S-plane parallel to hornblende cleavage. Long axes of titanites are not parallel to mylonitic fabric elements, suggesting they may have crystallized prior to onset of mylonitization.

Figure 8. (a) Photomicrograph of zoned, euhedral zircons with minor inclusions, sample M90-K73, Symvolon pluton. Anhedral cores are faintly visible in crystals at left and right. Plane polarized light. See Fig. 6 for location. (b) Scanning electron microscopic image of polished zircon section from sample M90-K73. Anhedral, chemically (?) eroded core of probable late Paleozoic age (see discussion in text) is surrounded by euhedral overgrowths inferred to have formed during crystallization of the Symvolon pluton ~21 - 22 Ma. Euhedral crystal facets were removed by air abrasion with pyrite prior to preparation of grain mount.

Figure 9. Concordia plots of U-Pb zircon and titanite analyses from the central part of the Symvolon granodiorite, northeastern Greece. (a) Poorly constrained chord regressed using multigrain zircon analyses only. Upper intercept age $\leq$~350 Ma (see text). (b) Detail of (a) shows $^{206}Pb/^{238}U$ titanite ages clustering in range 19.7 $\pm$ 0.3 Ma to 21.1 $\pm$ 0.8 Ma.

Figure 10.1. $^{40}Ar/^{39}Ar$ incremental-heating age spectrum (a) and inverse isotope correlation plot (b) for sample M90-K5 K-feldspar, south central Symvolon granodiorite, Nea Peramos vicinity, northeastern Greece.

Figure 10.2. $^{40}Ar/^{39}Ar$ incremental-heating age spectrum (a) and inverse isotope correlation plot (b) for sample M90-K5 biotite, south central Symvolon granodiorite, Nea Peramos vicinity, northeastern Greece.

Figure 10.3. $^{40}Ar/^{39}Ar$ incremental-heating age spectrum (a) and inverse isotope correlation plot (b) for sample M90-K71 hornblende, south central Symvolon granodiorite, Nea Peramos vicinity, northeastern Greece.

Figure 10.4. $^{40}Ar/^{39}Ar$ incremental-heating age spectrum (a) and inverse isotope correlation plot (b) for sample M90-K73 K-feldspar, south central Symvolon granodiorite, Nea Peramos vicinity, northeastern Greece.

Figure 10.5. $^{40}Ar/^{39}Ar$ incremental-heating age spectrum (a) and inverse isotope correlation plot (b) for sample M90-K73 biotite, 80 - 150 mesh size fraction, south central Symvolon granodiorite, Nea Peramos vicinity, northeastern Greece.

Figure 10.6. $^{40}Ar/^{39}Ar$ incremental-heating age spectrum (a) and inverse isotope correlation plot (b) for sample M90-K73 biotite, 60 - 80 mesh size fraction, south central Symvolon granodiorite, Nea Peramos vicinity, northeastern Greece.

Figure 10.7. $^{40}Ar/^{39}Ar$ incremental-heating age spectrum (a) and inverse isotope correlation plot (b) for sample M90-K79 K-feldspar, south central Symvolon granodiorite, Nea Peramos vicinity, northeastern Greece.

Figure 10.8. $^{40}Ar/^{39}Ar$ incremental-heating age spectrum (a) and inverse isotope correlation plot (b) for sample M90-K79 biotite, south central Symvolon granodiorite, Nea Peramos vicinity, northeastern Greece.

Figure 10.9. $^{40}Ar/^{39}Ar$ incremental-heating age spectrum (a) and inverse isotope correlation plot (b) for sample M90-K79 hornblende, south central Symvolon granodiorite, Nea Peramos vicinity, northeastern Greece.

Figure 11.1. $^{40}Ar/^{39}Ar$ laser-fusion inverse isotope correlation plot (a) and apparent age distribution (b) for sample M90-K5 biotite, south central Symvolon granodiorite, Nea Peramos vicinity, northeastern Greece.

Figure 11.2. $^{40}Ar/^{39}Ar$ laser-fusion inverse isotope correlation plot (a) and apparent age distribution (b) for sample M90-K5 hornblende, south central Symvolon granodiorite, Nea Peramos vicinity, northeastern Greece.

Figure 11.3. $^{40}Ar/^{39}Ar$ laser-fusion inverse isotope correlation plot (a) and apparent age distribution (b) for sample M90-K12 biotite, south central Symvolon granodiorite, Nea Peramos vicinity, northeastern Greece.

Figure 11.4. $^{40}Ar/^{39}Ar$ laser-fusion inverse isotope correlation plot (a) and apparent age distribution (b) for sample M90-K71 hornblende, south central Symvolon granodiorite, Nea Peramos vicinity, northeastern Greece.

Figure 11.5. $^{40}Ar/^{39}Ar$ laser-fusion inverse isotope correlation plot (a) and apparent age distribution (b) for sample M90-K73 biotite, south central Symvolon granodiorite, Nea Peramos vicinity, northeastern Greece.

Figure 11.6. $^{40}Ar/^{39}Ar$ laser-fusion inverse isotope correlation plot (a) and apparent age distribution (b) for sample M90-K73 hornblende, south central Symvolon granodiorite, Nea Peramos vicinity, northeastern Greece.

Figure 11.7. $^{40}Ar/^{39}Ar$ laser-fusion inverse isotope correlation plot (a) and apparent age distribution (b) for sample M90-K79 biotite, south central Symvolon granodiorite, Nea Peramos vicinity, northeastern Greece.

Figure 11.8. $^{40}Ar/^{39}Ar$ laser-fusion inverse isotope correlation plot (a) and apparent age distribution (b) for sample M90-K79 hornblende, south central Symvolon granodiorite, Nea Peramos vicinity, northeastern Greece.

Figure 12. Schematic Tertiary temperature-time (T-t) evolution of the south central Symvolon pluton near Nea Peramos, northeastern Greece. U-Pb closure temperatures assumed for zircon and titanite are 750°C and 600°C, respectively (Ghent et al., 1988); assumed Ar closure temperatures are 500°C for hornblende (Harrison, 1981), 300°C for biotite (Harrison et al., 1985), and 150°C for K-feldspar (e.g., McDougall and Harrison, 1988). Data points in zircon and titanite fields are $^{206}Pb/^{238}U$ dates, and in hornblende, biotite, and K-feldspar fields, $^{40}Ar/^{39}Ar$ incremental-heating and laser-fusion dates. Numbered cooling-path segments refer to distinct stages in the pluton's thermal and deformational evolution: 1 - emplacement of magma at mid-crustal depths and simultaneous mylonitization within the gently northeast-dipping Symvolon shear zone, interpreted as an extensional rupture of the upper greenschist-facies Falakron marble series (see text); 2 - inferred slow cooling for 4 - 5 m.y. after emplacement; 2' - alternate moderate-rate cooling path from ~500°C to 300°C allowed by the data in the absence of $^{40}Ar/^{39}Ar$ muscovite dates; 3 - renewed rapid cooling as a result of tectonic unroofing of the Rhodope metamorphic core complex in the footwall of the Strymon Valley detachment system; 4 - inferred cooling at moderate rates during isostatic uplift and erosion. 3' and 4' segments apply to southwestern parts of the pluton, unroofed later than more northeasterly exposures.

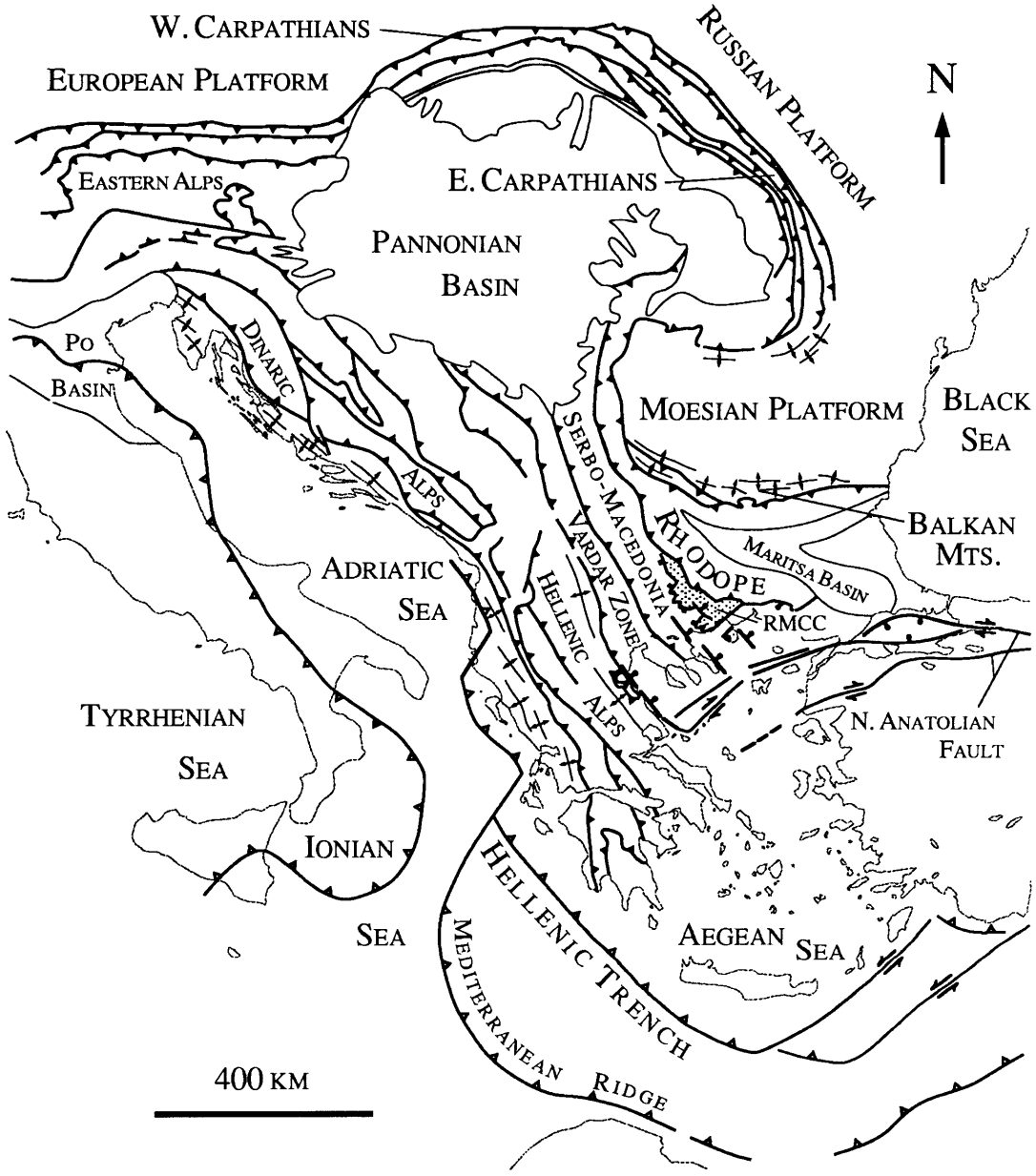

Figure 1. Sketch map of major tectonic elements in southeastern Europe and the northeastern Mediterranean region. RMCC - Rhodope metamorphic core complex (stipple pattern). Modified from Burchfiel (1980), Royden (1988), and Dinter and Royden (1993).

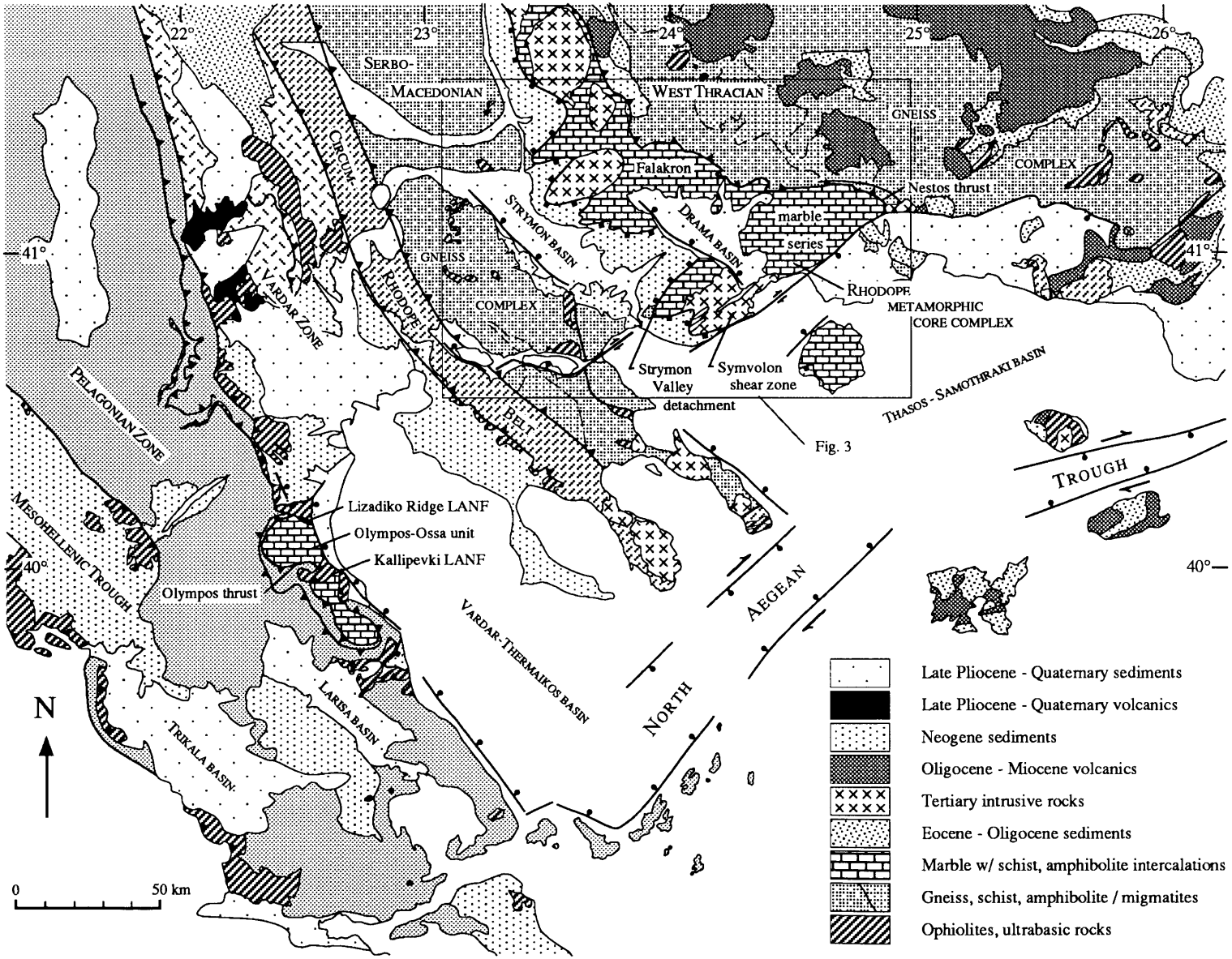

Figure 2. Generalized tectonic map of the north Aegean region. See Fig. 3 for explanation of contact symbols.

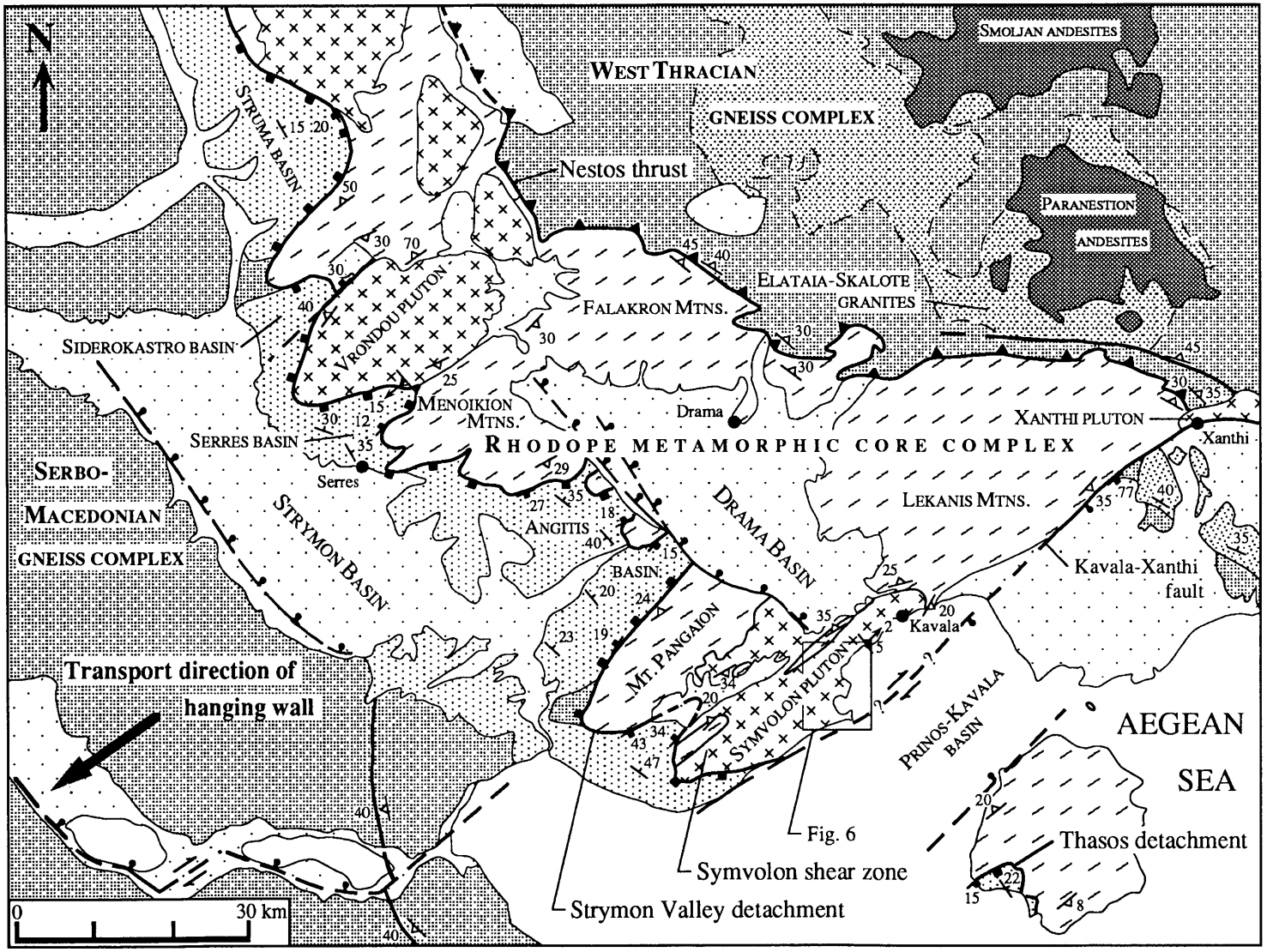

Figure 3. Generalized geology of the Strymon Valley region. See Fig. 2 for location, Fig. 4 for explanation of tectonostratigraphic units.

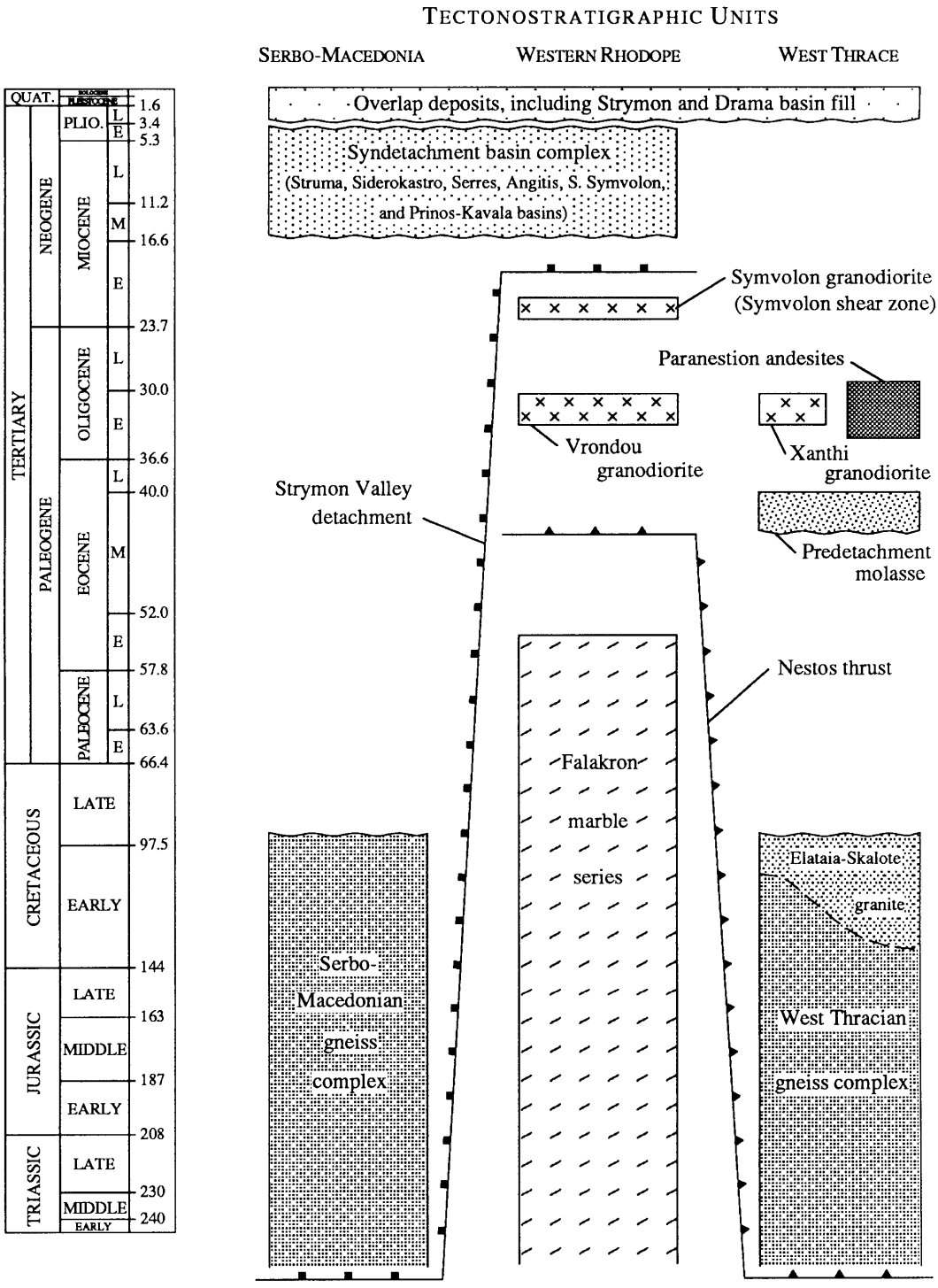

Figure 4. Generalized tectonostratigraphy of the Strymon-Nestos region, northeastern Greece.

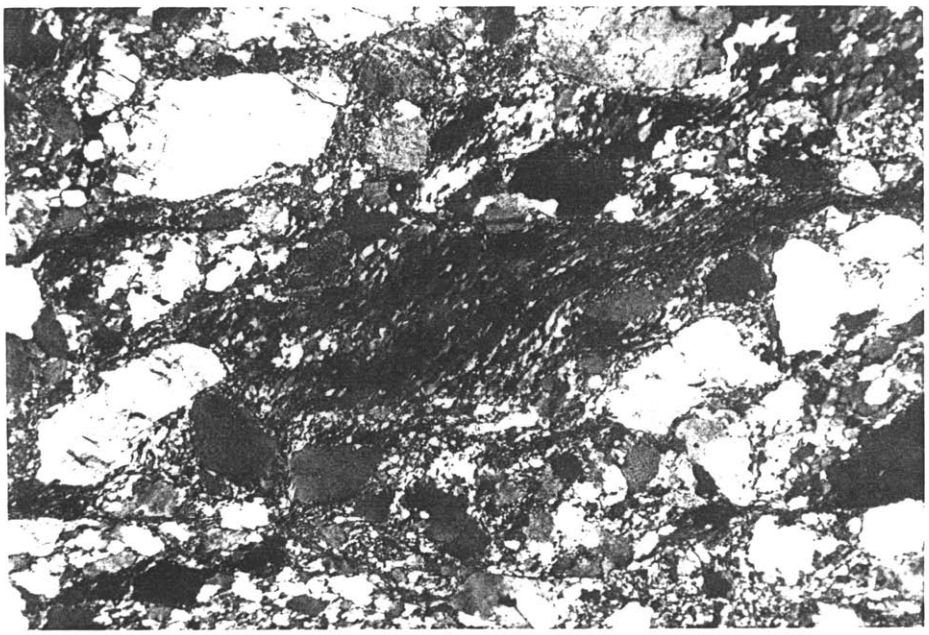

a

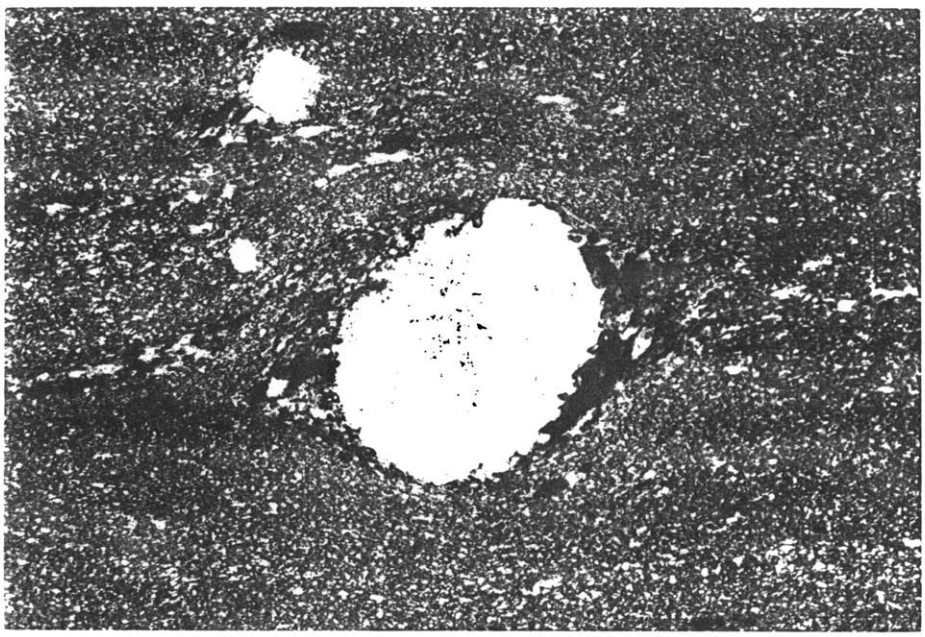

b

Figure 5. Photomicrographs of dextral mylonitic fabrics in the Symvolon pluton, northeastern Greece. (a) Asymmetric shape fabric defined by dynamically recrystallized quartz in S-C mylonite (e.g., Hanmer and Passchier, 1991). (b) K-feldspar porphyroclast showing well-developed tails of fine-grained biotite and dynamically recrystallized quartz in granitic ultramylonite.

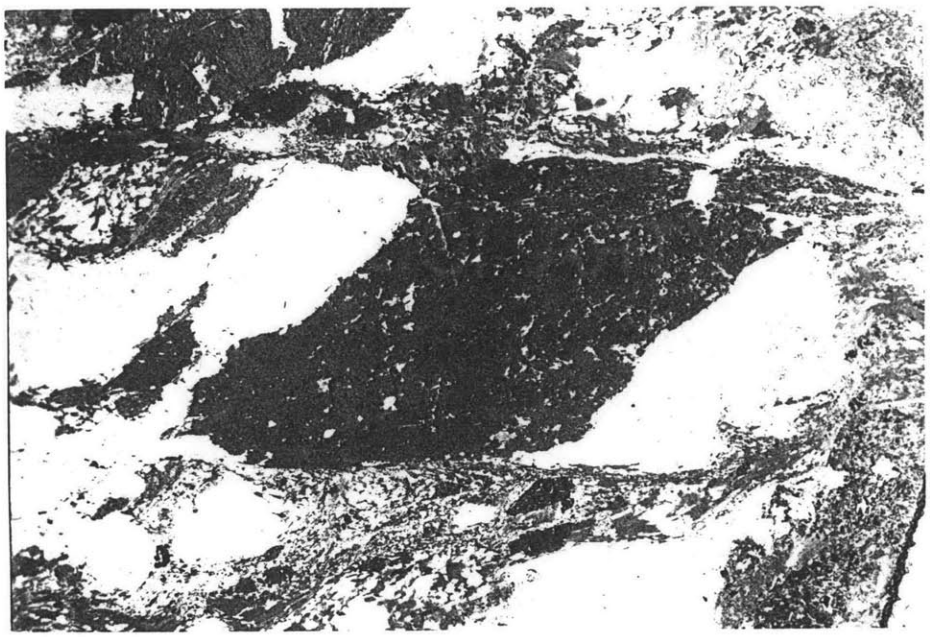

c

Figure 5 (c). Asymmetric hornblende porphyroblast in granitic S-C mylonite.

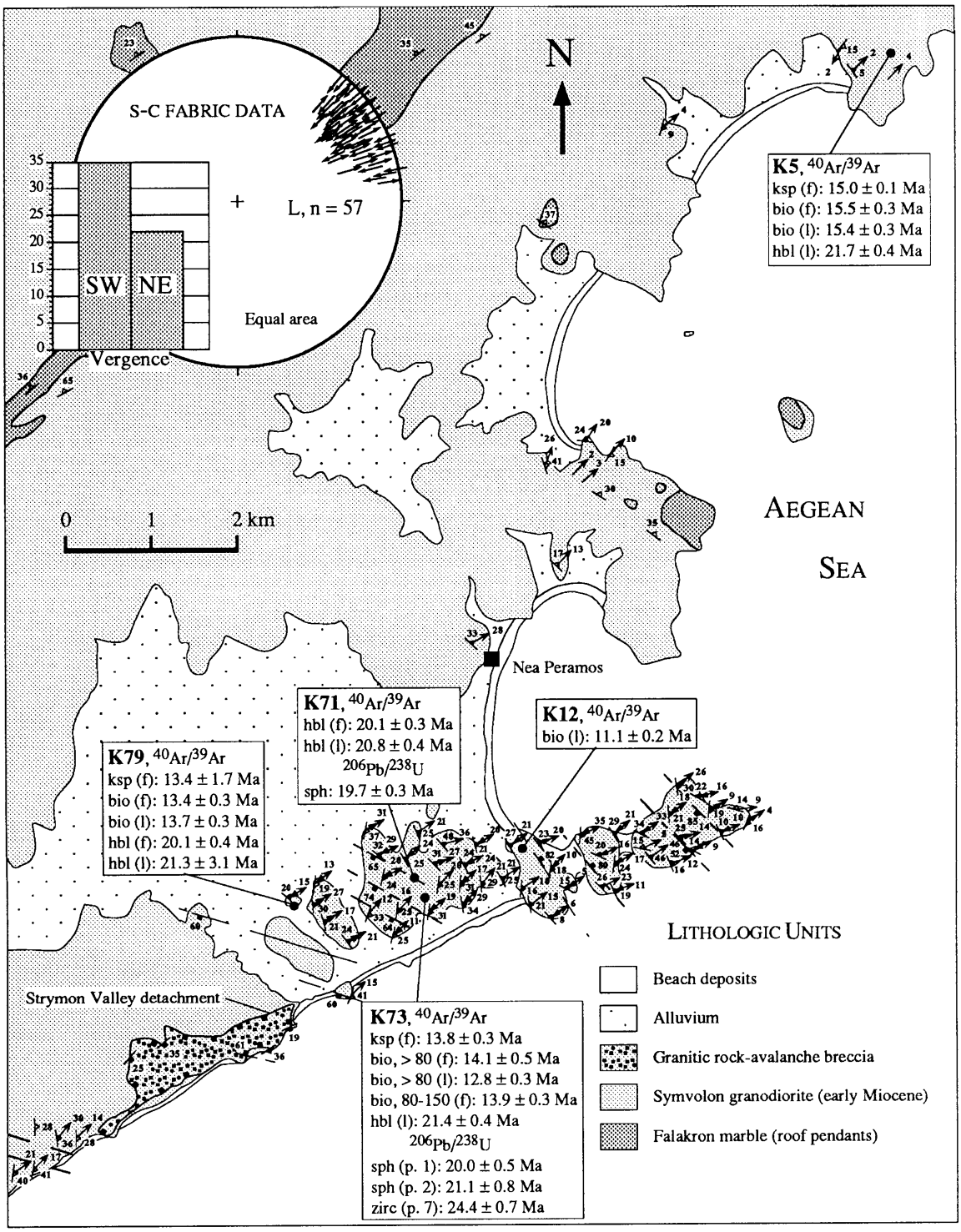

Figure 6. Structural and geochronological data, central Symvolon pluton. Attitudes with boxes are on brittle shear surfaces; attitudes with triangles are on mylonitic C-planes. Arrows represent stretching lineations. Single barb or outer barb of double-barbed arrows gives plunge of lineation. Inner barb gives sense of shear based on mylonitic fabric indicators. (Barb points in transport direction of material above shear plane). In data boxes, (f) indicates furnace step-heating analysis, (l) indicates laser-fusion analysis. Inset: Stretching lineations plotted with mylonitic sense of shear on equal area net. (Arrows point in transport direction of material above shear plane.) Bar graph tabulates SW vs. NE sense-of-shear indicators based on field determinations of S-C asymmetries. See Fig. 3 for location.

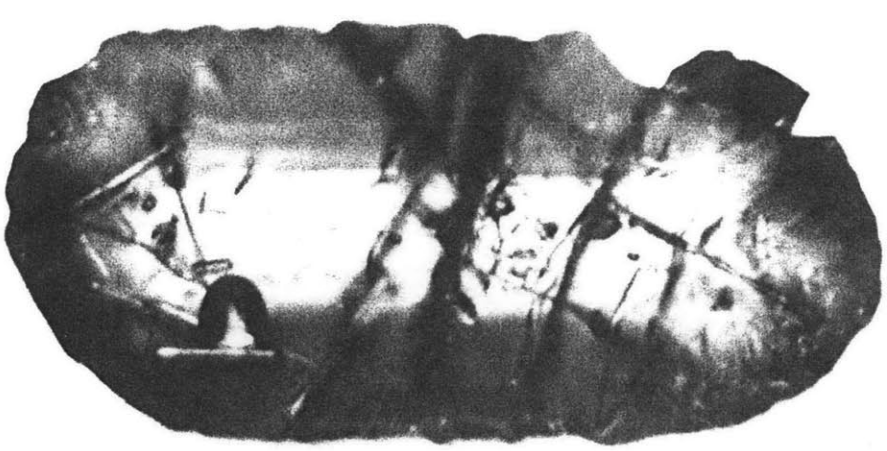

a

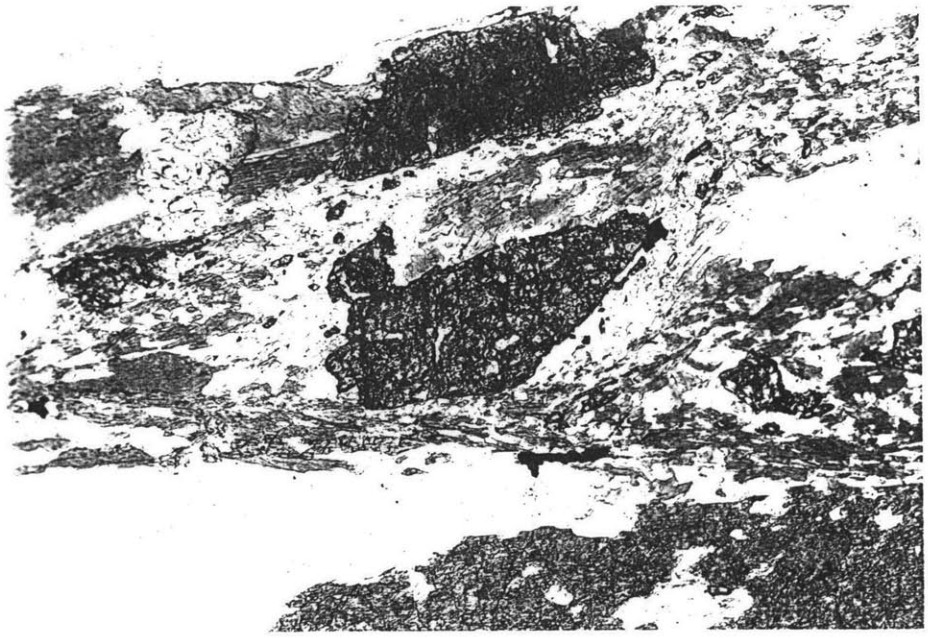

b

Figure 7. Photomicrographs of titanites from the Symvolon pluton, representative of those analyzed by U-Pb methods in the present study. Plane polarized light. See Fig. 6 for sample locations. (a) Cracked, euhedral titanite with minor needle-shaped inclusions from sample M90-K73. (b) Cracked, subhedral titanites with long axes oriented parallel to S-planes defined by fine-grained biotite in dextral S-C mylonite sample M90-K79; interpreted as evidence that titanite crystallized prior to or early in the Symvolon mylonitic environment.

c

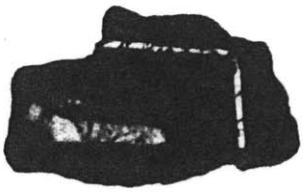

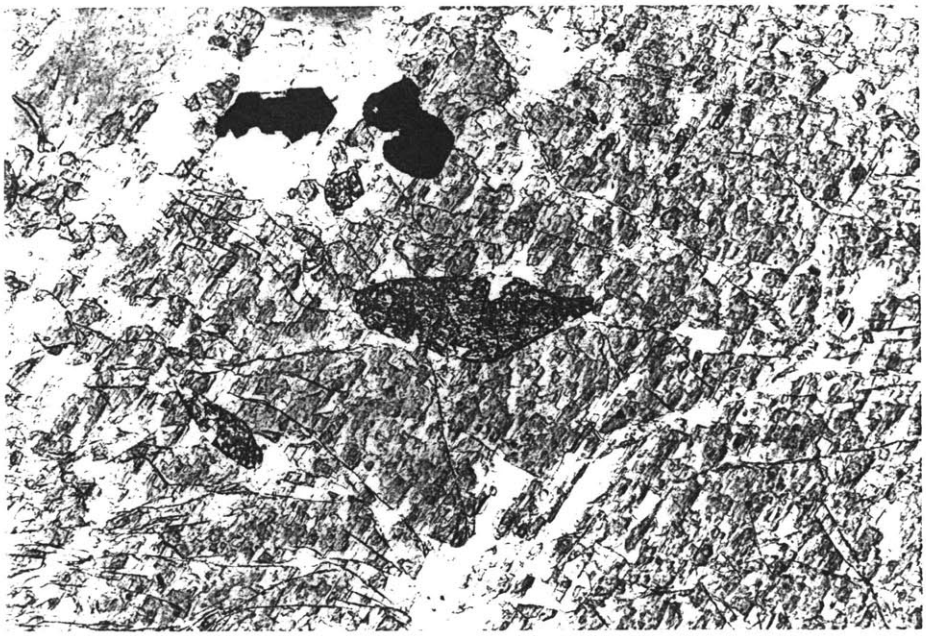

d

Figure 7. (c) Euhedral titanite from sample M90-K79 showing two distinct growth periods. (d) Euhedral titanite inclusions in an M90-K79 hornblende porphyroblast that crystallized within the mylonitic environment; S-plane parallel to hornblende cleavage. Long axes of titanites are not parallel to mylonitic fabric elements, suggesting they may have crystallized prior to onset of mylonitization.

a

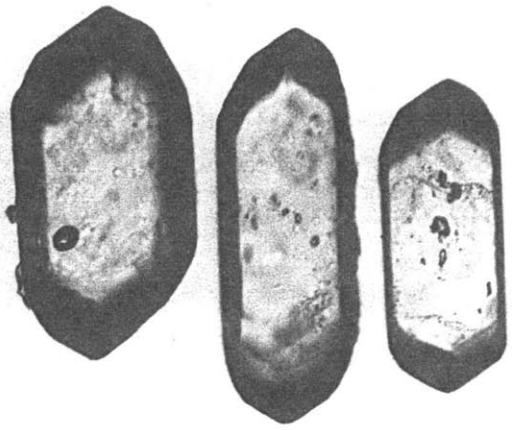

b

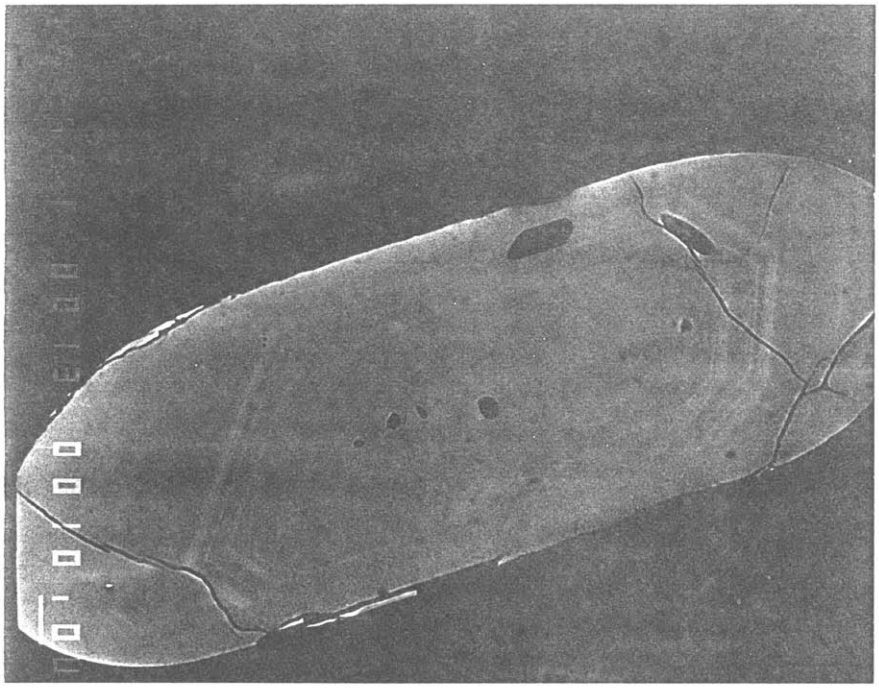

Figure 8. (a) Photomicrograph of zoned, euhedral zircons with minor inclusions, sample M90-K73, Symvolon pluton. Anhedral cores are faintly visible in crystals at left and right. Plane polarized light. See Fig. 6 for location. (b) Scanning electron microscopic image of polished zircon section from sample M90-K73. Anhedral, chemically (?) eroded core of probable late Paleozoic age (see discussion in text) is surrounded by euhedral overgrowths inferred to have formed during crystallization of the Symvolon pluton ~21 - 22 Ma. Euhedral crystal facets were removed by air abrasion with pyrite prior to preparation of grain mount.

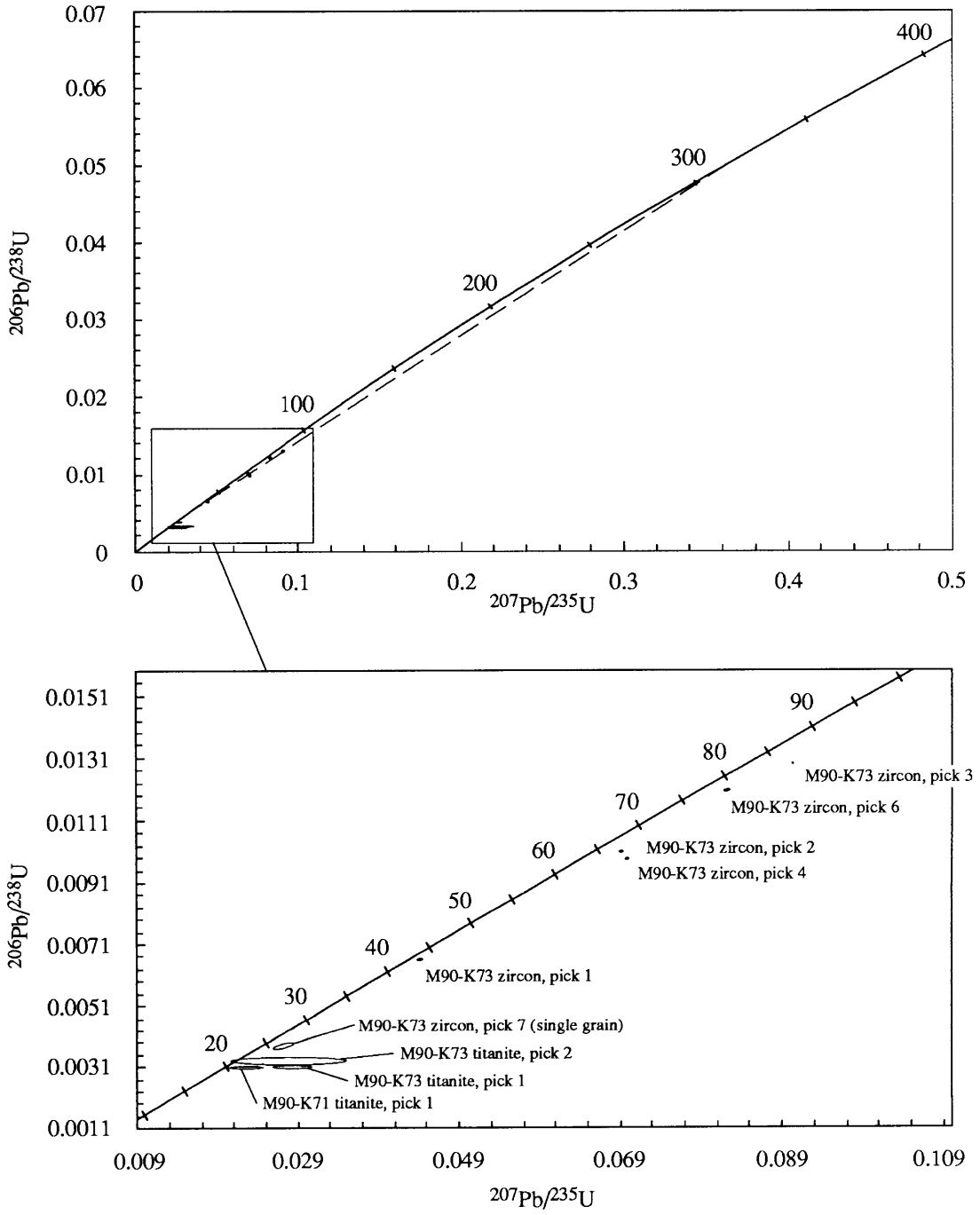

Figure 9. Concordia plots of U-Pb zircon and titanite analyses from the central part of the Symvolon granodiorite, northeastern Greece. (a) Poorly constrained chord regressed using multigrain zircon analyses only. Upper intercept age $\leq$ ~350 Ma (see text). (b) Detail of (a) shows $^{206}Pb/^{238}U$ titanite ages cluster in range 19.7 $\pm$ 0.3 Ma to 21.1 $\pm$ 0.8 Ma.

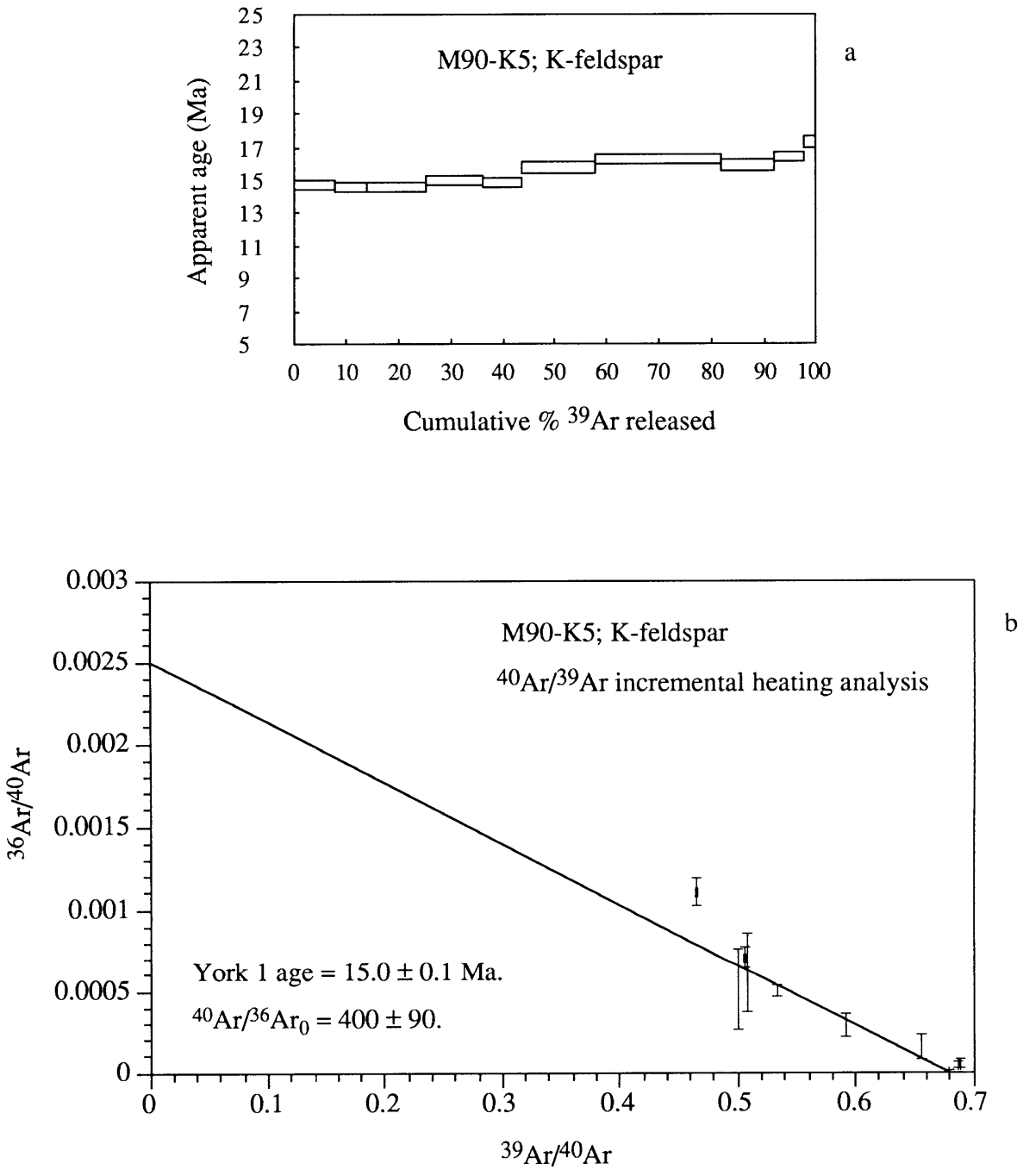

Figure 10.1. $^{40}Ar/^{39}Ar$ incremental-heating age spectrum (a) and inverse isotope correlation plot (b) for sample M90-K5, K-feldspar, south central Symvolon granodiorite pluton, Nea Peramos vicinity, northeastern Greece.

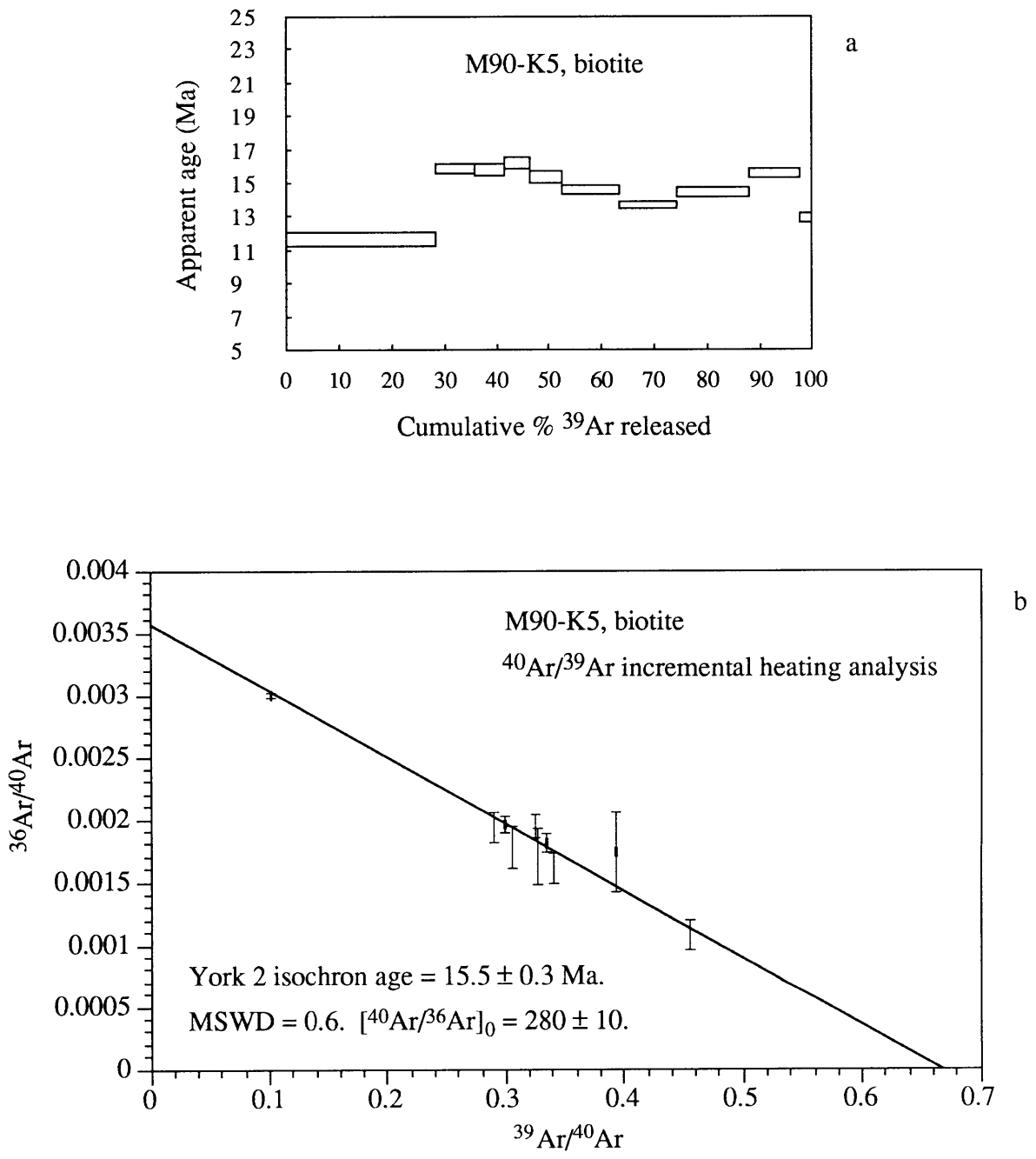

Figure 10.2. $^{40}Ar/^{39}Ar$ incremental-heating release spectrum (a) and inverse isotope correlation plot (b) for sample M90-K5, biotite, south central Symvolon granodiorite, Nea Peramos vicinity, northeastern Greece.

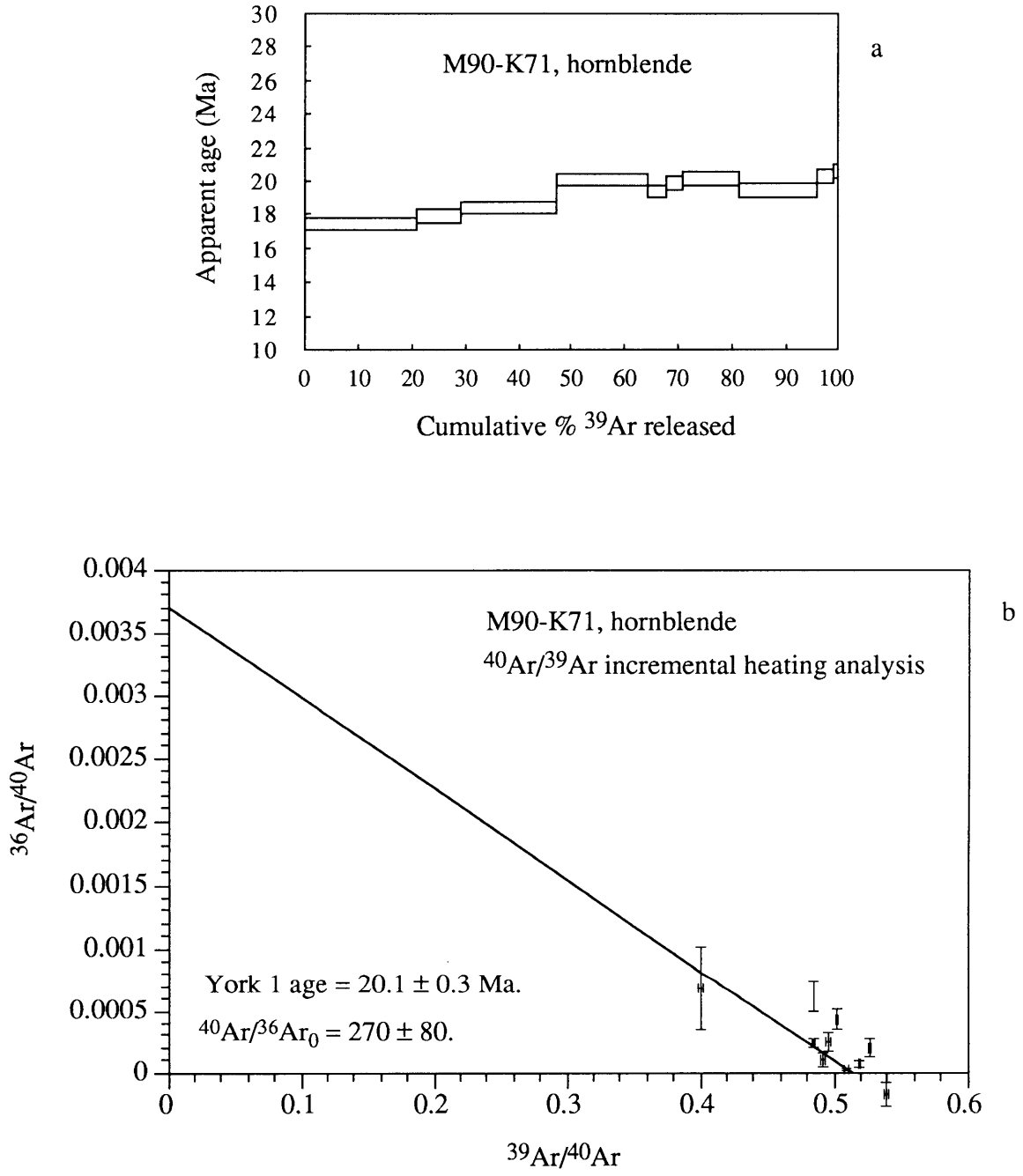

Figure 10.3. $^{40}Ar/^{39}Ar$ incremental-heating release spectrum (a) and inverse isotope correlation plot (b) for sample M90-K71, hornblende, south central Symvolon granodiorite, Nea Peramos vicinity, northeastern Greece.

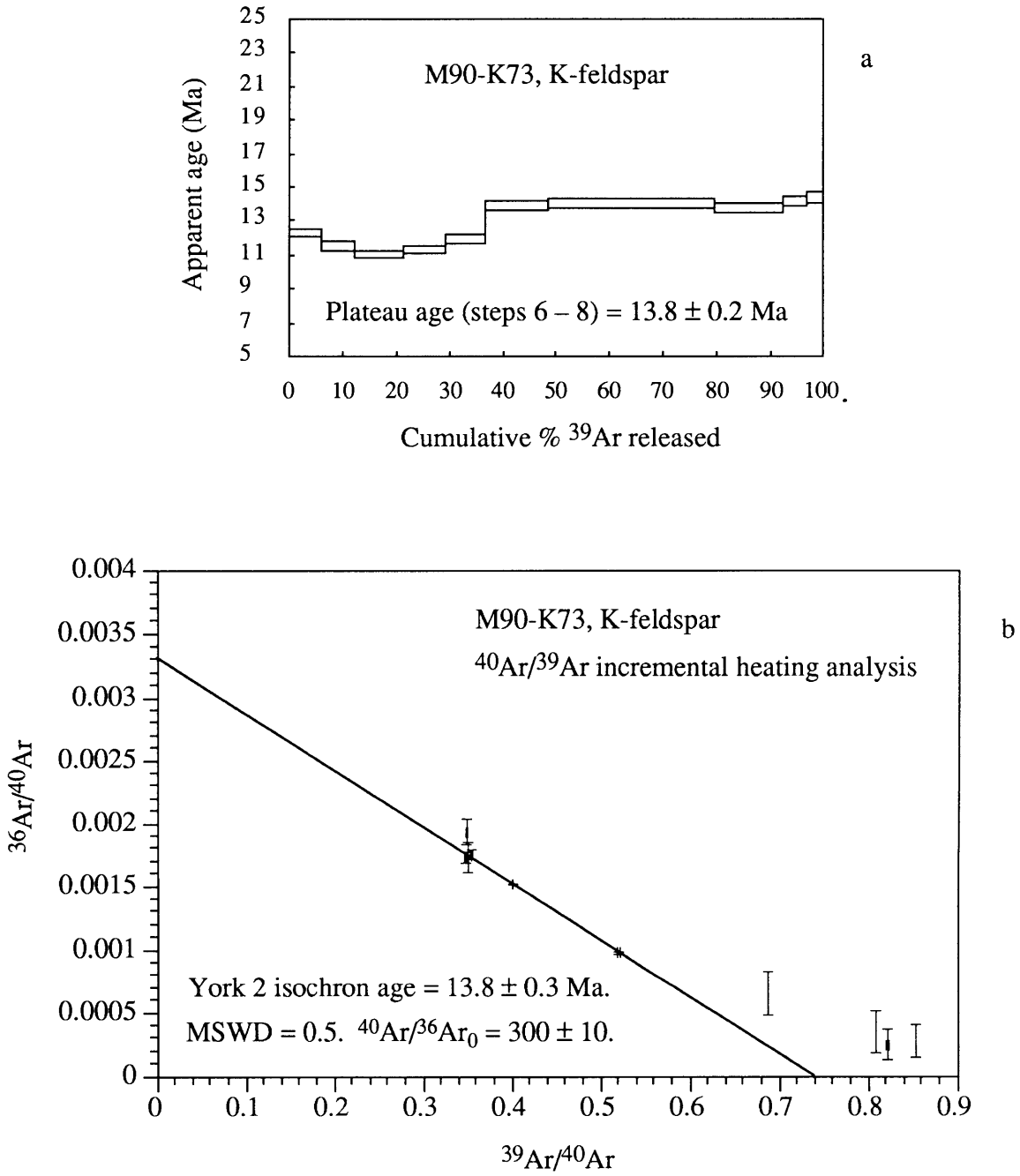

Figure 10.4. $^{40}Ar/^{39}Ar$ incremental-heating age spectrum (a) and inverse isotope correlation plot (b) for sample M90-K73, K-feldspar, south central Symvolon granodiorite, Nea Peramos vicinity, northeastern Greece.

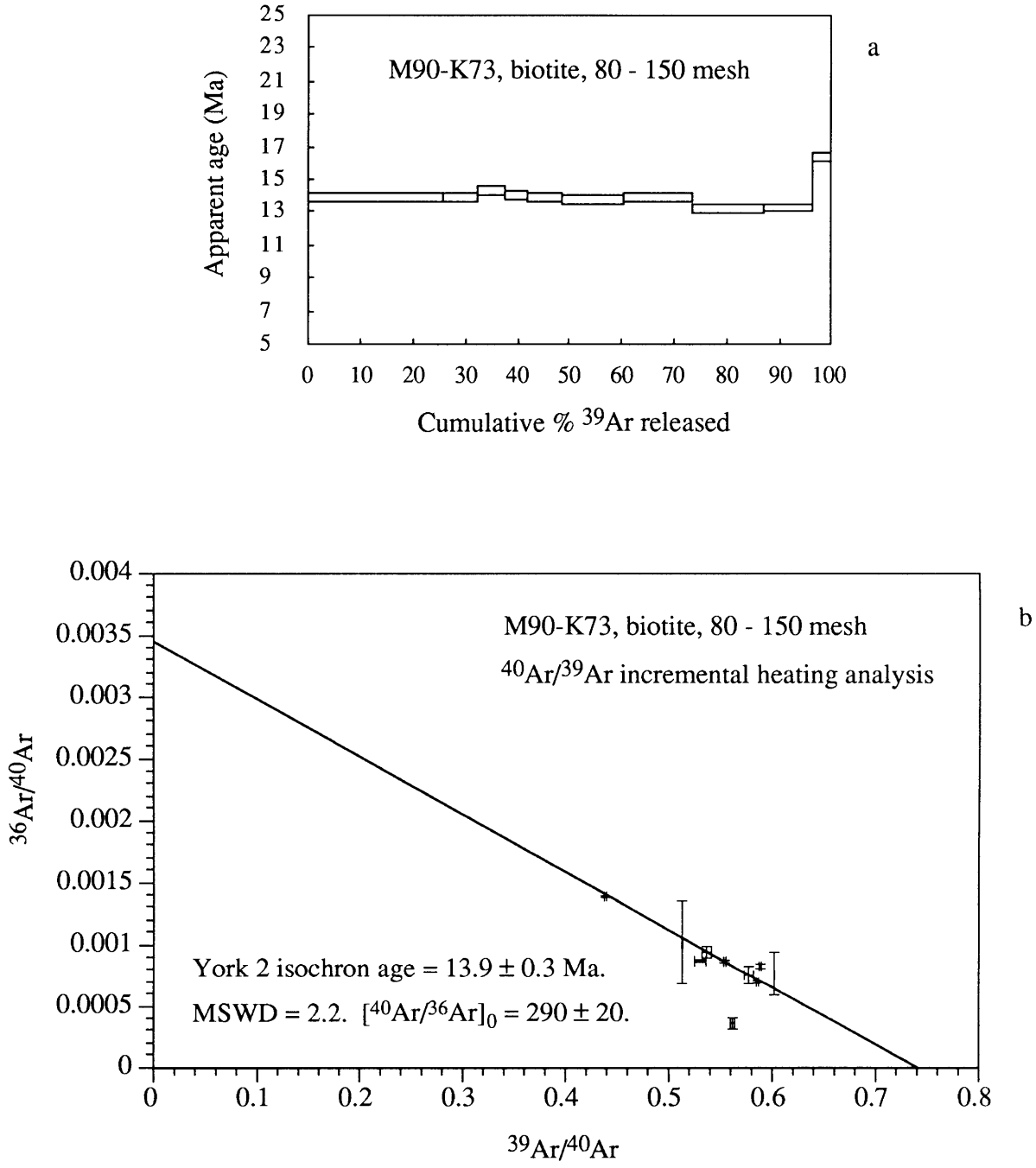

Figure 10.5. $^{40}Ar/^{39}Ar$ incremental-heating release spectrum (a) and inverse isotope correlation plot (b) for sample M90-K73, biotite, 80 - 150 mesh size fraction, south central Symvolon granodiorite, Nea Peramos vicinity, northeastern Greece.

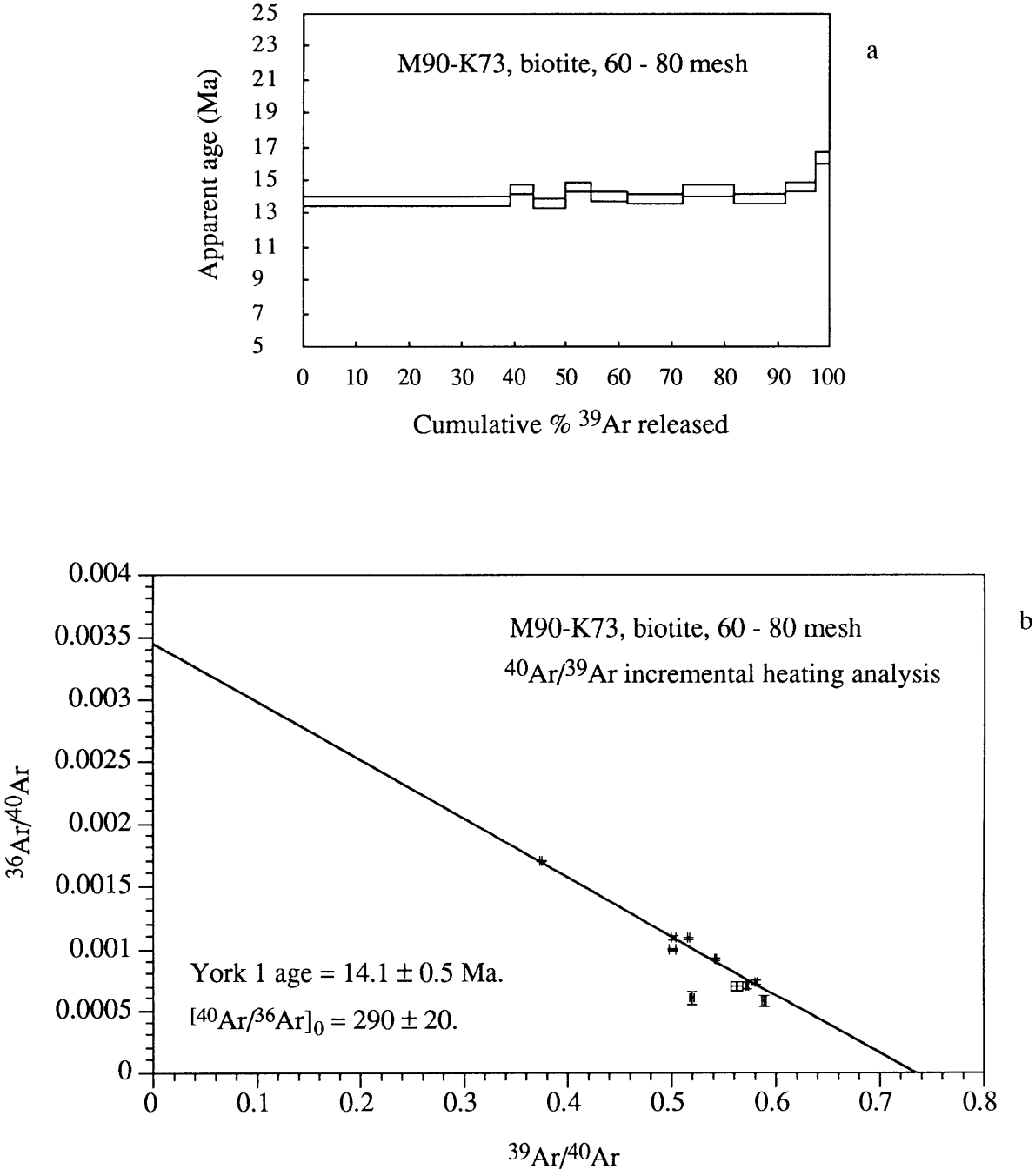

Figure 10.6. $^{40}Ar/^{39}Ar$ incremental-heating release spectrum (a) and inverse isotope correlation plot (b) for sample M90-K73, biotite, 60 - 80 mesh size fraction, south central Symvolon granodiorite, Nea Peramos vicinity, NE Greece.

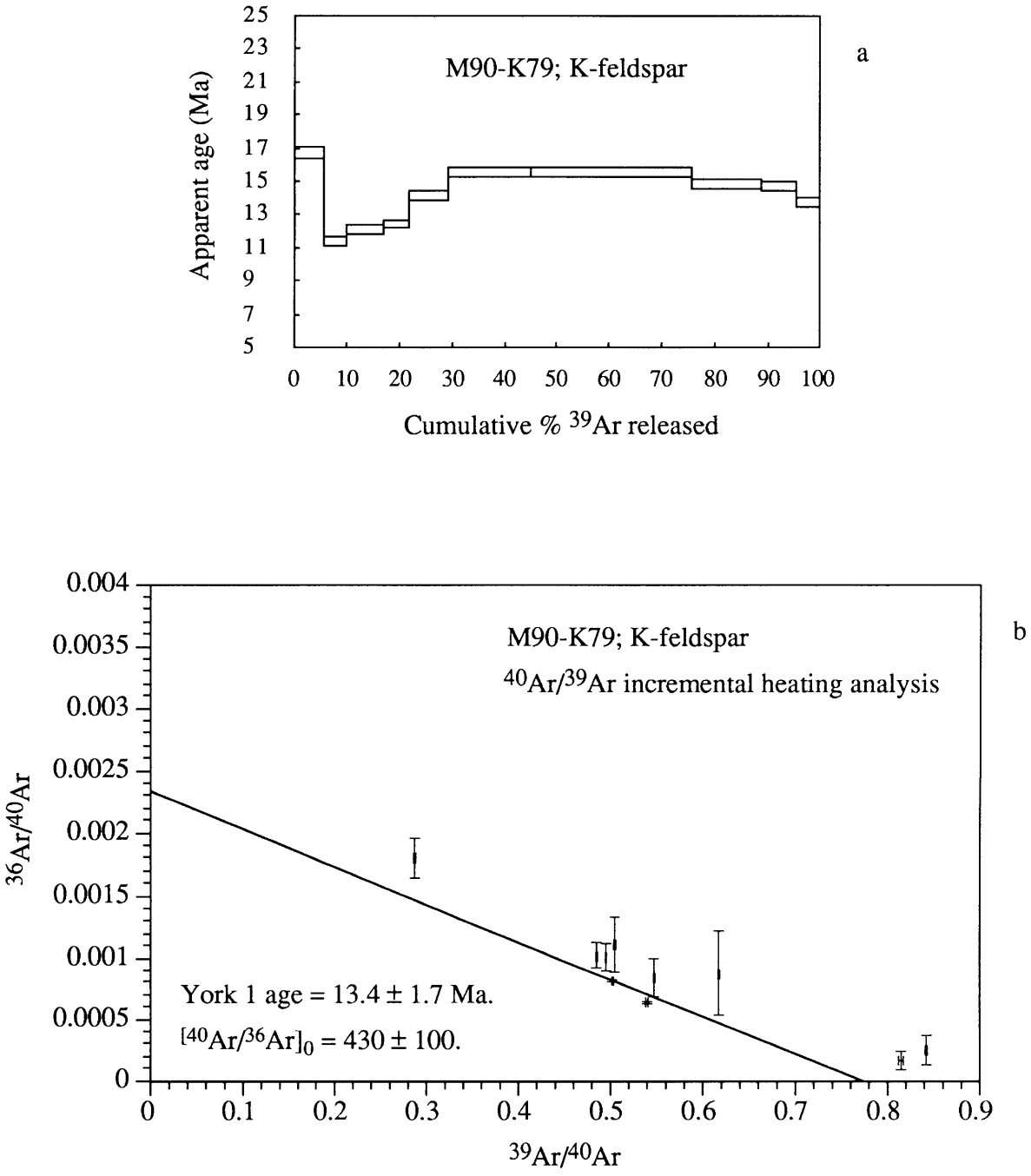

Figure 10.7. $^{40}Ar/^{39}Ar$ incremental-heating age spectrum (a) and inverse isotope correlation plot (b) for sample M90-K79, K-feldspar, south central Symvolon granodiorite, Nea Peramos vicinity, northeastern Greece.

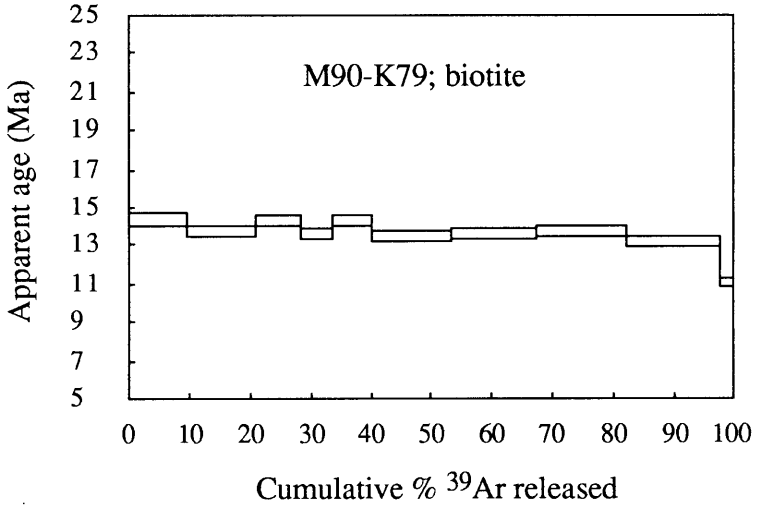

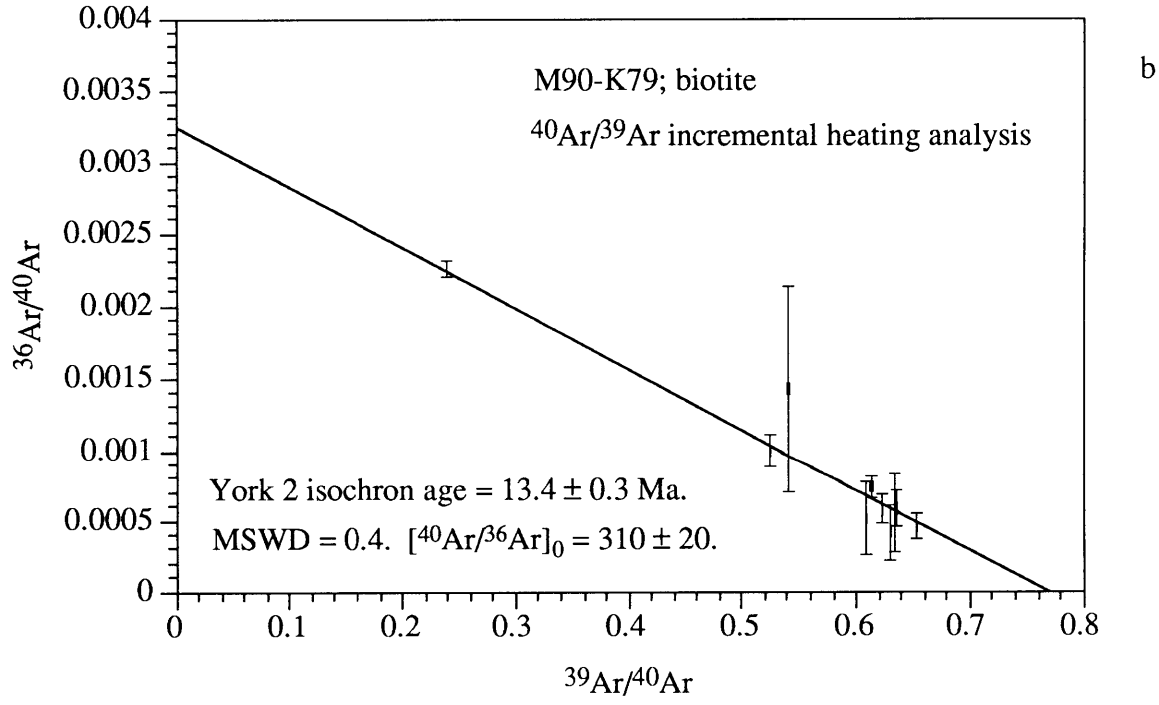

Figure 10.8. $^{40}Ar/^{39}Ar$ incremental-heating age spectrum (a) and inverse isotope correlation plot (b) for sample M90-K79, biotite, south central Symvolon granodiorite, Nea Peramos vicinity, northeastern Greece.

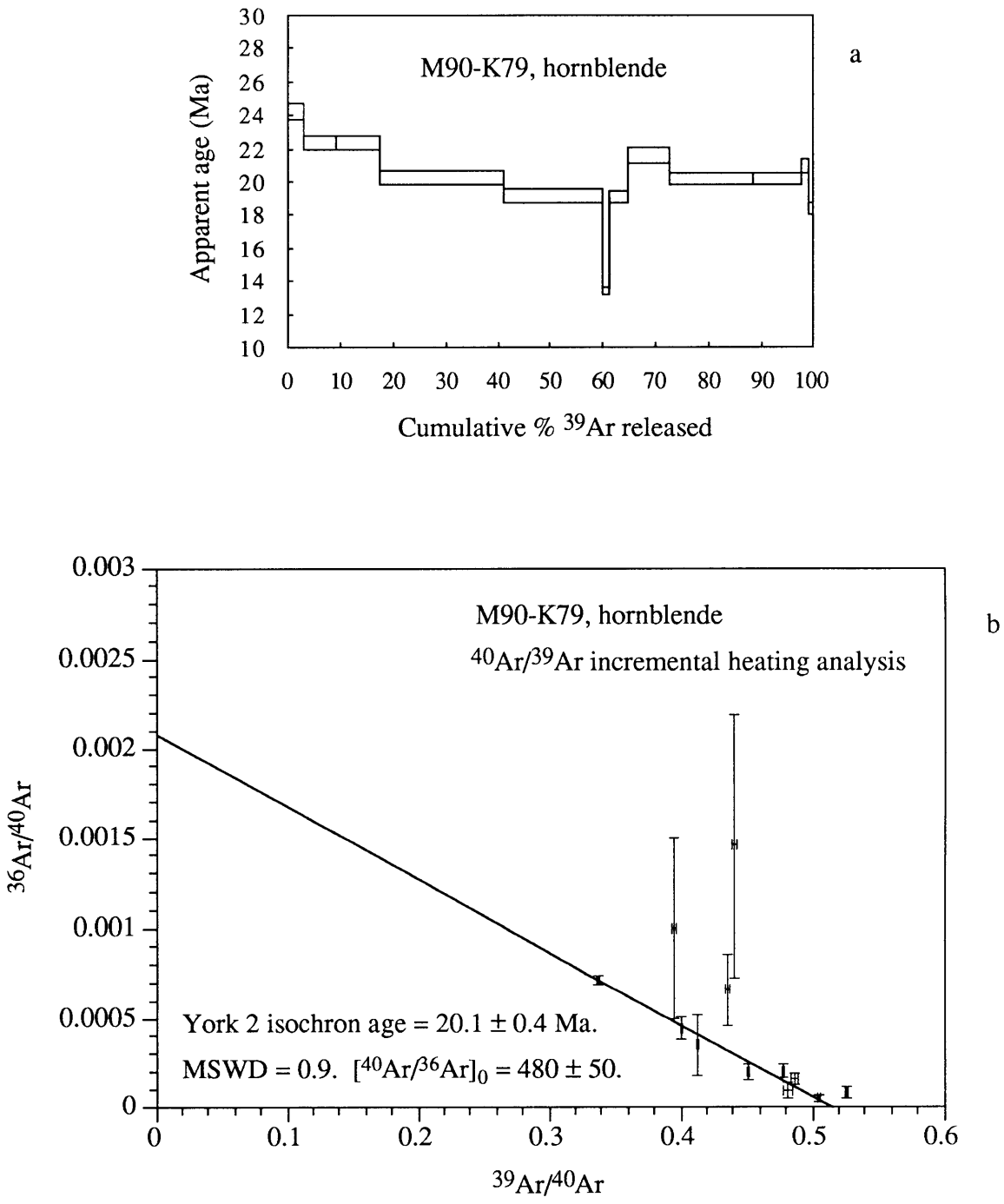

Figure 10.9. $^{40}Ar/^{39}Ar$ incremental heating age spectrum (a) and inverse isotope correlation plot (b) for sample M90-K79, hornblende, south central Symvolon granodiorite, Nea Peramos vicinity, northeastern Greece.

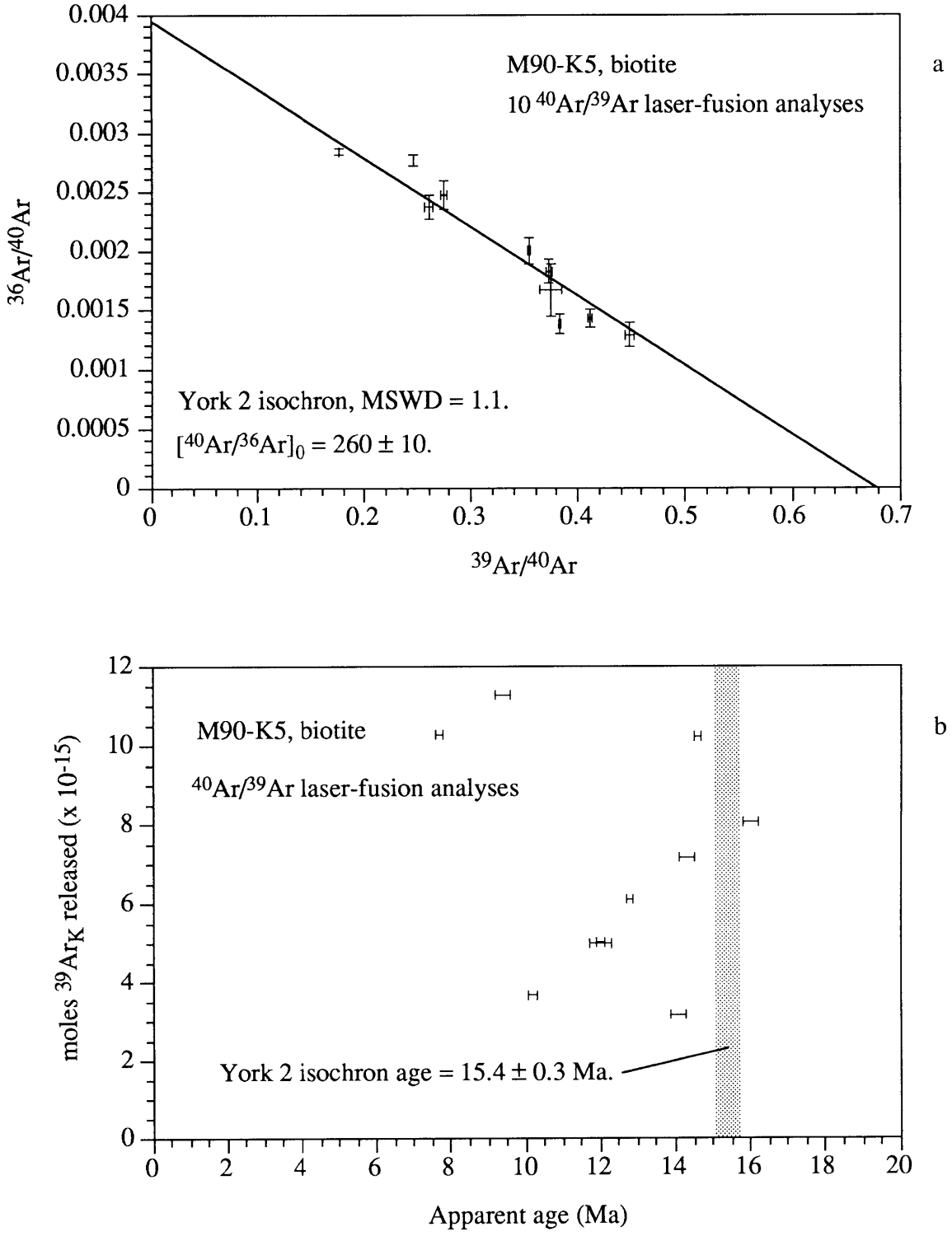

Figure 11.1. $^{40}Ar/^{39}Ar$ laser-fusion inverse isotope correlation plot (a) and apparent age distribution (b) for sample M90-K5, biotite, south central Symvolon granodiorite, Nea Peramos vicinity, northeastern Greece.

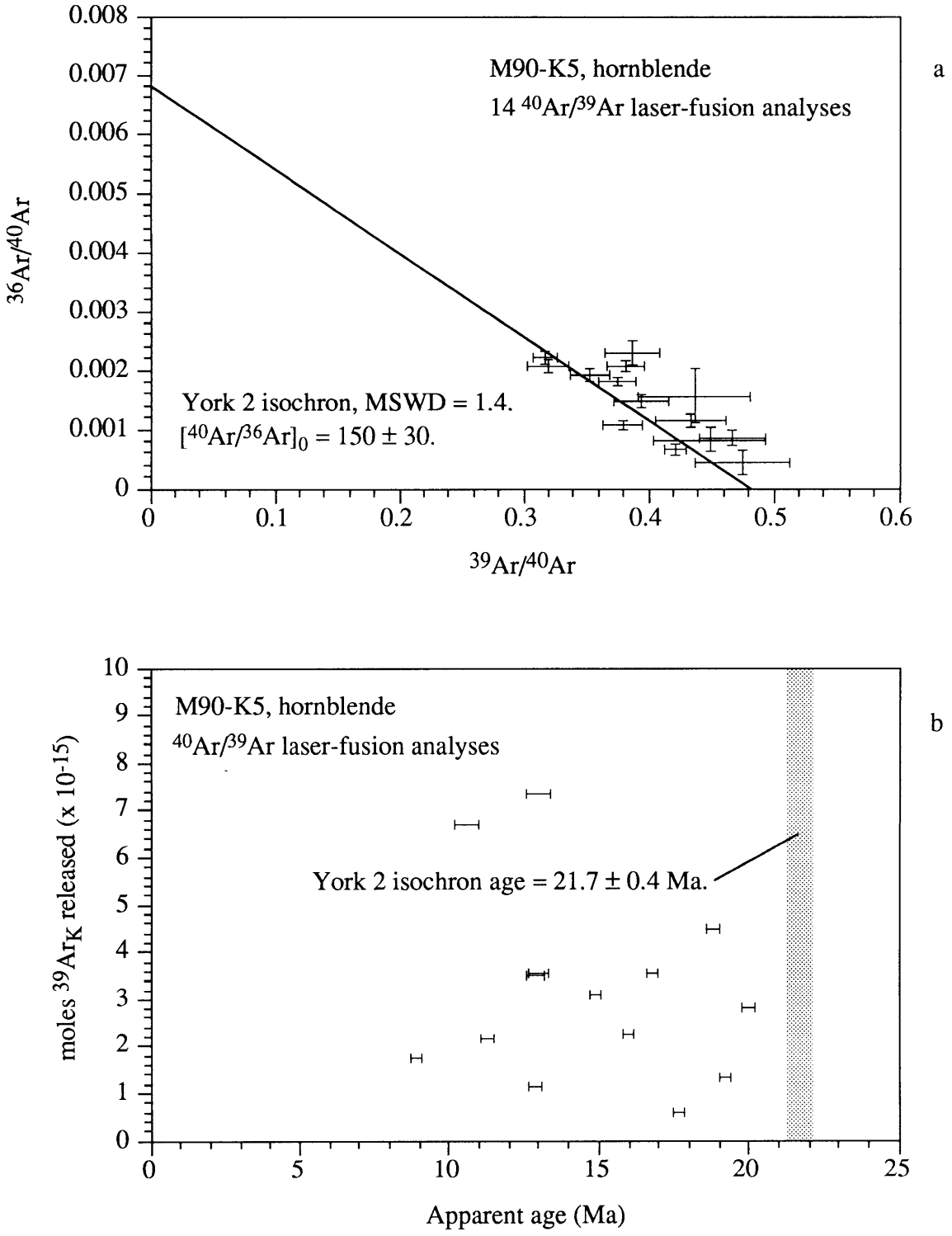

Figure 11.2. $^{40}Ar/^{39}Ar$ laser-fusion inverse isotope correlation plot (a) and apparent age distribution (b) for sample M90-K5, hornblende, south central Symvolon granodiorite, Nea Peramos vicinity, northeastern Greece.

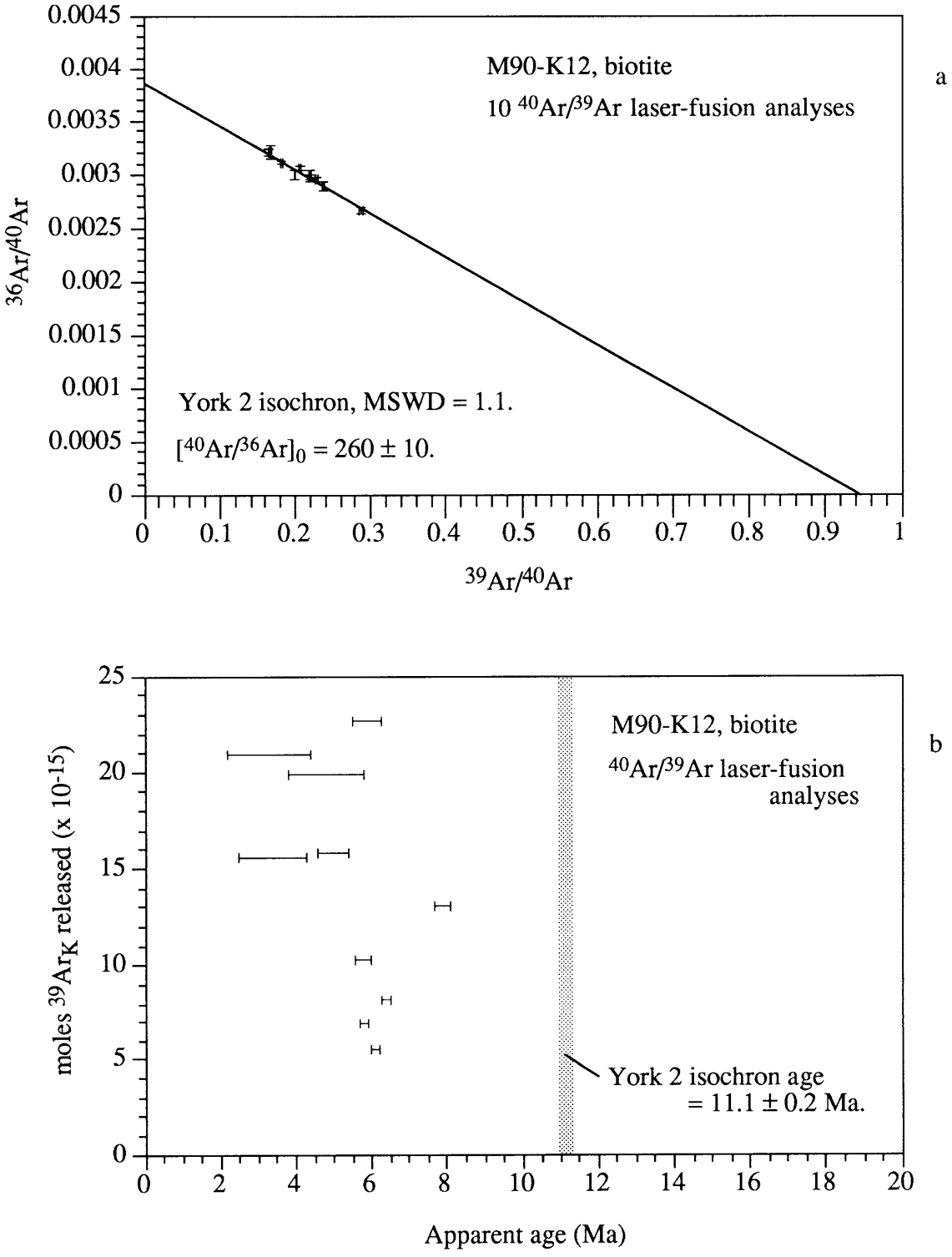

Figure 11.3. $^{40}Ar/^{39}Ar$ laser-fusion inverse isotope correlation plot (a) and apparent age distribution (b) for sample M90-K12, biotite, south central Symvolon granodiorite, Nea Peramos vicinity, northeastern Greece.

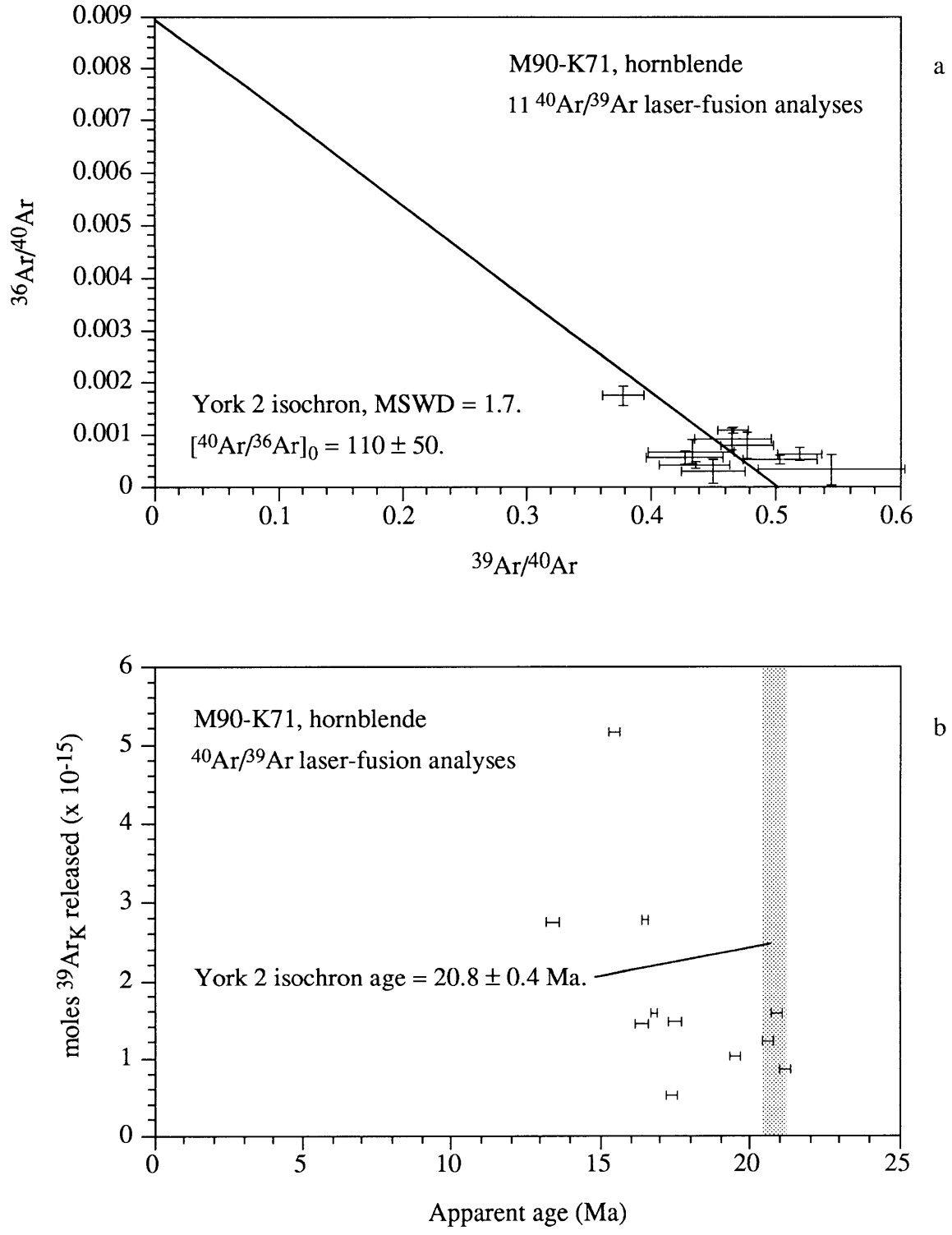

Figure 11.4. $^{40}Ar/^{39}Ar$ laser-fusion inverse isotope correlation plot (a) and apparent age distribution (b) for sample M90-K71, hornblende, south central Symvolon granodiorite, Nea Peramos vicinity, northeastern Greece.

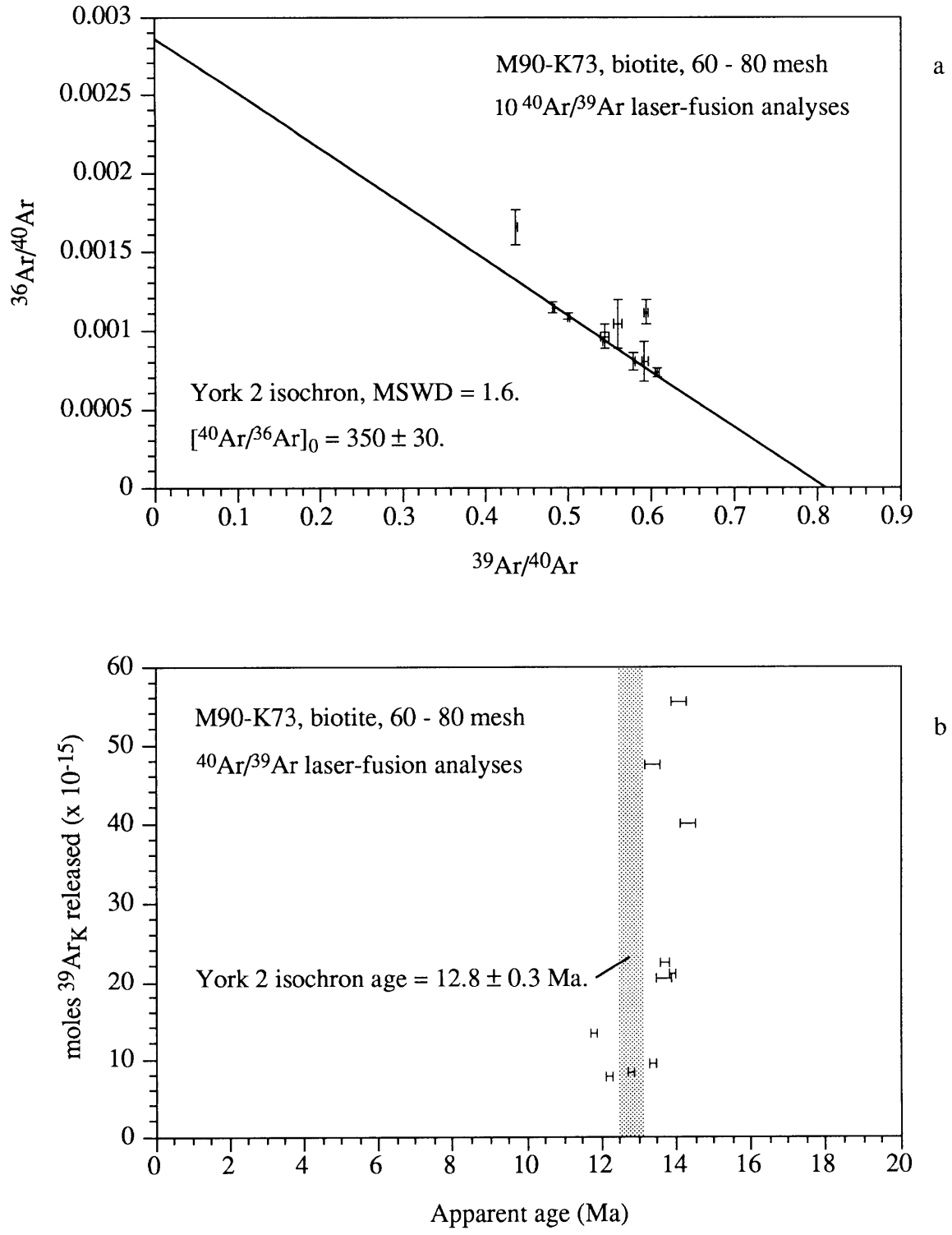

Figure 11.5. $^{40}Ar/^{39}Ar$ laser-fusion inverse isotope correlation plot (a) and apparent age distribution (b) for sample M90-K73, biotite, south central Symvolon granodiorite, Nea Peramos vicinity, northeastern Greece.

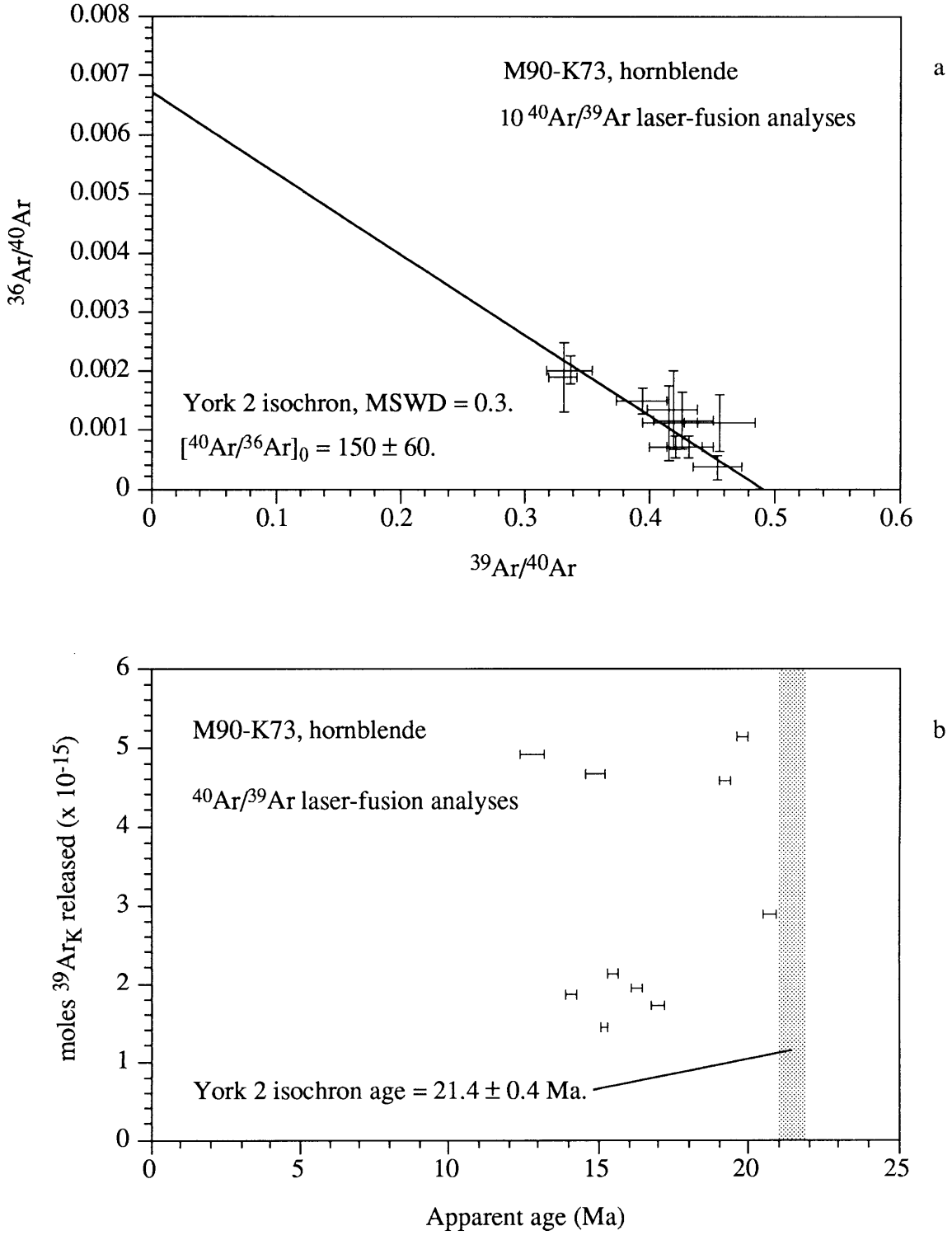

Figure 11.6. $^{40}Ar/^{39}Ar$ laser-fusion inverse isotope correlation plot (a) and apparent age distribution (b) for sample M90-K73, hornblende, south central Symvolon granodiorite, Nea Peramos vicinity, northeastern Greece.

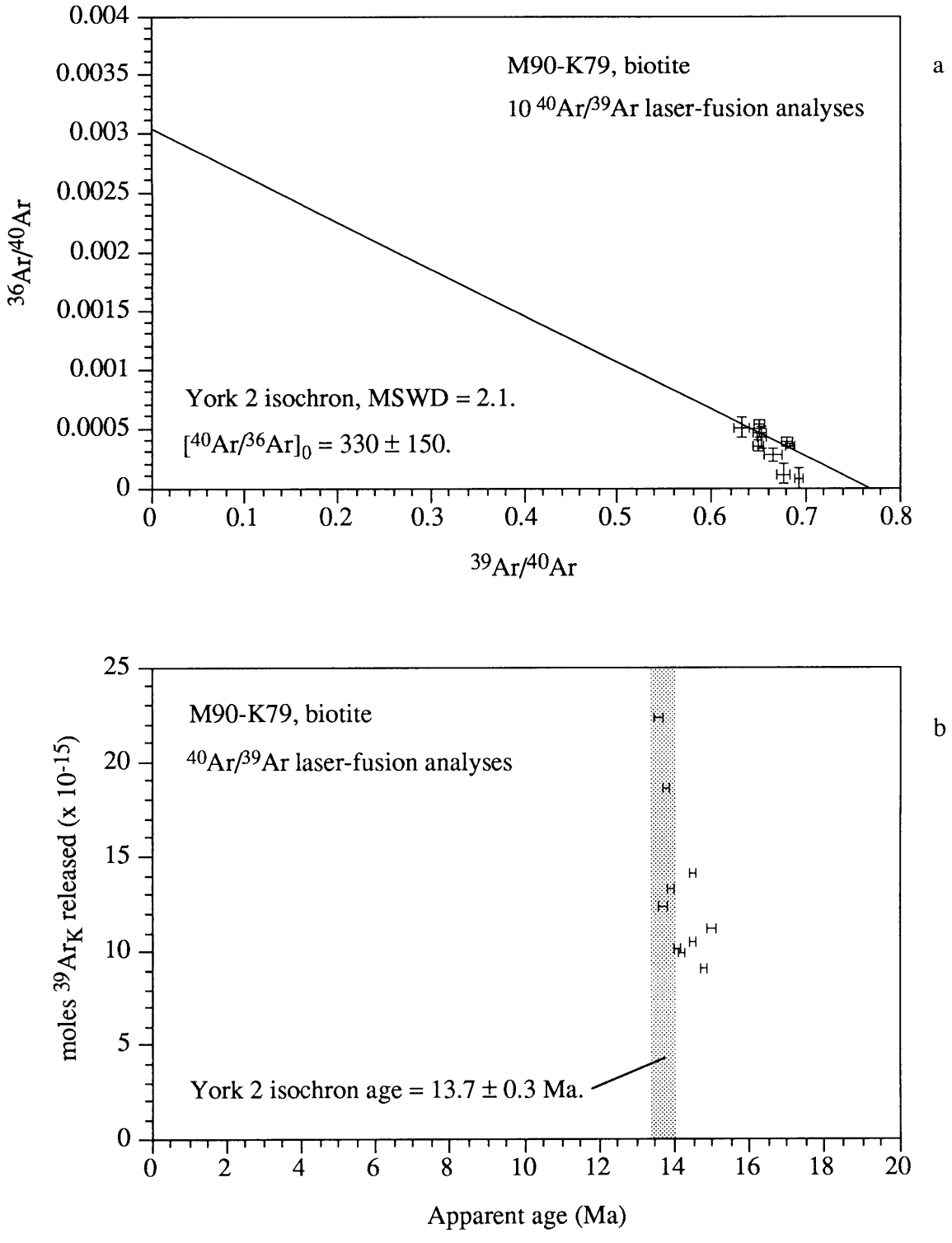

Figure 11.7. $^{40}Ar/^{39}Ar$ laser-fusion inverse isotope correlation plot (a) and apparent age distribution (b) for sample M90-K79, biotite, south central Symvolon granodiorite, Nea Peramos vicinity, northeastern Greece.

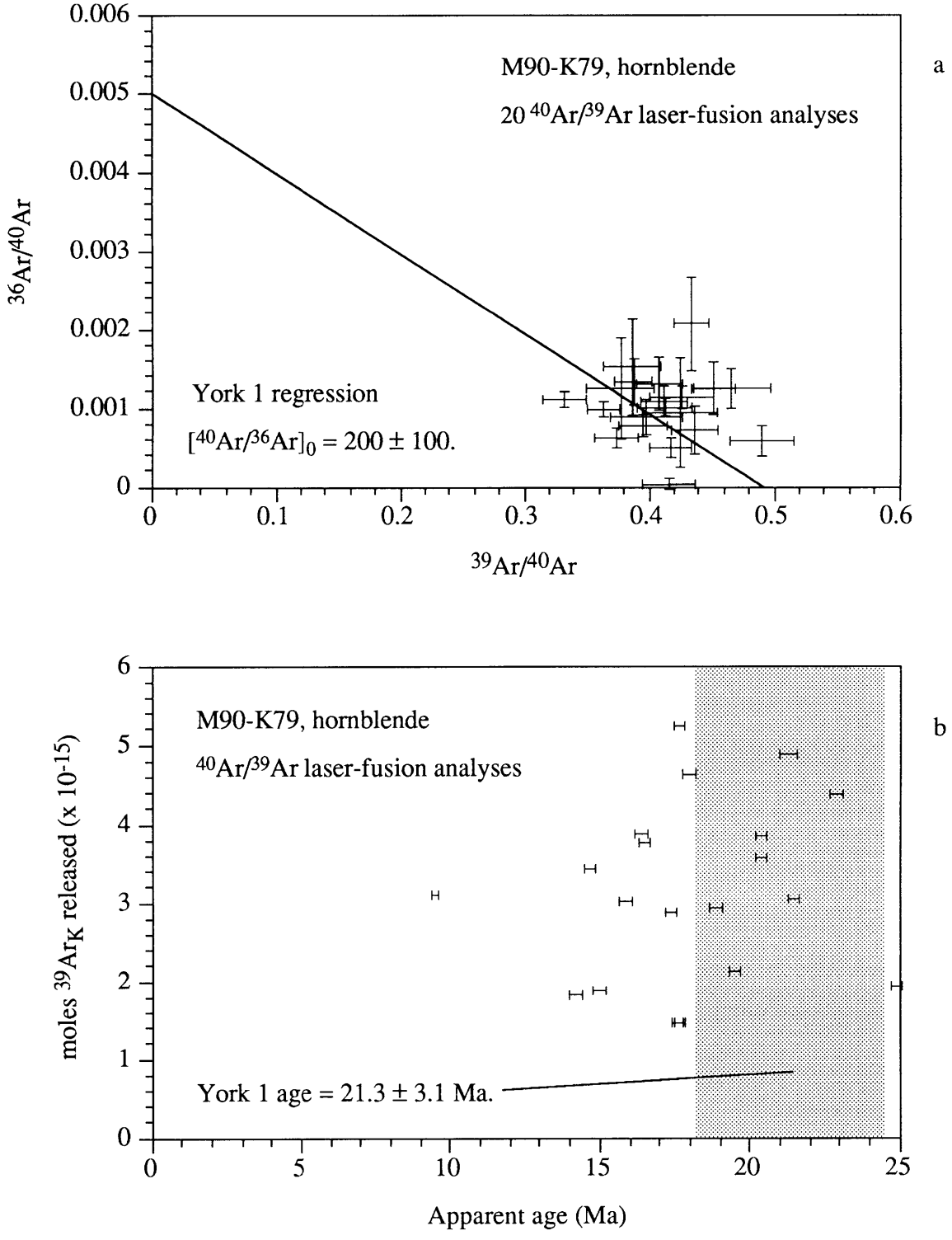

Figure 11.8. $^{40}Ar/^{39}Ar$ laser-fusion inverse isotope correlation plot (a) and apparent age distribution (b) for sample M90-K79, hornblende, south central Symvolon granodiorite, Nea Peramos vicinity, northeastern Greece.

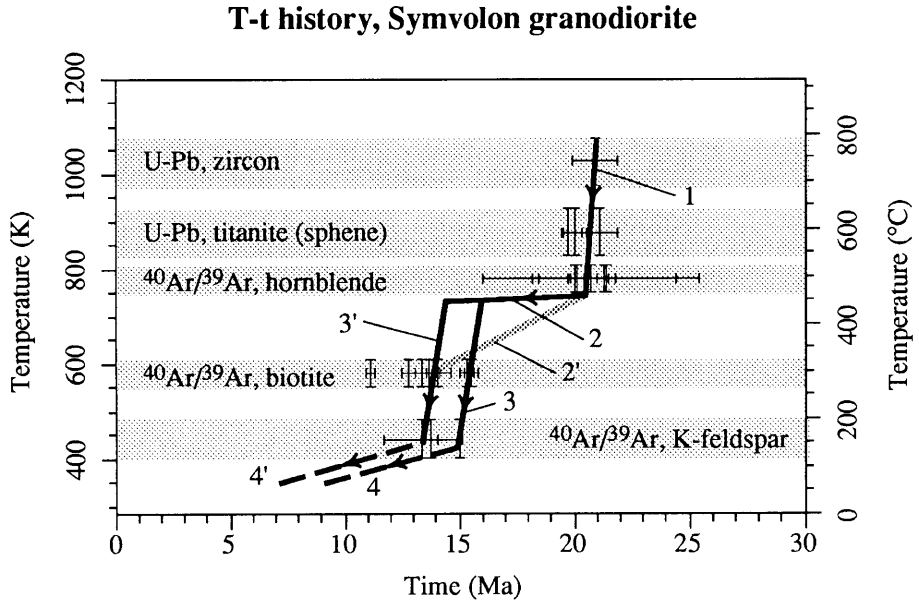

Figure 12. Schematic Tertiary temperature-time (T-t) history of the south central Symvolon pluton near Nea Peramos, northeastern Greece. U-Pb closure temperatures assumed for zircon and titanite are 750°C and 600°C, respectively (Ghent et al., 1988); assumed Ar closure temperatures are 500°C for hornblende (Harrison, 1981), 300°C for biotite (Harrison et al., 1985, and 150°C for K-feldspar (e.g., McDougall and Harrison, 1988). Data points in zircon and titanite fields are $^{206}Pb/^{238}U$ dates, and in hornblende, biotite, and K-feldspar fields, $^{40}Ar/^{39}Ar$ step-heating and laser-fusion dates. Numbered segments of the cooling path refer to distinct stages in the pluton's thermal and deformational evolution: 1 - emplacement of magma at mid-crustal depths within the upper greenschist facies Falakron marble series and simultaneous mylonitization within the gently northeast-dipping Symvolon shear zone; 2 - inferred slow cooling for 4 - 5 m.y. after emplacement; 2' - alternate moderate-rate cooling path from 500°C to 300°C allowed by the data; 3 - renewed rapid cooling as a result of tectonic unroofing of the Rhodope metamorphic core complex in the footwall of the Strymon Valley detachment system; 4 - inferred cooling at moderate rates during isostatic uplift and erosion. 3' - and 4' - segments apply to southwestern parts of the pluton, unroofed later than more northeasterly exposures.

Table 1. U-Pb dates and sample characteristics, Symvolon granodiorite, Rhodope metamorphic core complex, NE Greece

Sample	Mineral	Pick	Size	Color	# grains	weight (mg)	$^{206}Pb^*/^{238}U$ age†	$^{207}Pb^*/^{235}U$ age†	$^{207}Pb^*/^{206}Pb^*$ age†
M90-K71	titanite	1	80-100	honey	>400	2.1641	19.7 ± 0.3	22.6 ± 2.3	345.4 ± 35.7
M90-K73	"	1	100-140	amber	>400	3.4380	20.0 ± 0.5	28.4 ± 2.5	808.3 ± 69.4
"	"	2	80-100	"	>400	1.9940	21.1 ± 0.8	27.9 ± 7.3	663.3 ± 174.6
M90-K73	zircon	1	140-200	none	44	0.0756	42.5 ± 0.1	43.8 ± 0.2	116.3 ± 0.5
	"	2	100-140	"	22	0.0790	64.7 ± 0.1	67.9 ± 0.2	185.6 ± 0.4
	"	3	100-140	"	31	0.1440	82.6 ± 0.04	87.9 ± 0.1	233.1 ± 0.3
	"	4	140-200	"	57	0.1290	63.1 ± 0.1	68.6 ± 0.1	265.4 ± 0.3
	"	5	100-140	hyacinth	30	0.1560	96.9 ± 0.1	101.9 ± 1.0	221.0 ± 2.1
	"	6	140-200	"	26	0.0624	77.1 ± 0.1	80.4 ± 0.3	177.2 ± 0.5
	"	7	80-100	"	1	0.0147	24.4 ± 0.7	27.2 ± 1.3	281.8 ± 9.3

* Denotes radiogenic isotope.

† Ma

Table 2. U-Pb data corrected for mass fractionation, spike, and blank; titanite and zircon fractions, Symvolon granodiorite, NE Greece

Fractions	U (ppm)	Pb* (ppm)	$^{206}Pb^*/^{204}Pb$	$^{208}Pb^*/^{206}Pb^*$	$^{206}Pb^*/^{238}U$	$^{207}Pb^*/^{235}U$	$^{207}Pb^*/^{206}Pb^*$	corr. coeff.	common Pb (pg)
M90-K71 titanite									
pick 1	335.0	1.0	33.3	0.094	0.003061 ± 0.000039	0.0225 ± 0.0023	0.05339 ± 0.00546	0.019	9660.1
M90-K73 titanite									
pick 1	314.8	1.0	34.2	0.134	0.003109 ± 0.000073	0.0283 ± 0.0025	0.06606 ± 0.00567	0.234	13814.4
pick 2	250.8	0.9	23.6	0.172	0.003278 ± 0.000124	0.0279 ± 0.0073	0.06169 ± 0.01624	0.022	21075.8
M90-K73 zircon									
pick 1	855.9	5.3	404.7	0.043	0.006620 ± 0.000010	0.0441 ± 0.0002	0.04835 ± 0.00022	0.295	74.3
pick 2	1299.5	12.3	941.2	0.046	0.010080 ± 0.000016	0.0692 ± 0.0002	0.04980 ± 0.00009	0.640	75.0
pick 3	1160.2	14.0	1459.9	0.037	0.012900 ± 0.000006	0.0904 ± 0.0001	0.05082 ± 0.00006	0.390	98.9
pick 4	1566.1	14.8	1680.2	0.069	0.009837 ± 0.000009	0.0699 ± 0.0001	0.05155 ± 0.00006	0.610	79.9
pick 5	891.8	14.5	44.7	0.100	0.015151 ± 0.000079	0.1056 ± 0.0055	0.05056 ± 0.00262	0.015	4079.8
pick 6	1188.6	13.7	2093.2	0.061	0.012038 ± 0.000020	0.0824 ± 0.0003	0.04961 ± 0.00013	0.563	31.0
pick 7	319.1	1.2	122.3	0.145	0.003792 ± 0.000106	0.0271 ± 0.0013	0.05192 ± 0.00174	0.760	12.2

* Denotes radiogenic isotope.
Note: Estimated Pb blank for all analyses = 3.5 pg.

Table 3.1. U-Pb analytical data for sample M90-K71 titanite, pick 1

sample weight: 2164.1 µgm | Pb blank: 3.5 pg | Pb alpha (%/amu) 0.1240

spike weight: 0.0248 grams | U blank: 1.0 pg | U alpha (%/amu) 0.1547

RAW DATA

206/204	33.2874298	± 0.0548 %
206/207	2.03601	± 0.0210 %
206/208	0.837126	± 0.0220 %
206/205	47.9401981	± 0.1890 %
238/235	48.64395	± 0.0274 %
233/235	0.6537704	± 0.0000 %

Total Common Pb: 9660.1 pg

Radiogenic/Common: 1.2

(238/235)fc: 48.869681 Faraday/Daly

RATIOS CORRECTED FOR SPIKE AND BLANK

206/204	206/207	206/208
33.34	2.0316	0.8343
±0.091%	±0.042%	±0.076%

INITIAL PB S&K 0.03 Ga

206/204	18.665456
207/204	15.627084
208/204	38.584952

	total	radiogenic
PPM Pb	5.47	1.01
PPM U	334.96183	

208*/206* 0.094

common Pb 9656.6 pg (4.46 ppm)

Pb TOTAL LOAD 11936 pg

U TOTAL LOAD 743676 pg

206/238		207/235		207/206		Rho
0.00306	± 1.2924 %	0.02254	± 10.1751 %	0.053390	± 10.2328 %	.018775
19.7 Ma		22.6 Ma		345.4 Ma		

SPIKE: MIT1B-C

206/205	0.052928
206/204	1523.933
206/207	97.467635
206/208	41.881202
[205]	1.76906E-11 moles/gram
[235]	1.61084E-09 moles/gram
235/205	91.0559

BLANK COMPOSITION

206/204	19.10205 ±0.05
207/204	15.71470 ±0.05
208/204	38.65319 ±0.05

MOLES PB PER GRAM

206	9.7182E-09
207	4.7836E-09
208	1.1649E-08
204	2.9150E-10
TOTAL	2.6442E-08

MOLES URANIUM PER GRAM

238	1.3972E-06
235	1.0133E-08

MOLES RADIOGENIC PB PER GRAM

206*	4.2773E-09
207*	2.2837E-10
208*	4.0147E-10

TOTAL PB = 11846.2 pg

RAD Pb = 2189.6 pg

TOTAL U = 724890.9 pg

Table 3.2. U-Pb analytical data for sample M90-K73 titanite, pick 1

sample weight: 3438 µgm | Pb blank: 3.5 pg | Pb alpha (%/amu) 0.1240

spike weight: 0.0287 grams | U blank: 1.0 pg | U alpha (%/amu) -0.3741

RAW DATA

206/204	34.16068	± 0.2000 %
206/207	2.0587911	± 0.1400 %
206/208	0.8441992	± 0.0400 %
206/205	60.7946	± 2.0000 %
238/235	57.816006	± 0.0700 %
233/235	0.5866036	± 0.0000 %

Total Common Pb: 13814.4 pg

Radiogenic/Common: 1.3

(238/235)fc: 57.167118 Faraday/Daly

RATIOS CORRECTED FOR SPIKE AND BLANK

206/204	206/207	206/208
34.22	2.0547	0.8415
±0.213%	±0.145%	±0.083%

INITIAL PB S&K 0.03 Ga

206/204	18.665456
207/204	15.627084
208/204	38.584952

	total	radiogenic
PPM Pb	5.03	1.01
PPM U	314.78383	

208*/206* 0.134

common Pb 13810.9 pg (4.02 ppm)

Pb TOTAL LOAD 17388 pg

U TOTAL LOAD 1103966 pg

206/238		207/235		207/206		Rho
0.00311	± 2.3514 %	0.02832	± 8.8199 %	0.066062	± 8.5803 %	.233808

20.0 Ma **28.4** Ma **808.3** Ma

SPIKE:	MIT1B-C
206/205	0.052928
206/204	1523.933
206/207	97.467635
206/208	41.881202
[205]	1.76906E-11 moles/gram
[235]	1.61084E-09 moles/gram
235/205	91.0559

BLANK COMPOSITION	
206/204	19.10205 ±0.05
207/204	15.71470 ±0.05
208/204	38.65319 ±0.05

MOLES PB PER GRAM

206	8.9802E-09
207	4.3706E-09
208	1.0672E-08
204	2.6242E-10
TOTAL	2.4285E-08

MOLES URANIUM PER GRAM

238	1.3130E-06
235	9.5228E-09

MOLES RADIOGENIC PB PER GRAM

206*	4.0819E-09
207*	2.6966E-10
208*	5.4637E-10

TOTAL PB = 17284.0 pg

RAD Pb = 3473.1 pg

TOTAL U = 1082226.8 pg

Table 3.3. U-Pb analytical data for sample M90-K73 titanite, pick 2

sample weight: 1994 µgm | Pb blank: 3.5 pg | Pb alpha (%/amu) 0.1240

spike weight: 0.0242 grams | U blank: 1.0 pg | U alpha (%/amu) -0.0792

RAW DATA

206/204	23.58867	± 0.0760 %
206/207	1.4859684	± 0.0140 %
206/208	0.6010569	± 0.0200 %
206/205	75.9554	± 0.2000 %
238/235	38.64496	± 0.0392 %
233/235	0.726137	± 0.0000 %

Total Common Pb: 21075.8 pg

Radiogenic/Common: 1.1

(238/235)fc: 38.553132 Faraday/Daly

RATIOS CORRECTED FOR SPIKE AND BLANK

206/204	206/207	206/208
23.63	1.4832	0.5992
±0.105%	±0.039%	±0.075%

INITIAL PB

S&K	0.03 Ga
206/204	18.665456
207/204	15.627084
208/204	38.584952

	total	radiogenic
PPM Pb	11.44	0.87

208*/206* 0.172

Pb TOTAL LOAD 22900 pg

U TOTAL LOAD 518376 pg

PPM U 250.77518

common Pb 21072.3 pg (10.57 ppm)

206/238		207/235		207/206		Rho
0.00328	± 3.7849 %	0.02788	± 26.1363 %	0.061687	± 26.3275 %	.021697

21.1 Ma **27.9** Ma 663.3 Ma

SPIKE: MIT1B-C

206/205	0.052928
206/204	1523.933
206/207	97.467635
206/208	41.881202
[205]	1.76906E-11 moles/gram
[235]	1.61084E-09 moles/gram
235/205	91.0559

BLANK COMPOSITION

206/204	19.10205 ±0.05
207/204	15.71470 ±0.05
208/204	38.65319 ±0.05

MOLES PB PER GRAM

206	1.6314E-08
207	1.1000E-08
208	2.7228E-08
204	6.9036E-10
TOTAL	5.5233E-08

MOLES URANIUM PER GRAM

238	1.0460E-06
235	7.5864E-09

MOLES RADIOGENIC PB PER GRAM

206*	3.4285E-09
207*	2.1150E-10
208*	5.9072E-10

TOTAL PB = 22812.7 pg

RAD Pb = 1740.4 pg

TOTAL U = 500045.7 pg

Table 3.4. U-Pb analytical data for sample M90-K73 zircons, pick 1

sample weight: 75.6 µgm | Pb blank: 3.5 pg | Pb alpha (%/amu) 0.1240

spike weight: 0.0267 grams | U blank: 1.0 pg | U alpha (%/amu) -0.0514

RAW DATA

206/204	389.544	± 0.0740 %
206/207	11.7194687	± 0.0484 %
206/208	7.2207014	± 0.0480 %
206/205	4.0224385	± 0.0424 %
238/235	6.0194351	± 0.0560 %
233/235	0.9645809	± 0.0508 %

Total Common Pb: 74.3 pg

Radiogenic/Common: 6.4

(238/235)fc: 6.010156 Faraday/Daly

RATIOS CORRECTED FOR SPIKE AND BLANK

206/204	206/207	206/208
404.70	11.8019	7.3524
±2.337%	±1.009%	±1.608%

INITIAL PB

S&K	0.05 Ga
206/204	18.635073
207/204	15.625643
208/204	38.548436

	total	radiogenic
PPM Pb	6.25	5.31

208*/206* 0.043

Pb TOTAL LOAD 569 pg

U TOTAL LOAD 84928 pg

PPM U 855.87076

common Pb 70.8 pg (0.94 ppm)

206/238		207/235		207/206		Rho
0.00662	± 0.1494 %	0.04413	± 0.4653 %	0.048347	± 0.4449 %	.294543

206/238 Ma	207/235 Ma	207/206 Ma
42.5	43.8	116.3

SPIKE: MIT1B-C

206/205	0.052928
206/204	1523.933
206/207	97.467635
206/208	41.881202
[205]	1.76906E-11 moles/gram
[235]	1.61084E-09 moles/gram
235/205	91.0559

BLANK COMPOSITION

206/204	19.10205 ±0.05
207/204	15.71470 ±0.05
208/204	38.65319 ±0.05

MOLES PB PER GRAM

206	2.4775E-08
207	2.0992E-09
208	3.3696E-09
204	6.1219E-11
TOTAL	3.0305E-08

MOLES URANIUM PER GRAM

238	3.5700E-06
235	2.5892E-08

MOLES RADIOGENIC PB PER GRAM

206*	2.3634E-08
207*	1.1426E-09
208*	1.0097E-09

TOTAL PB = 472.6 pg

RAD Pb = 401.8 pg

TOTAL U = 64703.8 pg

Table 3.5. U-Pb analytical data for sample M90-K73 zircons, pick 2

sample weight: 79 µgm Pb blank: 3.5 pg Pb alpha (%/amu) 0.1240

spike weight: 0.0391 grams U blank: 1.0 pg U alpha (%/amu) -0.0358

RAW DATA

206/204	899.416	± 0.1200 %
206/207	15.24	± 0.0200 %
206/208	11.4283	± 0.0320 %
206/205	6.41707	± 0.0080 %
238/235	6.494222	± 0.1360 %
233/235	0.96139	± 0.0000 %

Total Common Pb: 75.0 pg

Radiogenic/Common: 13.9

(238/235)fc: 6.487242 Faraday/Daly

RATIOS CORRECTED FOR SPIKE AND BLANK

206/204	206/207	206/208
941.24	15.2872	11.5814
±2.380%	±0.571%	±1.107%

INITIAL PB S&K 0.05 Ga

206/204	18.635073
207/204	15.625643
208/204	38.548436

	total	radiogenic
PPM Pb	13.25	12.34
PPM U	1299.46434	

208*/206* 0.046

common Pb 71.5 pg (0.91 ppm)

Pb TOTAL LOAD 1188 pg

U TOTAL LOAD 132275 pg

206/238		207/235		207/206		Rho
0.01008	± 0.1567 %	0.06921	± 0.2423 %	0.049799	± 0.1862 %	.639865

64.7 Ma 67.9 Ma 185.6 Ma

SPIKE:	MIT1B-C
206/205	0.052928
206/204	1523.933
206/207	97.467635
206/208	41.881202
[205]	1.76906E-11 moles/gram
[235]	1.61084E-09 moles/gram
235/205	91.0559

BLANK COMPOSITION

206/204	19.10205 ±0.05
207/204	15.71470 ±0.05
208/204	38.65319 ±0.05

MOLES PB PER GRAM

206	5.5738E-08
207	3.6460E-09
208	4.8127E-09
204	5.9217E-11
TOTAL	6.4256E-08

MOLES URANIUM PER GRAM

238	5.4203E-06
235	3.9311E-08

MOLES RADIOGENIC PB PER GRAM

206*	5.4634E-08
207*	2.7207E-09
208*	2.5300E-09

TOTAL PB = 1046.6 pg

RAD Pb = 975.1 pg

TOTAL U = 102657.7 pg

Table 3.6. U-Pb analytical data for sample M90-K73 zircons, pick 3

sample weight: 144 µgm | Pb blank: 3.5 pg | Pb alpha (%/amu) 0.1240

spike weight: 0.033 grams | U blank: 1.0 pg | U alpha (%/amu) -0.0107

RAW DATA

206/204	1406.168	± 0.1600 %
206/207	16.3959	± 0.0200 %
206/208	15.6116	± 0.0200 %
206/205	15.6385	± 0.0200 %
238/235	11.9828	± 0.0200 %
233/235	0.921671	± 0.0000 %

Total Common Pb: 98.9 pg

Radiogenic/Common: 21.4

(238/235)fc

11.978966 Faraday/Daly

RATIOS CORRECTED FOR SPIKE AND BLANK

206/204	206/207	206/208
1459.85	16.4267	15.7682
±1.804%	±0.301%	±0.739%

INITIAL PB

S&K	0.05 Ga
206/204	18.635073
207/204	15.625643
208/204	38.548436

	total	radiogenic
PPM Pb	14.66	14.00

208*/206* 0.037

Pb TOTAL LOAD 2231 pg

U TOTAL LOAD 192064 pg

PPM U 1160.19070

common Pb 95.4 pg (0.66 ppm)

206/238		207/235		207/206		Rho
0.01290	± 0.0540 %	**0.09039**	± 0.1348 %	**0.050822**	± 0.1241 %	.389757
82.6 Ma		**87.9** Ma		**233.1** Ma		

SPIKE: MIT1B-C

206/205	0.052928
206/204	1523.933
206/207	97.467635
206/208	41.881202
[205]	1.76906E-11 moles/gram
[235]	1.61084E-09 moles/gram
235/205	91.0559

BLANK COMPOSITION

206/204	19.10205 ±0.05
207/204	15.71470 ±0.05
208/204	38.65319 ±0.05

MOLES PB PER GRAM

206	6.3234E-08
207	3.8495E-09
208	4.0102E-09
204	4.3315E-11
TOTAL	7.1137E-08

MOLES URANIUM PER GRAM

238	4.8393E-06
235	3.5098E-08

MOLES RADIOGENIC PB PER GRAM

206*	6.2427E-08
207*	3.1726E-09
208*	2.3405E-09

TOTAL PB = 2111.6 pg

RAD Pb = 2016.3 pg

TOTAL U = 167067.5 pg

Table 3.7. U-Pb analytical data for sample M90-K73 zircons, pick 4

sample weight: 129 µgm | Pb blank: 3.5 pg | Pb alpha (%/amu) 0.1240

spike weight: 0.0293 grams | U blank: 1.0 pg | U alpha (%/amu) -0.0840

RAW DATA

206/204	1603.6778	± 0.1800 %
206/207	16.5483611	± 0.0312 %
206/208	10.955233	± 0.0380 %
206/205	16.213633	± 0.0320 %
238/235	15.855	± 0.0600 %
233/235	0.89228	± 0.0000 %

Total Common Pb: 79.9 pg

Radiogenic/Common: 24.9

(238/235)fc: 15.815039 Faraday/Daly

RATIOS CORRECTED FOR SPIKE AND BLANK

206/204	206/207	206/208
1680.18	16.5908	11.0217
±2.257%	±0.330%	±0.557%

INITIAL PB S&K 0.03 Ga

206/204	18.665456
207/204	15.627084
208/204	38.584952

	total	radiogenic
PPM Pb	15.43	14.84
PPM U	1566.10200	

208*/206* 0.069

common Pb 76.4 pg (0.59 ppm)

Pb TOTAL LOAD 2097 pg

U TOTAL LOAD 224221 pg

206/238		207/235		207/206		Rho
0.00984	± 0.0879 %	0.06991	± 0.1432 %	0.051546	± 0.1135 %	.609906
63.1 Ma		68.6 Ma		265.4 Ma		

SPIKE: MIT1B-C

206/205	0.052928
206/204	1523.933
206/207	97.467635
206/208	41.881202
[205]	1.76906E-11 moles/gram
[235]	1.61084E-09 moles/gram
235/205	91.0559

BLANK COMPOSITION

206/204	19.10205 ±0.05
207/204	15.71470 ±0.05
208/204	38.65319 ±0.05

MOLES PB PER GRAM

206	6.4983E-08
207	3.9168E-09
208	5.8959E-09
204	3.8676E-11
TOTAL	7.4834E-08

MOLES URANIUM PER GRAM

238	6.5324E-06
235	4.7378E-08

MOLES RADIOGENIC PB PER GRAM

206*	6.4261E-08
207*	3.3124E-09
208*	4.4036E-09

TOTAL PB = 1990.4 pg

RAD Pb = 1914.0 pg

TOTAL U = 202027.2 pg

Table 3.8. U-Pb analytical data for sample M90-K73 zircons, pick 5

sample weight: 156 µgm | Pb blank: 3.5 pg | Pb alpha (%/amu) 0.1240

spike weight: 0.0305 grams | U blank: 1.0 pg | U alpha (%/amu) -0.0001

RAW DATA

206/204	44.6903665	± 0.0424 %
206/207	2.6881096	± 0.0078 %
206/208	1.1039249	± 0.0072 %
206/205	24.6800962	± 0.0338 %
238/235	10.88722	± 0.0200 %
233/235	0.92986	± 0.0000 %

Total Common Pb: 4079.8 pg

Radiogenic/Common: 1.6

(238/235)fc: 10.887189 Faraday/Daly

RATIOS CORRECTED FOR SPIKE AND BLANK

206/204	206/207	206/208
44.73	2.6802	1.0993
±0.086%	±0.042%	±0.075%

INITIAL PB S&K 2.00 Ga

206/204	15.160221
207/204	15.193093
208/204	34.798778

	total	radiogenic
PPM Pb	40.66	14.53

208*/206* 0.199

Pb TOTAL LOAD 6454 pg

U TOTAL LOAD 162224 pg

PPM U 891.80196

common Pb 4076.3 pg (26.13 ppm)

206/238		207/235		207/206		Rho
0.01515	± 0.5176 %	0.10562	± 5.1692 %	0.050557	± 5.1874 %	.014833
96.9 Ma		101.9 Ma		221.0 Ma		

SPIKE: MIT1B-C

206/205	0.052928
206/204	1523.933
206/207	97.467635
206/208	41.881202
[205]	1.76906E-11 moles/gram
[235]	1.61084E-09 moles/gram
235/205	91.0559

BLANK COMPOSITION

206/204	19.10205 ±0.05
207/204	15.71470 ±0.05
208/204	38.65319 ±0.05

MOLES PB PER GRAM

206	8.5257E-08
207	3.1810E-08
208	7.7554E-08
204	1.9061E-09
TOTAL	1.9653E-07

MOLES URANIUM PER GRAM

238	3.7198E-06
235	2.6979E-08

MOLES RADIOGENIC PB PER GRAM

206*	5.6360E-08
207*	2.8494E-09
208*	1.1222E-08

TOTAL PB = 6343.4 pg

RAD Pb = 2267.1 pg

TOTAL U = 139121.1 pg

Table 3.9. U-Pb analytical data for sample M90-K73 zircons, pick 6

sample weight: 62.4 µgm | Pb blank: 3.5 pg | Pb alpha (%/amu) 0.1240

spike weight: 0.0234 grams | U blank: 1.0 pg | U alpha (%/amu) 0.0807

RAW DATA

206/204	1853.5852	± 0.4000 %
206/207	17.490136	± 0.2000 %
206/208	12.397799	± 0.1400 %
206/205	9.12966	± 0.1200 %
238/235	7.73585	± 0.1000 %
233/235	0.954339	± 0.0000 %

Total Common Pb: 31.0 pg

Radiogenic/Common: 28.4

(238/235)fc: 7.754571 Faraday/Daly

RATIOS CORRECTED FOR SPIKE AND BLANK

206/204	206/207	206/208
2093.23	17.6562	12.6659
±6.277%	±0.807%	±1.429%

INITIAL PB S&K 0.03 Ga

206/204	18.665456
207/204	15.627084
208/204	38.584952

	total	radiogenic
PPM Pb	14.10	13.66
PPM U	1188.62282	

208*/206* 0.061

common Pb 27.5 pg (0.44 ppm)

Pb TOTAL LOAD 965 pg

U TOTAL LOAD 91895 pg

206/238	207/235	207/206	Rho
0.01204 ± 0.1748 %	0.08235 ± 0.3127 %	0.049614 ± 0.2585 %	.562647
77.1 Ma	80.4 Ma	177.2 Ma	

SPIKE:	MIT1B-C	MOLES PB PER GRAM		MOLES RADIOGENIC PB PER GRAM	
206/205	0.052928	206	6.0221E-08	206*	5.9684E-08
206/204	1523.933	207	3.4107E-09	207*	2.9612E-09
206/207	97.467635	208	4.7546E-09	208*	3.6445E-09
206/208	41.881202	204	2.8769E-11		
[205]	1.76906E-11 moles/gram	TOTAL	6.8415E-08		
[235]	1.61084E-09 moles/gram				
235/205	91.0559			TOTAL PB = 880.1 pg	
BLANK COMPOSITION		MOLES URANIUM PER GRAM		RAD Pb = 852.6 pg	
206/204	19.10205 ±0.05	238	4.9579E-06	TOTAL U = 74170.1 pg	
207/204	15.71470 ±0.05	235	3.5958E-08		
208/204	38.65319 ±0.05				

Table 3.10. U-Pb analytical data for sample M90-K73 zircons, pick 7 (single grain)

sample weight: 14.7 µgm | Pb blank: 3.5 pg | Pb alpha (%/amu) 0.1240

spike weight: 0.0308 grams | U blank: 1.0 pg | U alpha (%/amu) 0.0329

RAW DATA

206/204	125.3264116	± 0.2012 %
206/207	6.6214088	± 0.3310 %
206/208	2.7301379	± 0.1204 %
206/205	0.2133777	± 0.0372 %
238/235	0.40139	± 0.0600 %
233/235	1.0073	± 0.0000 %

Total Common Pb: 12.2 pg

Radiogenic/Common: 2.2

(238/235)fc 0.401786 Faraday/Daly

RATIOS CORRECTED FOR SPIKE AND BLANK

206/204	206/207	206/208
122.26	6.0571	2.5005
±14.079%	±10.389%	±10.583%

INITIAL PB S&K 2.85 Ga

206/204	13.283344
207/204	14.527559
208/204	33.047706

	total	radiogenic
PPM Pb	1.84	1.25

208*/206* 0.145

Pb TOTAL LOAD 139 pg

U TOTAL LOAD 28021 pg

PPM U 319.11376

common Pb 8.7 pg (0.59 ppm)

206/238		207/235		207/206		Rho
0.00379	± 2.7987 %	**0.02714**	± 4.9477 %	**0.051915**	± 3.3567 %	.759911

24.4 Ma **27.2** Ma **281.8** Ma

SPIKE: MIT1B-C

206/205	0.052928
206/204	1523.933
206/207	97.467635
206/208	41.881202
[205]	1.76906E-11 moles/gram
[235]	1.61084E-09 moles/gram
235/205	91.0559

BLANK COMPOSITION

206/204	19.10205 ±0.05
207/204	15.71470 ±0.05
208/204	38.65319 ±0.05

MOLES PB PER GRAM

206	5.6623E-09
207	9.3482E-10
208	2.2645E-09
204	4.6312E-11
TOTAL	8.9079E-09

MOLES URANIUM PER GRAM

238	1.3311E-06
235	9.6538E-09

MOLES RADIOGENIC PB PER GRAM

206*	5.0471E-09
207*	2.6202E-10
208*	7.3397E-10

TOTAL PB = 27.1 pg

RAD Pb = 18.3 pg

TOTAL U = 4691.0 pg

Table 4. $^{40}Ar/^{39}Ar$ dates and sample characteristics, Symvolon granodiorite, Rhodope metamorphic core complex, NE Greece

Sample	Mineral	Size fraction	J*	Heating method	Steps†	Age (Ma)	Correlation method
M90-K5	K-feldspar	80 – 100	0.00567	furnace step-heat	10	15.0 ± 0.1	York 1
"	biotite	80 – 150	0.00576	furnace step-heat	10	15.5 ± 0.3	York 2; MSWD‡ = 0.6
"	"	80 – 150	0.00581	laser fusion	10	15.4 ± 0.3	York 2; MSWD = 1.1
"	hornblende	80 – 150	0.00581	laser fusion	14	21.7 ± 0.4	York 2; MSWD = 1.4
M90-K12	biotite	80 – 100	0.00583	laser fusion	10	11.1 ± 0.2	York 2; MSWD = 1.1
M90-K71	hornblende	80 – 150	0.00574	furnace step-heat	10	20.1 ± 0.3	York 1
"	"	80 – 150	0.00581	laser fusion	11	20.8 ± 0.4	York 2; MSWD = 1.7
M90-K73	K-feldspar	80 – 100	0.00566	furnace step-heat	10	13.8 ± 0.3	York 2; MSWD = 0.5
"	biotite	60 – 80	0.00576	furnace step-heat	10	14.1 ± 0.5	York 1
"	"	60 – 80	0.00581	laser fusion	10	12.8 ± 0.3	York 2; MSWD = 1.6
"	"	80 – 150	0.00573	furnace step-heat	10	13.9 ± 0.3	York 2; MSWD = 2.2
"	hornblende	80 – 100	0.00583	laser fusion	10	21.4 ± 0.4	York 2; MSWD = 0.3
M90-K79	K-feldspar	60 – 80	0.00576	furnace step-heat	10	13.4 ± 1.7	York 1
"	biotite	60 – 80	0.00573	furnace step-heat	10	13.4 ± 0.3	York 2; MSWD = 0.4
"	"	60 – 80	0.00584	laser fusion	10	13.7 ± 0.3	York 2; MSWD = 2.1
"	hornblende	60 – 80	0.00576	furnace step-heat	12	20.1 ± 0.4	York 2; MSWD = 0.9
"	"	60 – 80	0.00584	laser fusion	20	21.3 ± 3.1	York 1

* ±0.00005

† Number of heating increments for furnace step-heat analyses; number of 1- to 5-grain subsamples for laser-fusion analyses.

‡ Mean squared weighted deviation.

Table 5.1. $^{40}Ar/^{39}Ar$ ANALYTICAL DATA FOR SAMPLE M90-K5, K-FELDSPAR

T(K)	$^{39}Ar/^{40}Ar$	$^{36}Ar/^{40}Ar$	^{39}Ar (%)	$^{40}Ar^*$ (%)	K/Ca	Age (Ma) (± 2σ)
800	0.4662	0.0011	7.5	67.5	21.5	14.8 ± 0.3
900	0.6879	0.0000	6.3	98.8	25.0	14.6 ± 0.3
1000	0.6883	0.0001	11.6	98.4	22.5	14.6 ± 0.3
1100	0.6789	0.0000	10.9	100.0	22.1	15.0 ± 0.3
1200	0.6560	0.0002	7.3	95.4	34.0	14.8 ± 0.3
1300	0.5923	0.0003	14.0	91.5	32.3	15.7 ± 0.3
1400	0.5331	0.0005	24.4	85.1	84.2	16.3 ± 0.3
1500	0.5054	0.0007	10.0	79.0	112.2	15.9 ± 0.3
1600	0.5084	0.0006	5.4	81.9	49.1	16.4 ± 0.3
1700	0.4999	0.0005	2.6	85.0	37.9	17.3 ± 0.3

York 1 age = 15.0 ± 0.1 Ma. $[^{40}Ar/^{36}Ar]_0$ = 400 ± 90. J = 0.00567 ± 0.00005.

Table 5.2. $^{40}Ar/^{39}Ar$ ANALYTICAL DATA FOR SAMPLE M90-K5, BIOTITE

T(K)	$^{39}Ar/^{40}Ar$	$^{36}Ar/^{40}Ar$	^{39}Ar (%)	$^{40}Ar^*$ (%)	K/Ca	Age (Ma) (± 2σ)
900	0.1026	.0030	28.3	11.6	73.9	11.7 ± 0.4
950	0.3410	.0016	7.3	52.3	137.6	15.9 ± 0.3
1000	0.3267	.0017	6.0	49.8	59.5	15.8 ± 0.3
1050	0.3064	.0018	4.8	47.8	21.6	16.2 ± 0.3
1100	0.2901	.0019	6.0	43.0	13.7	15.3 ± 0.3
1150	0.3012	.0020	11.1	42.4	29.9	14.6 ± 0.3
1200	0.3260	.0019	10.8	43.1	8.3	13.7 ± 0.3
1250	0.3343	.0018	13.5	46.6	7.7	14.4 ± 0.3
1350	0.4551	.0011	10.0	68.3	3.4	15.5 ± 0.3
1550	0.3927	.0017	2.2	48.8	3.7	12.9 ± 0.3

York 2 isochron age = 15.5 ± 0.3 Ma. MSWD = 0.6. $[^{40}Ar/^{36}Ar]_0$ = 280 ± 10. J = 0.00576 ± 0.00005.

Table 5.3. $^{40}Ar/^{39}Ar$ ANALYTICAL DATA FOR SAMPLE M90-K71, HORNBLENDE

T(K)	$^{39}Ar/^{40}Ar$	$^{36}Ar/^{40}Ar$	^{39}Ar (%)	$^{40}Ar^*$ (%)	K/Ca	Age (Ma) (± 2σ)
1100	0.4846	0.0008	20.7	76.4	0.2	16.3 ± 0.3
1150	0.5016	0.0004	8.4	87.3	0.2	17.9 ± 0.4
1175	0.5275	0.0002	18.1	94.3	0.2	18.4 ± 0.4
1200	0.5391	-0.0001	17.0	103.9	0.2	19.9 ± 0.4
1225	0.4955	0.0002	3.4	93.1	0.2	19.4 ± 0.4
1250	0.4842	0.0002	3.3	93.2	0.2	19.8 ± 0.4
1275	0.5091	0.0000	10.5	99.8	0.2	20.2 ± 0.4
1300	0.5191	0.0001	14.5	98.1	0.2	19.5 ± 0.4
1350	0.4921	0.0001	3.1	96.7	0.2	20.2 ± 0.4
1550	0.4012	0.0007	1.0	80.1	0.2	20.6 ± 0.4

York 1 age = 20.1 ± 0.3 Ma. $[^{40}Ar/^{36}Ar]_0$ = 270 ± 80. J = 0.00574 ± 0.00005.

Table 5.4. $^{40}Ar/^{39}Ar$ ANALYTICAL DATA FOR SAMPLE M90-K73, K-FELDSPAR

T(K)	$^{39}Ar/^{40}Ar$	$^{36}Ar/^{40}Ar$	^{39}Ar (%)	$^{40}Ar^*$ (%)	K/Ca	Age (Ma) (± 2σ)
800	0.3499	0.0020	6.1	42.3	9.5	12.3 ± 0.2
900	0.8208	0.0002	6.1	92.9	9.1	11.5 ± 0.2
1000	0.8533	0.0003	9.2	92.2	8.2	11.0 ± 0.2
1100	0.8090	0.0003	7.8	89.7	8.0	11.3 ± 0.2
1200	0.6886	0.0006	7.5	81.0	13.5	12.0 ± 0.2
1300	0.5213	0.0010	11.6	71.3	16.4	13.9 ± 0.3
1400	0.4002	0.0015	31.1	55.3	32.6	14.1 ± 0.3
1500	0.3535	0.0018	12.8	47.6	24.7	13.7 ± 0.3
1600	0.3521	0.0017	4.5	48.9	19.0	14.1 ± 0.3
1700	0.3477	0.0017	3.3	49.1	13.5	14.4 ± 0.3

York 2 isochron age = 13.8 ± 0.3 Ma. MSWD = 0.5. $[^{40}Ar/^{36}Ar]_0$ = 300 ± 10. J = 0.00566 ± 0.00005.

Table 5.5. $^{40}Ar/^{39}Ar$ ANALYTICAL DATA FOR SAMPLE M90-K73, BIOTITE (100-150 MESH)

T(K)	$^{39}Ar/^{40}Ar$	$^{36}Ar/^{40}Ar$	^{39}Ar (%)	$^{40}Ar^*$ (%)	K/Ca	Age (Ma) (± 2σ)
900	0.4395	0.0014	25.8	59.2	101.7	13.9 ± 0.3
950	0.5784	0.0007	6.7	77.9	274.4	13.9 ± 0.3
1000	0.5317	0.0009	5.1	73.7	63.0	14.3 ± 0.3
1050	0.5139	0.0010	4.5	70.2	31.9	14.1 ± 0.3
1100	0.5363	0.0009	6.2	72.6	45.3	13.9 ± 0.3
1150	0.5553	0.0009	12.1	74.2	76.5	13.8 ± 0.3
1200	0.5861	0.0007	13.0	79.2	56.1	13.9 ± 0.3
1250	0.5905	0.0008	13.6	75.7	44.4	13.2 ± 0.3
1350	0.6024	0.0008	9.5	77.6	31.6	13.3 ± 0.3
1550	0.5632	0.0004	3.5	89.6	59.5	16.4 ± 0.3

York 2 isochron age = 13.9 ± 0.3 Ma. MSWD = 2.2. $[^{40}Ar/^{36}Ar]_0$ = 290 ± 20. J = 0.00573 ± 0.00005.

Table 5.6. $^{40}Ar/^{39}Ar$ ANALYTICAL DATA FOR SAMPLE M90-K73, BIOTITE (>80 MESH)

T(K)	$^{39}Ar/^{40}Ar$	$^{36}Ar/^{40}Ar$	^{39}Ar (%)	$^{40}Ar^*$ (%)	K/Ca	Age (Ma) (± 2σ)
900	0.3748	0.0017	39.4	49.7	122.4	13.7 ± 0.3
950	0.5659	0.0007	4.4	78.8	86.1	14.4 ± 0.3
1000	0.5175	0.0011	5.8	67.8	32.7	13.6 ± 0.3
1050	0.5014	0.0010	5.0	70.7	28.0	14.6 ± 0.3
1100	0.5025	0.0011	7.0	68.0	36.5	14.0 ± 0.3
1150	0.5433	0.0009	10.6	73.0	70.2	13.9 ± 0.3
1200	0.5711	0.0007	9.5	79.3	35.6	14.4 ± 0.3
1250	0.5826	0.0007	9.6	78.1	42.6	13.9 ± 0.3
1350	0.5897	0.0006	5.7	83.0	12.1	14.6 ± 0.3
1550	0.5199	0.0006	3.0	82.0	17.1	16.3 ± 0.3

York 1 age = 14.1 ± 0.5 Ma. $[^{40}Ar/^{36}Ar]_0$ = 290 ± 20. J = 0.00576 ± 0.00005.

Table 5.7. $^{40}Ar/^{39}Ar$ ANALYTICAL DATA FOR SAMPLE M90-K79, K-FELDSPAR

T(K)	$^{39}Ar/^{40}Ar$	$^{36}Ar/^{40}Ar$	^{39}Ar (%)	$^{40}Ar^*$ (%)	K/Ca	Age (Ma) (± 2σ)
800	0.2897	0.0018	5.5	46.8	10.2	16.7 ± 0.3
900	0.8435	0.0002	4.5	92.7	23.2	11.4 ± 0.2
1000	0.8156	0.0002	6.8	95.4	20.1	12.1 ± 0.2
1100	0.6189	0.0009	5.1	74.3	16.3	12.4 ± 0.2
1200	0.5481	0.0008	7.1	75.3	30.2	14.2 ± 0.3
1300	0.5399	0.0006	15.8	81.1	48.3	15.5 ± 0.3
1400	0.5038	0.0008	30.8	75.9	93.6	15.6 ± 0.3
1500	0.4852	0.0010	13.1	69.9	65.6	14.9 ± 0.3
1600	0.4953	0.0010	6.8	70.2	42.8	14.7 ± 0.3
1700	0.5069	0.0011	4.5	67.4	26.3	13.8 ± 0.3

York 1 age = 13.4 ± 1.7 Ma. $[^{40}Ar/^{36}Ar]_0$ = 430 ± 110. J = 0.00576 ± 0.00005.

Table 5.8. $^{40}Ar/^{39}Ar$ ANALYTICAL DATA FOR SAMPLE M90-K79, BIOTITE

T(K)	$^{39}Ar/^{40}Ar$	$^{36}Ar/^{40}Ar$	^{39}Ar (%)	$^{40}Ar^*$ (%)	K/Ca	Age (Ma) (± 2σ)
900	0.2402	0.0022	9.6	33.6	303.9	14.4 ± 0.3
950	0.5257	0.0010	11.0	70.5	193.7	13.8 ± 0.3
1000	0.6306	0.0004	7.5	87.7	154.5	14.3 ± 0.3
1050	0.6345	0.0006	5.4	83.7	85.0	13.6 ± 0.3
1100	0.6091	0.0005	6.5	84.9	58.1	14.3 ± 0.3
1150	0.6353	0.0006	13.3	82.8	22.0	13.4 ± 0.3
1200	0.6531	0.0005	14.1	86.5	9.7	13.6 ± 0.3
1250	0.6234	0.0006	15.0	83.0	7.0	13.7 ± 0.3
1350	0.6148	0.0007	15.3	78.5	15.2	13.2 ± 0.3
1550	0.5421	0.0014	2.3	58.3	10.2	11.1 ± 0.2

York 2 isochron age = 13.4 ± 0.3 Ma. MSWD = 0.4. $[^{40}Ar/^{36}Ar]_0$ = 300 ± 20. J = 0.00573 ± 0.00005.

Table 5.9. $^{40}Ar/^{39}Ar$ ANALYTICAL DATA FOR SAMPLE M90-K79, HORNBLENDE

T(K)	$^{39}Ar/^{40}Ar$	$^{36}Ar/^{40}Ar$	^{39}Ar (%)	$^{40}Ar^*$ (%)	K/Ca	Age (Ma) (± 2σ)
1100	0.3362	0.0007	2.8	79.0	0.2	24.2 ± 0.5
1150	0.4004	0.0004	6.3	86.8	0.2	22.4 ± 0.4
1175	0.4137	0.0003	8.2	89.7	0.1	22.4 ± 0.4
1200	0.4782	0.0002	23.8	94.1	0.1	20.3 ± 0.4
1220	0.5264	0.0001	18.9	97.7	0.2	19.2 ± 0.4
1240	0.4405	0.0015	1.2	57.0	0.2	13.4 ± 0.3
1260	0.4353	0.0007	3.6	80.6	0.1	19.1 ± 0.4
1280	0.4509	0.0002	7.6	94.2	0.1	21.6 ± 0.4
1300	0.4874	0.0002	16.0	95.3	0.1	20.2 ± 0.4
1325	0.5048	0.0000	9.2	98.8	0.1	20.2 ± 0.4
1350	0.4809	0.0001	1.2	97.4	0.1	20.9 ± 0.4
1550	0.3949	0.0010	1.2	70.4	0.1	18.4 ± 0.4

York 2 isochron age = 20.1 ± 0.4 Ma. MSWD = 0.9. $[^{40}Ar/^{36}Ar]_0$ = 480 ± 50. J = 0.00576 ± 0.00005.

Table 6.1. $^{40}Ar/^{39}Ar$ LASER-FUSION ANALYTICAL DATA FOR SAMPLE M90-K5, BIOTITE

Subsample	$^{40}Ar^*$ (x10^{-15} moles)	$^{39}Ar_K$ (x10^{-15} moles)	$^{38}Ar_{Cl}$ (x10^{-17} moles)	$^{37}Ar_{Ca}$ (x10^{-17} moles)	$^{36}Ar_{atm.}$ (x10^{-17} moles)	Age (Ma) (± 2σ)‡
1	5.7491 ± 0.0002	4.9606 ± 0.0001	6.9110 ± 0.0006	2.7157 ± 0.0021	2.7811 ± 0.0016	12.0 ± 0.1
2	10.1802 ± 0.0002	11.2635 ± 0.0003	24.9595 ± 0.0012	24.2089 ± 0.0032	18.1426 ± 0.0018	9.4 ± 0.2
3	3.5914 ± 0.0004	3.6401 ± 0.0001	6.4372 ± 0.0005	3.6109 ± 0.0021	3.2784 ± 0.0016	10.2 ± 0.1
4	14.3862 ± 0.0005	10.2084 ± 0.0001	12.3708 ± 0.0005	31.0897 ± 0.0021	3.5215 ± 0.0017	14.6 ± 0.1
5	12.4462 ± 0.0003	8.0259 ± 0.0001	14.5608 ± 0.0009	5.7337 ± 0.0025	5.7337 ± 0.0025	16.0 ± 0.2
6	7.6685 ± 0.0001	10.2835 ± 0.0003	32.3903 ± 0.0023	19.9790 ± 0.0040	11.5165 ± 0.0016	7.7 ± 0.1
7	4.2623 ± 0.0010	3.1302 ± 0.0005	5.3864 ± 0.0017	1.9192 ± 0.0032	1.3856 ± 0.0019	14.1 ± 0.2
8	9.8789 ± 0.0009	7.1416 ± 0.0001	10.4809 ± 0.0007	19.3565 ± 0.0021	2.0389 ± 0.0016	14.3 ± 0.2
9	7.5279 ± 0.0005	6.0745 ± 0.0002	10.4909 ± 0.0006	0.8312 ± 0.0036	2.9451 ± 0.0016	12.8 ± 0.1
10	5.767 ± 0.0009	4.9708 ± 0.0002	9.3061 ± 0.0010	5.9009 ± 0.0023	4.5140 ± 0.0017	12.0 ± 0.3

York 2 isochron age = 15.4 ± 0.3 Ma. MSWD = 1.1. $[^{40}Ar/^{36}Ar]_0$ = 260 ± 10. J value: 0.00581 ± 0.00005. Size fraction: 80 - 150.

* denotes radiogenic isotope. ‡ Apparent age assuming $[^{40}Ar/^{36}Ar]_0$ = 295.5 (atmospheric).

Table 6.2. $^{40}Ar/^{39}Ar$ LASER-FUSION ANALYTICAL DATA FOR SAMPLE M90-K5, HORNBLENDE

Subsample	$^{40}Ar^*$ (x10^{-15} moles)	$^{39}Ar_K$ (x10^{-15} moles)	$^{38}Ar_{Cl}$ (x10^{-17} moles)	$^{37}Ar_{Ca}$ (x10^{-15} moles)	$^{36}Ar_{atm.}$ (x10^{-17} moles)	Age (Ma) (± 2σ)‡
1	2.3224 ± 0.0007	2.1407 ± 0.0001	15.2068 ± 0.0020	7.3417 ± 0.0006	1.4982 ± 0.0005	11.3 ± 0.2
2	1.0305 ± 0.0010	0.6073 ± 0.00002	5.1541 ± 0.0004	3.8297 ± 0.0003	0.1090 ± 0.0001	17.7 ± 0.2
3	2.4080 ± 0.0019	1.3089 ± 0.00004	11.6705 ± 0.0011	7.9474 ± 0.0003	0.1172 ± 0.0002	19.2 ± 0.2
4	1.4713 ± 0.0008	1.7349 ± 0.0001	28.8046 ± 0.0016	7.6197 ± 0.0004	1.0165 ± 0.0006	8.9 ± 0.2
5	4.3836 ± 0.0024	3.0648 ± 0.00001	23.8303 ± 0.0019	17.9119 ± 0.0009	1.1459 ± 0.0005	14.9 ± 0.2
6	3.4644 ± 0.0022	2.2608 ± 0.0002	17.4514 ± 0.0031	12.1164 ± 0.0010	0.5887 ± 0.0002	16.0 ± 0.2
7	8.0196 ± 0.0034	4.4539 ± 0.0001	55.0548 ± 0.0066	18.7395 ± 0.0013	1.2548 ± 0.0004	18.8 ± 0.2
8	1.4305 ± 0.0005	1.1602 ± 0.0002	8.0580 ± 0.0010	7.3206 ± 0.0008	0.4148 ± 0.0008	12.9 ± 0.2
9	5.7168 ± 0.0031	3.55818 ± 0.0003	24.0677 ± 0.0030	19.2598 ± 0.0014	0.6411 ± 0.0005	16.8 ± 0.2
10	4.2976 ± 0.0022	3.4829 ± 0.0002	36.0832 ± 0.0067	14.4450 ± 0.0011	2.2373 ± 0.0002	12.9 ± 0.3
11	5.3541 ± 0.0011	2.7915 ± 0.0002	27.9307 ± 0.0023	10.6284 ± 0.0006	0.4305 ± 0.0004	20.0 ± 0.2
12	4.3956 ± 0.0020	3.5416 ± 0.0003	35.0496 ± 0.0014	12.7727 ± 0.0020	1.9061 ± 0.0007	13.0 ± 0.3
13	9.1550 ± 0.0036	7.3600 ± 0.0003	67.5138 ± 0.0039	21.2414 ± 0.0009	3.5270 ± 0.0005	13.0 ± 0.4
14	6.7971 ± 0.0026	6.6841 ± 0.0001	57.6405 ± 0.0059	21.6186 ± 0.0012	3.6233 ± 0.0004	10.6 ± 0.4

York 2 isochron age = 21.7 ± 0.4 Ma. MSWD = 1.4. $[^{40}Ar/^{36}Ar]_0$ = 150 ± 30. J value: 0.00581 ± 0.00005. Size fraction: 80 - 150.

* denotes radiogenic isotope. ‡ Apparent age assuming $[^{40}Ar/^{36}Ar]_0$ = 295.5 (atmospheric).

Table 6.3. $^{40}Ar/^{39}Ar$ LASER-FUSION ANALYTICAL DATA FOR SAMPLE M90-K12, BIOTITE

Subsample	$^{40}Ar^*$ (x10^{-15} moles)	$^{39}Ar_K$ (x10^{-15} moles)	$^{38}Ar_{Cl}$ (x10^{-16} moles)	$^{37}Ar_{Ca}$ (x10^{-17} moles)	$^{36}Ar_{atm.}$ (x10^{-17} moles)	Age (Ma) (± 2σ)‡
1	4.9898 ± 0.0001	8.2143 ± 0.0002	3.8598 ± 0.0001	9.1170 ± 0.0020	9.9294 ± 0.0015	6.4 ± 0.1
2	5.6369 ± 0.0001	10.2581 ± 0.0002	6.2102 ± 0.0003	13.4904 ± 0.0021	13.7595 ± 0.0011	5.8 ± 0.2
3	9.0468 ± 0.0003	19.8376 ± 0.0007	9.6642 ± 0.0006	22.3333 ± 0.0023	34.0343 ± 0.0011	4.8 ± 1.0
4	5.0290 ± 0.0001	15.5918 ± 0.0009	7.5216 ± 0.0004	16.7654 ± 0.0076	29.5198 ± 0.0064	3.4 ± 0.9
5	3.2266 ± 0.0001	5.5363 ± 0.0002	2.5334 ± 0.0001	8.2146 ± 0.0012	8.2617 ± 0.0010	6.1 ± 0.1
6	3.7695 ± 0.0001	6.8646 ± 0.0003	3.4022 ± 0.0001	14.1922 ± 0.0022	9.2834 ± 0.0014	5.8 ± 0.1
7	12.6806 ± 0.0003	22.6482 ± 0.0004	10.5360 ± 0.0007	91.7982 ± 0.0096	29.3199 ± 0.0024	5.9 ± 0.4
8	6.4696 ± 0.0001	20.8990 ± 0.0013	10.0197 ± 0.0008	32.3267 ± 0.0050	40.6922 ± 0.0031	3.3 ± 1.1
9	9.8809 ± 0.0003	13.0431 ± 0.0008	5.5243 ± 0.0004	10.2096 ± 0.0051	12.0062 ± 0.0017	7.9 ± 0.2
10	7.5272 ± 0.0001	15.7695 ± 0.0008	7.4812 ± 0.0001	20.4898 ± 0.0023	23.1030 ± 0.0018	5.0 ± 0.4

York 2 isochron age = 11.1 ± 0.2 Ma. MSWD = 1.1. $[^{40}Ar/^{36}Ar]_0$ = 260 ± 10. J value: 0.00583 ± 0.00005. Size fraction: 80 - 100.

* denotes radiogenic isotope. ‡ Apparent age assuming $[^{40}Ar/^{36}Ar]_0$ = 295.5 (atmospheric).

Table 6.4. $^{40}Ar/^{39}Ar$ LASER-FUSION ANALYTICAL DATA FOR SAMPLE M90-K71, HORNBLENDE

Subsample	$^{40}Ar^*$ (x10^{-15} moles)	$^{39}Ar_K$ (x10^{-15} moles)	$^{38}Ar_{Cl}$ (x10^{-16} moles)	$^{37}Ar_{Ca}$ (x10^{-15} moles)	$^{36}Ar_{atm.}$ (x10^{-17} moles)	Age (Ma) (± 2σ)‡
1	1.8896 ± .0015	1.0123 ± .0002	3.5234 ± .0011	5.2619 ± .0005	0.1500 ± .0005	19.5 ± 0.2
2	1.7007 ± .0009	0.8372 ± .0002	2.5841 ± .0004	4.3505 ± .0004	0.0533 ± .0004	21.2 ± 0.2
3	3.1408 ± .0019	1.5640 ± .0003	4.5888 ± .0007	7.5385 ± .0007	0.1505 ± .0002	20.9 ± 0.2
4	2.3997 ± .0016	1.2143 ± .0003	3.7477 ± .0002	6.2608 ± .0009	0.1500 ± .0003	20.6 ± 0.2
5	7.6706 ± .0019	5.1629 ± .0007	5.3271 ± .0004	19.9446 ± .0039	1.1589 ± .0005	15.5 ± 0.2
6	2.2637 ± .0015	1.4409 ± .0003	4.5654 ± .0005	7.2854 ± .0002	0.2794 ± .0006	16.4 ± 0.2
7	4.3559 ± .0014	2.7593 ± .0003	1.8598 ± .0002	2.4206 ± .0002	0.3220 ± .0007	16.5 ± 0.1
8	3.5346 ± .0015	2.7464 ± .0003	2.0841 ± .0005	9.5364 ± .0011	1.2570 ± .0013	13.4 ± 0.2
9	2.4440 ± .0014	1.4580 ± .0001	4.6682 ± .0008	7.4239 ± .0008	0.1509 ± .0002	17.5 ± 0.2
10	0.8428 ± .0009	0.5057 ± .0001	1.5794 ± .0002	2.6028 ± .0003	0.0284 ± .0003	17.4 ± 0.2
11	2.5272 ± .0011	1.5704 ± .0002	2.0093 ± .0004	6.6337 ± .0009	0.2556 ± .0008	16.8 ± 0.1

York 2 isochron age = 20.8 ± 0.4 Ma. MSWD = 1.7. $[^{40}Ar/^{36}Ar]_0$ = 110 ± 50. J value: 0.00581 ± 0.00005. Size fraction: 80 - 150.

* denotes radiogenic isotope. ‡ Apparent age assuming $[^{40}Ar/^{36}Ar]_0$ = 295.5 (atmospheric).

Table 6.5. $^{40}Ar/^{39}Ar$ LASER-FUSION ANALYTICAL DATA FOR SAMPLE M90-K73, BIOTITE

Subsample	$^{40}Ar^{*}$ (x10^{-15} moles)	$^{39}Ar_{K}$ (x10^{-15} moles)	$^{38}Ar_{Cl}$ (x10^{-16} moles)	$^{37}Ar_{Ca}$ (x10^{-17} moles)	$^{36}Ar_{atm.}$ (x10^{-17} moles)	Age (Ma) (± 2σ)‡
1	29.4813 ± 0.0003	22.4724 ± 0.0007	9.3558 ± 0.0005	5.3658 ± 0.0062	3.1107 ± 0.0019	13.7 ± 0.1
2	10.0711 ± 0.0011	8.1753 ± 0.0001	3.6829 ± 0.0006	2.4902 ± 0.0062	1.5194 ± 0.0022	12.8 ± 0.1
3	14.7803 ± 0.0002	13.0924 ± 0.0005	5.7975 ± 0.0003	17.2387 ± 0.0087	2.4433 ± 0.0019	11.8 ± 0.1
4	12.2074 ± 0.0006	9.4768 ± 0.0004	4.2348 ± 0.0001	10.5983 ± 0.0057	1.2732 ± 0.0020	13.4 ± 0.1
5	28.0747 ± 0.0004	21.0842 ± 0.0007	9.6659 ± 0.0001	64.2855 ± 0.0056	3.5978 ± 0.0020	13.9 ± 0.1
6	54.6533 ± 0.0008	39.9320 ± 0.0011	18.6383 ± 0.0012	18.4278 ± 0.0031	9.4409 ± 0.0024	14.3 ± 0.2
7	26.8394 ± 0.0020	20.4649 ± 0.0016	9.5952 ± 0.0003	13.9302 ± 0.0040	3.6188 ± 0.0025	13.7 ± 0.2
8	60.9855 ± 0.0010	47.3117 ± 0.0024	20.9080 ± 0.0004	102.9407 ± 0.0040	5.6616 ± 0.0020	13.4 ± 0.2
9	8.8251 ± 0.0001	7.5565 ± 0.0001	3.6226 ± 0.0002	3.9180 ± 0.0021	2.8451 ± 0.0019	12.2 ± 0.1
10	75.1796 ± 0.0009	55.4827 ± 0.0011	24.3184 ± 0.0009	37.9531 ± 0.0023	11.9536 ± 0.0019	14.1 ± 0.2

York 2 isochron age = 12.8 ± 0.3 Ma. MSWD = 1.6. $[^{40}Ar/^{36}Ar]_0$ = 350 ± 30. J value: 0.00581 ± 0.00005. Size fraction: 60 - 80.

* denotes radiogenic isotope. ‡ Apparent age assuming $[^{40}Ar/^{36}Ar]_0$ = 295.5 (atmospheric).

Table 6.6. $^{40}Ar/^{39}Ar$ LASER-FUSION ANALYTICAL DATA FOR SAMPLE M90-K73, HORNBLENDE

Subsample	$^{40}Ar^{*}$ (x10^{-15} moles)	$^{39}Ar_{K}$ (x10^{-15} moles)	$^{38}Ar_{Cl}$ (x10^{-16} moles)	$^{37}Ar_{Ca}$ (x10^{-15} moles)	$^{36}Ar_{atm.}$ (x10^{-17} moles)	Age (Ma) (± 2σ)‡
1	5.7201 ± 0.0023	2.8915 ± 0.0003	9.8019 ± 0.0008	9.5930 ± 0.0005	0.2175 ± 0.0014	20.7 ± 0.2
2	2.7727 ± 0.0014	1.7030 ± 0.0003	4.7613 ± 0.0006	5.1420 ± 0.0007	0.4436 ± 0.0026	17.0 ± 0.2
3	8.4353 ± 0.0035	4.5850 ± 0.0005	13.1993 ± 0.0005	14.9573 ± 0.0016	0.7311 ± 0.0021	19.2 ± 0.2
4	2.4970 ± 0.0009	1.8513 ± 0.0002	5.9327 ± 0.0008	6.5824 ± 0.0005	1.0437 ± 0.0032	14.1 ± 0.2
5	2.0818 ± 0.0010	1.4334 ± 0.0002	4.9497 ± 0.0018	4.9501 ± 0.0005	0.4520 ± 0.0023	15.2 ± 0.1
6	5.9801 ± 0.0032	4.9082 ± 0.0009	11.9603 ± 0.0012	9.9839 ± 0.0007	2.9064 ± 0.0032	12.8 ± 0.4
7	9.7160 ± 0.0048	5.1405 ± 0.0004	15.6982 ± 0.0015	18.1722 ± 0.0013	0.8390 ± 0.0021	19.8 ± 0.2
8	3.1342 ± 0.0019	2.1238 ± 0.0003	7.1140 ± 0.0014	7.2178 ± 0.0005	0.5106 ± 0.0023	15.5 ± 0.2
9	6.6429 ± 0.0032	4.6575 ± 0.0008	12.5566 ± 0.0009	13.2511 ± 0.0009	1.7438 ± 0.0025	14.9 ± 0.3
10	2.9961 ± 0.0016	1.9230 ± 0.0004	6.5463 ± 0.0016	6.5628 ± 0.0009	0.5078 ± 0.0014	16.3 ± 0.2

York 2 isochron age = 21.4 ± 0.4 Ma. MSWD = 0.3. $[^{40}Ar/^{36}Ar]_0$ = 150 ± 60. J value: 0.00583 ± 0.00005. Size fraction: 80 - 100.

* denotes radiogenic isotope. ‡ Apparent age assuming $[^{40}Ar/^{36}Ar]_0$ = 295.5 (atmospheric).

Table 6.7. $^{40}Ar/^{39}Ar$ LASER-FUSION ANALYTICAL DATA FOR SAMPLE M90-K79, BIOTITE

Subsample	$^{40}Ar^*$ (x10^{-15} moles)	$^{39}Ar_K$ (x10^{-15} moles)	$^{38}Ar_{Cl}$ (x10^{-16} moles)	$^{37}Ar_{Ca}$ (x10^{-17} moles)	$^{36}Ar_{atm.}$ (x10^{-17} moles)	Age (Ma) (± 2σ)‡
1	13.4229 ± 0.0016	9.9486 ± 0.0002	3.3645 ± 0.0004	2.4766 ± 0.0037	0.7850 ± 0.0014	14.2 ± 0.1
2	14.4491 ± 0.0018	10.4533 ± 0.0006	3.1308 ± 0.0003	2.6636 ± 0.0025	0.4294 ± 0.0010	14.2 ± 0.1
3	15.9061 ± 0.0013	11.1402 ± 0.0005	3.5514 ± 0.0002	1.0748 ± 0.0027	0.1869 ± 0.0013	15.0 ± 0.1
4	13.5944 ± 0.0010	10.1308 ± 0.0002	3.8785 ± 0.0002	3.5981 ± 0.0029	0.6449 ± 0.0014	14.1 ± 0.1
5	24.3584 ± 0.0007	18.5561 ± 0.0012	6.1215 ± 0.0006	13.8318 ± 0.0076	0.9393 ± 0.0006	13.8 ± 0.1
6	12.8430 ± 0.0009	9.1262 ± 0.0002	2.6168 ± 0.0005	3.9252 ± 0.0053	0.1061 ± 0.0011	14.8 ± 0.1
7	17.6902 ± 0.0017	13.3084 ± 0.0005	4.3458 ± 0.0004	2.0561 ± 0.0030	0.9252 ± 0.0008	13.9 ± 0.1
8	19.3902 ± 0.0016	14.0607 ± 0.0003	4.4860 ± 0.0002	4.7196 ± 0.0071	0.7523 ± 0.0010	14.5 ± 0.1
9	16.0164 ± 0.0012	12.2850 ± 0.0002	3.9252 ± 0.0006	5.6542 ± 0.0037	0.6869 ± 0.0008	13.7 ± 0.1
10	28.8201 ± 0.0018	22.2991 ± 0.0017	7.3364 ± 0.0005	7.5701 ± 0.0051	1.8131 ± 0.0011	13.6 ± 0.1

York 2 isochron age = 13.7 ± 0.3 Ma. MSWD = 2.1. $[^{40}Ar/^{36}Ar]_0 = 330 \pm 150$. J value: 0.00584 ± 0.00005. Size fraction: 60 - 80.

* denotes radiogenic isotope. ‡ Apparent age assuming $[^{40}Ar/^{36}Ar]_0 = 295.5$ (atmospheric).

Table 6.8. $^{40}Ar/^{39}Ar$ LASER-FUSION ANALYTICAL DATA FOR SAMPLE M90-K79, HORNBLENDE

Subsample	$^{40}Ar^*$ (x10^{-15} moles)	$^{39}Ar_K$ (x10^{-15} moles)	$^{38}Ar_{Cl}$ (x10^{-16} moles)	$^{37}Ar_{Ca}$ (x10^{-15} moles)	$^{36}Ar_{atm.}$ (x10^{-17} moles)	Age (Ma) (± 2σ)‡
1	4.6000 ± 0.0022	1.9296 ± 0.0004	4.4755 ± 0.0014	5.6155 ± 0.0010	0.0130 ± 0.0003	24.9 ± 0.2
2	8.8400 ± 0.0042	5.2276 ± 0.0010	11.0991 ± 0.0018	12.5471 ± 0.0032	0.6243 ± 0.0020	17.7 ± 0.2
3	5.3112 ± 0.0020	2.9325 ± 0.0005	7.2320 ± 0.0015	7.9161 ± 0.0008	0.4758 ± 0.0020	18.9 ± 0.2
4	5.9244 ± 0.0020	3.7657 ± 0.0006	8.3475 ± 0.0017	9.6423 ± 0.0008	1.2829 ± 0.0028	16.5 ± 0.2
5	4.7924 ± 0.0018	3.4235 ± 0.0004	8.2339 ± 0.0014	9.6731 ± 0.0021	0.9434 ± 0.0026	14.7 ± 0.2
6	4.5613 ± 0.0020	3.0114 ± 0.0004	7.3241 ± 0.0015	8.4167 ± 0.0015	0.9522 ± 0.0024	15.9 ± 0.2
7	2.7009 ± 0.0015	1.8890 ± 0.0004	4.6409 ± 0.0017	5.3626 ± 0.0007	0.7405 ± 0.0030	15.0 ± 0.2
8	2.4743 ± 0.0017	1.4677 ± 0.0003	3.9040 ± 0.0014	4.0657 ± 0.0003	0.4751 ± 0.0024	17.6 ± 0.2
9	2.4846 ± 0.0017	1.4660 ± 0.0003	3.7216 ± 0.0016	3.9519 ± 0.0007	0.3257 ± 0.0024	17.7 ± 0.2
10	2.7904 ± 0.0008	3.0940 ± 0.0005	8.4888 ± 0.0021	8.4865 ± 0.0012	1.4685 ± 0.0042	9.5 ± 0.1
11	6.2464 ± 0.0023	3.0403 ± 0.0004	7.6410 ± 0.0002	11.2316 ± 0.0006	0.3521 ± 0.0009	21.5 ± 0.2
12	7.4826 ± 0.0035	3.8376 ± 0.0005	9.0929 ± 0.0004	13.4987 ± 0.0008	0.7556 ± 0.0013	20.4 ± 0.2
13	9.9338 ± 0.0049	4.8683 ± 0.0007	11.4380 ± 0.0013	17.9670 ± 0.0018	1.5998 ± 0.0011	21.3 ± 0.3
14	7.9419 ± 0.0040	4.6296 ± 0.0006	10.9964 ± 0.0006	15.9855 ± 0.0008	1.1137 ± 0.0011	18.0 ± 0.2
15	3.9640 ± 0.0028	2.1237 ± 0.0003	4.9856 ± 0.0006	7.4301 ± 0.0007	0.4677 ± 0.0011	19.5 ± 0.2
16	2.4689 ± 0.0016	1.8180 ± 0.0002	4.7132 ± 0.0007	6.0078 ± 0.0006	0.4846 ± 0.0009	14.2 ± 0.2
17	9.5635 ± 0.0043	4.3736 ± 0.0003	11.4998 ± 0.0010	15.3732 ± 0.0010	0.7193 ± 0.0015	22.9 ± 0.2
18	6.0518 ± 0.0035	3.8659 ± 0.0004	9.3481 ± 0.0009	13.7753 ± 0.0010	1.0248 ± 0.0010	16.4 ± 0.2
19	4.7677 ± 0.0021	2.8751 ± 0.0003	6.9068 ± 0.0006	10.7128 ± 0.0010	0.7491 ± 0.0013	17.4 ± 0.2
20	6.9339 ± 0.0023	3.5605 ± 0.0003	8.7659 ± 0.0006	12.7162 ± 0.0004	0.9577 ± 0.0009	20.4 ± 0.2

York 1 age = 21.3 ± 3.1 Ma. $[^{40}Ar/^{36}Ar]_0$ = 200 ± 100. J value: 0.00584 ± 0.00005. Size fraction: 60 - 80.

* denotes radiogenic isotope. ‡ Apparent age assuming $[^{40}Ar/^{36}Ar]_0$ = 295.5 (atmospheric).

CHAPTER 4

NEOGENE EXTENSION OF AN ALPINE COLLISIONAL OROGEN, NORTHEASTERN GREECE

David A. Dinter
Department of Earth, Atmospheric and Planetary Sciences
Massachusetts Institute of Technology
Cambridge, MA 02139

ABSTRACT

During the latter stages of Alpine convergence in the north Aegean region, the Falakron marble series, a continental platform carbonate sequence >5000 m thick, was subducted to the northeast beneath a high-grade gneiss complex at the southwest margin of the Rhodope metamorphic province in northeastern Greece. In middle Miocene - early Pliocene time, the marble unit reemerged from the core of the Alpine orogen in the footwall of a gently southwest-dipping low-angle normal fault, the Strymon Valley detachment. The Tertiary tectonic evolution of the southwestern Rhodope region is chronicled here as a succession of four deformational events: D_1 comprises the ductile folding, penetrative deformation, and dynamic metamorphism of the Falakron series in middle - late Eocene time during its descent to mid-crustal depths in the footwall of the southwest-vergent Nestos thrust. A number of granodiorite plutons were emplaced within the Falakron marble series in mid-Oligocene time, and correlative arc-type andesitic lavas blanketed a large region above the overlying gneiss complex. The northeast-southwest extensional collapse of the Alpine nappe pile began ~15 m.y. after the cessation of continental subduction and appears to have been accommodated by three successive shear systems that alternated in polarity. Early Miocene extension (D_2) is recorded by the emplacement and mylonitization of the Symvolon granodiorite beginning ~22 Ma within a northeast-dipping coaxial shear zone that may represent an extensional rupture of the Falakron carbonate slab. The Symvolon shear zone was succeeded in middle Miocene time by the southwest-dipping

Strymon Valley detachment system (D_3), which facilitated the southwestward-progressive tectonic unroofing of the Rhodope metamorphic core complex and a consequent transition from ductile to brittle deformation from ~16 - 3.5 Ma. Continuing extension from late Pliocene time to the present (D_4) is principally expressed by the subsidence of the Strymon and Drama basins, whose northwest-striking bounding faults may sole into an active northeast-dipping detachment that terminates to the southeast at the North Aegean trough.

INTRODUCTION

The geographical designation "Rhodope" has been applied in several tectonic contexts. The *Rhodope continental fragment* subsumes the entire region between the Vardar zone and the Carpathian-Balkan branch of the Alpine chain, whereas the *Rhodope massif* includes only the mountainous central portion of this "fragment", bounded by the Struma-Strymon and Maritsa Basins (Figs. 1 and 2). This region is referred to here simply as the *Rhodope metamorphic province*, because it does not exemplify the tectonic stability implied by the term "massif" (see below). *The Rhodope metamorphic core complex* comprises only the southwestern segment of the Rhodope province, approximately bounded by the Strymon and Nestos Rivers. The Rhodope continental fragment has been interpreted as one of several pieces of western Tethyan lithosphere that were isolated by rifting during the early Mesozoic breakup of Pangaea (Burchfiel, 1980). Its southern remnant on the southeastern Balkan peninsula comprises three major crystalline domains – the Serbo-Macedonian and Rhodope metamorphic provinces, and the north-vergent thrust nappes of the Balkan Mountains (Fig. 1). During Alpine convergence between Africa and Europe, the northern (Balkan) margin of the Rhodope fragment was underthrust by the Moesian continental platform, and its southwestern (Vardar) margin lay at the leading edge of the overriding plate above a northeast-dipping subduction zone. The last of the "Vardar ocean" was consumed in this subduction zone by latest Cretaceous or Paleocene time,

resulting in a collision between Rhodope and another Tethyan continental fragment, Apulia, which comprises much of Italy, western former Yugoslavia, Albania and western mainland Greece (e.g., Smith, 1971; Bernoulli and Laubscher, 1972; Zimmerman, 1972; Mercier et al., 1975; Burchfiel, 1980). Following the collision, convergence continued within and immediately west of the Vardar zone throughout most of Eocene time, accommodated by northeastward A-type subduction of the eastern Apulian margin (Schermer, 1990, 1993). Subsequently, the locus of shortening migrated incrementally westward across the Hellenic and Dinaric Alps, reaching its present position at the eastern verge of the Adriatic Sea ~12 - 13 Ma (Le Pichon and Angelier, 1979).

Serbo-Macedonia and the Balkans, the marginal crystalline provinces of the southern Rhodope fragment, were clearly deformed during Alpine orogenesis because they are disrupted by thrust faults involving late Mesozoic sediments (e.g., Kauffmann et al.; 1976; Jacobshagen et al., 1978). The central portion of the fragment, the Rhodope metamorphic province, was long considered to represent a Precambrian or Hercynian "massif" or "Zwischengebirge" that remained essentially stable during Alpine deformation around its margins (e.g., Kober, 1931; Schwan, 1962; Georgiev, 1963; Boncev, 1971); however, detailed structural mapping and geochronologic studies have shown to the contrary that this region, too, was strongly folded, sheared, and metamorphosed during the Alpine orogeny (Kronberg, 1969; Meyer, 1969; Birk et al., 1970; Papanikolaou and Panagopoulos, 1980; Zachos and Dimadis, 1983; Ivanov, 1981; Burg et al., 1990). It has been suggested that this deformation represents intracratonic shortening of the Rhodope continental fragment owing to stresses transmitted inward from the convergent zones at its boundaries (Burchfiel, 1980). Major kinematic and temporal aspects of the regional structure have previously been poorly resolved, however, so that the tectonic setting of the Rhodope province during Alpine orogenesis has remained largely an open question.

A key element in the Tertiary tectonic evolution of the north Aegean region has recently been recognized: The Strymon Valley detachment is a southwest-dipping low-angle normal fault that forms the southwestern boundary of the Rhodope metamorphic province for >200 km along strike in southwestern Bulgaria, northeastern Greece, and on the island of Thasos (Figs. 2 and 3; Dinter, 1991, 1993; Dinter and Royden, 1993). Southwestward transport of the hanging wall in this detachment system from ~16 to 3.5 Ma may have exceeded 80 km, resulting in the unroofing of the Rhodope metamorphic core complex, which is exposed northeast of the Strymon Valley beneath a strongly disrupted veneer of syndetachment basinal deposits. The large-magnitude lateral displacement of major tectonostratigraphic units on low-angle normal faults accounts for thinning that must approach 100% in the north Aegean region based on measurements of crustal thickness (Jongsma et al., 1977; Makris, 1976; Makris and Vees, 1977). An appreciation of the kinematic evolution of the Strymon Valley detachment system is requisite to understanding the origin and deformation of Cenozoic basins in northeastern Greece. Moreover, the detachment geometry bears strongly on the interpretation of earlier tectonic events. A palinspastic restoration of units displaced in the detachment system to their preextensional positions necessitates a reevaluation of several long-accepted tenets of the regional geology and serves as the underpinning to a fundamentally new model for the tectonic evolution of southwestern Rhodope and Serbo-Macedonian metamorphic provinces.

GEOLOGIC SETTING OF THE STRYMON VALLEY REGION

The gross structural geometry of the southwestern Rhodope province in northeastern Greece is quite simple: The Falakron marble series, an enormously thick, highly strained, platform carbonate unit of unknown age exposed between the Strymon and Nestos Rivers, is overlain at its northeastern margin on a ductile, northeast-dipping shear zone by a unit referred to in this study as the "West Thracian gneiss complex", and at its

southwestern margin on a brittle, low-angle, southwest-dipping fault by the "Serbo-Macedonian gneiss complex" and by strongly deformed, unmetamorphosed Neogene deposits conventionally assigned to the Siderokastro, Serres, Angitis, Akropotamos, and South Symvolon basins (Figs. 2, 3, and 4). The Falakron marble series bears upper greenschist-facies mineral assemblages (Schenk, 1970; Kronberg et al., 1970), whereas the overlying Serbo-Macedonian and West Thracian gneiss complexes were both regionally metamorphosed under upper amphibolite-facies conditions with local anatectic melting (Kockel et al., 1977; Kronberg and Raith, 1977, respectively).

The northeast-dipping mylonitic contact between the West Thracian gneiss complex and the underlying Falakron marble, exposed in the Nestos River vicinity, is referred to here as the "Nestos thrust". Metamorphic foliations in the juxtaposed units dip northeast within several kilometers of the contact zone (Kronberg and Eltgen, 1973), and northeast-plunging minor fold axes and stretching lineations are also common to the marble (Meyer, 1968; Kronberg, 1969) and the gneiss complex (Kilias and Mountrakis, 1990; Koukouvelas and Doutsos, 1990). While acknowledging that the contact is strongly sheared, early workers presumed that it preserved essentially primary stratigraphy (e.g., Kronberg, 1969; Kronberg and Raith, 1977). Based on the contrast in metamorphic grade between the two units, however, Papanikolaou and Panogopoulos (1981) suggested that the contact might be a thrust fault, and Zachos and Dimadis (1983) openly favored a thrust origin. Kilias and Mountrakis (1990) studied mylonitic fabric asymmetries within the Nestos thrust zone, establishing that the vergence is uniformly to the southwest. Koukouvelas and Doutsos (1990) describe structural aspects of the overlying West Thracian gneiss complex, which they interpret as a southwest-vergent stack of Alpine nappes. The age, kinematic character, and tectonic significance of the Nestos thrust and related structures are discussed in greater detail below.

The cataclasized, low-angle, southwest-dipping contact between the Serbo-Macedonian gneiss complex and the underlying Falakron marble series is exposed in two short segments at the northeast margin of the Strymon Valley (Kockel and Walther, 1965; Koukouzas, 1972). Kockel and Walther interpreted this shear zone as a northeast-vergent Alpine thrust, the "Strimonüberschiebung", which they believed to have accommodated the emplacement of Serbo-Macedonian rocks over the southwest margin of the Rhodope province. Schenk (1970) concluded that the latest displacement on this fault was Tertiary or later because unmetamorphosed sediments of indefinite Tertiary age are locally sheared in the fault zone. He also argued that the fault cannot be older than Miocene, because it cuts ductile strain fabrics preserved in the footwall in the Messolakia pluton, which yielded Miocene K-Ar biotite dates (Meyer, 1968). The 'Neogene thrust' identity of this structure is generally accepted and widely cited as an expression of mid-Tertiary compression in the Strymon Valley area (e.g., Jacobshagen et al., 1978; Koukouvelas and Doutsos, 1990). Recently, however, the supposed thrust exposures have been remapped as segments of the extensional Strymon Valley detachment (Dinter and Royden, 1993).

TECTONOSTRATIGRAPHY

Rocks exposed northeast of the Strymon River in northeastern Greece may be divided into three broad tectonostratigraphic sequences based on their structural positions with respect to the Strymon Valley detachment. They either lie in its footwall and so belong to the Rhodope metamorphic core complex, in its hanging wall, or are part of an "overlap sequence" deposited after detachment motion ceased. The Rhodope core complex comprises the Falakron marble series and a number of granodiorite plutons that intruded it in mid-Oligocene and early Miocene time, prior to its middle Miocene - early Pliocene emergence in the footwall of the Strymon Valley detachment system (Dinter and Royden, 1993). The hanging-wall suite includes, in addition to high-grade Serbo-Macedonian

metamorphic rocks, a strongly deformed, unmetamorphosed, syndetachment basin complex that comprises Neogene deposits conventionally assigned to the Struma, Siderokastro, Serres, Angitis, Akropotamos, South Symvolon, and Prinos-Kavala basins (Fig. 3). The "overlap sequence", which includes the Strymon and Drama basins, consists of late Pliocene - Quaternary marine and nonmarine deposits that either unconformably or tectonically overlie units that were displaced in the Strymon Valley detachment system.

Footwall rocks: the Rhodope metamorphic core complex

Three major tectonostratigraphic units were mapped in the footwall of the Strymon Valley detachment. The Falakron marble series of this study corresponds exactly to the "lower tectonic unit" of the Greek Rhodope province of Papanikolaou and Panagopoulos (1981) and the "Pangeon unit" of Kilias and Mountrakis (1990); it is of unknown pre-mid-Oligocene age. The Vrondou pluton is one of a chain of calc-alkaline intrusives inferred to have been emplaced ~31 - 33 Ma in the southern Rhodope province (Marakis, 1969; Liati, 1986; Del Moro et al., 1988), and the Symvolon (or "Kavala") granodiorite was emplaced ~21 - 22 Ma (Dinter et al., submitted). Structural relationships surrounding a second mid-Oligocene pluton, the Xanthi granodiorite, bear strongly on the conclusions of this study and will therefore be discussed below, but were not mapped by the author.

Falakron marble series

The Falakron marble series crops out over an area covering >4000 km^2 between the Strymon and Nestos Rivers and on the island of Thasos (Figs. 2 and 3; Zachos, 1982; Bornovas and Rondogianni-Tsiambaou, 1983; Vavelidis et al., 1987). Its thickness increases dramatically from southwest to northeast, from <200 m in southwestern Mount Pangaion and the Menoikion Mountains to >5000 m in the central Falakron and Lekanis

Mountains (Kronberg, 1969; Schenk, 1970; de Boer, 1970). The dominant carbonate lithology is a massive, white to light gray, granular marble so strongly sheared and recrystallized that virtually all primary sedimentary features have been obliterated. The trends of nearly ubiquitous mineral stretching lineations and recumbent, tight to isoclinal outcrop-scale folds cluster strongly in the range N40°-60°E and most commonly plunge gently northeast (Meyer, 1969). Intercalations of micaceous gneiss, two-mica schist, and actinolite schist appear locally in lenses and layers <1 m to >400 m thick, and were mapped where they are thick enough (at least 10 m, typically) to appear at the local map scale. Mineral compositions and assemblages observed in metapelites and impure marbles throughout the mainland exposure area of the Falakron series are typical of greenschist-facies (quartz-albite-epidote-biotite subfacies) regional metamorphism (Kronberg et al., 1970). On the island of Thasos, greenschist assemblages also predominate (Vavelidis et al., 1987); however, relict kyanite and sillimanite are locally present in gneiss and schist layers, preserving evidence of an earlier higher-grade metamorphism (Atzori et al., 1990).

The age of the Falakron series is poorly constrained. Meyer and Pilger (1963) reported a single colonial (?) coral find from the central part of the unit, constraining the marbles to be post-Cambrian; however, preservation proved too poor for the specimen to be identified (Kronberg et al., 1970). The Falakron unit is intruded by the mid-Oligocene Vrondou and Xanthi plutons and must, therefore, be early Oligocene or older. Based on structural arguments presented below, the unit is inferred to be older than middle Eocene.

Earlier workers divided Falakron marble series into an upper sequence dominated by massive marbles, the "Marmorserie F" of Osswald (1938) or "Marmor-Folge" of Meyer and Pilger (1963), and a lower sequence of gneiss and schist with sparse marble intercalations, the "Gneis-Serie E" of Osswald (1938) or "Untere Schiefergneis-Folge" of Meyer and Pilger (1963). According to Kronberg (1969; 1973) and Schenk (1970), the

gneiss and schist crop out primarily beneath marbles on the southeast flank of Mount Pangaion and as a country-rock carapace overlying the Symvolon pluton at its northwest flank. However, Kokkinakis (1980a) remapped the latter exposures as a marginal blastomylonitic phase of the Symvolon granodiorite and, based on my own observations, many of the Pangaion exposures also appear to be strongly mylonitized plutonic rocks rather than paragneisses. Although muscovite and two-mica schists and gneisses representing country rock do crop out locally in both areas, their thickness and tectonic position within the footwall is presently uncertain. As they are petrographically indistinguishable from schist and paragneiss intercalated within marbles elsewhere in the core complex (Kronberg et al., 1970), these units are assigned here to the Falakron series.

Tertiary calc-alkaline intrusives

Tertiary intrusives ranging in composition from gabbro to granite crop out in scattered locations throughout the Rhodope metamorphic core complex, but occur in especially great volumes beneath its southwestern margin, corresponding to the thinnest part of the Falakron marble series (Meyer, 1968; de Boer, 1970; Schenk, 1970). With the addition of new $^{40}Ar/^{39}Ar$ and U-Pb dates summarized in Tables 1 and 2 for the Symvolon granodiorite (Dinter et al., submitted), there are now sufficient radiometric data from the major intrusive bodies in the Rhodope core complex to facilitate their division into two groups representing distinct magmatic episodes.

Mid-Oligocene intrusives

The Xanthi granodiorite truncates the Nestos thrust at the southeast corner of the Rhodope metamorphic core complex (Figs. 2 and 3; Kronberg and Eltgen, 1973; Liati, 1986). Radiometric data from the Xanthi pluton include K-Ar biotite dates of 27.1 ± 0.4

Ma, 27.9 ± 0.9 Ma (Meyer, 1968), and 28.8 ± 0.3 Ma (Table 3; Liati, 1986), and a K-Ar hornblende date of 30.4 ± 0.6 Ma (Liati, 1986), which provides a minimum emplacement age. At its eastern margin the Xanthi body intrudes andesitic dykes from which hornblende phenocrysts yielded a K-Ar date of 33.5 ± 1.2 Ma (Table 3; Eleftheriadis et al.,1984). This date provides a maximum emplacement age for the pluton providing that the Ar system of the extrusive hornblendes was not partially reset as a result of the intrusion. This assumption is probably valid, because a large tract of andesitic volcanics that overlies the West Thracian gneiss complex 20 km to the northwest has yielded K-Ar dates clustering in the range of 28.7 Ma to 35.0 Ma (Table 3; Eleftheriadis and Lippolt, 1984).

The Vrondou pluton, composed predominantly of quartz monzonite, crops out as a N55°E-elongate dome ~35 km long and 10 - 15 km wide at the western margin of the Rhodope core complex just south of Bulgaria (Fig. 3). Its northeastern margin is an undeformed intrusive contact that cuts northeast-trending structural elements in the Falakron series and is associated with a narrow contact aureole. Its southern margin, by contrast, is strongly mylonitized and bears uniformly southwest-plunging stretching lineations (Kolocotroni and Dixon, 1991; Dinter and Royden, 1993). K-Ar hornblende dates from Vrondou quartz monzonites range from 29 ± 1 Ma to 33 ± 2 Ma (Table 3; Marakis, 1969), and a biotite separate from the Vrondou pluton yielded a K-Ar date of 30.0 ± 3.0 Ma (Dürr et al., 1978), documenting a rapid cooling of the Vrondou body in mid-Oligocene time from > 500°C to < 300°C, the approximate Ar closure temperatures of hornblende and biotite, respectively (Harrison, 1981; Harrison et al., 1985). These data must be interpreted *sensu strictu* to indicate a minimum emplacement age for the Vrondou pluton in the range 31 - 33 Ma. However, the Vrondou body is similar in composition and radiometric age characteristics to the Xanthi pluton (Kotopouli and Pe-Piper, 1989a), and both the Xanthi pluton and the eastern margin of the Vrondou pluton truncate structures inferred to have formed as late as 36 Ma within the Falakron marble series (see below). It

appears likely, therefore, that the eastern part, at least, of the Vrondou body was emplaced during the same mid-Oligocene intrusive event represented by the Xanthi pluton.

Early Miocene Symvolon pluton

The Symvolon granodiorite crops out from the port of Kavala southwest along the north Aegean coastline for ~40 km as a N50°-55°E-elongate dome 10 - 15 km wide. Its margins are pervasively mylonitized and contacts with country rocks are, in general, ductile shear zones in which calc-silicates such as diopside and tremolite are common. No discrete contact aureole is preserved. The interior of the pluton is also mylonitic, and characterized by gently-plunging, northeast-trending stretching lineations and outcrop-scale folds subparallel to those that are widely developed in the Falakron marble series (Kokkinakis, 1980a). The emplacement age of the Symvolon (or "Kavala") intrusive is a subject of some debate. Meyer (1968) proposed a pre-middle Eocene age for the pluton because he believed it to have been mylonitized with the Falakron series during a single episode of ductile shear in the southwestern Rhodope province, interpreted to be pre-middle Eocene based on stratigraphic relationships in eastern Thrace. Kokkinakis (1980b) interpreted a Carboniferous emplacement age from the results of a single U-Pb zircon analysis that gave discordant $^{206}Pb/^{238}U$ and $^{207}Pb/^{235}U$ model ages of 95 ± 5 Ma and 101 ± 8 Ma, respectively, and a $^{207}Pb/^{206}Pb$ age of 335 ± 40 Ma (Table 4).

Newly acquired radiometric data from the Symvolon pluton include $^{40}Ar/^{39}Ar$ K-feldspar, biotite, and hornblende dates, and U-Pb titanite dates (Tables 1 and 2; Dinter et al., submitted). Middle Miocene biotite and K-feldspar model ages are discussed below in the context of the Strymon Valley detachment system. $^{40}Ar/^{39}Ar$ hornblende and $^{206}Pb/^{238}U$ titanite dates fall in the range 19.7 ± 0.3 Ma to 21.7 ± 0.4 Ma, and register cooling through closure temperatures of ~500°C for hornblende (Harrison, 1981) and

600°C for titanite (Ghent et al., 1988). Their convergence in earliest Miocene time records an abrupt cooling event associated with the emplacement of the pluton (Dinter et al., submitted). Rb-Sr muscovite dates of 22.3 ± 0.7 Ma and 22.6 ± 0.7 Ma obtained by Del Moro et al.(1990) from gneisses intruded by the Symvolon pluton in the Marmara Valley area are consistent with this interpretation.

Hanging-wall units

The Serbo-Macedonian gneiss complex, conventionally regarded as the deformed western margin of the Rhodope continental fragment (e.g., Jacobshagen et al., 1978; Burchfiel, 1980), constitutes the crystalline portion of the hanging wall that was displaced southwestward in the Strymon Valley detachment system (Dinter and Royden, 1993). Kockel et al. (1971, 1977) divide this unit into two "series", separated by a southwest-dipping cataclastic shear zone. The western "Vertiskos" series, composed of upper amphibolite-facies gneiss and schist intruded by several strongly sheared felsic, basic, and ultrabasic bodies, has yielded Early - Late Cretaceous K-Ar and $^{40}Ar/^{39}Ar$ biotite and muscovite dates (Table 5; Harre et al., 1968; Marakis; 1969; Papadopoulos and Kilias, 1985; De Wet et al., 1989). The underlying eastern "Kerdilion" series, predominantly biotite gneiss and migmatitic gneiss intercalated with marble and minor amphibolite, is characterized by middle Eocene - early Oligocene K-Ar mica ages (Harre et al., 1968). Mylonitic, micaceous, plagioclase-microcline gneiss belonging to the Kerdilion series lies in direct detachment contact with the underlying Falakron marble series in two small exposures northeast of the Strymon Valley (Figs. 2 and 3). Aspects of the structural evolution and tectonic significance of the Serbo-Macedonian gneiss complex are considered briefly in a later section.

Along the remainder of its exposed length, the Strymon Valley detachment is immediately overlain by tilted, strongly faulted, unmetamorphosed Neogene deposits that are customarily assigned to the Struma, Siderokastro, Serres, Angitis, Akropotamos, and South Symvolon basins (Fig. 3). These "basins", together with the offshore Prinos-Kavala and Thasos-Samothraki basins, were recognized by Dinter and Royden (1993) as lobes of a syndetachment basin complex that accumulated at the trailing edge of the hanging wall above the Strymon Valley detachment (cf. Fedo and Miller, 1992). The syndetachment basin complex persists for >200 km in a belt trending ~N35°W. Its width in the direction of hanging-wall transport increases southward from <5 km in western Bulgaria to ~40 km at the north Aegean coastline, and still greater widths may be attained offshore. Thicknesses of syndetachment deposits increase southward from ~850 m in western Bulgaria (Zagorcev, 1992) to >3500 m in the offshore Prinos-Kavala basin (Pollak, 1979; Proedrou, 1979). The Struma basin in Bulgaria and the Siderokastro basin in northernmost Greece contain only terrigenous deposits (Kojumdgieva et al., 1982; Zagorcev, 1992), whereas the Serres basin (von Freyberg, 1951; Armour-Brown et al., 1979), and syndetachment deposits surrounding the southern margin of Strymon Valley (Gramann and Kockel, 1969; Dermitzakis et al., 1985), preserve a thin lower Pliocene shallow marine interval separating thicker nonmarine sequences. The Akropotamos, South Symvolon, and Prinos-Kavala basins preserve both Messinian evaporites and lower Pliocene marine beds between predominantly nonmarine sequences (Psilovikos and Syrides, 1983; Dermitzakis et al., 1985; Pollak, 1979; Proedrou, 1979). Ages of fossils presently known from these deposits range from middle Miocene (Kojumdgieva et al., 1982) to early Pliocene (Armour-Brown et al., 1979). Detailed descriptions of units mapped within the syndetachment basin complex and interpretations of their depositional environments are beyond the scope of this paper, but appear in Dinter (1994).

Postdetachment overlap deposits

Post-Strymon Valley detachment sediments preserved near the southern margin of the Rhodope core complex include (1) marine and nonmarine deposits generally not exceeding ~150 m in thickness that unconformably overlie Rhodope bedrock, deformed supradetachment basin strata, and the detachment itself between the Strymon and Drama basins, and at least 1000 m of basin fill within the Strymon and Drama basins. As the youngest known syndetachment deposits are ~3.5 Ma in age (Armour-Brown et al., 1979), all late Pliocene and younger sediments in the Strymon Valley area are considered to belong to the postdetachment overlap sequence.

Where the Strymon Valley detachment coincides with the base of a marble mountain front as at Mts. Pangaion and Menoikion, it is commonly covered by 1 - 10 m of consolidated marble talus breccia, which in some places is actively accumulating. Over much of the Angitis basin, however, coalescing sheets of this breccia define a planation surface that is graded to a base level at least 200 m higher than present sea level. The breccia is not observed below ~200 m and is deeply incised by modern streams. At an elevation of ~290 m above the village of Galypsos on the southern flank of Mt. Pangaion, a horizontal wave-cut platform pierced by *Lithodomus* borings marks the top of an undeformed, late Pliocene or Quaternary nearshore marine gritstone (Psilovikos and Syrides, 1983). This unit depositionally overlaps the Strymon Valley detachment, and erosional remnants of similar marine deposits overlie deformed syndetachment strata at an angular unconformity throughout much of the Angitis basin at elevations lower than ~260 m (cf. Xidas, 1984). Flat-lying beach and shallow marine strata are also exposed at elevations of ~200 m within basin fill at the eastern margin of the Drama basin. These deposits represent a late Pliocene or Quaternary highstand of the Aegean Sea that probably defined the base level for the coalescing subaerial breccias described above. Several small

marine terraces that crop out at lower elevations surrounding the lower Strymon River presumably formed during subsequent Quaternary transgressions.

The stratigraphy of the Strymon basin is known principally from the Strymon 1 and Strymon 2 boreholes ~12 km south-southeast of Serres. Summary logs in Erki et al. (1984) show ~900 m of Quaternary, 900 m of Pliocene, and 1800 m of Miocene sand, silt, marl, conglomerate, and sedimentary breccia overlying schist of probable Serbo-Macedonian affinity in the central part of the basin. The entire sedimentary section in these cores has conventionally been regarded as Strymon basin fill; however, all lower Pliocene and older deposits predate the formation of the Strymon basin and actually belong to the supradetachment basin complex (Dinter and Royden, 1993). A similar situation probably prevails in the Drama basin, and a presently unrecognized syndetachment-postdetachment unconformity presumably exists in both basins.

CENOZOIC DEFORMATION IN THE STRYMON VALLEY REGION

Stretching lineations and minor folds are remarkably uniform in morphology and orientation throughout the Rhodope core complex, typically plunging 0° - 25° northeast or southwest in the Falakron marble series (Jordan, 1969; Meyer, 1969; Kronberg, 1969; Birk et al., 1970; Dinter and Royden, 1993), in the Symvolon granodiorite (Kokkinakis, 1980a), and at the western margin of the Vrondou pluton (Kolocotroni and Dixon, 1991). Northeasterly plunges are most common, varying in trend from about N30°E to N60°E, but clustering strongly in the range N40°-50°E (Meyer, 1969; Kokkinakis, 1980a). These northeast-trending structural elements have conventionally been interpreted as products of a single, early Tertiary (?), Alpine convergent event (e.g., Meyer, 1968, 1969; Kronberg, 1969; Kronberg et al., 1970; Kokkinakis, 1980b; Kilias and Mountrakis, 1990). The Symvolon and western Vrondou plutons and several smaller intrusives were considered

syntectonic to this Alpine deformation because they appeared to share the regional shear fabric, and the Xanthi pluton was interpreted as post-tectonic because its intrusive margins cut this fabric (Meyer, 1968; Kokkinakis, 1980a; Kilias and Mountrakis, 1990).

Geologic relationships described below provide unequivocal evidence that northeast-trending folds and stretching lineations in the Rhodope metamorphic core complex actually represent at least three distinct episodes of ductile shear, the latter two of which accommodated *extensional* rather than contractional strain. The undeformed northern and eastern intrusive margins of the Xanthi and Vrondou plutons, respectively, cut northeast-plunging mylonitic elements in the Falakron series that must, therefore, predate the mid-Oligocene emplacement of those bodies. The Symvolon pluton, emplaced ~21 - 22 Ma, bears pervasive, synintrusional, northeast-plunging folds and lineations that represent early Miocene ductile shearing (Dinter et al., submitted). Finally, the southwest margins of the Vrondou pluton (Kolocotroni and Dixon, 1991; Dinter and Royden, 1993), and of the Falakron series and the Symvolon pluton (Dinter, 1991), are deformed by gently southwest-plunging folds and stretching lineations produced within the Strymon Valley detachment zone, which originated ~16 Ma and facilitated a transition from ductile to brittle strain in the Rhodope core complex in middle Miocene time (Dinter and Royden, 1993).

During three field seasons from 1989 to 1991 the Strymon Valley detachment and adjacent hanging-wall and footwall rocks were mapped by the author from the north Aegean coastline southwest of Kavala around the southwestern margins of Mts. Symvolon and Pangaion, and north and south of the Angitis River between the Strymon and Drama basins at a scale of 1:25,000 using topographic and SPOT satellite image bases. Parts of the northeastern Angitis basin were mapped at 1:6000 on stereographic air photos. In addition, short segments of the detachment and adjacent rocks were examined in reconnaissance fashion at the base of the Serres and Siderokastro supradetachment basin

lobes to verify the continuity of the detachment north of the study area. Footwall rocks at structural levels considerably deeper than the Strymon Valley detachment were mapped in small areas north and east of the Drama basin. Limited observations of hanging-wall rocks belonging to the Serbo-Macedonian province were made at the southwest margin of Mt. Pangaion and in the Kerkini Range, which bounds the Strymon basin to the north (Fig. 3).

Based on the results of this mapping and on subsequent geochronologic work (Dinter et al., submitted), the deformation and juxtaposition of tectonostratigraphic units exposed in the Strymon Valley region are rationalized here as products of four broadly successive Cenozoic deformational phases, D_1 - D_4 (Table 6). D_1 corresponds to the Alpine convergent event recognized by earlier workers (see above). The Vrondou and Xanthi granodiorite plutons and several smaller igneous bodies were emplaced within the Falakron series ~31 - 33 Ma, during an interval of relative tectonic quiescence between events D_1 and D_2 that lasted ~14 m.y. D_2 - D_4 designate distinct phases in the quasi-continuous early Miocene to Recent extension of the north Aegean Alpine nappe pile in a back-arc setting relative to the Hellenic subduction system.

D_1: Early Tertiary Alpine convergence

D_1 shearing and metamorphism pervasively and penetratively disrupted the Falakron marble series between the Strymon and Nestos Rivers, destroying all but crude compositional expressions of original stratigraphic layering. Open folds with 10- to 20-km wavelengths and gently-plunging, northeast-trending axes persisting for up to 70 km, modified in some places by slightly younger northwest-trending folds, were defined by early workers as the major structures associated with the D_1 event (Jordan, 1969; Kronberg, 1969; Meyer, 1969; Schenk, 1970; de Boer, 1970). It was later recognized that these structures formed within the footwall of the most prominent regional D_1 structure, the

gently northeast-dipping Nestos thrust, which accommodated the emplacement of the upper amphibolite-facies West Thracian gneiss complex over upper greenschist-facies Falakron series rocks (Papanikolaou and Panagopoulos, 1981; Zachos and Dimadis, 1983; Liati, 1986; Kilias and Mountrakis, 1990; Koukouvelas and Doutsos, 1990).

As noted above, D_1 was the first of three deformational periods during which gently plunging, northeast-trending outcrop-scale folds and mineral lineations formed within the Falakron marble series. Such structural elements are confidently attributed to the D_1 event where they are cut by undeformed intrusive margins of mid-Oligocene plutons, as at Xanthi and eastern Mt. Vrondou, and in areas distant from the influence of the D_2 and D_3 shear zones, including most of the region north and east of the Drama basin, where the structural thickness of the Falakron series reaches 5000 - 7000 m (Jordan, 1969; Kronberg, 1969). Outcrop-scale F_1 folds are commonly tight to isoclinal and warp S_1 metamorphic foliations that are defined by grain size contrasts, color banding, or the alignment of flattened calcite crystals in pure marble, and by compositional banding in impure marble. In general, minor F_1 fold axes trend in the range N35°-45°E and plunge gently northeast in the Falakron and Lekanis Mountains and eastern Mt. Pangaion, where they have conventionally been interpreted as products of intralimb shear on the upright, open, northeast-trending folds believed to dominate the regional structure (Birk, 1970; Jordan, 1969; Kronberg, 1969; Kronberg et al., 1970; Meyer and Pilger, 1963; Meyer, 1969). Kilias and Mountrakis (1990) recognized that many outcrop-scale F_1 structures are actually sheath folds, especially in zones of concentrated ductile shear near the Nestos thrust. Based on outcrop patterns shown on published geologic maps of the Lekanis Mountains (Kronberg, 1973; Kronberg and Eltgen, 1973), it appears plausible that some of the larger F_1 folds considered by earlier workers to be open anticlines and synclines (e.g., Kronberg et al., 1970), might alternatively be interpreted as sheath folds, as well.

L_1 lineations coincide with very low-angle intersections of tightly to isoclinally folded, white, coarse-grained marble laminations with axial planar foliations to those folds (Plates 1 and 2). Coarse calcite grains and grain aggregates that define these intersection lineations in marble lithologies are strongly elongated parallel to the intersections, and so also represent stretching lineations. Similar stretching lineations are defined within schist and gneiss intervals in the Falakron series by elongated and aligned quartz and mica. L_1 stretching lineations are oriented parallel to subparallel to F_1 fold axes throughout the Rhodope metamorphic core complex, most commonly plunging gently to the northeast (Meyer, 1969). Along the northeastern margin of the Drama basin, however, L_1 lineations plunge predominantly to the southwest, with attitudes clustering strongly about 10°, S38°W (Fig. 5). I tentatively ascribe this variance from the regional northeasterly plunges of D_1 structures to a southwesterly rotation of hanging wall strata above northeast-dipping D_4 normal faults that accommodated the subsidence of the Drama basin (Fig. 3; see below). East to east-northeasterly trends of outcrop-scale F_1 fold axes and L_1 lineations adjacent to the Nestos thrust north of Drama (Meyer, 1969) may be the result of D_3 doming in the breakaway region of the Strymon Valley detachment.

Foliation planes defined by the alignment of either mica or augen in schist and gneiss lithologies of the Falakron series show a fairly strong tendency toward shallow to moderate northeasterly dips (Fig. 6; see additional data in de Boer, 1970), even in areas such as the Menoikion Mountains, where marble foliations have typically been transposed such that they are subparallel to the local orientation of the Strymon Valley detachment. The age of the gneiss foliations is generally unknown and may vary from place to place; however, their uniformity in orientation over large areas may imply a common D_1 origin, because only D_1 deformation is pervasive in the core complex.

D_1 kinematics and timing

A gently to moderately northeast-plunging axis of D_1 shear transport in the Falakron series is indicated by the orientation of L_1 stretching lineations. Major and minor F_1 fold axes are, therefore, oriented subparallel to the direction of shear transport, a common attribute of rock units that have accommodated large magnitudes of ductile shear strain (e.g., Hansen, 1971). The associated sense of shear is typically ambiguous because carbonate lithologies of the Falakron series preserve few well-developed, asymmetric mylonitic fabrics or other sense-of-shear indicators. Steep, closed, extensional fractures oriented approximately perpendicular to L_1 lineations locally offset S_1 foliations a few mm down-to-the-SW, and are interpreted as evidence of a top-to-the-SW sense of D_1 shearing.

Due to the destruction of original stratigraphy in the Falakron series and the consequent obscurity of tectonostratigraphic omissions or repetitions, it is likewise difficult to ascertain solely on the basis of structural relationships exposed *within* the Rhodope core complex whether D_1 shearing accommodated regional contraction or extension. The convergent nature of the D_1 event is apparent, however, owing to its unambiguous association with the Nestos thrust: D_1 mylonitic fabrics are continuous and congruent upward from the top of the Falakron series through the thrust zone and into the base of the West Thracian gneiss complex, where they are associated with the development of a retrograde greenschist-facies mineral assemblage (Liati, 1986). A uniform top-to-the-southwest sense of D_1 shearing within and adjacent to the Nestos thrust zone has been established on the basis of S-C mylonitic fabrics, σ- and δ-structures developed around rotated feldspar porphyroclasts, asymmetric recrystallized quartz fabrics, and quartz c-axis orientations (Kilias and Mountrakis, 1990).

The undeformed, intrusive northern margin of the Xanthi granodiorite truncates both the Nestos thrust and a major, northeast-plunging D_1 anticline expressed by S_1 foliations in the Falakron marble at the southeast corner of the Rhodope core complex, and the undeformed, intrusive western margin of the Vrondou pluton cuts D_1 structural elements northwest of the Drama basin (Fig. 3; Meyer, 1968; Kronberg and Eltgen, 1973; Liati, 1986). It is possible that the Vrondou pluton acquired its northeast-elongate domal shape as a result of being emplaced in the core of a D_1 anticline. Both of these plutons were emplaced at least 31 - 33 Ma (see above), constraining D_1 deformation to be pre-mid-Oligocene in age. Regional geochronologic data that provide closer constraints on the age and tectonic significance of the D_1 event are discussed in a later section.

D_2: Early Miocene intrusion and coaxial shearing (Symvolon shear zone)

The Symvolon or "Kavala" granodiorite intrudes the Falakron marble series at the southwest margin of the Rhodope metamorphic core complex (Fig. 3). Its interior and margins are pervasively mylonitic, characterized by outcrop-scale folds and stretching lineations that plunge gently to moderately east-northeast, subparallel to D_1 folds and lineations in the Falakron series (see above). The congruity of mylonitic structural elements in these units has predicated a nearly uniform view among earlier workers that the Symvolon pluton was emplaced earlier than the relatively undeformed Xanthi and Vrondou bodies and mylonitized concurrently with the Falakron series during the convergent D_1 event (e.g., Meyer, 1968; Kokkinakis, 1980a; Kilias and Mountrakis, 1990). Recently acquired U-Pb titanite and zircon ages and $^{40}Ar/^{39}Ar$ hornblende ages establish unequivocally, however, that the Symvolon granodiorite was emplaced ~21 - 22 Ma, at least 10 m.y. *later* than the Xanthi and Vrondou plutons (Tables 1 and 2, Dinter et al., submitted). Thus, the mylonitic character of the Symvolon body cannot be a product of pre-mid-Oligocene D_1 deformation; it must represent Miocene or younger ductile shearing

(D_2) that produced folds and lineations similar in form and orientation to those that formed during D_1. Whereas D_1 shearing penetratively deformed the entire Falakron marble series, however, the D_2 ductile-fabric-forming event appears to have strongly affected only the southwest margin of the Rhodope core complex, between the Strymon and Drama basins. In that region, it is commonly difficult to discriminate between D_1 and D_2 folds and lineations within the Falakron series because they are so alike in form and attitude. D_2 structural elements can be confidently identified only in the pluton itself and within calc-silicate-bearing shear zones as wide as ~100 m around its margins.

Mylonitic C-planes (S_2) spaced a few mm apart throughout much of the Symvolon intrusive coincide with narrow zones of strongly sheared, very fine-grained biotite and recrystallized quartz. S-planes (S_2') in variably developed S-C mylonites are most commonly defined by fish-like shapes of biotite and hornblende and by asymmetric recrystallized quartz fabrics (Plate 3). Mineral stretching lineations (L_2) that have a pasty appearance in the field are defined by a pronounced elongation and streaking of biotite and quartz on C-planes, and also by strongly developed K-feldspar phenocryst tails (Plate 4). C-planes in the south central part of the pluton typically dip gently northeast and associated L_2 stretching lineations have orientations in the range 10°-25°, N50°-70°E, with a well-defined mean value of 18°, N58°E (Figs. 7 and 8). Similar results obtain for the remainder of the pluton (Kokkinakis, 1980a), except in a narrow band along its southwest margin, where northeast-plunging D_2 structural elements appear to be overprinted by southwest-plunging D_3 mylonitic fabrics associated with the Strymon Valley detachment (Dinter and Royden, 1993). An average 10° - 15° difference in trend between L_1 and L_2 stretching lineations appears to be statistically significant regionally, and is interpreted to be diagnostic of slightly differing azimuths of shear transport during D_1 and D_2 deformation.

D_2 kinematics

Mylonitic fabrics including S-C geometries, K-feldspar porphyroclast and hornblende porphyroblast tails, and oblique recrystallized quartz patterns examined in ten oriented thin sections from the central Symvolon pluton are equally divided between top-to-the-southwest and top-to-the-northeast shear asymmetries (Dinter et al., submitted). Estimates of shear sense based on field observations in 62 locations show an approximate 5:3 bias toward southwest-vergent shear, which I consider to be statistically insignificant owing to the uncertainties inherent in distinguishing S- and C-foliations in the field (Fig. 7). The indeterminacy of shear sense in the Symvolon mylonites contrasts markedly with the uniform southwest vergence characteristic of D_1 deformation (Kilias and Mountrakis, 1990) and also with the later Strymon Valley shear zone (Kolocotroni and Dixon, 1991; Dinter, 1991; Dinter and Royden, 1993), and may indicate a strong component of flattening (coaxial or "pure" shear) associated with D_2 mylonitization.

A critical issue concerning the tectonic significance of D_2 shearing is whether the mylonitization of the Symvolon pluton was syn- or post-intrusional. Hornblende grains in Symvolon mylonites must have crystallized in the D_2 shear environment, because they are not mechanically deformed and exhibit asymmetric "fish" shapes congruent with the ambient S-C shear geometries expressed by other D_2 fabric elements (Dinter et al., submitted). $^{40}Ar/^{39}Ar$ dates on these hornblendes are minimum crystallization ages, and so also serve as minimum ages for the onset of D_2 shearing. As these ages fall in the same range as U-Pb titanite and zircon ages that date the emplacement of the pluton, the Symvolon granodiorite must have been emplaced and concurrently mylonitized within a coaxial shear environment that was active at the southwest margin of the Rhodope core complex by ~21 - 22 Ma. In a pure-shear setting and in the absence of evidence for significant post-D_2 rotation of D_2 structural elements, the mean principal stretching axis

indicated by L_2 stretching lineations, 18°, N58°E, may be taken to approximate the finite extensional axis associated with the "Symvolon shear zone".

D_2 coaxial shearing is inferred to have occurred in an extensional environment primarily because the Symvolon pluton coincides areally with an order-of-magnitude thinning of the Falakron marble series at the southwest margin of the Rhodope core complex (Kronberg, 1969; Schenk, 1970). The magnitude of D_2 extension may amount to ~40 km based on the width of the Symvolon pluton. It is not clear how far north of Mt. Pangaion the effects of D_2 deformation persist because it is difficult to discriminate between D_1 and D_2 structural elements in the absence of clarifying intrusive relationships. The marked southwestward thinning of the Falakron series, however, is evident at least as far north as the Bulgarian border (de Boer, 1970).

D_2 timing

As noted above, the minimum crystallization ages of mylonitic hornblende provided by $^{40}Ar/^{39}Ar$ analyses indicate that D_2 shearing began no later than ~20 - 22 Ma. Such hornblende does not appear to have been deformed by further shearing subsequent to cooling below ~500°C shortly after the intrusion of the pluton. Nonetheless, mylonitization of the pluton may have continued at lower temperatures for several m.y. after its intrusion, accommodated principally by the deformation and recrystallization of biotite and quartz along C- and S-planes. D_2 shearing ceased no later than ~16 Ma, when D_2 fabrics were transected at the southwest margin of the Rhodope metamorphic core complex by the nascent Strymon Valley shear zone (Dinter and Royden, 1993).

D_3: Middle Miocene - early Pliocene extension (Strymon Valley detachment system)

The northeast-dipping Symvolon shear zone (D_2) was succeeded in middle Miocene time by the Strymon Valley detachment system (D_3), which comprises a regionally southwest-dipping low-angle normal fault and related structures in its footwall and hanging wall (Dinter and Royden, 1993). The main detachment forms the southwestern boundary of the Rhodope metamorphic core complex, cutting across D_1 and D_2 structural elements for >200 km along strike in the region northeast of the Strymon River and on the island of Thasos. Hanging-wall rocks, which were displaced relatively southwestward in the detachment system, include the Serbo-Macedonian gneiss complex and a strongly deformed syndetachment basin complex (Fig. 3).

The Rhodope metamorphic core complex emerged from mid-crustal depths in the footwall of the Strymon Valley detachment and in doing so, passed upward through the ductile-brittle transition in the crust, resulting in the overprinting of early Strymon Valley mylonitic fabrics (D_{3a}) by increasingly brittle structures (D_{3b}). The unroofing of the core complex progressed from northeast to southwest such that brittle deformation within upper levels of the detachment system proceeded contemporaneously with ductile shear down dip to the southwest (Dinter and Royden, 1993).

D_{3a} (ductile deformation): Rhodope metamorphic core complex

Along most of its sinuous outcrop length northeast of the Strymon River, the Strymon Valley detachment coincides with the structural top of the Falakron marble unit (Fig. 3). Even in areas where gneiss or granitoid constitutes the dominant footwall lithology, a highly tectonized marble carapace up to several meters thick is commonly

observed immediately beneath the detachment surface. Indeed, with few exceptions, marble responded with significantly greater ductility and mobility to D_{3a} shearing in the footwall of the detachment system than did silicic rocks at comparable structural levels. D_{3a} ductile deformation also apparently penetrated to greater depths beneath the detachment surface in carbonate rocks.

Calcite stretching lineations measured within ~5 m beneath the Strymon Valley detachment in Falakrons at the southwest perimeter of Mt. Pangaion and in the Menoikion Mountains are plotted with associated metamorphic foliations in Fig. 9 and with brittle linear shear elements measured on the detachment plane in Fig. 10. Additional data for the Vrondou, Menoikion, west Pangaion, and Symvolon areas, all of which lie along the southwest margin of the Rhodope metamorphic core complex, appear in Kolocotroni and Dixon (1991), de Boer (1970), Schenk (1970), and Kokkinakis (1980a), respectively. Surfaces interpreted as S_{3a} foliations in these areas typically have northeasterly strikes and dip at low to moderate angles, subparallel to the local orientation of the overlying detachment. L_{3a} stretching lineations vary in trend from N45°E to N65°E, but cluster strongly in the range N50°-60°E; they most commonly plunge southwest, but gentle northeast plunges are observed, as well. L_{3a} lineations within a few m beneath the detachment at the southwest perimeter of the Symvolon pluton are inferred to overprint northeast-plunging L_2 lineations that characterize the remainder of the pluton (see above), but exposure is poor and the cross-cutting relationships are generally obscure. Although post-tectonic block rotations have occurred locally, a general association of northeasterly fold and lineation plunges with deformational events D_1 and D_2, and of southwesterly plunges with event D_3 appears to be valid regionally in the Rhodope core complex, and is consistent with the inferred orientations of the Nestos, Symvolon, and Strymon Valley shear zones, respectively.

D_{3b}: Brittle deformation

Strymon Valley detachment

Although the regional dip of the Strymon Valley detachment is southwestward (Dinter and Royden, 1993), southwest-dipping detachment outcrops are rarely observed in the field because the fault surface is strongly corrugated about an axis that plunges gently to the southwest (Figs. 3 and 10). The largest corrugations, with 10 - 35 km wavelengths and amplitudes as great as ~1 km, control the gross regional structural geometry and strongly influence modern topography. Ridges in the fault surface correspond to northeast-elongate domal exposures of footwall rocks that appear in map view as a series of southwest-facing scallops at the southwest margin of the Rhodope metamorphic province, whereas depressions are occupied by southwest-thickening lobes of the syndetachment basin complex that were transported to their present positions in the hanging wall of the detachment system (Fig. 3). Smaller-scale corrugations of the detachment surface are also characteristic, ranging from undulations with 50 - 300 m wavelengths and 10 - 50 m amplitudes superimposed on the limbs of the principal corrugations (Plate 5), to outcrop-scale fluting with 1 - 5 m wavelengths and 0.2 - 1.0 m amplitudes. The regional corrugation axis defined by predominantly northeast-striking detachment-surface attitudes on the limbs of major corrugations throughout the field area is consistent in orientation with outcrop-scale fluting axes, plunging roughly 3° to S53°W (Fig. 10). There is no evidence to suggest that the corrugations at any scale are folds: syndetachment hanging-wall strata are not folded on southwest-trending axes. The corrugations therefore appear to be "fault mullions", that is, primary cylindrical undulations of the detachment surface (cf. John, 1987). Locations of major ridges and depressions in the detachment may be related in part to contrasting material properties in the footwall. The Vrondou and Symvolon plutons both

correspond to prominent footwall domes, whereas Falakron marble or schist lithologies tend to underlie major depressions (Fig. 3).

Strymon Valley low-angle normal fault exposures are of two general types, the type developed in any given area being primarily dependent on the nature of the overlying hanging-wall material. Discrete, well-polished detachment surfaces, commonly streaked with chloritic microbreccia and overlain by a layer of white, calcareous rock flour, typically underlie hanging-wall sections dominated by poorly consolidated clastic sediment. By contrast, fault zones as thick as 40 - 50 m, characterized by distributed shear and intense brecciation, occur where the hanging-wall material is highly indurated limestone or crystalline metamorphic rock.

Discrete detachment surfaces

Cross-sectional exposures of discrete detachment planes developed on marble or granitic footwall lithologies preserve 2 - 5 cm, rarely up to a meter, of polished, resistant, dark brown chloritic microbreccia, which contains angular fragments up to 5 mm in diameter of the underlying footwall material. Flat-iron exposures typically preserve only a few mm of this microbreccia arrayed in diffuse streaks that trend within a few degrees of S53°W, subparallel to outcrop-scale fluting of the detachment surface (Plate 6). Rare slickenside grooves have similar orientations. Marble weathers faintly pink for several cm immediately below the microbreccia layer; granitic rocks weather to a rust color.

Discrete detachment surfaces are commonly overlain by a distinctive white- to offwhite-weathering, highly calcareous, very fine-grained, poorly to moderately consolidated layer of rock flour (ultracataclasite) 1 - 5 m thick (Plate 7). In most exposures the rock flour is unfoliated and contains 5 - 30% angular to subrounded fragments derived

from both footwall and hanging-wall rocks dispersed with random orientations in the white, fine-grained matrix. Angular marble fragments and gneissic quartz augen are common footwall-derived clasts; highly weathered, strongly foliated, granitic or gneissic cobbles and sheared, angular clasts of dark gray laminated mudstone represent the hanging wall. Thin sections of the matrix material show it to consist of 50 - 90% cryptocrystalline calcite, locally recrystallized, presumably derived primarily from marble in the footwall, and up to 50% angular to subrounded, randomly oriented, microclasts of feldspar and quartz ≤ 1 mm in diameter (Plate 8). Relatively minor constituents include up to 3% coarse, detrital muscovite, typically crimped and folded on a microscopic scale, 1% fine- to medium-grained biotite, and 1% subhedral red garnet ≤ 0.5 mm in diameter. The muscovite, which occurs in flakes as large as 1 cm in diameter, appears to be derived from cobbles of pegmatite and two-mica gneiss that appear in basal conglomerates of the supradetachment basin complex.

Diffuse low-angle fault zones

Discrete low-angle fault surfaces rarely underlie hanging-wall suites dominated by well-consolidated marl, algal limestone, or marble breccia; rather, shear strain in such settings is distributed throughout a brecciated zone as thick as 40 - 50 m. Mixtures of angular hanging-wall and footwall clasts ranging from boulder-size down to fine grit are characteristic of such zones, which are plausible sources of landslide and debris flow breccias that occur intermittently within the supradetachment basin. Matrix material in diffuse shear zones is gritty, angular, poorly-sorted sand derived at least in part by tectonic abrasion of larger clasts. Approximately the lower third of a typical low-angle breccia zone contains clasts derived primarily from the footwall, the upper third is dominated by hanging-wall clasts, and the central section contains a thorough mixture of clasts from above and below. Where the hanging-wall material is limestone, the portion of the breccia

zone dominated by limestone clasts weathers deep tuscan red. Diffuse low-angle shear zones terminate through transitional intervals ~5 - 10 m thick in which fracturing becomes progressively less severe. The Strymon Valley low-angle normal fault was mapped at the top of intact footwall material in areas of distributed shear.

Rhodope metamorphic core complex

Immediately beneath the main detachment, marble is commonly highly fractured within an allochthonous slab as thick as 10 m bounded below by an intrafootwall detachment, and granite and gneiss are divided by anastamosing, microbrecciated shear surfaces into axe-blade-shaped lenses 2 - 3 m wide and up to 1 m thick, elongate in the direction of detachment displacement. Angular blocks of marble, gneiss, or granite up to 10 m thick that were probably incised from this zone occur sporadically at the base of the hanging wall. In most places they lie in direct contact with the detachment plane or are separated from it by a few cm of highly sheared mudstone.

Gently southwest-dipping, planar to slightly curviplanar, microbrecciated, intrafootwall detachments are common in the Falakron marble series, and are also found locally within the Symvolon pluton. They are generally restricted to the upper 80 - 100 m beneath the main detachment plane, and commonly develop subparallel to local S_{3a} metamorphic foliations. As many as three such surfaces in a vertical section divide the marble or granite into distinct tabular masses 5 - 20 m thick. The intrafootwall detachments must have formed earlier than the main detachment because they are commonly trucated by it up dip at very low angles (Plate 9). Given the lack of stratigraphic control in the Falakron series and the Symvolon granodiorite, it is difficult to determine whether the intrafootwall detachments omit section. They are assumed to have accommodated regional

extension, however, because of their unambiguous spatial and geometric affinities to the Strymon Valley detachment.

Minor normal faults with offsets of 0.1–3.0 cm, spaced at 0.1–3.0 m intervals in the Symvolon granodiorite, strike in the range N55°–85°W and most commonly dip steeply to the southwest (Fig. 11). Although these structures strike parallel to major normal faults associated with the subsidence of the Strymon and Drama basins (D_4), they are not brecciated, and so probably represent deeper and, therefore, somewhat older deformation. I tentatively regard these and similar faults in the Falakron series (Fig. 12) as D_{3b} structures that facilitated the isostatic uplift of emerged northeasterly sections of the Rhodope core complex relative to yet-to-be-unroofed southwesterly sections.

Supradetachment basin complex

The D_3 syndetachment basin complex, represented in the present map area by the Angitis, Akropotamos, and South Symvolon basin lobes, was strongly disrupted by both high- and low-angle normal faults as it moved southwestward over the emerging Rhodope core complex in the hanging wall of the Strymon Valley detachment (Plate 10). Moderate- to high-angle, N20°-70°W-striking normal faults commonly sole into or are truncated by the main detachment. Low-angle normal faults are also widely developed, many representing splays from the main detachment. Angular unconformities within the basin section indicate that deformation proceeded concurrently with deposition.

The white, calcareous rock flour that commonly mantles the main detachment (see above) was highly mobile during D_3 deformation and appears in pods and lenses scattered along shear zones throughout the supradetachment basin. Above the basal rock-flour layer, a strongly sheared interval as thick as ~30 m consists of small shear-bounded lenses of

siltstone, lignite, laminated, dark gray mudstone, and poorly consolidated sandstone and conglomerate. Anastamosing shear surfaces both subparallel to and strongly discordant with the main detachment are pervasive in this interval, which appears to serve locally, with the underlying rock flour, as a basal accommodation zone for bookshelf-style block rotations of overlying hanging-wall strata on normal faults both synthetic and antithetic to the main detachment.

Bedding planes in clastic strata of the northeast Angitis basin characteristically dip 10° - 40° southwest, with a well-defined mean attitude of N38°W, 28°SW (Fig. 13). The tilting of these beds was facilitated by moderate- to high-angle, N25°-65°W-striking, northeast-dipping normal faults *antithetic* to the Strymon Valley detachment (Fig. 14). As such faults are locally observed to sole into or be truncated by the main detachment, they must be syndetachment structures (D_{3b}). Tilted blocks bounded by these relatively major faults are internally extended on minor northwest-striking normal faults spaced ≤ 2 m apart, with offsets ranging up to ~0.5 m (Plate 11). The Menoikion carbonate breccia, interpreted as a large-rock avalanche deposit (Dinter, 1994; cf. Yarnold and Lombard, 1989; de Boer, 1970), overlies the southwest-tilted siliciclastic section at the northern margin of the Angitis basin, where its base is truncated by the Strymon Valley detachment. The structural affinities (D_{3b} vs. D_4) of moderate- to high-angle, northwest-striking shear zones in this unit are difficult to establish because their relationship to the detachment is unclear and bedding is less regular than in the underlying section (Fig. 15). In the Akropotamos and south Symvolon basin lobes (Fig. 3), syndetachment strata typically dip 10° - 45° northeast, with a mean attitude of N50°W, 32°NE (Fig. 16). They were tilted into these orientations on moderate- to high-angle, southwest-dipping D_{3b} normal faults *synthetic* to the Strymon Valley detachment, with strikes in the range N35°-65°W (Fig. 17). Southwest-dipping shear zones in the northeast Angitis basin and northeast-dipping shear

zones in the Akropotamos and south Symvolon basins apparently did not cause significant rotation of bedding, and are tentatively regarded as D_4 structures (see below).

Intrabasinal low-angle shear zones, microbrecciated and suffused with distorted pods of white, calcareous rock flour, are typically localized in fissile mudstone or siltstone beds and persist over areas as large as several km^2 (Plate 12). They also occur as bedding-parallel shears in algal carbonate and evaporite lithologies. In many instances these structures displace the D_{3b} high-angle normal faults described above and represent splays of the main detachment. Elsewhere, the low-angle surfaces are not tectonic faults, but surficial shear zones that facilitated the emplacement both of relatively intact gravity slides and of highly deformed landslide-breccia sheets such as the Menoikion carbonate breccia. The presence of such deposits at numerous stratigraphic levels attests to an active tectonic environment during the accumulation of the supradetachment basin complex.

Serbo-Macedonian metamorphic province

The crystalline portion of the Strymon Valley hanging wall, the Serbo-Macedonian metamorphic province, was not examined in detail because it rarely crops out in the area mapped northeast of the Strymon River. A small tract of Serbo-Macedonian gneiss exposed immediately above the Strymon Valley detachment at the southwest margin of Mt. Pangaion bears northeast-trending stretching lineations of uncertain tectonic affinity (Schenk, 1970). Steep, southwest-dipping, N15°-55°W-striking shear zones prominent in quarry exposures of Serbo-Macedonian schist and paragneiss in the Kerkini Mountains at the northern boundary of the Strymon basin may represent D_{3b} normal faults; however, their relationship to the underlying Strymon Valley detachment is unknown.

D_3 kinematics

Top-to-the-southwest shear asymmetries associated with gently plunging, northeast-trending stretching lineations are characteristic of D_{3a} mylonites at the southwest margin of the Symvolon pluton and in isolated orthogneiss windows beneath the Serres basin (Dinter, 1991; Dinter and Royden, 1993). The Vrondou pluton also bears gently southwest-plunging stretching lineations and S-C fabrics indicative of uniform top-to-the-southwest shearing along its strongly mylonitized southern margin. Kolocotroni and Dixon (1991) argue that the mylonitization of the Vrondou body was synintrusional, because the mylonites are intruded by "later melts" that are also somewhat mylonitic. This conclusion is difficult to reconcile, however, with the undeformed nature of the pluton's northern and eastern intrusive margins and much of its interior, and with the lack of any regional evidence for mid-Oligocene shear deformation. I interpret the Vrondou mylonites as products of D_{3a} shearing because (1) they are restricted to areas immediately underlying the Strymon Valley detachment, and (2) both the orientation and sense of shear in the mylonites are congruent with later brittle displacement on the detachment (D_{3b}). The "later melts" are inferred to represent minor synextensional magmatism unrelated to the mid-Oligocene emplacement of the main Vrondou body. The age of the "later melts" is crucial to resolving this issue; unfortunately, they have not yet been dated.

Closed or "fused" tensional cracks are commonly observed subperpendicular to calcite stretching lineations in Falakron series marbles. Two generations of such cracks are visible in the Menoikion Mountains (Plate 13). The older set is associated with ~S35°W-trending lineations, inferred to be D_1 shear elements (see above), and the younger set with ~S53°W-trending lineations, presumed to represent Strymon Valley detachment deformation. Where the third dimension is visible, the cracks typically dip steeply in the inferred direction of upper plate transport, top-to-the-southwest for both the D_1 and D_3

events. In some places, the cracks offset metamorphic foliations a few mm in a normal sense, down-to-the-southwest for both D_1 and D_3 deformation.

Brittle linear shear elements associated with displacement on the Strymon Valley detachment include corrugation or "mullion" axes at outcrop- to regional scales, microbreccia streaks, and rare slickenside grooves, all of which define a regional D_{3b} shear axis of 3°, S53°W (Fig. 10). A uniform top-to-the-southwest sense of D_{3b} shearing is implied by the southwest-facing geometries of small duplex structures that are commonly developed on the detachment surface where the substrate is marble and the hanging wall consists of poorly consolidated clastic deposits (Dinter and Royden, 1993). The duplexes are constructed of marble slivers 1 - 4 cm thick thrust successively into a nested stack 5 - 15 cm high and 1 - 2 m wide (Plate 14). They typically terminate at a roughly lunate, southwest-facing fracture that may have an accumulation of chloritic microbreccia at its base, in the structural shadow of the stacked slivers (Fig. 18; Plate 15).

Weak foliations defined by the alignment of coarse detrital muscovite and finer biotite grains are locally developed in the white cataclasite layer immediately overlying the detachment surface. Such foliations typically dip gently northeast and intersect the regionally southwest-dipping detachment surface at a low angle, defining a megascopic shear fabric that geometrically resembles a mylonitic S-C fabric indicative of top-to-the-SW shear. If the sense-of-shear implications of the two fabrics are similar, then the orientations of the cataclasite foliations provide additional evidence that the hanging wall of the detachment system moved southwest with respect to its footwall.

D_3 timing and rate constraints

The Strymon Valley detachment truncates the ~21 - 22 Ma Symvolon pluton at its southwest margin and is itself displaced by high-angle normal faults bounding the late Pliocene(?) - Quaternary Strymon and Drama basins. Closer constraints on the timing of D_3 deformation are provided by the ages of fossils contained in the syndetachment basin complex and by $^{40}Ar/^{39}Ar$ dates on biotite and K-feldspar separates from the Symvolon pluton, which cooled through the Ar closure temperatures of those minerals as it emerged in the footwall of the Strymon Valley detachment.

Syndetachment basin strata are pervasively disrupted by syn- and post-depositional faults and their faunal suites generally lack reliable stratigraphic context as a result. Nonetheless, these deposits have been widely sampled for fossils so that the *range* of ages they represent is fairly well characterized and provides a primary constraint on the timing of Strymon Valley detachment activity. The oldest specimen presently known from the syndetachment basin complex is a tooth of *Micromeryx flourensianus* Lartet recovered in a borehole from the oldest unit in the Struma basin, the Delcevo Formation (Kojumdgieva et al., 1982). This is an early Miocene species on the Balkan Peninsula (MN3 – MN6) and is probably 15 - 18 Ma in age (R. Bernor, personal commun., 1992). The youngest known syndetachment deposits are nonmarine sandstones of the Spilia formation in the Serres basin, which bear MN15 rodent fauna that may be as young as 3.5 Ma (Armour-Brown et al., 1979; Steininger and Rögl, 1984).

K-Ar biotite dates of 15.5 ± 0.5 Ma and 17.8 ± 0.8 Ma from the Symvolon pluton (Kokkinakis, 1980b) and 13.8 ± 0.2 Ma and 15.0 ± 0.3 Ma from the Mesolakkia pluton, which intrudes the Falakron series beneath Mt. Pangaion (Harre et al., 1968), were interpreted by Dinter and Royden (1993) as cooling ages related to the emergence of the

Rhodope metamorphic core complex in the footwall of the Strymon Valley detachment. More reliable $^{40}Ar/^{39}Ar$ biotite and K-feldspar ages from the central part of the Symvolon pluton range from 11.1 ± 0.2 Ma to 15.5 ± 0.3 Ma, defining a general trend of more youthful cooling ages to the southwest that is consistent with a southwestward-progressive unroofing of the pluton during D_3 deformation (Fig. 7; Table 1; Dinter et al., submitted).

Assuming *a priori* that the southwestward decrease in $^{40}Ar/^{39}Ar$ biotite and K-feldspar ages from the Symvolon pluton is related linearly to the southwestward-progressive unroofing of the core complex, a speculative estimate of ~6.0 mm/yr may be calculated for the average middle Miocene horizontal displacement rate on the Strymon Valley detachment using a biotite date of 15.4 Ma for sample M90-K5 at the northeast margin of the study area and a value of 13.4 Ma representing a group of samples collected ~12 km to the southwest (Fig. 7). An independent reckoning of the average displacement rate along any displacement-parallel cross section may be derived by dividing the width of the core complex there by the total duration of detachment activity, ~12.0 - 14.5 m.y. based on the range of fossil ages in the supradetachment basin. At the latitude of the Symvolon pluton the core complex is ~80 km wide, corresponding to displacement rates in the range 5.5 - 6.7 mm/yr, which brackets the value inferred from the $^{40}Ar/^{39}Ar$ cooling ages.

D_4: Late Pliocene - Quaternary extension (Strymon and Drama Basins)

Northwest-striking, high-angle normal faults bounding the Strymon and Drama basins are the defining elements of a D_4 extensional system that superseded the Strymon Valley detachment ~3.5 Ma (Dinter and Royden, 1993). Such faults offset the Strymon Valley detachment by as much as 3.5 km vertically based on the depth to the base of unconsolidated deposits in the Strymon 1 borehole (Erki et al., 1984). D_4 range-front faults are commonly covered by highly consolidated marble talus breccia; however, rare

stream cuts at the southwest margin of the Drama basin reveal D_4 fault zones as wide as 15 m composed of angular breccia blocks up to ~1 m in diameter in an unconsolidated, sandy, porous, dark-red weathering matrix. As noted above, relatively minor northwest-trending shear zones that cut but do not rotate D_3 strata between the Strymon and Drama basins are also regarded as probable D_4 structures (Figs. 14 and 17).

Relatively steep faults of at least three general orientations have modified the margins of the Strymon and Drama basins and are considered here to represent late D_4 deformation (Fig. 19). Steep faults striking in the range N40°-50°E appear to be mainly dextral(?) strike-slip structures, although they may accommodate some normal displacement as well. Three major faults of this type were recognized (Fig. 3): The "Tower Bluff fault" parallels the North Aegean coastline southeast of Mt. Symvolon and may be a segment of the regionally developed Kavala-Xanthi-Komotini strike-slip fault (e.g., Lybéris, 1984; Koukouvelas and Doutsos, 1990). It juxtaposes a carbonate conglomerate of unknown age against poorly consolidated D_3 and D_4 sediments. The "Achladochorian fault" forms the southeast boundary of the small Achladochorian basin near the Bulgarian border, juxtaposing the Falakron marble laterally against the northwest margin of the Vrondou pluton. The "Angitis fault" is identified solely on morphologic grounds. The N50°E-trending Angitis Gorge deeply incises the Falakron marble between the Strymon and Drama basins and is offset by several right steps of ~100 m, each associated with an apparent dextral rhombochasm defined by the gorge walls. On this basis the Angitis River is tentatively inferred to follow the trace of a N50°E-trending dextral strike-slip fault with relatively minor cumulative offset.

Steep normal faults striking N75°-85°W and bearing near-vertical slickenside grooves displace the Strymon Valley detachment up to ~50 m vertically and also appear to cut northwest-striking D_4 range-front faults at the southwest margin of the Drama basin

(Plate 16). I interpret such faults, which are commonly associated with dramatic scarps, as secondary extensional structures in a modern (late-D_4) tectonic regime dominated by distributed dextral shear on the northeast-trending strike-slip faults described above. Relatively minor, steep faults trending N25°-40°E that displace range-front faults by as much as 10 - 15 m in a normal and/or strike-slip sense may represent splays or tertiary shears ("P-shears") within this system (e.g., Twiss and Moores, 1992).

Widely developed, rough to smooth, steep, disjunctive joints spaced at regular intervals of 0.3 - 3.0 m in the Falakron marble series strike predominantly in the range N15°-45°E (Fig. 20; Plate 17). Most were measured on Mt. Menoikion, but scattered attitudes from the Falakron Mts. and western Mt. Pangaion are also included. In some places, two sets of steep joints nearly parallel in strike and intersecting at angles ≤20° are developed, neither set offsetting the other (Plate 18). S_{3a}(?) metamorphic foliations are not significantly offset by these joints, but display some disjuncture across them owing to the origin of the joints as pressure solution surfaces. Gentle corrugations of joint surfaces about subhorizontal axes are common. The joints must be D_{3b} or D_4 structures owing to their brittle nature. As disjunctive joints are thought to coincide with the plane of principal flattening at the time of their formation (e.g., Twiss and Moores, 1992), I tentatively consider the observed joints to be late D_4 structures, because flattening on high-angle planes striking N15°-45°E is dynamically consistent within the northeast-striking dextral strike-slip system that appears to control the geometry of late D_4 deformation (see above).

D_4 kinematics and timing

The southwest margins of the Strymon and Drama basins are steep, faulted contacts between bedrock and modern basin fill, whereas their northeast margins slope more gently toward the basin axes. This asymmetry is suggestive of a half-graben morphology, and is

shared by the Vardar-Thermaikos basin west of Thessaloniki (Bornovas and Rondogianni-Tsiambaou, 1983) and by several offshore basins in the north Aegean Sea (e.g., Lybéris, 1984). Dinter and Royden (1993) suggest that these basins may be subsiding above an active, northeast-dipping "North Aegean detachment" that succeeded the Strymon Valley detachment as the major structure accommodating extension in the north Aegean region. The D_4 detachment system probably terminates southward at the N45°E-trending North Aegean Trough, which represents the offshore continuation of the dextral North Anatolian strike-slip fault (Fig. 2). The sole chronological datum presently constraining the transition from D_3 to D_4 detachment activity is the youngest known age of deposits within the D_3 supradetachment basin complex, ~3.5 Ma (see above).

Subsidence in the Strymon and Drama basins was accompanied by significant uplift of the region between them. The Menoikion carbonate breccia, inferred to have been deposited at or near sea level in Messinian time (Dinter, 1994), now appears at elevations of nearly 1500 m in the footwall of normal faults bounding the Drama basin at its southwest margin. Assuming that this uplift began upon the cessation of Strymon Valley detachment activity ~3.5 Ma, the average uplift rate since that time is ~0.4 mm/yr. A second sea level datum is provided by an undeformed late Pliocene or Quaternary (D_4) wave-cut platform that lies at an elevation of ~290 m on the southwest flank of Mt. Pangaion. As glacioeustatic variations can only account for sea levels up to ~60 m higher than at present from late Pliocene through Quaternary time (e.g., Dinter et al., 1990), this platform must have risen at least 230 m since it formed.

Northwest-striking D_4 normal faults bounding the Strymon and Drama basins may still be active in some places. The modern kinematic environment appears to be dominated, however, by a system of N40°-50°E-striking dextral strike-slip faults that includes, as secondary components, steep normal faults striking N75°-85°W and relatively minor, steep

strike-slip(?) faults striking N25°-40°E. Focal plane mechanisms of large earthquakes suggest that such faults may be responsible for modern seismicity in the north Aegean region: Events centered in the North Aegean Trough have yielded dextral strike-slip mechanisms on vertical, northeast-striking planes, and the Thessaloniki (1978) and Volos (1980) earthquakes involved normal slip on high-angle surfaces trending ~N80°W (e.g., Jackson and McKenzie, 1983). A chain of Plio-Quaternary trachyte-rhyolite fissure eruptions that trends N75°W across the northern part of the Greek Serbo-Macedonian province (Panagos et al., 1978) may also coincide with a major zone of secondary normal faulting within the northeast-trending late-D_4 wrenching regime.

DISCUSSION

Paleogeographic implications of D_3 displacement: A proposed correlation

The Serbo-Macedonian gneiss complex moved relatively southwestward in the hanging wall of the Strymon Valley detachment as the Rhodope metamorphic core complex emerged to the northeast in its footwall. The minimum offset on the detachment in northern Greece is constrained by the displacement-parallel width over which supradetachment basinal deposits are tilted and truncated at the detachment surface, ~25 km (Dinter and Royden, 1993). A more realistic minimum of cumulative detachment offset in any given location may be provided by the width of the core complex, which approximately coincides with the exposed width of the Falakron marble series and increases southward to ~80 km at the north Aegean coastline. Restoration of the Serbo-Macedonian province to its pre-D_3 position overlying the Falakron series implies that prior to ~16 Ma, the Serbo-Macedonian and West Thracian gneiss complexes were adjacent, and it is tempting on geometric grounds to suggest that they may be correlative (Fig. 3). The gross lithologic,

geochemical, and structural characteristics of these units are compared briefly below in an effort to establish whether they are sufficiently similar to support such a correlation.

Gneiss, schist, and amphibolite assigned to the Vertiskos series constitute the bulk of the Serbo-Macedonian gneiss complex in Greece (Kockel et al., 1971). The dominant foliations in this unit dip southwest, and formed during a regional metamorphic event that reached upper amphibolite-facies conditions (Kockel et al., 1977). The southwest-dipping fabrics are cut by northeast-dipping shear zones at the southwestern margin of the Vertiskos series, where it is underthrust by weakly metamorphosed Triassic to Lower Jurassic(?) sediments of the circum-Rhodope belt (Kauffmann et al., 1976). This underplating by relatively cool continental material may be related to the Early to Late Cretaceous cooling of Vertiskos rocks indicated by K-Ar and $^{40}Ar/^{39}Ar$ biotite and muscovite dates ranging from 136.8 ± 1.5 Ma to 87.8 ± 4.2 Ma (Harre et al., 1968; Marakis; 1969; Papadopoulos and Kilias, 1985; De Wet et al., 1989). The Volvi ultramafic complex, the largest of numerous basic and ultrabasic bodies within the Vertiskos series, is interpreted by Dixon and Dimitriadis (1984) as a Mesozoic intracontinental rift complex. K-Ar hornblende dates from amphibolites near its northeast margin fall in the range 113 - 116 Ma (Harre et al., 1968). Schist, migmatitic gneiss, and amphibolite of the Kerdilion series, which underlies the Vertiskos series beneath a brittle, southwest-dipping shear zone, yielded 32 - 38.5 Ma K-Ar biotite dates, 36 - 43 Ma K-Ar muscovite dates, and a single K-Ar hornblende date of 79.5±1 Ma (Harre et al., 1968).

The West Thracian gneiss complex, which overlies the Falakron marble series at the northeast-dipping Nestos thrust, consists primarily of quartzo-feldspathic and pelitic gneisses, migmatites, amphibolites, and partially amphibolitized eclogites, with ultramafic bodies, including large tracts of serpentinite, becoming increasingly common to the east (Kronberg, 1969; Kronberg and Eltgen, 1973; Liati, 1986, 1988; Mposkos, 1989). Three

successive metamorphisms have affected this unit: (1) a high-P event that produced eclogites from tholeiitic basalt protoliths, (2) a regional amphibolite-facies event during which the eclogites were almost completely converted to amphibolites and gneissic rocks were partially melted to form migmatites, and (3) a retrograde greenschist-facies event that strongly affected only the lower part of the gneiss complex, adjacent to the Nestos thrust (Kronberg and Raith, 1977; Liati, 1986, 1988; Mposkos, 1987, 1988, 1989, Mposkos and Perdikatsis, 1987; Mposkos et al., 1988; Liati and Mposkos, 1990; Kotopouli and Pe-Piper, 1989b; Kotopouli et al., 1991). An Eocene age has been interpreted for the amphibolite-facies event on the basis of K-Ar dates ranging from 37.3 ± 0.6 Ma to 46.9 ± 0.7 Ma on recrystallized hornblendes (Liati, 1986; Koukouvelas and Doutsos, 1990; Kotopouli et al., 1991). However, as K-Ar dates represent *cooling* ages, and temperatures attained during the high-grade event were much higher than the ~500°C closure of hornblende to Ar (Harrison, 1981), these dates must be considered minimum metamorphic ages. A Rb-Sr whole rock isochron of 87.7 ± 27 Ma (initial $^{87}Sr/^{86}Sr = 0.706 \pm 0.0002$) reported for the Elataia granodiorite by Soldatos (1985) may approximate more closely the time of peak amphibolite-facies metamorphism. K-Ar hornblende dates of 57.4 ± 0.6 Ma, 78.9 ± 0.6 Ma, and 95.1 ± 1.1 Ma yielded by partially recrystallized eclogites are considered by Liati (1986) to result from excess Ar. Alternatively, if these dates represent partially reset ages related to the initial crystallization of the eclogitic amphiboles, then a minimum Albian - Cenomanian age is indicated for the early high-P event.

It is apparent from the foregoing discussion that the Serbo-Macedonian and West Thracian gneiss complexes are markedly similar in pre-D_3 tectonic position, lithology, metamorphic grade, and radiometric age characteristics. I propose here that they are correlative, and that prior to their Neogene separation on the Strymon Valley detachment, they formed a single, continuous tectonostratigraphic unit. The composite Serbo-Macedonian-West Thracian gneiss complex consists of strongly sheared metasediments,

metabasites, metaeclogites, serpentinites, ophiolitic remnants, and syndeformational intrusives that were first metamorphosed under extremely high-P conditions and later subjected to regional high-T metamorphism. These characteristics are inconsistent with the established interpretation of the Serbo-Macedonian and West Thracian metamorphic provinces as components of a Rhodope continental fragment that was deformed in the hinterland of the Vardar subduction zone (e.g., Jacobshagen et al., 1978; Burchfiel, 1980). The composite gneiss unit more likely represents a pre-Cretaceous accretionary subduction complex that was subducted and then transferred, perhaps by underplating, to a position within a thickening marginal orogen (cf. Platt, 1986). Early Cretaceous cooling ages are common in the Serbo-Macedonian Vertiskos series, whereas the oldest ages known from the West Thracian complex are Cenomanian, which may imply that the unroofing of the orogen progressed from southwest to northeast (Tables 5 and 7).

The D_1 Nestos thrust: Middle-late Eocene continental subduction

The D_1 shear event in the Rhodope metamorphic core complex corresponds to the ductile thrust emplacement of the upper amphibolite-facies Serbo-Macedonian-West Thracian gneiss complex over the upper greenschist-facies Falakron marble series. As detailed above, northeast-plunging D_1 stretching lineations and folds indicate an azimuth of D_1 shear in the range N40°-50°E (Meyer, 1969; Kronberg and Eltgen, 1973; Kronberg and Raith, 1977), mylonitic fabric asymmetries imply southwest thrust vergence (Kilias and Mountrakis, 1990), and crosscutting relationships with the Vrondou and Xanthi plutons constrain a pre-mid-Oligocene age for D_1 deformation. The presence of relict high-P metamorphic assemblages in the Falakron series on the island of Thasos (Atzori et al., 1990) suggests that the Rhodope core complex was subducted during the D_1 event; upper greenschist-facies mineral assemblages characteristic of that unit elsewhere presumably represent retrograde metamorphic conditions that prevailed during its exhumation. D_3

extensional displacement opened a tectonic window into the D_1 subduction zone. Indeed, it is possible that the Strymon Valley detachment represents a reactivation of a segment of the Nestos thrust as a low-angle normal fault. Owing to the near parallelism of D_1 and D_3 shearing, the width of the "Falakron window" constrains not only the magnitude of D_3 extension (see above), but also the minimum amount of D_1 shortening, which is thus >80 km without accounting for folding or ductile strain.

Radiometric data from the West Thracian gneiss complex reported in Liati (1986) may provide more precise constraints on the age of D_1 deformation (Table 7). K-Ar hornblende dates in the range 45.5 - 46.9 Ma from mafic rocks <1 km above the Nestos thrust zone, and somewhat younger dates of 37.3 - 41.4 Ma from similar rocks 1 - 3 km structurally higher in the gneiss complex, were interpreted by Liati (1986), Koukouvelas and Doutsos (1990), and Kotopouli et al. (1991) as peak amphibolite-facies metamorphic ages (see above). I propose instead that these dates record the abrupt cooling of amphibolites near the base of the West Thracian gneiss complex to temperatures below ~500°C as a result of being underthrust by the relatively cool Falakron carbonate slab beginning ~47 Ma. Inverted metamorphic and cooling gradients within and above the Nestos thrust are inferred to reflect the thermal equilibration of the West Thracian gneiss complex to this continental subduction event. Upward-progressive cooling of the gneiss complex through ~37.3 Ma probably indicates continued subduction of the Falakron slab until at least that date, because thermal models of the subduction process imply that sustained underthrusting of cool material is required to maintain low-T conditions at depth in a subduction zone (e.g., Oxburgh and Turcotte, 1974; Draper and Bone, 1981; England and Thompson, 1984; Rubie, 1984; Peacock, 1987). K-Ar muscovite dates of 36.8 ± 0.6 Ma to 42.0 ± 1.0 Ma obtained from the Kerdilion series west of the Strymon Valley record the cooling of the lower part of Serbo-Macedonian gneiss complex below ~420°C, and are

consistent with the inferred middle-late Eocene age of D_1 continental subduction (Table 5; Harre et al., 1968; Robbins, 1972).

Subduction-related mid-Oligocene magmatism

Intrusives with compositions, radiometric ages, and structural settings similar to those of the Vrondou and Xanthi plutons are scattered throughout the southern Rhodope province. The small Granitis and Krinides (or Philippi) granites, which intrude the Falakron series between the Vrondou and Xanthi bodies, yielded 28.2 ± 0.5 Ma and 26.0 ± 0.5 Ma K-Ar biotite dates, respectively (Meyer, 1968). Del Moro et al. (1988) interpret Rb-Sr biotite-whole rock isochron ages in the 28 - 32 Ma range obtained from several small granodiorite and quartz monzonite bodies in eastern Thrace, 50 - 70 km east of Xanthi, as emplacement ages. Together with the Vrondou and Xanthi bodies, these granitoids define a prominent belt of mid-Oligocene (~28 - 33 Ma) calc-alkaline plutonism that trends ~N80°W for more than 200 km across the southern Rhodope province (Fig. 2). This belt is closely related spacially, temporally, and compositionally to the Paranestion volcanic series, a calc-alkaline arc suite composed of andesites, rhyolites, and dacites that overlies the West Thracian gneiss complex along the Greek-Bulgarian border (Fig. 3; Fytikas et al., 1984). The Xanthi granodiorite and rhyolitic Paranestion tuffs are nearly identical in composition, and are interpreted by Kotopouli and Pe-Piper (1991) as magmatic equivalents. Biotite and sanidine separates from the Paranestion volcanics yielded K-Ar dates ranging from 28.7 ± 1.1 Ma to 30.6 ± 1.1 Ma (Eleftheriadis and Lippolt, 1984).

Given the association with arc volcanics and a geochemical character consistent with a fractionated mantle source contaminated by crustal constituents, the Vrondou and Xanthi plutons are considered by Kotopouli and Pe-Piper (1989a), Kolocotroni and Dixon (1991), and Koukouvelas and Pe-Piper (1991) to be products of subduction-related

magmatism. A similar origin is inferred for the mid-Oligocene granitoids and volcanics of eastern Thrace by Innocenti et al. (1984) and Del Moro et al. (1988). Thus the west-northwest-trending Vrondou-Xanthi-Thracian intrusive belt appears to have been emplaced above a mid-Oligocene subduction zone.

Structural context of coaxial D_2 shearing

The Symvolon pluton was emplaced and mylonitized beginning ~22 Ma in a northeast-dipping zone of relatively pure (coaxial) shear at the southwest margin of the Rhodope metamorphic core complex. The tectonic context of the Symvolon shear zone remains somewhat enigmatic. It may be significant, however, that the Falakron marble series is >5000 m thick north and east of the Drama basin, but only 200 - 500 m thick to the southwest, where it is intruded by the Symvolon pluton (Kronberg et al., 1970; Schenk, 1970). Owing to the paucity of original sedimentary horizons in the Falakron series, a stratigraphic origin for its dramatic southwestward thinning cannot be ruled out. However, given the areal coincidence of the attenuated marble section with the Symvolon body and the strong evidence of congruent, synintrusional stretching and shearing in the intrusive and its Falakron cover rocks, I propose as a more likely alternative that the Symvolon shear zone represents an extensional rupturing of the Falakron carbonate slab that occurred while it still lay at mid-crustal depths beneath the Serbo-Macedonian gneiss complex. Such a rupture might have accommodated the mid-crustal termination of a northeast-dipping, early Miocene extensional detachment; alternatively, it could represent a ramp space that facilitated the descent of such a detachment to a deeper structural level. The up-dip portion of any northeast-dipping detachment linked to the Symvolon rupture would be expected to daylight somewhere west of Serbo-Macedonia. It may be notable in this context northeast-dipping low-angle normal faults active ~23 - 16 Ma have been mapped in the Mt. Olympos region immediately west of the Vardar zone (Fig. 2; Schermer, 1993).

The Symvolon pluton is not an isolated early Miocene magmatite. It occurs at the northern end of an enormous tract of andesitic volcanics dated at 22.7 - 15.5 Ma that crops out in a northwest-trending belt on numerous northeast Aegean islands and covers much of the northwest corner of Turkey (Fytikas et al., 1984). If this belt is localized above a mid-crustal extensional rupture, then this rupture may persist southeastward for >200 km.

Tectonic implications of D_2 - D_4 extension

Aegean crust appears to have extended by ~100% in the back-arc of the Hellenic subduction system, because its ~22 - 32 km thickness is only about half that of mainland Greece and Turkey (Jongsma et al., 1977; Makris, 1976; Makris and Vees, 1977). Results presented here imply that in the northeast Aegean region, much of this extension was accommodated by up to 80 km of displacement on the southwest-dipping Strymon Valley detachment. If the coaxial Symvolon shear zone was kinematically linked to an extensional detachment, and if the Strymon and Drama basins are subsiding above an active, northeast-dipping, "North Aegean detachment" as posited by Dinter and Royden (1993), then virtually all Neogene thinning in northeastern Greece may have been facilitated by a succession of three detachment systems that alternated in polarity.

As noted above, segments of the Strymon Valley detachment have previously been interpreted as outcrops of a northeast-vergent Neogene thrust, the "Strimonüberschiebung" (Kockel and Walther, 1965; Schenk, 1970; Koukouzas, 1972). This structure has long been cited as evidence of a regional compressional event in late Oligocene or early Miocene time, to which the folding and tilting of Paleogene basinal deposits in various parts of the north Aegean have also been ascribed (e.g., Mercier, 1968; Lybéris, 1984; Koukouvelas and Doutsos, 1990). The occurrence of such an event is questionable in light of the

reinterpretation of the "Strimonüberschiebung" as a low-angle normal fault and the realization that Tertiary strata in the hanging wall of the Strymon Valley detachment were folded and tilted in an *extensional* environment.

The recognition of the Siderokastro, Serres, Angitis, and Akropotamos basins as lobes of a deformed supradetachment basin complex necessitates a reevaluation of two common assumptions regarding their tectonic origins: first, that they represent *in situ* grabens filled principally by clastic material derived from the surrounding highlands, and second, that they are genetically related to the Strymon Basin (von Freyberg, 1951; Gramann and Kockel, 1969; Armour-Brown et al., 1979; Psilovikos et al., 1981; Psilovikos and Syrides, 1983; Dermitzakis et al., 1985; Karistineos and Georgiades-Dikeoulia, 1986; Karistineos and Ioakim, 1989). In fact, the southwest-thickening, lobate wedge shapes of these "basins" do not express underlying graben morphologies or even original depositional geometries, but correspond to large, primary, southwest-plunging structural troughs in the Strymon Valley detachment surface (Dinter and Royden, 1993). Sediments within these wedges are not locally derived, nor do they lie in depositional contact with the underlying Rhodope basement rock. Rather, they were deposited some tens of km to the northeast and transported to their present positions in the hanging wall of the detachment system. Relatively undeformed sediments of the Strymon and Drama basins were superposed on the highly tectonized syndetachment deposits only after the Strymon Valley detachment system became extinct. Neogene sediments exposed in the Strymon Valley region therefore represent not one prolonged episode of extensional subsidence as previously supposed, but two successive basin systems, distinct in age, provenance, and tectonic origin.

CONCLUSIONS

The Rhodope metamorphic province has conventionally been regarded as the interior of a Tethyan continental fragment that was deformed in the hinterland of a Mesozoic to early Tertiary subduction zone, remnants of which are preserved in the ophiolitic Vardar suture in northern Greece and rump Yugoslavia. Results of the present study imply a fundamentally different origin for the Rhodope province, in Greece at least, as an Alpine collisional orogen that accommodated at least 80 km of shortening in middle to late Eocene time, and was subsequently greatly extended on a series of detachment systems in the back-arc of the Hellenic subduction zone. Two major tectonostratigraphic sequences are recognized in the Greek Rhodope province: The composite, upper amphibolite-facies Serbo-Macedonian-West Thracian gneiss complex, which bears metaeclogites, serpentinites, and other ophiolitic remnants, is interpreted as a pre-Cretaceous accretionary prism that was first subducted and later incorporated at the base of a thickening marginal orogen. The Falakron carbonate platform was subducted to the northeast beneath this gneiss complex from ~47 Ma to 36 Ma, producing an inverted metamorphic gradient above the subduction zone. Upon the cessation of continental subduction, high-P metamorphic assemblages in the Falakron series were almost completely converted to upper greenschist-facies assemblages, as predicted by thermal models of the subduction process.

The Oligocene epoch was a period of relative tectonic quiescence at mid-crustal depths in the southern Rhodope province, punctuated by the emplacement of a N80°W-trending belt of arc-related granodiorite plutons ~28 - 33 Ma. Northeast-southwest extension of the thickened Alpine orogen commenced in early Miocene time. In the Rhodope core complex this was evidenced by the emplacement and synintrusional mylonitization of the Symvolon granodiorite beginning ~22 Ma in a widening, northeast-dipping, coaxial shear zone that may represent an extensional rupture of the Falakron

marble series. Early Miocene stretching at the southwest margin of the Rhodope core complex may have amounted to ~40 km based on the width of the Symvolon pluton. The Symvolon shear zone was succeeded by the Strymon Valley detachment system, active from ~16 Ma to 3.5 Ma. The Serbo-Macedonian gneiss complex was displaced southwestward by as much as 80 km in the hanging wall of the Strymon Valley detachment, carrying with it a syndetachment basin complex that accumulated at its trailing edge. The Rhodope metamorphic core complex emerged northeastward in the footwall of the detachment, exposing the effects of earlier ductile deformation and igneous activity in the "Falakron window" between the Strymon and Nestos Rivers. Continuing extension in late Pliocene(?) - Quaternary time is expressed by the subsidence of the Strymon and Drama basins, whose northeast-dipping bounding faults may sole into an active northeast-dipping detachment. A poorly defined system of active faults, possibly forming within a N60°E-trending strike-slip setting, has modified the boundaries of the Strymon and Drama basins and may be responsible for modern seismicity in northern Greece. The structures described above have accommodated >120 km of stretching in Neogene time, a factor that must be considered in reconstructions of earlier deformation in the southern Balkan region.

REFERENCES

Armour-Brown, A., de Bruijn, H., Maniati, C., Siatos, G. and Neisen, P., 1979, The geology of the Neogene sediments north of Serrai and the use of rodent faunas for biostratigraphic control, in Kallergis, G., ed., VI Colloquium on the Geology of the Aegean Region, Proceedings, II, Athens, Institute of Geological and Mining Research, p. 615-622.

Atzori, P., Lo Giudice, A., Kokkinakis, A., Kyriakopoulos, K., Magganas, A., Pezzino, A. and Sideris, K., 1990, Petrological and geochemical study of crystalline rocks from Thassos Island, northern Greece: Proceedings of the 2nd Hellenic-Bulgarian Symposium, Thessaloniki, 1989, Geologica Rhodopica, v. 2, p. 157-165.

Bernoulli, D. and Laubscher, H., 1972, The palinspastic problem of the Hellenides: Ecologae geologicae Helvetiae, v. 65, 107-118.

Birk, F., de Boer, H. U., Kronberg, P., Meyer, W., Pilger, A. and Schenck, P., 1970, Zur Geologie des Rhodopen-Kristallins im Gebiet zwischen Strimon und Nestos (Griechisch-Ostmazedonien): Beihefte zum Geologischen Jahrbuch, v. Heft 88, p. 179.

Birk, F., 1970, Zur Geologie und Petrographie des östlichen Bos-Dag-Massivs bei Drama in Griechisch-Mazedonien, in Birk, F., de Boer, H. U., Kronberg, P., Meyer, W., Pilger, A. and Schenck, P., ed., Zur Geologie des Rhodopen-Kristallins im Gebiet zwischen Strimon und Nestos (Griechisch-Ostmazedonien), Beihefte zum Geologischen Jahrbuch, Heft 88, Hannover, p. 5-42.

Boncev, E., 1971, Problems of Bulgarian Geotectonics, Sofia, Technika, 204 p.

Bornovas, J., and Rondogianni-Tsiambaou, T., 1983, Geological map of Greece, second edition: Athens, Institute of Geology and Mineral Exploration, scale 1:500,000.

Burchfiel, B. C., 1980, Eastern European Alpine system and the Carpathian orocline as an example of collision tectonics: Tectonophysics, v. 63, p. 31-61.

Burg, J.-P., Ivanov, Z., Ricou, L.-E., Dimor, D. and Klain, L., 1990, Implications of shear-sense criteria for the tectonic evolution of the Central Rhodope massif, southern Bulgaria: Geology, v. 18, p. 451-454.

Cheshitev, G., and Kancev, I., 1989, Geological Map of the People's Republic of Bulgaria: Sofia, Committee of Geology, Department of Geophysical Prospecting and Geological Mapping, scale 1:500,000.

de Boer, H. U., 1970, Geologisch-petrographische Untersuchungen im Rhodope-Massiv Griechisch-Ostmazedoniens: Der Menikion-Bergzug nordöstlich Serrai, in Birk, F., de Boer, H. U., Kronberg, P., Meyer, W., Pilger, A. and Schenck, P., ed., Zur Geologie des Rhodopen-Kristallins im Gebiet zwischen Strimon und Nestos (Griechisch-Ostmazedonien), Beihefte zum Geologischen Jahrbuch, Heft 88, Hannover, p. 43-79.

Del Moro, A., Innocenti, F., Kyriakopoulos, C., Manetti, P. and Papadopoulos, P., 1988, Tertiary granitoids from Thrace (northern Greece): Sr isotopic and petrochemical data: Neues Jahrbuch für Mineralogie, Abhandlungen, v. 159, p. 113-135.

Del Moro, A., Kyriakopoulos, K., Pezzino, A., Atzori, P. and Lo Giudice, A., 1990, The metamorphic complex associated to the Kavala plutonites: an Rb-Sr geochronological, petrological and structural study: Proceedings of the 2nd Hellenic-Bulgarian Symposium, Thessaloniki, 1989, Geologica Rhodopica, v. 2, p. 143-152.

Dermitzakis, M. D., Georgiades-Dikeoulia, E. and Velitzelos, E., 1985, Ecostratigraphic observations on the Messinian deposits of Akropotamos area (Kavala, N. Greece): Annales Géologiques des pays Helléniques, v. 33, p. 367-376.

De Wet, A. P., Miller, J. A., Bickle, M. J. and Chapman, H. J., 1989, Geology and geochronology of the Arnea, Sithonia, and Ouranopolis intrusions, Chalkidiki Peninsula, northern Greece: Tectonophysics, v. 161, p. 65-79.

Dinter, D. A., 1991, Neogene detachment faulting and the Rhodope metamorphic core complexes, northern Greece [abs.]: Eos, Transactions, American Geophysical Union, v. 72, p. 460.

Dinter, D. A., 1993, Tertiary extensional evolution of the Rhodope metamorphic core complex, northeastern Greece [abs.]: Abstracts, Annual Meeting of the Geological Society of America, Boston, October 25-28, 1993, p. A-474.

Dinter, D. A., Carter, L. D. and Brigham-Grette, J., 1990, Late Cenozoic geologic evolution of the Alaskan North Slope and adjacent continental shelves, in Grantz, A., Johnson, L. and Sweeney, J. F., ed., The Arctic Ocean region, L, The Geology of North America, Boulder, Colorado, Geological Society of America, p. 459-490.

Dinter, D. A., Macfarlane, A. M., Hames, W., Isachsen, C., and Royden, L., 1994, U-Pb and $^{40}Ar/^{39}Ar$ geochronology of the Symvolon granodiorite: Implications for the thermal and structural evolution of the Rhodope metamorphic core complex, northeastern Greece, submitted to Tectonics.

Dinter, D. A. and Royden, L., 1993, Late Cenozoic extension in northeastern Greece: Strymon Valley detachment and Rhodope metammorphic core complex: Geology, v. 21, p. 45-48.

Dixon, J. E. and Dimitriades, S., 1984, Metamorphosed ophiolitic rocks from the Serbo-Macedonian Massif, near Lake Volvi, North-east Greece, in Dixon, J. E. and Robertson, A. H. F., ed., The Geological Evolution of the Eastern Mediterranean, Geological Society Special Publication No. 17, Oxford, Blackwell Scientific Publications, p. 603-618.

Draper, G. and Bone, R., 1981, Denudation rates, thermal evolution, and preservation of blueschist terrains: Journal of Geology, v. 89, p. 601-613.

Dürr, S., Altherr, R., Keller, J., Okrusch, M. and Seidel, E., 1978, The median Aegean crystalline belt: stratigraphy, structure, metamorphism, magmatism, in Closs, H., Roeder, D. and Schmidt, K., ed., Alps, Apennines, Hellenides, Inter-Union Commission on Geodynamics Scientific Report No. 38, Stuttgart, E. Schweizerbart'sche Verlagsbuchhandlung, p. 455-477.

Eleftheriadis, G., Christofides, G. and Kassoli-Fournaraki, A., 1984, Geochemistry of the high-K calc-alkaline basaltic sills and dykes in the south Rhodope massif (N. Greece): Bulletin Volcanologique, v. 47, p. 569-579.

Eleftheriadis, G. and Lippolt, H. J., 1984, Altersbestimmungen zum oligozänen vulkanismus der Süd-Rhodopen/Nord Griechenland: Neues Jahrbuch für Geologie und Paläontologie, Monatshefte, v. 3, p. 179-191.

England, P. C. and Thompson, A. B., 1984, Pressure-temperature-time paths of regional metamorphism, Part I: Heat transfer during the evolution of regions of thickened continental crust: Journal of Petrology, v. 25, p. 894-928.

Erki, I., Kolios, N. and Stegena, L., 1984, Heat flow density determination in the Strymon basin, NE Greece: Journal of Geophysics, v. 54, p. 106-109.

Fedo, C. M. and Miller, J. M. G., 1992, Evolution of a Miocene half-graben basin, Colorado River extensional corridor, southeastern California: Geological Society of America Bulletin, v. 104, p. 481-493.

Freyberg, v. B., 1951, Geologie und Lagerstättenkunde des Braunkohlenrevier von Serrae (Makedonien): Annales géologiques des pays Hélleniques, v. 3, p. 87-154.

Fytikas, M., Innocenti, F., Manetti, P., Mazzuoli, R., Peccerillo, A. and Villari, L., 1984, Tertiary to Quaternary evolution of volcanism in the Aegean region, in Dixon, J. E. and Robertson, A. H. F., ed., The Geological Evolution of the Eastern Mediterranean, Blackwell Scientific Publications, p. 687-699.

Georgiev, G., 1963, Petrographie der metamorphen Gesteine, Sofia, Verlag Technika, 272 p.

Ghent, E. D., Stout, M. Z. and Parrish, R. R., 1988, Determination of metamorphic pressure-temperature-time (PTt) paths., in Nisbet, E. G. and Fowler, C. M. R., ed., Short Course on Heat, Metamorphism, and Tectonics, Saint John's, Mineralogical Association of Canada, p. 155-188.

Gramann, H. and Kockel, F., 1969, Das Neogen im Strymon-becken (Griechisch-Ostmazedonien), Teil 1, Lithologie, stratigraphie und paläogeographie: Geologisches Jahrbuch, v. 87, p. 445-484.

Hansen, E., 1971, Strain Facies, Berlin, Springer-Verlag, 207 p.

Harre, W., Kockel, F., Kreuzer, H., Lenz, H., Müller, P. and Walther, H. W., 1968, Über Rejuvenationen im Serbo-Madzedonischen Massiv (Deutung radiometrischer Altersbestimmungen) [abs.]: Proceedings of the 23rd International Geological Congress, Prague, p. 223-236.

Harrison, T. M., 1981, Diffusion of ^{40}Ar in hornblende: Contributions in Mineralogy and Petrology, v. 78, p. 324-331.

Harrison, T. M., Duncan, I. and McDougall, I., 1985, Diffusion of ^{40}Ar in biotite: temperature, pressure, and compositional effects: Geochimica Cosmochimica Acta, v. 49, p. 2461-2468.

Innocenti, F., Kolios, N., Manetti, P., Mazzuoli, R., Peccerillo, G., Rita, F. and Villari, L., 1984, Evolution and geodynamic significance of the Tertiary orogenic volcanism in northeastern Greece: Bulletin Volcanologique, v. 47, p. 25-37.

Ivanov, R., 1981, The deep-seated central Rhodope nappe and interference tectonics of the Rhodope crystalline basement: Geologica Balcanica, v. 11, p. 47-66.

Jackson, J. A. and McKenzie, D. P., 1983, The geometrical evolution of normal fault systems: Journal of Structural Geology, v. 5, p. 471-482.

Jacobshagen, V., Dürr, S., Kockel, F., Kopp, K.-O., Kowalczyk, G., Berckhemer, H. and Büttner, D., 1978, Structure and geodynamic evolution of the Aegean region, in Closs, H., Roeder, D. and Schmidt, K., ed., Alps, Apennines, Hellenides, Inter-Union Commission on Geodynamics Scientific Report No. 38, Stuttgart, E. Schweizerbart'sche Verlagsbuchhandlung, p. 537-564.

John, B. E., 1987, Geometry and evolution of a mid-crustal extensional fault system: Chemehuevi Mountains, southeastern California, in Coward, M. P., Dewey, J. F. and Hancock, P. L., eds., Continental Extensional Tectonics, Geological Society Special Publication No. 28, Oxford, Blackwell Scientific Publications, p. 313-335.

Jongsma, D., Wissman, G., Hinz, K., and Garde, S., 1977. Seismic studies in the Cretan Sea, 2, The southern Aegean Sea: an extensional marginal basin without seafloor spreading?, "Meteor" Forschungsergeb. Reihe C, p. 27.

Jordan, H., 1969, Geologie und Petrographie im Zentralteil des Bos Dag (Drama, Griechisch-Makedonien): Geotectonische Forschungen, v. 31, p. 50-85.

Karistineos, N. K. and Georgiades-Dikeoulia, E., 1986, The marine transgression in the Serres basin: Annales Géologiques Des Pays Helléniques, v. 33, p. 221-232.

Karistineos, N. and Ioakim, C., 1989, Palaeoenvironmental and palaeoclimatic evolution of the Serres basin (N. Greece) during the Miocene: Palaegeography, Palaeoclimatology, Palaeoecology, v. 70, p. 275-285.

Kauffmann, G., Kockel, F. and Mollat, H., 1976, Notes on the stratigraphic and palaeogeographic position of the Svoula formation in the innermost zone of the Hellenides (northern Greece): v. 18, p. 225-230.

Kilias, A. and Mountrakis, D., 1990, Kinematics of the crystalline sequences in the western Rhodope massif, in Konstantinos, S., ed., Geologica Rhodopica, Proceedings of the 2nd Hellenic-Bulgarian Symposium, Thessaloniki, 1989, v. 2, Thessaloniki, Aritstotle University Press, p. 100-116

Kober, L., 1931, Das alpine Europa un sein Rahment, Berlin, Borntraeger, 310 p.

Kockel, F., Mollat, H. and Walther, H. W., 1971, Geologie des Serbo-Mazedonischen Massivs und seines mesozoischen Rahmens (Nordgriechenland): Geologisches Jahrbuch, v. 89, p. 529-551.

Kockel, F., Mollat, H. and Walther, H. W., 1977, Erläuterungen zur Geologischen Karte der Chalkidhiki und angrenzender Gebiete 1:100,000 (Nord-Griechenland), Hannover, Bundesanstalt für Geowissenschaften und Rohstoffe, 119 p.

Kockel, F. and Walther, H. W., 1965, Die Strimonlinie als Grenze zwischen Serbo-Mazedonischem und Ril-Rhodope-Massiv in Ost-Mazedonien: Geologisches Jahrbuch, v. 83, p. 575-602.

Kojumdgieva, E., Nikolov, I., Nedjalkov, P. and Busev, A., 1982, Stratigraphy of the Neogene in Sandanski graben: Geologica Balcanica, v. 12, p. 69-81.

Kokkinakis, A., 1980a, Zum faltenbau des Symvolongebirges und des gebietes von Kavala (Griechisch-Ostmakedonien): Annales Géologiques des Pays Helléniques, v. 30, p. 398-420.

Kokkinakis, A., 1980b, Altersbeziehungen zwischen Metamorphosen, mechanischen Deformationen und Intrusionen am Südrand des Rhodope-Massivs (Makedonien, Grieschenland): Geologische Rundschau, v. 69, p. 726-744.

Kolocotroni, C. and Dixon, J. E., 1991, The origin and emplacement of the Vrondou granite, Serres, N.E. Greece: Bulletin of the Geological Society of Greece, v. 25, p. 469-483.

Kotopouli, C. N. and Pe-Piper, G., 1989a, Geochemical characteristics of felsic intrusive rocks within the Hellenic Rhodope: A comparative study and petrogenetic implications: Neues Jahrbuch für Mineralogie, Abhandlungen, v. 161, p. 141-169.

Kotopouli, C. N. and Pe-Piper, G., 1989b, Chemical composition of pargasite and hornblende in low to high grade metamorphic rocks of the Rhodope zone, Xanthi, Greece: Mineralogy and Petrology, v. 40, p. 275-288.

Kotopouli, C. N. and Pe-Piper, G., 1991, Geochemistry of the Paranestion volcanic rocks, Hellenic Rhodope, Greece: Chemie der Erde, v. 51, p. 13-22.

Kotopouli, C. N., Pe-Piper, G. and Katagas, C. G., 1991, The metamorphism and migmatization of the Xanthe-Echinos metamorphic complex, Central Rhodope, Greece: Lithos, v. 27, p. 79-93.

Koukouvelas, I. and Doutsos, T., 1990, Tectonic stages along a traverse cross cutting the Rhodopian zone (Greece): Geologische Rundschau, v. 79, p. 753-776.

Koukouvelas, I. and Pe-Piper, G., 1991, The Oligocene Xanthi pluton, northern Greece: a granodiorite emplaced during regional extension: Journal of the Geological Society, London, v. 148, p. 749-758.

Koukouzas, C., 1972, Le chévauchement de Strymon dans la région Strymon dans la région de la frontiére Gréco-Bulgare: Zeitung der deutsche geologische Gesellschaft, v. 123, p. 343-347.

Kronberg, P., 1969, Gliederung, Petrographie und Tectogenese des Rhodopen-Kristallins im Tsal-Dag, Simvolon und Ost-Pangäon (Griechisch-Makedonien): Geotektonische Forschungen, v. 31, p. 1-49.

Kronberg, P., 1973, Geological Map of Greece, Kavala sheet: Athens, Institute of Geology and Mineral Exploration, scale 1:50,000.

Kronberg, P. and Eltgen, H., 1973, Geological Map of Greece, Xanthi sheet: Athens, Institute of Geology and Mineral Exploration, scale 1:50,000.

Kronberg, P., Meyer, W. and Pilger, A., 1970, Geologie der Rila-Rhodope-Masse zwischen Strimon und Nestos (Nordgriechenland), in Birk, F., de Boer, H. U., Kronberg, P., Meyer, W., Pilger, A. and Schenck, P., eds., Zur Geologie des Rhodopen-Kristallins im Gebiet zwischen Strimon und Nestos (Griechisch-Ostmazedonien), Beihefte zum Geologischen Jahrbuch, Heft 88, Hannover, p. 133-180.

Kronberg, P. and Raith, M., 1977, Tectonics and metamorphism of the Rhodope crystalline complex in Eastern Greek Macedonia and parts of Western Thrace: Neues Jahrbuch für Geologie und Paläontologie, Monatshefte, v. 11, p. 697-704.

Le Pichon, X. and Angelier, J., 1979, The Hellenic Arc and Trench system: A key to the neotectonic evolution of the eastern Mediterranean area: Tectonophysics, v. 60, p. 1-42.

Liati, A., 1986, Regional metamorphism and overprinting contact metamorphism of the Rhodope zone, near Xanthi (N. Greece). Petrology, geochemistry, geochronology [Ph.D. thesis]: Techn. Univ. Braunschweig, 186 p.

Liati, A., 1988, Amphibolitized eclogites in the Rhodope crystalline complex, near Xanthi (N. Greece): Neues Jahrbuch für Mineralogie, Monatshefte, v. H. 1, p. 1-8.

Liati, A. and Mposkos, E., 1990, Evolution of the eclogites in the Rhodope zone of northern Greece: Lithos, v. 25, p. 89-99.

Lybéris, N., 1984, Tectonic evolution of the North Aegean trough, in Dixon, J. E. and Robertson, A. H. F., ed., The Geological Evolution of the Eastern Mediterranean, Geological Society Special Publication No. 17, Oxford, Blackwell Scientific Publications, p. 709-725.

Makris, J., 1976. Crustal structure of the Aegean Sea and the Hellenides obtained from geophysical surveys: Journal of Geophysics, v. 41, 441.

Makris, J., and Vees, R., 1977. Crustal structure of the central Aegean Sea and the islands of Evvia and Crete, Greece, obtained by refraction seismic experiments: Journal of Geophysics, v. 42, p. 329.

Marakis, G. I., 1969, Geochronologic studies of some granites from Macedonia: Annales Géologiques des Pays Helléniques, v. 21, p. 121-152.

Mercier, J., 1968, Étude géologique des zones internes des Hellenides en Macédoine centrale (Grèce): Annales Géologiques des pays Helléniques, v. 20, p. 1-792.

Mercier, J., Vergely, P. and Bebein, J., 1975, Les ophiolites helléniques "obductés" au Jurassique supérior sont-elles les vestiges d'un océan tethysien ou d'une mer marginale périeuropéene?: Compte rendu sommaire des Sciences de la Societe géologique de France, v. 17, p. 108-112.

Meyer, W., 1968, Zur Alterstellung des Plutonismus im Südteil der Rila-Rhodope-Masse (Nordgriechenland): Geologica et Paleontologica, v. 2, p. 173-192.

Meyer, W., 1969, Die Faltenachsen im Rhodopen-Kristallin östlich des Strimon (Nordost-Griechenland): Geotektonische Forschungen, v. 31, p. 86-96.

Meyer, W. and Pilger, A., 1963, Zur Geologie des Gebietes zwischen Strimon und Nestos (Rhodopen-Massiv) in Griechisch-Makedonien: Neues Jahrbuch für Geologie und Paläontologie, Abhandlungen, v. 118, p. 272-280.

Mposkos, E., 1987, Polymetamorphism in central and east Rhodope Massif.: Proceedings of the First Bulgarian-Greek Symposium on the Geology and Physical Geography of the Rhodope Massif, Geologica Rhodopica, v. 1, p. 153-159.

Mposkos, E., 1988, The chloritoid-staurolite schists of the lower tectonic unit in east Rhodope: Bulletin of the Geological Society of Greece, v. 22, p. 393-411.

Mposkos, E., 1989, High-pressure metamorphism in gneisses and pelitic schists in the east Rhodope zone (N. Greece): Mineralogy and Petrology, v. 41, p. 25-39.

Mposkos, E. and Perdikatsis, V., 1987, High-pressure metamorphism in east Rhodope Massif (Greece): Fortschrift Mineralogie, v. 65, p. 140.

Mposkos, E., Perdikatsis, V. and Liati, A., 1988, Geochemical investigation of amphibolites from eastern and central Rhodope: Bulletin of the Geological Society of Greece, v. 22, p. 413-427.

Osswald, K., 1938, Geologische Geschichte von Griechisch-Nordmazedonien: Denkschrift der Geologische Landesantalt von Griechenland, v. Heft 3, p. 142 p.

Oxburgh, E. R. and Turcotte, D. L., 1974, Thermal and regional metamorphism in overthrust terrains with special reference to the Eastern Alps: Schweizerische Mineralogische und Petrographische Mitteilungen, v. 54, p. 641-662.

Panagos, A. G., Pe, G. G. and Varnavas, S. P., 1978, The volcanic rocks of Strymonikon-Metamorphosis, central Macedonia, Greece: Chemie der Erde, v. 37, p. 50-61.

Papadakis, A., 1971, On the age of the granitic intrusion near Stratonion, Chalkidiki (Greece): Annales Géologiques des Pays Helléniques, v. 23, p. 297-300.

Papadopoulos, V. C. and Kilias, A., 1985, Altersbeziehungen zwischen Metamorphose und Deformation im zentralen Teil des Serbomazedonischen Massivs (Vertiskos Gebirge, Nord-Griechenland): Geologische Rundschau, v. 74, p. 77-85.

Papanikolaou, D. and Panagopoulos, A., 1981, On the structural style of Southern Rhodope, Greece: Geologica Balcanica, v. 11, p. 13-22.

Peacock, S. M., 1987, Creation and preservation of subduction-related inverted metamorphic gradients: Journal of Geophysical Research, v. 92, p. 12,793-12,781.

Platt, J. P., 1986, Dynamics of orgenic wedges and the uplift of high-pressure metamorphic rocks: Geological Society of America Bulletin, v. 97, p. 1037-1053.

Pollak, W. H., 1979, Structural and lithological development of the Prinos-Kavala basin, Sea of Thrace, Greece: Annales Géologiques des pays Helléniques, tome hors série, v. fasc. II, p. 1003-1011.

Proedrou, P., 1979, The evaporites formation in the Nestos-Prinos graben in the northern Aegean Sea: Annales Géologiques des pays Helléniques, tome hors série, v. fasc. II, p. 1013-1020.

Psilovikos, A., Sotiriadis, L. and Vavliakis, E., 1981, Quaternary tectonics and morphological differentiation of the Siderokastro basin (in Greek): Annales Géologiques des pays Helléniques, v. 30, p. 588-601.

Psilovikos, A. and Syrides, G., 1983, Stratigraphy, sedimentation and palaeogeography of the Strymon Basin, eastern Macedonia/northern Aegean Sea, Greece: Clausthaler Geologische Abhandlungen, v. 44, p. 55-87.

Robbins, G. A., 1972, Radiogenic argon diffusion in muscovite under hydrothermal conditions [M.S. thesis]: Brown University, Providence, R.I.

Royden, L. H., 1988, Late Cenozoic tectonics of the Pannonian basin system, in Royden, L. H. and Horvath, F., ed., Pannonian Basin: A Study in Basin Evolution, AAPG Memoir 45, p. 27-48.

Rubie, D. C., 1984, A thermal-tectonic model for high-pressure metamorphism and deformation in the Sesia Zone, Western Alps: Journal of Geology, v. 92, p. 21-36.

Schenk, P.-F., 1970, Geologie des westlichen Pangaion in Griechisch-Ostmakedonien, in Birk, F., de Boer, H. U., Kronberg, P., Meyer, W., Pilger, A. and Schenck, P., ed., Zur Geologie des Rhodopen-Kristallins im Gebiet zwischen Strimon und Nestos (Griechisch-Ostmazedonien), Beihefte zum Geologischen Jahrbuch, Heft 88, Hannover, p. 81-132.

Schermer, E. R., 1990, Mechanisms of blueschist creation and preservation in an A-type subduction zone, Mount Olympos region, Greece: Geology, v. 18, p. 1130-1133.

Schermer, E. R., 1993, Geometry and kinematics of continental basement deformation during the Alpine orogeny, Mt. Olympos region, Greece: Journal of Structural Geology, v. 15, p. 571-591.

Schwan, W., 1962, Deckenfragen im Balkan—Mit einer Einführung in die geotektonischen Verhältnisse Bulgariens: Geologische Rundschau, v. 51, H. 1, p. 181-218.

Smith, A. G., 1971, Alpine deformation and the oceanic areas of the Tethys, Mediterranean and Atlantic: Geological Society of America Bulletin, v. 82, p. 2039-2070.

Soldatos, K., 1985, Petrology and geochemistry of the Elatia pluton [Ph.D. thesis]: Aristotle University of Thessaloniki, 262 p.

Steininger, F. F. and Rögl, F., 1984, Paleogeography and palinspastic reconstruction of the Neogene of the Mediterranean and Paratethys, in Dixon, J. E. and Robertson, A. H. F., ed., The Geological Evolution of the Eastern Mediterranean, Geological Society Special Publication No. 17, Oxford, Blackwell Scientific Publications, p. 659-668.

Twiss, R. J. and Moores, E. M., 1992, Structural Geology, New York, W.H. Freeman and Company, 532 p.

Vavelidis, M., Eleftheriadis, G. and Kassoli-Fournaraki, A., 1987, A petrological study of the crystalline complex in the island Thasos: Annales Géologiques des pays Helléniques, v. 33, p. 203-216.

Xidas, S., 1984, Geological Map of Greece, Rodholivos sheet: Athens, Institute of Geology and Mineral Exploration, scale 1:50,000.

Yarnold, J. C. and Lombard, J. P., 1989, A facies model for large rock-avalanche deposits formed in dry climates, in Colburn, I. P., Abbott, P. L. and Minch, J., eds., Conglomerates in Basin Analysis: A Symposium Dedicated to A.O. Woodward, 62, Pacific Section, Society of Economic Paleontologists and Mineralogists, p. 9-31.

Zachos, S., 1982, Geological Map of Greece, Thasos sheet: Athens, Institute of Geology and Mineral Exploration, scale 1:50,000.

Zachos, S. and Dimadis, E., 1983, The geotectonic position of the Skaloti-Echinos granite and its relationship to the metamorphic formations of Greek Western and Central Rhodope: Geologica Balcanica, v. 13, p. 17-24.

Zagorcev, I. S., 1992, Neotectonic development of the Struma (Kraistid) Lineament, southwest Bulgaria and northern Greece: Geological Magazine, v. 128, p. 197-222.

Zimmerman, J., Jr., 1972, Emplacement of the Vourinos ophiolitic complex, northern Greece, in Shagam, R. et al., eds., Studies in Earth and Space Sciences: Geological Society of America Memoir 132, p. 225-239.

FIGURE CAPTIONS

Figure 1. Sketch map of major tectonic elements in southeastern Europe and the northeastern Mediterranean region. RCF – Rhodope continental fragment (horizontal lines), RMP – Rhodope metamorphic province (vertical lines), RMCC – Rhodope metamorphic core complex (gray pattern). NAT – North Aegean trough. Modified from Burchfiel (1980), Royden (1988), and Dinter and Royden (1993).

Figure 2. Tectonic map of the north Aegean region. See text for discussion, Fig. 3 for explanation of contact symbols. Data compiled from Bornovas and Rondogianni-Tsiambaou (1983), Cheshitev and Kancev (1989), Schermer (1993), Dinter and Royden (1993), and unpublished mapping by the author.

Figure 3. Generalized geology of the Strymon Valley region. Heavy lines are faults, dashed where inferred: with barbs – thrust fault (barbs on hanging wall), with boxes – low-angle normal fault (boxes on hanging wall), with balls – high-angle normal fault (balls on hanging wall), with arrows parallel to fault trace – strike-slip fault, unadorned – fault of uncertain tectonic identity. Attitude symbols: open triangles – metamorphic foliations, solid boxes – fault planes, short lines – bedding. Light solid lines – depositional or intrusive contacts. Light dashed line in West Thracian gneiss complex – contact between migmatic granite and host rock. See Fig. 2 for location, Fig. 4 for explanation of tectonostratigraphic units.

Figure 4. Generalized tectonostratigraphy, Tertiary deformational sequence, and schematic structural relationships in the southern Rhodope province, northeastern Greece. Unit patterns keyed to Fig. 3. See text and Table 6 for explanation of deformational sequence.

Figure 5. Attitudes of foliations and stretching lineations interpreted as D_1 structural elements in the Falakron marble series northeast of the Drama basin. "+" signs – L_1 stretching lineations (n = 11). (a) Dots – poles to S_1 foliations (n = 32). (b) Shades – 1% area contours on poles to S_1 foliations.

Figure 6. Attitudes of principal foliations (S_1) in Falakron-series gneiss intercalations in the Menoikion and Falakron Mountains and on Mt. Pangaion. (a) Dots – poles to S_1 foliations (n = 38). (b) Shades – 1% area contours on poles to S_1 foliations.

Figure 7. Structural and geochronological data, central Symvolon pluton. Attitudes with boxes are on brittle shear surfaces (D_{3b}); attitudes with triangles are on mylonitic C-planes (S_2). Arrows represent L_2 stretching lineations. Single barb or outer barb of double-barbed arrows gives plunge of lineation. Inner barb gives sense of shear based on mylonitic fabric indicators. (Barb points in transport direction of material *above* shear plane.) In data boxes, (f) indicates furnace step-heating analysis, (l) indicates laser-fusion analysis. Inset: L_2 stretching lineations plotted with mylonitic sense of shear on equal area net. (Arrows point in transport direction of material *above* shear plane.) Bar graph tabulates top-to-the-southwest vs. top-to-the-northeast sense-of-shear based on field determinations of S-C asymmetries. See Fig. 3 for location.

Figure 8. Attitudes of mylonitic C-planes and stretching lineations, south central Symvolon pluton (see Fig. 3). (a) Boxes – poles to C-planes (S_2, n = 162), dots – stretching lineations (L_2, n = 165). (b) Shades –1% area contours on L_2 lineations and poles to S_2.

Figure 9. Attitudes of D_{3a} foliations and stretching lineations in the Falakron marble series within ~5 m beneath the Strymon Valley detachment at Mt. Menoikion and southwest Mt. Pangaion (see Fig. 3). "+" signs – stretching lineations (L_{3a}, n = 15). (a) Dots – poles to foliations (S_{3a}, n = 36). (b) Shades – 1% area contours on poles to S_{3a} foliations.

Figure 10. Attitudes of the Strymon Valley detachment and associated D_3 structural elements. Filled circles – poles to strongly corrugated detachment surface (S_{3b}, n = 74); shaded circle – mean regional corrugation axis of detachment = transport direction of hanging wall (3°, S53°W); "+" signs – microbreccia streaks and outcrop-scale fluting axes (L_{3b}, n = 15); open squares – mineral stretching lineations in extensional mylonites below the detachment surface (L_{3a}, n = 23).

Figure 11. Attitudes of brittle faults, typically normal and spaced at intervals ≤ 2 m, with offsets ≤ 20 cm, and brecciated shear zones, interpreted as D_{3b} structures in the south central Symvolon pluton (see text). (a) Dots – poles to shear planes (n = 116). (b) Shades – 1% area contours on poles to shear planes.

Figure 12. Attitudes of brittle faults and brecciated shear zones interpreted as D_{3b} structures within marble and gneiss of the Falakron series in the Menoikion and Falakron Mts., on southern Mt. Pangaion, and north of Mt. Vrondou (see Fig. 3). (a) Dots – poles to shear planes (n = 32). (b) Shades – 1% area contours on poles to shear planes.

Figure 13. Bedding attitudes in unmetamorphosed Neogene deposits overlying the Strymon Valley detachment in the Angitis lobe of the D_{3b} supradetachment basin complex north of Mt. Pangaion (see Fig. 3). Beds dip uniformly to the southwest at moderate angles. (a) Dots – poles to bedding planes (n = 66). Filled circle – mean bedding pole. (b) Shades = 1% area contours on poles to bedding planes.

Figure 14. Attitudes of faults and shear zones disrupting D_3 supradetachment deposits in the northeast part of the Angitis lobe of the syndetachment basin complex (see Fig. 3). Northeast-dipping faults (D_{3b}) antithetic to Strymon Valley detachment are responsible for uniform southwest dips of syndetachment deposits (Fig. 13). Southwest-dipping faults may be post-detachment (D_4). (a) Dots – poles to shear planes (n = 47). (b) Shades – 1% area contours on poles to shear planes.

Figure 15. Attitudes of bedding and shear planes in the late-D_{3b} Menoikion carbonate conglomerate, which crops out at elevations as great as 1500 m on the southern flank of the Menoikion Mts. between the Strymon and Drama basins. This unit overlies earlier syndetachment deposits in the Angitis lobe of the D_{3b} supradetachment basin complex at an angular unconformity that is locally sheared and microbrecciated, probably due to emplacement as a large rock-avalanche breccia (see text). Bedding is locally preserved in intact limestone blocks bearing algal laminations, storm rip-up breccias, talus breccias, and rounded marble pebble conglomerates. (a) Bedding attitudes (n = 22) show little uniformity. (b and c) However, shear surfaces (n = 43) within and at the base of the Menoikion conglomerate have strongly preferred northwesterly strikes similar to those in the underlying deposits (Fig. 14), and are probably syndetachment structures (D_{3b}).

Figure 16. Bedding attitudes in unmetamorphosed Neogene deposits overlying the Strymon Valley detachment in the Akropotamos and South Symvolon lobes of the D_{3b} supradetachment basin complex south of Mt. Pangaion (see Fig. 3). Most beds dip moderately to the northeast; however, beds near the main detachment are commonly rotated into northeast-striking orientations subparallel to it. (a) Dots – poles to bedding planes (n = 44). (b) Shades – 1% area contours on poles to bedding.

Figure 17. Attitudes of faults and shear zones disrupting D_3 supradetachment deposits in the Akropotamos and South Symvolon basin lobes south of Mt. Pangaion. Southwest-dipping faults (D_{3b}) synthetic to Strymon Valley detachment are responsible for predominantly northeast dips of syndetachment deposits (Fig. 16). Northeast-dipping faults are probably post-detachment (D_4). (a) Dots – poles to shear planes (n = 25). (b) Shades – 1% area contours on poles to shear planes.

Figure 18. Diagrammatic representation of detachment-plane duplex structure, commonly developed on marble substrate underlying poorly consolidated, clastic, supradetachment basin deposits (see Plates 14 and 15). (a) Plane view. (b) Cross section.

Figure 19. Attitudes of faults and shear zones that offset D_4 "overlap deposits" or are associated with modern scarps northeast of the Strymon River. High-angle faults striking N40°-50°W are interpreted as early D_4 structures related to the subsidence of the Strymon and Drama basins. Probable late-D_4 (active, possibly seismogenic) structures include high-angle faults striking in three ranges: N45°-65°E, N75°-85°W, and N20°-40°E, inferred to be forming within a kinematic environment dominated by dextral shear on northeasterly-striking strike-slip faults (see text). (a) Dots – poles to shear planes (n = 180). (b) Shades – 1% area contours on poles to shear planes.

Figure 20. Attitudes of smooth, disjunctive solution foliations (joints, J_4) interpreted to be approximately parallel to the plane of flattening during D_4 dextral (?) strike-slip displacement on faults trending ~N45°- 65°E. Each attitude is representive of joints that are similar in orientation over a wide outcrop area in the Menoikion or Falakron Mountains or on Mt. Pangaion. Spacing typically ranges from 0.3 – 1.2 m (see Plates 17 and 18). (a) Dots – poles to J_4 joints (n = 28). (b) Shades – 1% area contours on poles to J_4 joints.

PLATE CAPTIONS

Plate 1. Up-plunge view of minor F_1 isoclinal folds defined by coarse-grained, recrystallized, white calcite bands a few mm thick in marbles of the Falakron series. F_1 fold axes typically plunge gently northeast in the Rhodope metamorphic core complex, except where they have been rotated by later tectonism, as at the northeast margin of the Drama basin (see text).

Plate 2. L_1 lineations (parallel to pencil in photograph) coincide with very low-angle intersections of isoclinally folded S_1 marble foliations with axial planar foliations to F_1 folds. Coarse calcite grains and grain aggregates that define these intersection lineations are strongly elongated parallel to them, and so also represent mineral stretching lineations, inferred to indicate the azimuth of D_1 shear transport. L_1 lineations and F_1 folds are parallel to subparallel in the Rhodope metamorphic core complex, commonly plunging gently northeast. Similar lineations are defined in schist and gneiss intervals of the Falakron series by elongated and aligned quartz and mica.

Plate 3. Sinistral D_2 S-C mylonitic fabric in the Symvolon pluton. C-planes coincide with zones of strongly sheared biotite and recrystallized quartz spaced a few mm apart and typically dip northeast; S-planes are commonly defined by orientations of biotite and hornblende that crystallized in the shear environment, and by asymmetric recrystallized quartz fabrics.

Plate 4. L_2 stretching lineations in the Symvolon pluton (parallel to pencil in photograph) are defined by the elongation and streaking of K-feldspar porphyroclast tails and recrystallized quartz on mylonitic C-planes. L_2 lineations have orientations in the range 10° - 25°, N50°-70°E in the central part of the pluton, with a well-defined mean of 18°, N58°E.

Plate 5. Northeast-striking outcrop of the Strymon Valley detachment on a limb of a primary corrugation or "fault mullion" at the northern margin of the Angitis lobe of the supradetachment basin complex. Corrugations of this type have 50 - 300 m wavelengths and 10 - 50 m amplitudes and are superposed on the limbs of major corrugations with wavelengths up to ~30 km and amplitudes ≥ 0.5 km (Fig. 3). Outcrop-scale fluting with 1 - 5 m wavelengths and 0.2 - 1.0 m amplitudes is also apparent in this outcrop. Regional corrugation axis is consistent at all scales, plunging ~3°, S53°W (Fig. 10). Footwall is marble of the Falakron series; hanging wall consists of syndetachment clastic sediment (covered by vegetation in foreground).

Plate 6. Chloritic microbreccia on Strymon Valley detachment outcrop is streaked parallel to D_3 displacement direction: 3°, S53°W (parallel to hammer handle).

Plate 7. Strymon Valley detachment (foreground) is overlain by up to 5 m of white, calcareous rock flour (ultracataclasite) at the base of the supradetachment basin.

Plate 8. Photomicrograph of ultracataclasite that typically mantles the Strymon Valley detachment where hanging-wall material is unconsolidated clastic sediment. Angular microbreccia grains, predominantly feldspar and quartz, with sparse muscovite and accessory red garnet, are presumably derived from basal conglomerate and sandstone in the supradetachment basin. Cryptocrystalline calcite matrix probably derives from the Falakron marble substrate.

Plate 9. Intrafootwall low-angle shear surface inferred to be a D_3 structure within the Falakron marble series. Strymon Valley detachment coincides with top of outcrop. Intrafootwall shear dips slightly more steeply than the main detachment and is truncated by it up-dip (to the right of the photograph). As many as three such surfaces in a vertical section divide marble or granite into distinct tabular masses 5 - 20 m thick.

Plate 10. D_3 detachment (foreground) overlain by tilted syndetachment clastic strata (Thasos Island). Tilting of D_3 supradetachment deposits was facilitated by northwest-striking, high-angle, syndetachment normal faults that either sole into or are truncated by the main detachment. High-angle normal faults both synthetic and antithetic to the main detachment are common in the supradetachment basin complex.

Plate 11. Tilted blocks bounded by relatively major northwest-striking normal faults in the D_3 supradetachment basin complex are internally extended on minor northwest-striking normal faults spaced ≤ 2 m apart, with offsets ranging up to ~0.5 m.

Plate 12. Low-angle shear zones persist over areas as great as several km^2 within the D_3 supradetachment basin complex. Microbrecciated and suffused with distorted pods of white, calcareous ultracataclasite, they are typically localized in fissile mudstone or siltstone beds, but also occur as bedding-parallel shears in algal carbonates and evaporites. In many instances such structures represent splays of the main D_3 detachment.

Plate 13. Plan view showing two generations of closed or "fused" tensional cracks oriented subperpendicular to calcite stretching lineations in Falakron series marbles in the Menoikion Mountains. Older set, best developed in the center of this outcrop, is associated with ~S35°W-trending lineations, inferred to be D_1 shear elements. Younger set (left and right sides of outcrop) is associated with ~S53°W-trending lineations (parallel to siting arm of Brunton compass in photograph), presumed to represent D_3 shearing in the Strymon Valley detachment system. Where the third dimension is visible, such cracks typically dip steeply in the inferred direction of upper plate transport, top-to-the-southwest for both D_1 and D_3. The cracks locally displace metamorphic foliations a few mm in a normal sense, down-to-the-southwest for both D_1 and D_3 deformation. Dark brown material at base of photograph is D_3 chloritic microbreccia.

Plate 14. Oblique view of small duplex structure on the Strymon Valley detachment surface, constructed of marble slivers 1 - 4 cm thick thrust successively into a nested stack 5 - 15 cm high and 1 - 2 m wide. Such structures uniformly verge to the southwest, indicating a top-to-the-southwest sense of D_3 shearing. Siting arm of Brunton compass points S53°W.

Plate 15. Plan view of marble-sliver duplex on the Strymon Valley detachment, showing terminations of duplex slivers at a lunate fractures facing in the D_3 displacement direction (Siting arm of Brunton compass points S53°W). Accumulations of chloritic microbreccia are common in structural shadows of the stacked slivers (e.g., at left of compass).

Plate 16. Steep, N80°W-striking normal fault associated with a prominent scarp and near-vertical slickenside grooves has modified the southwest margin of the Drama basin and displaces the Strymon Valley detachment up to ~50 m vertically. Such faults are interpreted here as secondary extensional structures in an active (late-D_4) tectonic regime dominated by distributed dextral shear on northeast-striking strike-slip faults.

Plate 17. Steep, disjunctive J_4 joints spaced at regular intervals of 0.3 - 3.0 m in Falakron marbles in the Angitis Gorge south of Mt. Menoikion (Fig. 3). J_4 joints strike N15°-45°E and are tentatively considered to represent the plane of principal flattening during late D_4 deformation, because flattening on such planes is consistent within the northeast-striking dextral strike-slip system inferred to dominate the late D_4 kinematic enviroment.

Plate 18. J_4 joints exposed in a quarry wall on the north rim of the Angitis Gorge. In this area, two sets of steep joints nearly parallel in strike and intersecting at angles $\leq 20°$ are developed, neither set offsetting the other (see right side of photograph). Metamorphic foliations are not significantly offset by J_4 joints, but display some disjuncture across them owing to the origin of the joints as pressure solution surfaces. Gentle corrugations of joint surfaces about subhorizontal axes are common.

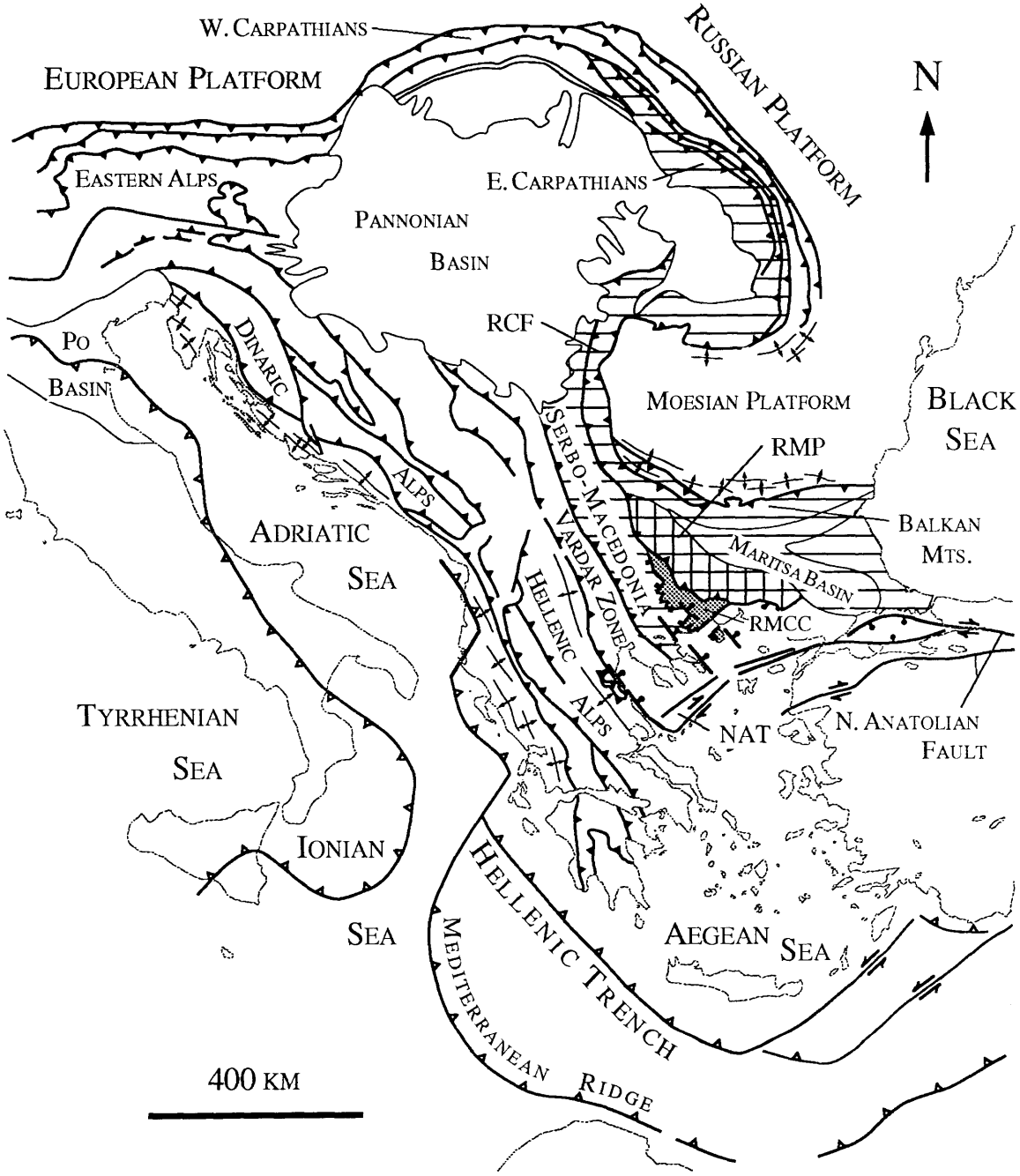

Figure 1. Sketch map of major tectonic elements in southeastern Europe and the northeastern Mediterranean region. RCF – Rhodope continental fragment (horizontal lines), RMP – Rhodope metamorphic province (vertical lines), RMCC – Rhodope metamorphic core complex (gray pattern). NAT – North Aegean Trough. Modified from Burchfiel (1980), Royden (1988), and Dinter and Royden (1993).

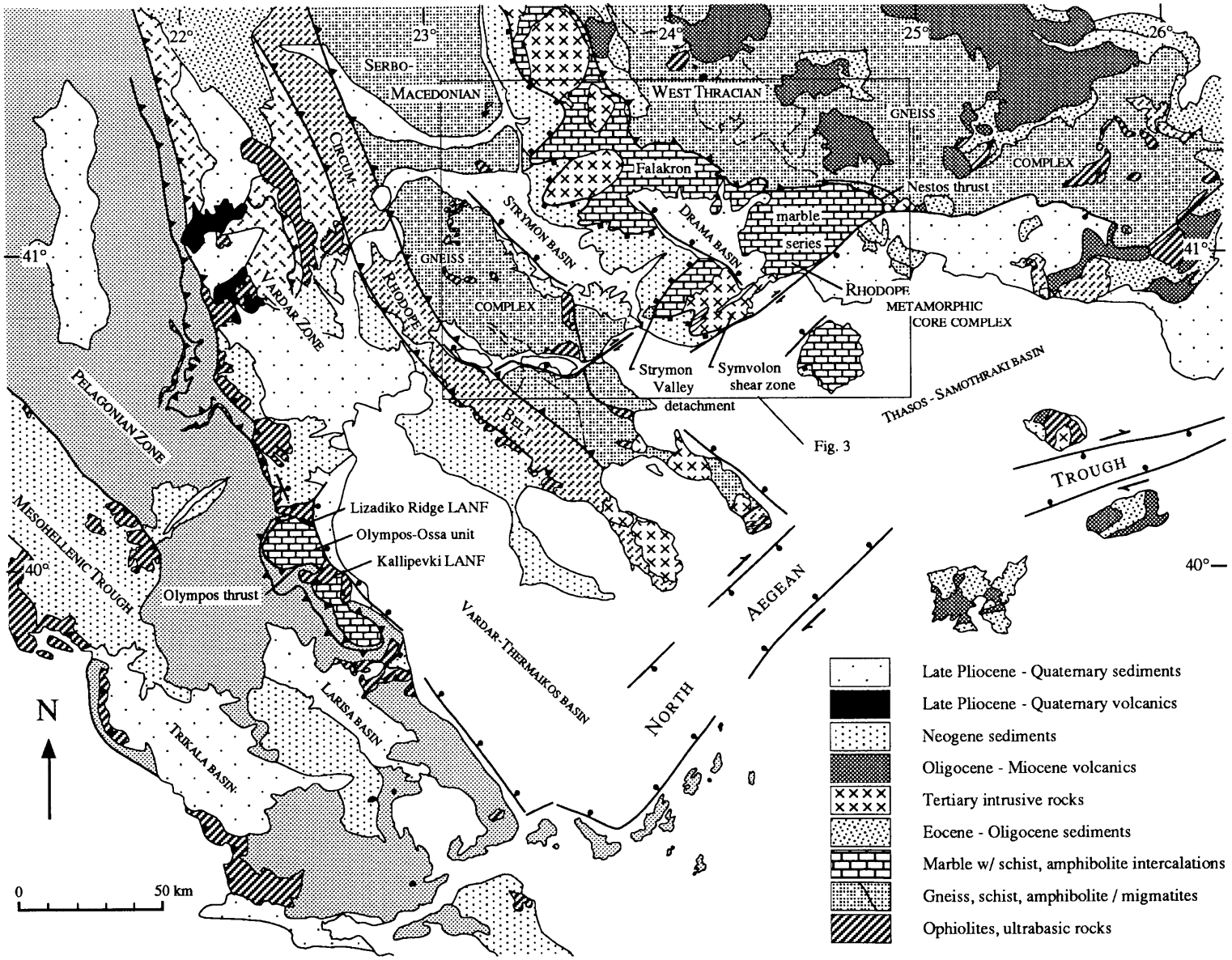

Figure 2. Generalized tectonic map of the north Aegean region. See Fig. 3 for explanation of contact symbols.

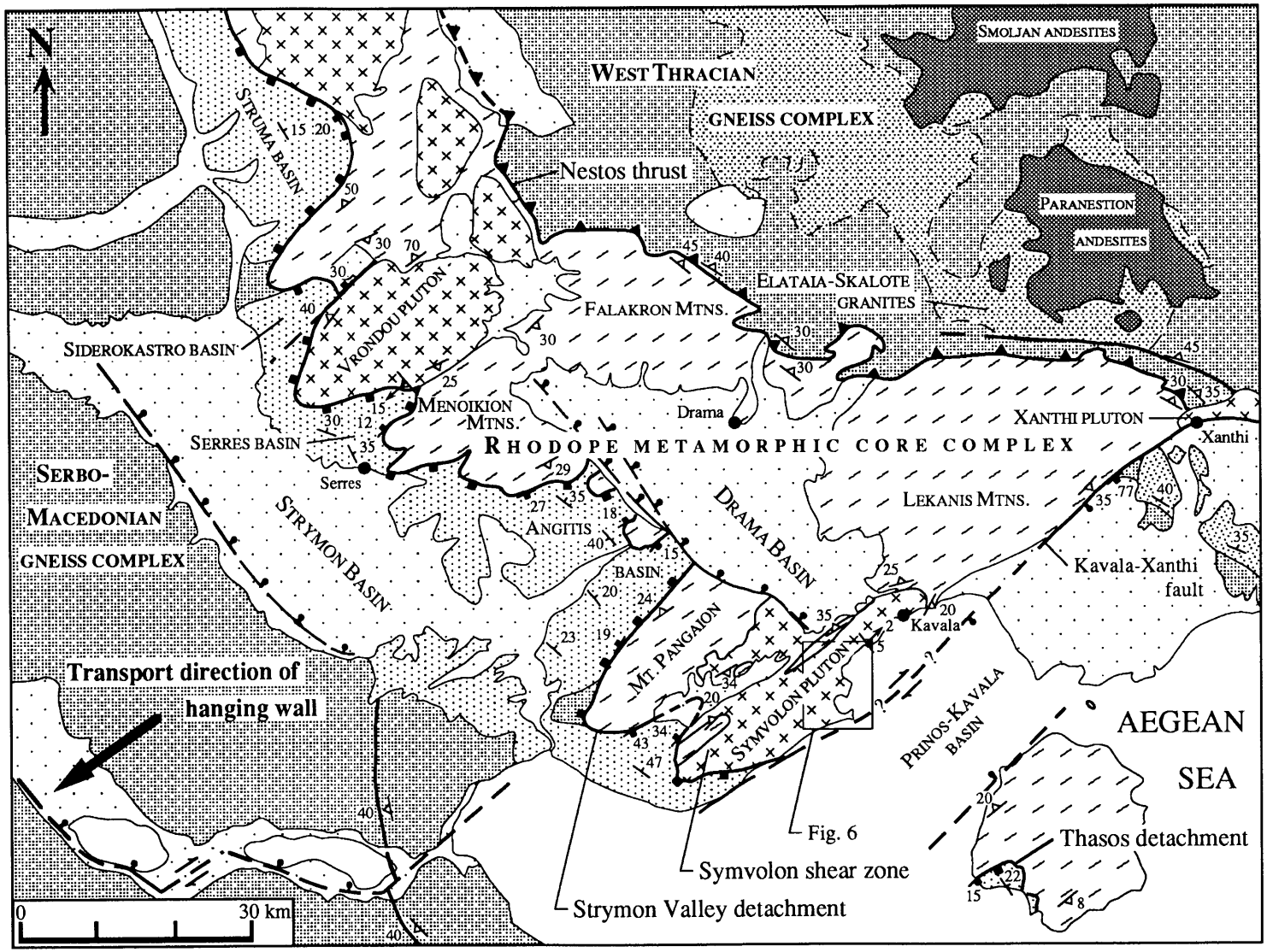

Figure 3. Generalized geology of the Strymon Valley region. See Fig. 2 for location, Fig. 4 for explanation of tectonostratigraphic units.

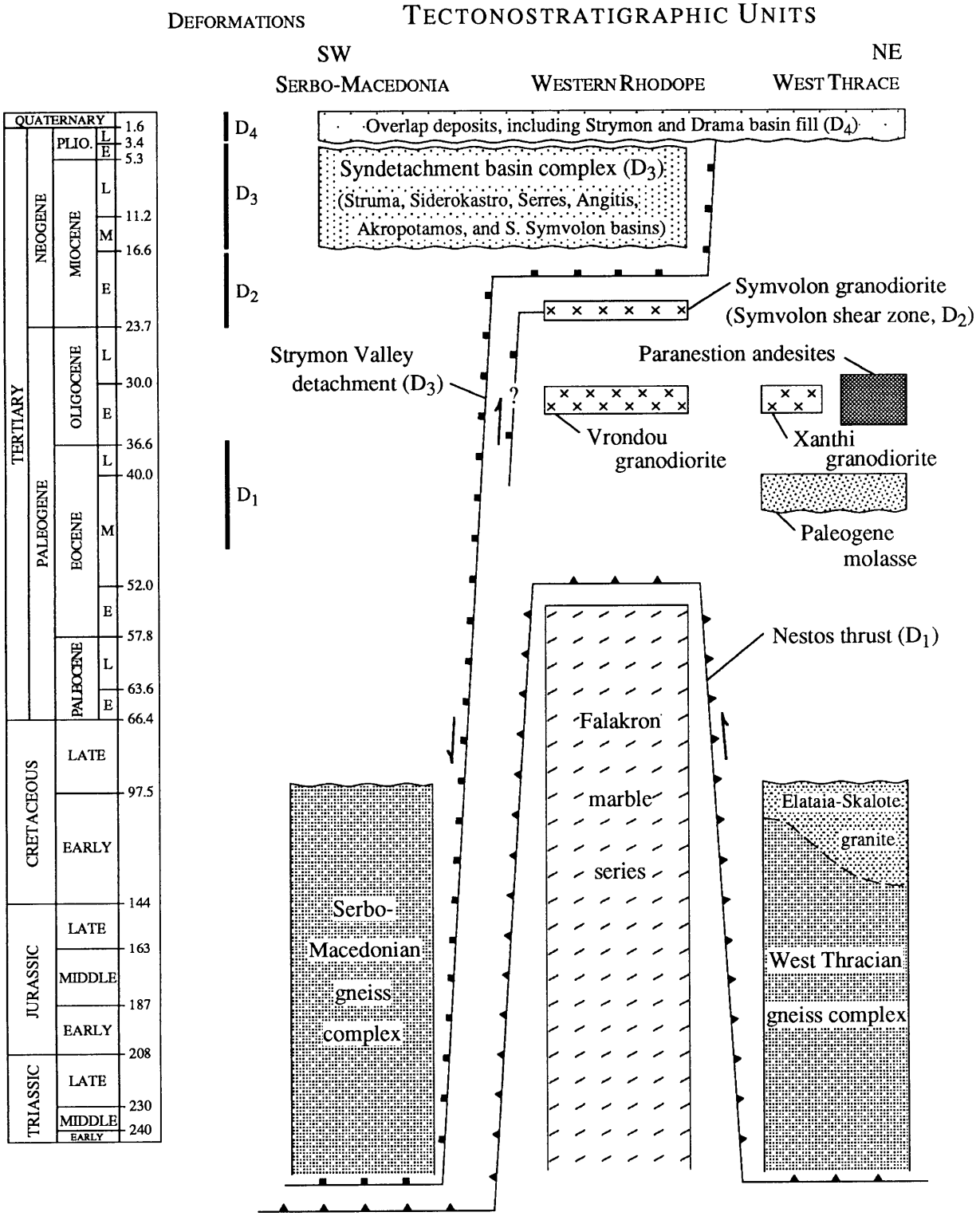

Fig. 4. Tertiary deformational-intrusive sequence, generalized tectonostratigraphy, and schematic structural relationships in the Strymon-Nestos region, northeastern Greece.

D_1 foliations and stretching lineations, Falakron marble

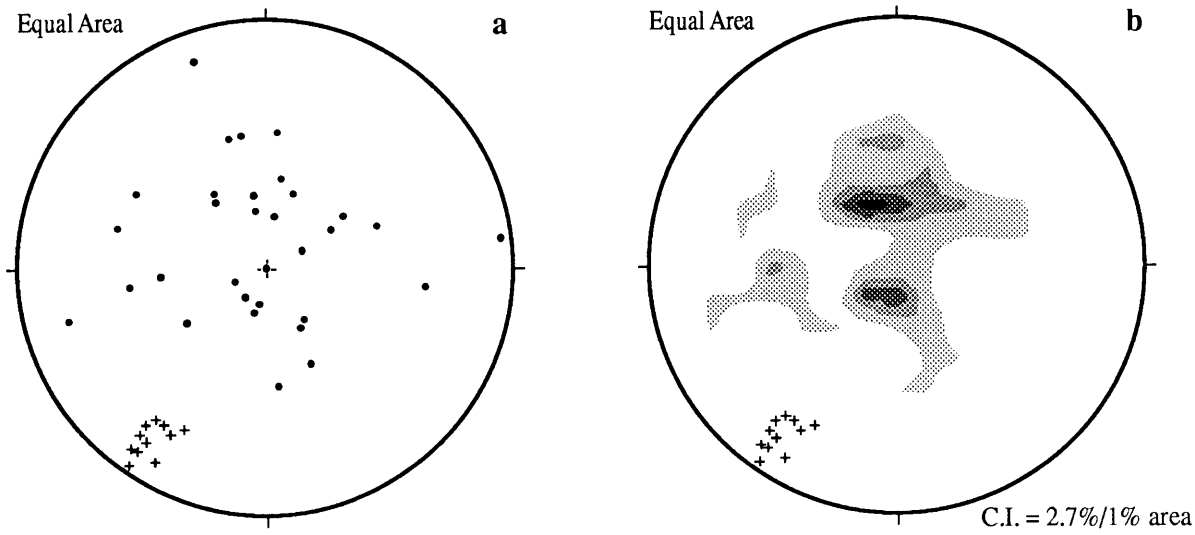

Fig. 5. Foliations and stretching lineations interpreted as D_1 structural elements in the Falakron marble series northeast of the Drama basin. "+" signs – stretching lineations (L_1, n = 11). (a) Dots – poles to foliation planes (S_1, n = 32). (b) Shades – 1% area contours on poles to foliations.

D_1 gneiss foliations, Falakron marble series

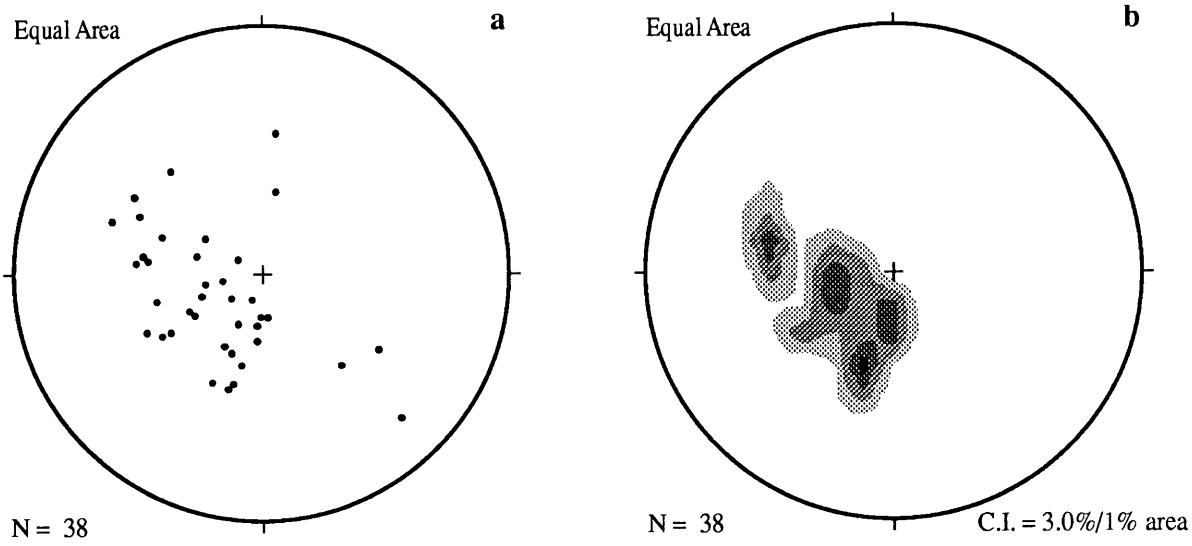

Fig. 6. Principal foliations (S_1) in Falakron-series gneiss intercalations in the Menoikion and Falakron Mountains and Mt. Pangaion. (a) Dots – poles to S_1. (b) Shades – 1% area contours on poles to S_1.

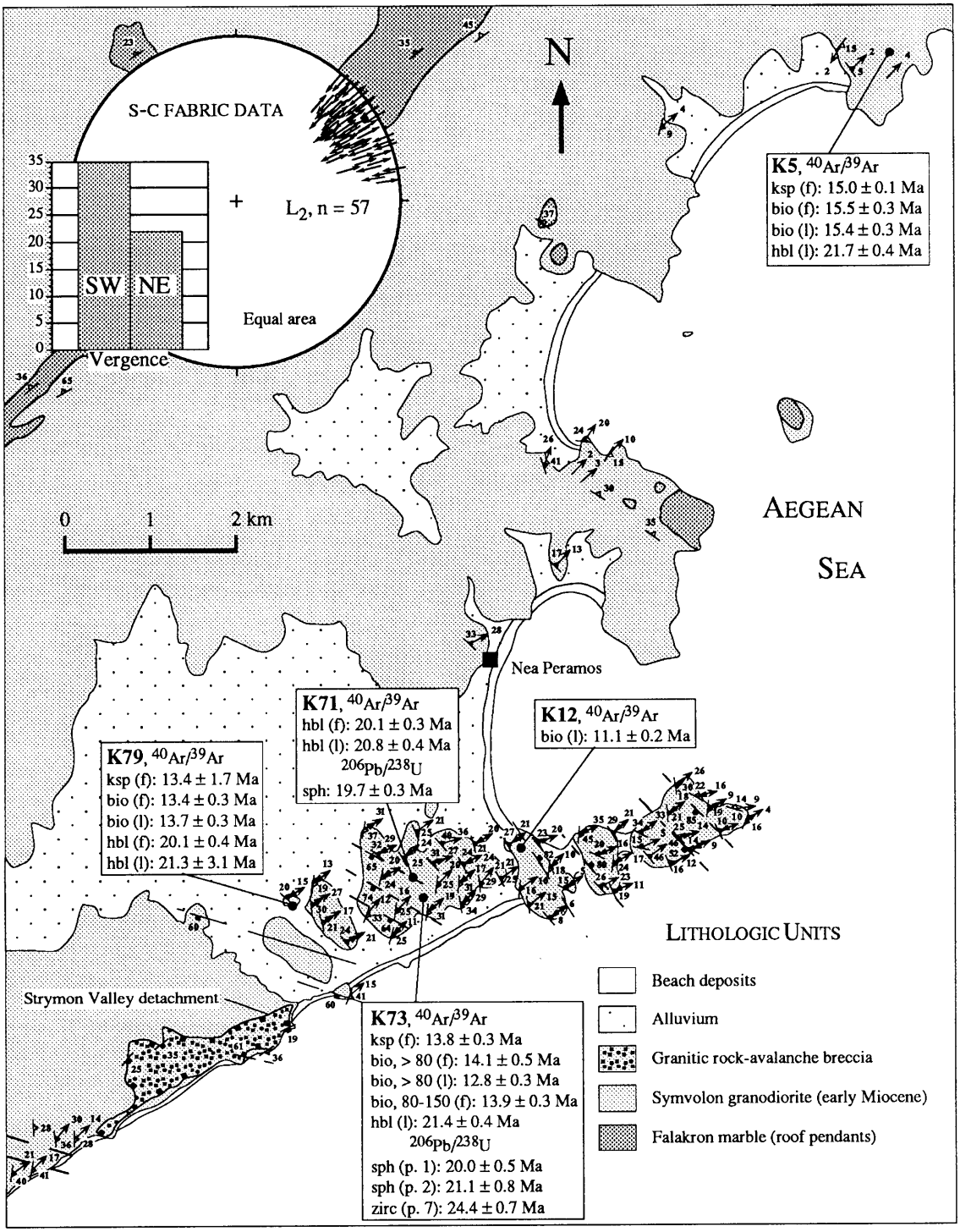

Fig. 7. Structural and geochronologic data, central Symvolon pluton. Attitudes with boxes are on brittle shear surfaces; attitudes with triangles on mylonitic C-planes. Arrows represent stretching lineations. Single barb or outer barb of double-barbed arrows gives plunge of lineation. Inner barb gives sense of shear based on mylonitic fabric indicators. (Barb points in transport direction of material *above* shear plane). In data boxes, (f) indicates furnace step-heating analysis, (l) indicates laser-fusion analysis. Inset: Stretching lineations plotted with mylonitic sense of shear on equal area net. Bar graph tabulates SW vs. NE sense-of-shear indicators.

D_2 foliations and stretching lineations, Symvolon pluton

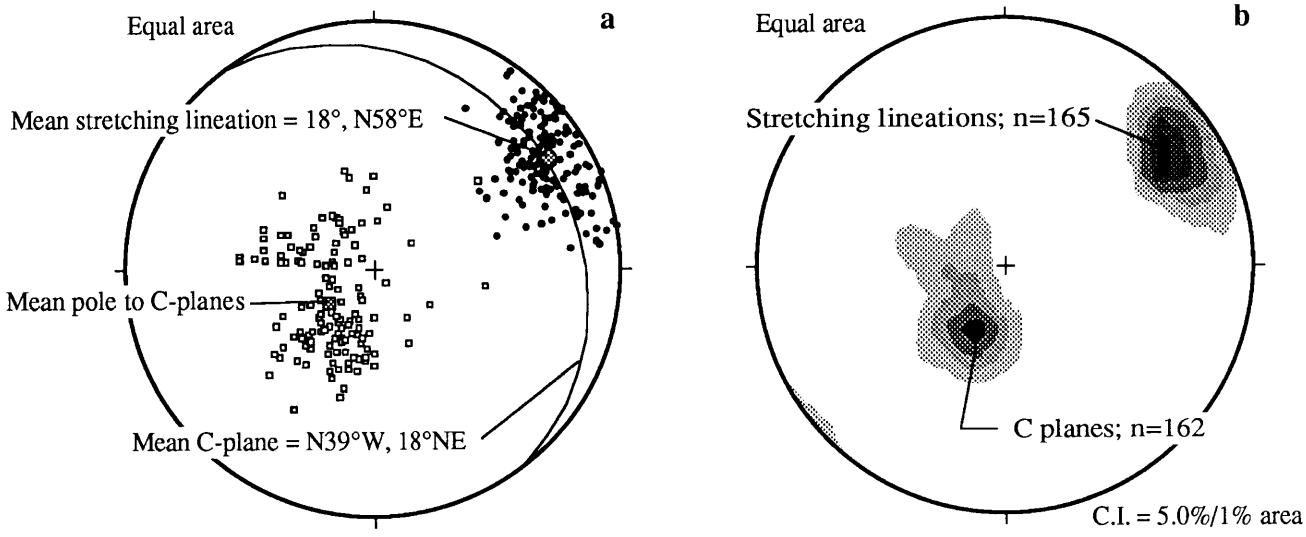

Fig. 8. Mylonitic C-planes and stretching lineations, south central Symvolon pluton.
(a) Boxes – poles to C-planes (S_2, n = 162), dots – stretching lineations (L_2, n = 165).
(b) Shades –1% area contours on L_2 lineations and poles to S_2.

D_{3a} foliations and stretching lineations, Falakron marble

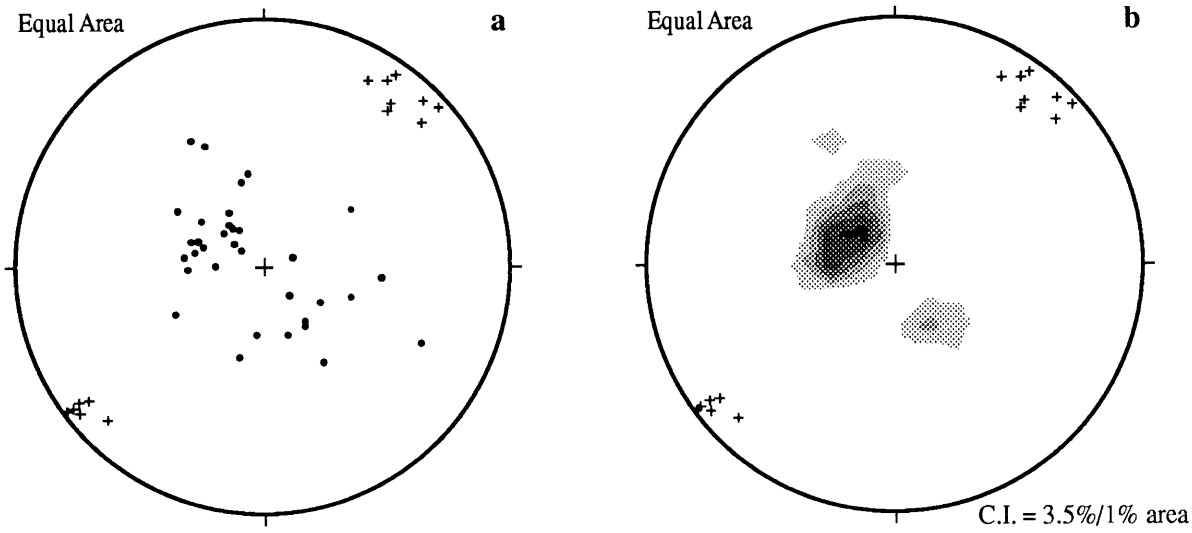

Fig. 9. D_{3a} foliations and stretching lineations in the Falakron marble series within ~5 m beneath the Strymon Valley detachment at Mt. Menoikion and southwest Mt. Pangaion. "+" signs – stretching lineations (L_{3a}, n = 15). (a) Dots – poles to foliations (S_{3a}, n = 36). (b) Shades – 1% area contours on poles to foliations.

Strymon Valley detachment (D_{3b})

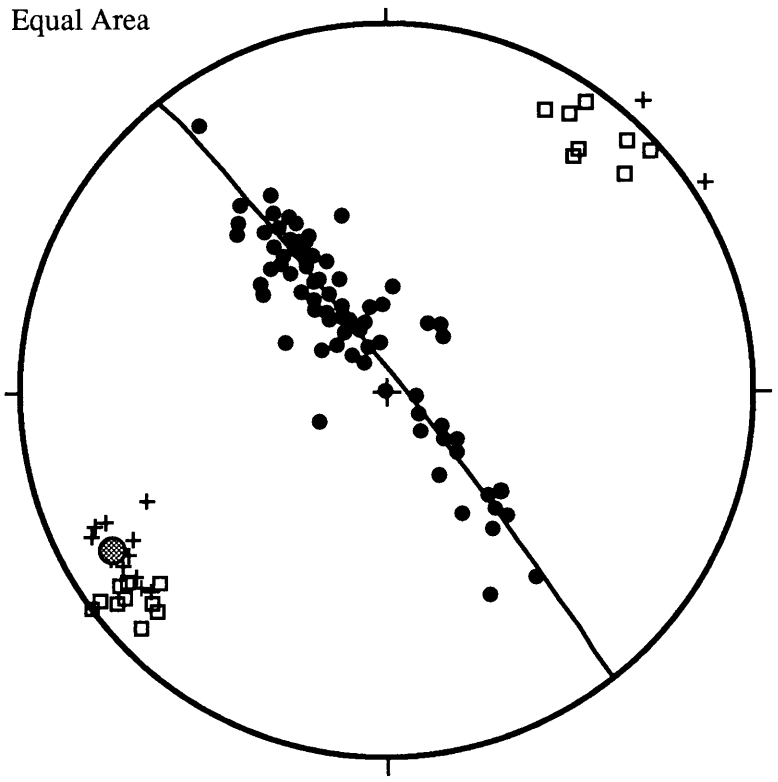

Figure 10. Strymon Valley detachment and associated structural elements. Filled circles – poles to detachment surface (S_{3b}, n = 74); shaded circle – mean regional corrugation axis of detachment = transport direction of hanging wall (3°, S53°W); plus signs – microbreccia streaks and outcrop-scale fluting axes (L_{3b}, n = 15); open squares – mineral stretching lineations in extensional mylonites below the detachment surface (L_{3a}, n = 23).

D_{3b} brittle faults and shear zones, Symvolon pluton

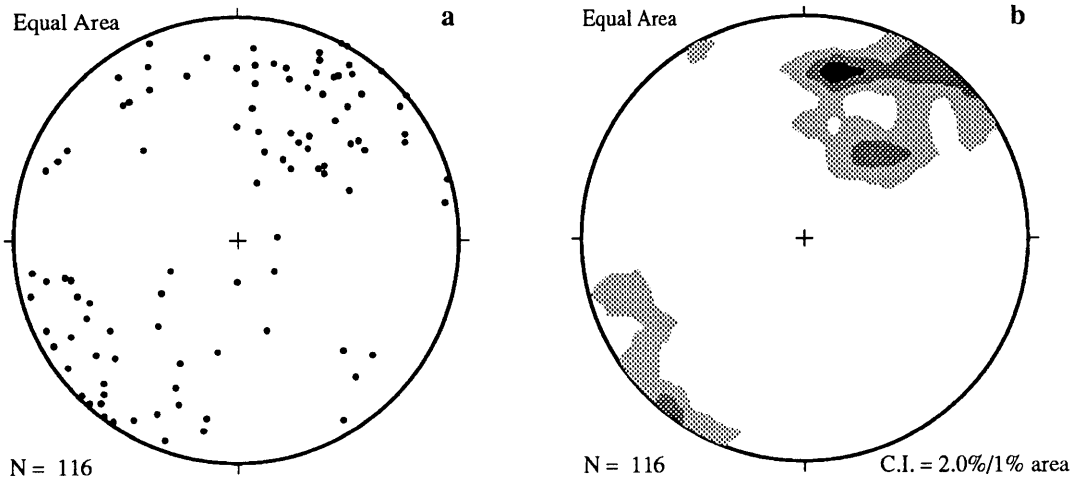

Fig. 11. Brittle faults, typically normal and spaced at intervals ≤ 2 m, with offsets ≤ 20 cm, and brecciated shear zones, interpreted as D_{3b} structures in the south central Symvolon pluton in the vicinity of Nea Peramos. (a) Dots – poles to shear planes. (b) Shades – 1% area contour intervals on poles to shear planes.

D_{3b} brittle faults and shear zones, Falakron marble series

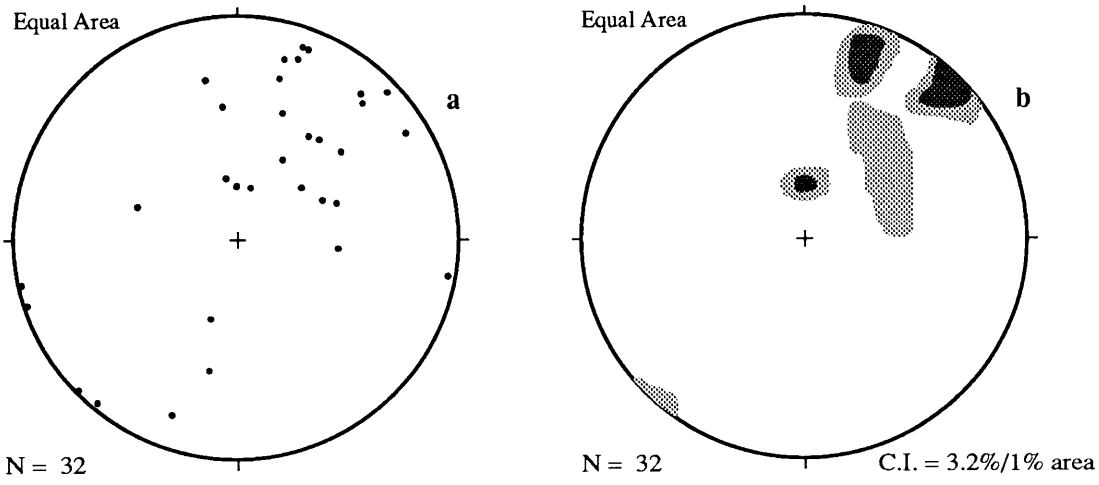

Fig. 12. Brittle faults and brecciated shear zones interpreted as D_{3b} structures within marble and gneiss of the Falakron marble series in the Menoikion and Falakron Mts., southern Mt. Pangaion, and north of Mt. Vrondou. (a) Dots – poles to shear planes. (b) Shades – 1% area contour intervals on poles to shear planes.

Bedding in syndetachment basin deposits, northeast Angitis basin

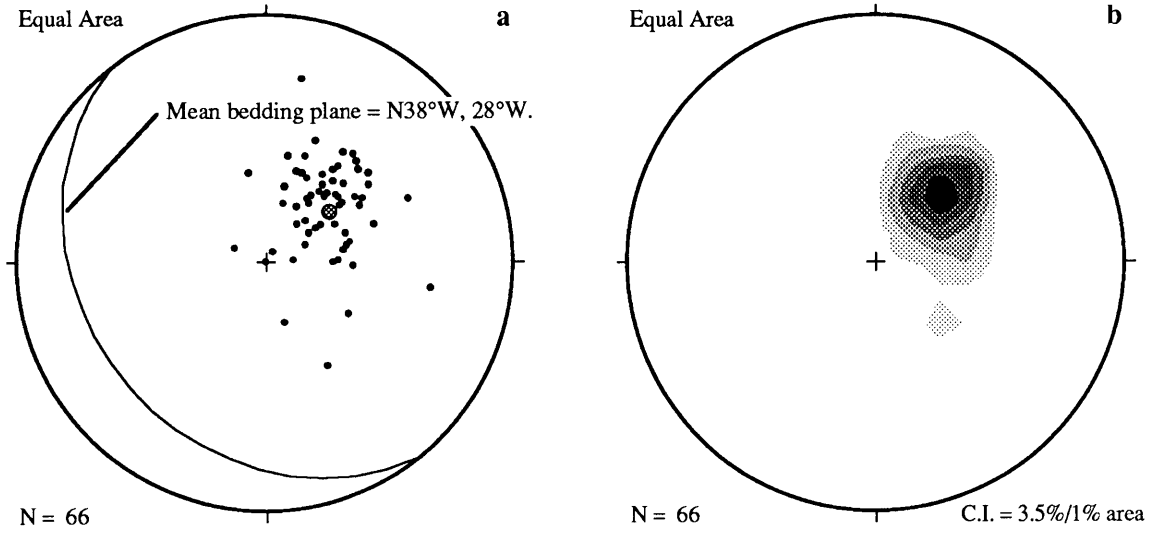

Fig. 13. Bedding planes in D_{3b} deposits overlying the Strymon Valley detachment in the Angitis lobe of the supradetachment basin north of Mt. Pangaion. Beds dip uniformly to the southwest at moderate angles. (a) Dots – poles to bedding planes. Filled circle – mean bedding pole. (b) Shades = 1% area contours on poles to bedding.

Faults and shear zones in syndetachment deposits, northeast Angitis basin

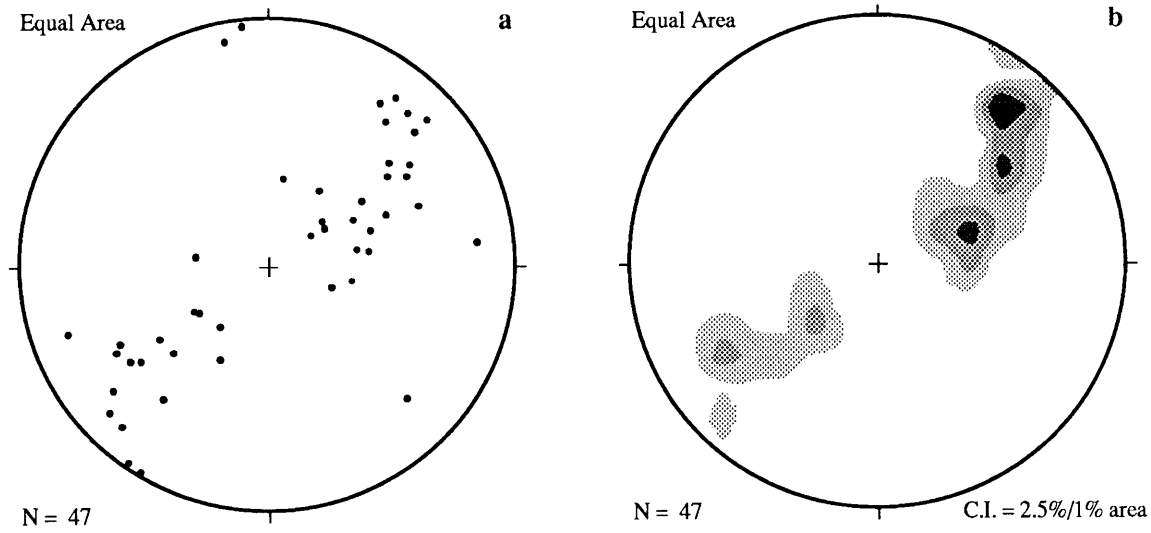

Fig. 14. Faults and shear zones disrupting hanging-wall deposits of the D_3 Strymon Valley detachment system in the northeast Angitis basin. Northeast-dipping faults (D_{3b}) antithetic to detachment displacement are responsible for uniform southwest dips of syndetachment deposits (Fig. 13). Southwest-dipping faults may be post-detachment (D_4). (a) Dots – poles to shear planes (n = 47). (b) Shades – 1% area contours on poles to shear planes.

Bedding and shear planes, Menoikion conglomerate, northeast Angitis basin

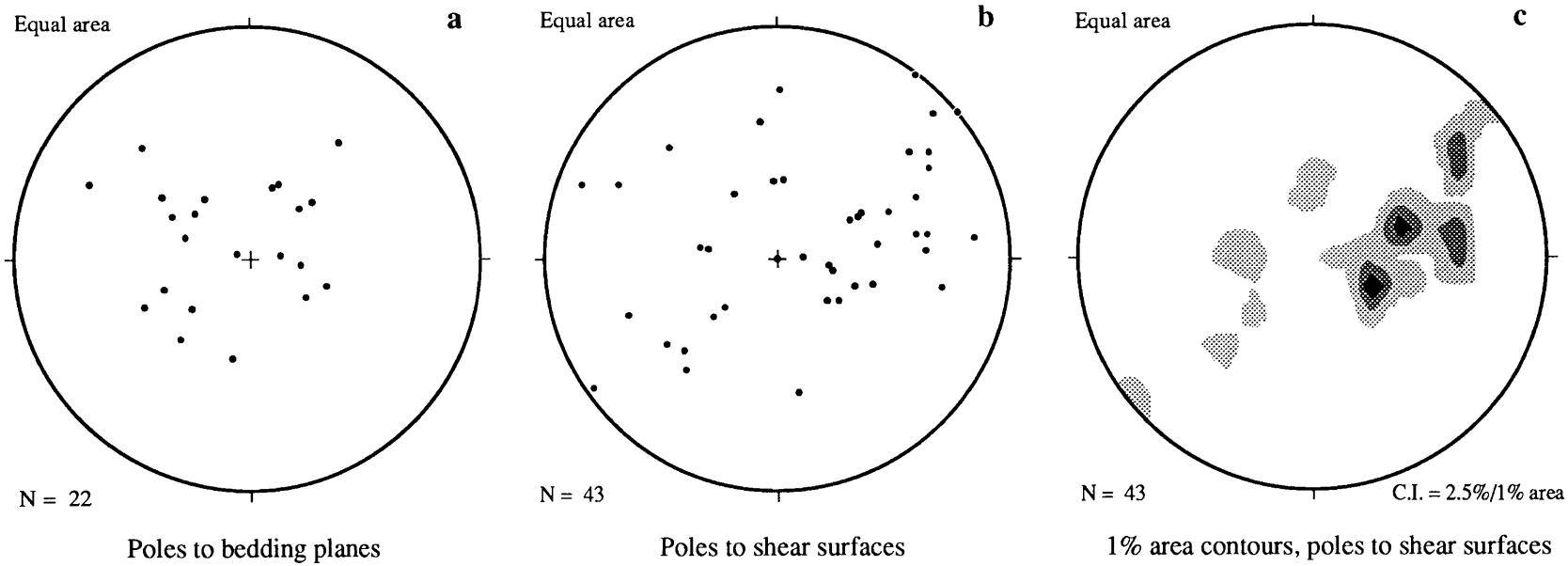

Fig. 15. Bedding and shear planes within the late syndetachment Menoikion carbonate conglomerate, which crops out at elevations as great as 1500 m on the southern flank of the Menoikion Mts. between the modern Strymon and Drama basins. This unit overlies earlier syndetachment deposits in the Angitis subbasin at an angular unconformity that is locally sheared and micro-brecciated, probably due to emplacement as a large rock-avalanche breccia. Bedding is locally preserved in intact limestone blocks bearing laminated algal structures, storm rip-up breccias, talus breccias, and rounded marble pebble conglomerates. Although bedding attitudes (a) show little uniformity, shear surfaces within and at the base of the Menoikion conglomerate (b and c) have strongly preferred northwesterly strikes similar to those in the underlying deposits (Fig. 14), and are probably syndetachment structures (D_{3b}).

Bedding in syndetachment basin deposits, south of Mt. Pangaion

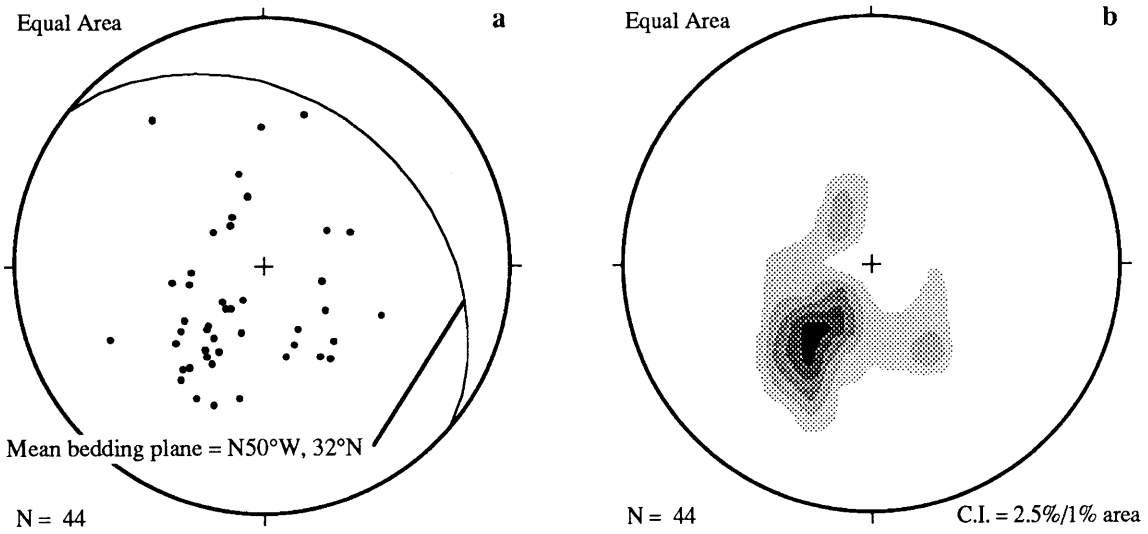

Fig. 16. Bedding planes in hanging-wall deposits of the Strymon Valley detachment system in the Akropotamos and South Symvolon subbasins south of Mt. Pangaion. Most beds dip moderately to the northeast; beds close to the main detachment surface are commonly rotated into northeast-striking orientations subparallel to it. (a) Dots – poles to bedding planes. (b) Shades – 1% area contour intervals on poles to bedding.

Faults and shear zones in syndetachment deposits, south of Mt. Pangaion

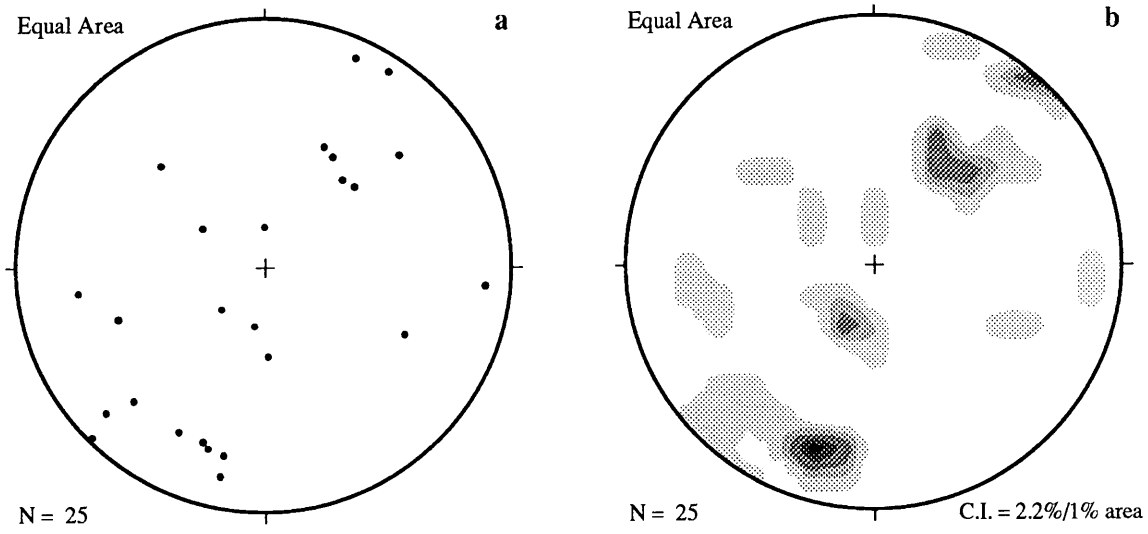

Figure 17. Faults and shear zones disrupting hanging-wall deposits of the Strymon Valley detachment system in the Akropotamos and south Symvolon subbasins south of Mt. Pangaion. Southwest-dipping faults (D_{3b}) synthetic to main detachment displacement are responsible for predominantly northeast dips of syndetachment deposits (Fig. 16). Northeast-dipping faults are probably post-detachment (D_4). (a) Dots – poles to shear planes. (b) Shades – 1% area contour intervals on poles to shear planes.

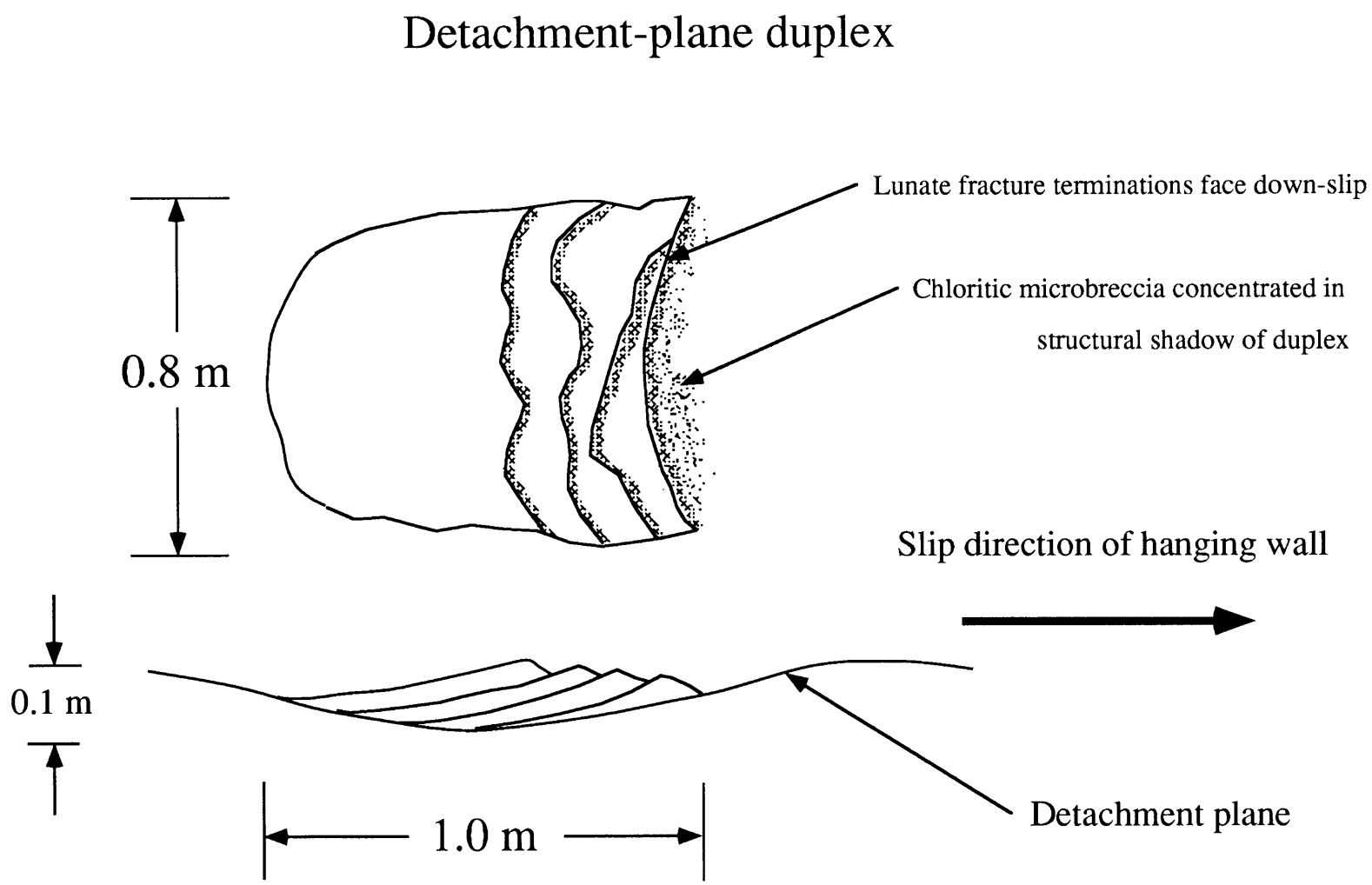

Figure 18. Diagrammatic representation of a detachment-plane duplex structure. (a) Plan view. (b) Cross section.

D_4 faults and shear zones

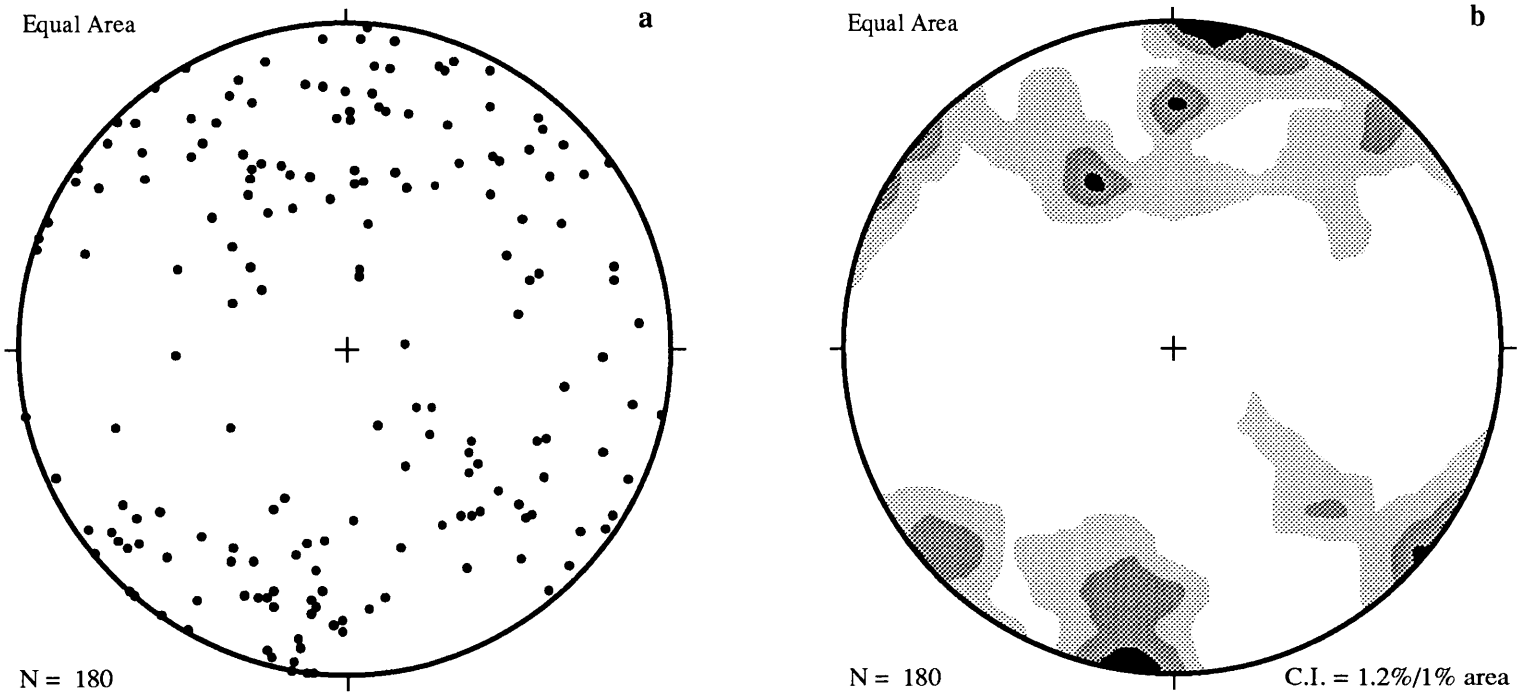

Fig. 19. Faults and shear zones that offset D_4 "overlap deposits" or are associated with modern scarps northeast of the Strymon River. High-angle faults striking N40°-50°W are interpreted as early D_4 structures related to the subsidence of the Strymon and Drama basins. Probable late D_4 structures include high-angle faults striking in three ranges: N45°-65°E, N75°-85°W, and N20°-40°E. (a) Dots – poles to shear planes. (b) Shades – 1% area contour intervals on poles to shear planes.

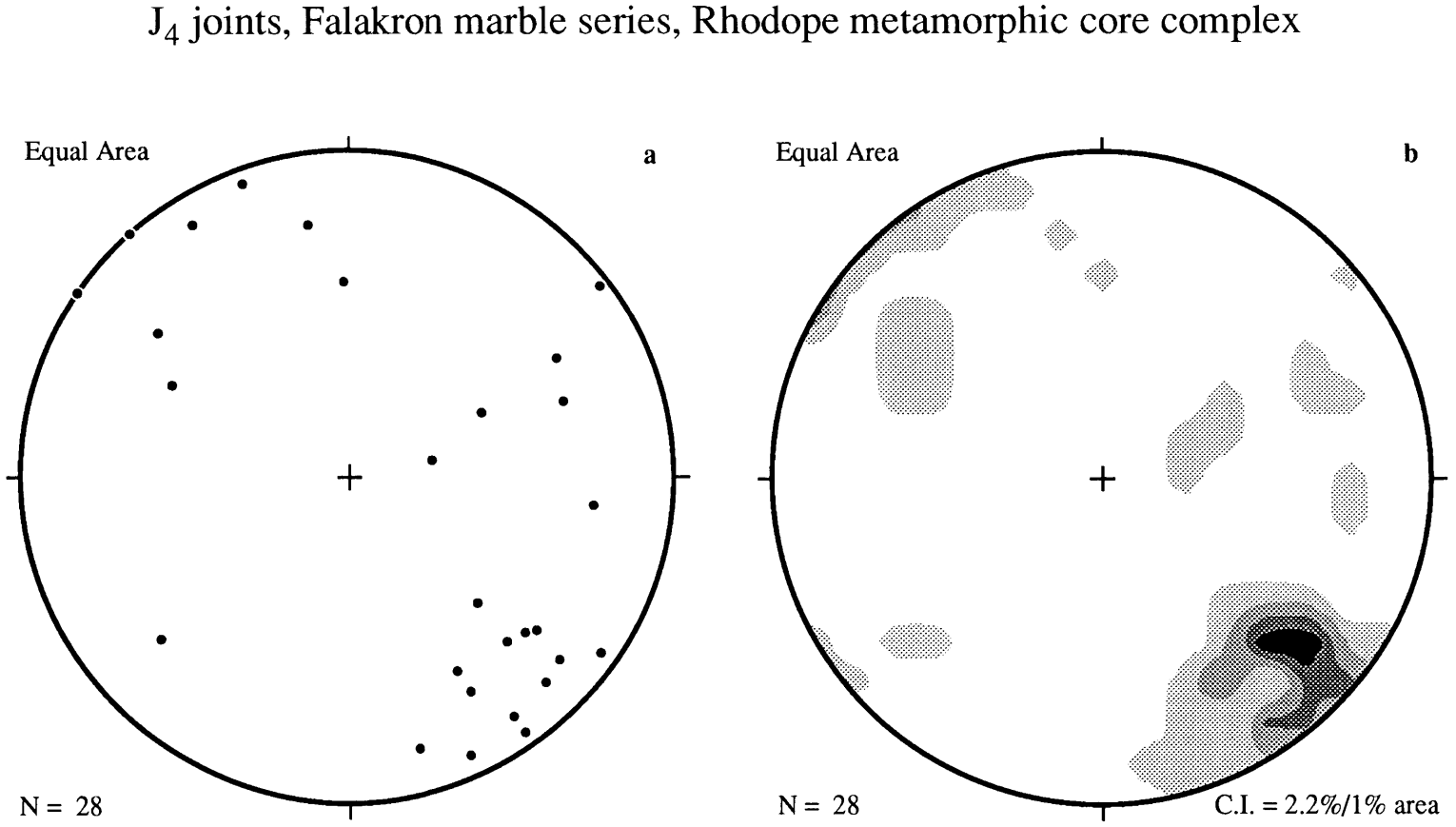

Fig. 20. Smooth, disjunctive solution foliations (joints, J_4) interpreted to be approximately parallel to the plane of flattening during D_4 dextral (?) strike-slip displacement on faults trending ~N40°- 50°E. Each point represents a set of joints characteristic of a wide outcrop area in the Menoikion or Falakron Mountains or on Mt. Pangaion. Spacing typically ranges from 0.3 – 1.2 m. (a) Dots – poles to J_4 joints. (b) Shades – 1% area contour intervals on poles to J_4 joints.

Plate 1. Up-plunge view of minor F_1 isoclinal folds defined by coarse-grained, recrystallized, white calcite bands a few mm thick in marbles of the Falakron series. F_1 fold axes typically plunge gently northeast in the Rhodope metamorphic core complex, except where they have been rotated by later tectonism, as at the northeast margin of the Drama basin (see text).

Plate 2. L_1 lineations (parallel to pencil in photograph) coincide with very low-angle intersections of isoclinally folded S_1 marble foliations with axial planar foliations to F_1 folds. Coarse calcite grains and grain aggregates that define these intersection lineations are strongly elongated parallel to them, and so also represent mineral stretching lineations, inferred to indicate the azimuth of D_1 shear transport. L_1 lineations and F_1 folds are parallel to subparallel in the Rhodope metamorphic core complex, commonly plunging gently northeast. Similar lineations are defined in schist and gneiss intervals of the Falakron series by elongated and aligned quartz and mica.

Plate 3. Sinistral D_2 S-C mylonitic fabric in the Symvolon pluton. C-planes coincide with zones of strongly sheared biotite and recrystallized quartz spaced a few mm apart and typically dip northeast; S-planes are commonly defined by orientations of biotite and hornblende that crystallized in the shear environment, and by asymmetric recrystallized quartz fabrics.

Plate 4. L_2 stretching lineations in the Symvolon pluton (parallel to pencil in photograph) are defined by the elongation and streaking of K-feldspar porphyroclast tails and recrystallized quartz on mylonitic C-planes. L_2 lineations have orientations in the range 10° - 25°, N50°-70°E in the central part of the pluton, with a well-defined mean of 18°, N58°E.

Plate 5. Northeast-striking outcrop of the Strymon Valley detachment on a limb of a primary corrugation or "fault mullion" at the northern margin of the Angitis lobe of the supradetachment basin complex. Corrugations of this type have 50 - 300 m wavelengths and 10 - 50 m amplitudes and are superposed on the limbs of major corrugations with wavelengths up to ~30 km and amplitudes ≥ 0.5 km (Fig. 3). Outcrop-scale fluting with 1 - 5 m wavelengths and 0.2 - 1.0 m amplitudes is also apparent in this outcrop. Regional corrugation axis is consistent at all scales, plunging ~3°, S53°W. Footwall is marble of the Falakron series; hanging wall consists of syndetachment clastic sediment (covered by vegetation in foreground).

Plate 6. Chloritic microbreccia on Strymon Valley detachment outcrop is streaked parallel to D_3 displacement direction: 3°, S53°W (parallel to hammer handle).

Plate 7. Strymon Valley detachment (foreground) is overlain by up to 5 m of white, calcareous rock flour (ultracataclasite) at the base of the supradetachment basin.

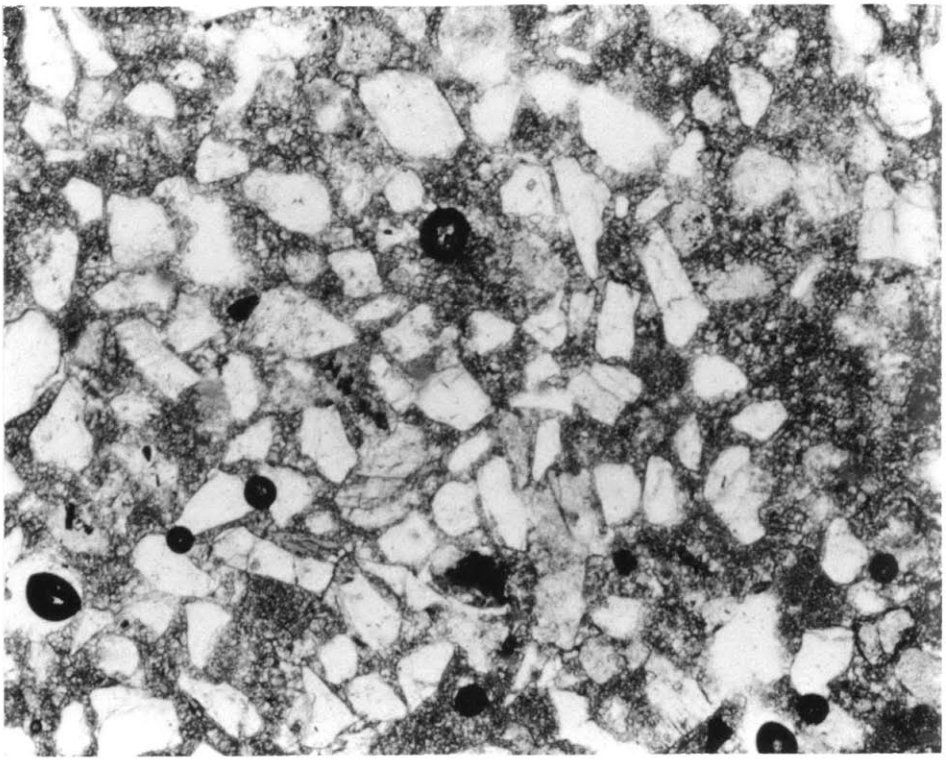

Plate 8. Photomicrograph of ultracataclasite that typically mantles the Strymon Valley detachment where hanging-wall material is unconsolidated clastic sediment. Angular microbreccia grains, predominantly feldspar and quartz, with sparse muscovite and accessory red garnet, are presumably derived from basal conglomerate and sandstone in the supradetachment basin. Cryptocrystalline calcite matrix probably derives from the Falakron marble substrate.

Plate 9. Intrafootwall low-angle shear surface inferred to be a D_3 structure within the Falakron marble series. Strymon Valley detachment coincides with top of outcrop. Intrafootwall shear dips slightly more steeply than the main detachment and is truncated by it up-dip (to the right of the photograph). As many as three such surfaces in a vertical section divide marble or granite into tabular masses 5 - 20 m thick.

Plate 10. D_3 detachment (foreground) overlain by tilted syndetachment clastic strata on the island of Thasos. Tilting of D_3 supradetachment deposits was facilitated by northwest-striking, high-angle, syndetachment normal faults that sole into or are truncated by the main detachment. High-angle normal faults both synthetic and antithetic to the main detachment are common in the supradetachment basin complex.

Plate 11. Tilted blocks bounded by relatively major northwest-striking normal faults in the D_3 supradetachment basin complex are internally extended on minor northwest-striking normal faults spaced ≤ 2 m apart, with offsets ranging up to ~0.5 m.

Plate 12. Low-angle shear zones persist over areas as great as several km^2 within the D_3 supradetachment basin complex. Microbrecciated and suffused with distorted pods of white, calcareous cataclasite, they are typically localized in fissile mudstone or siltstone, but also occur as bedding-parallel shears in algal carbonates and evaporites. In many instances such structures represent splays of the main D_3 detachment.

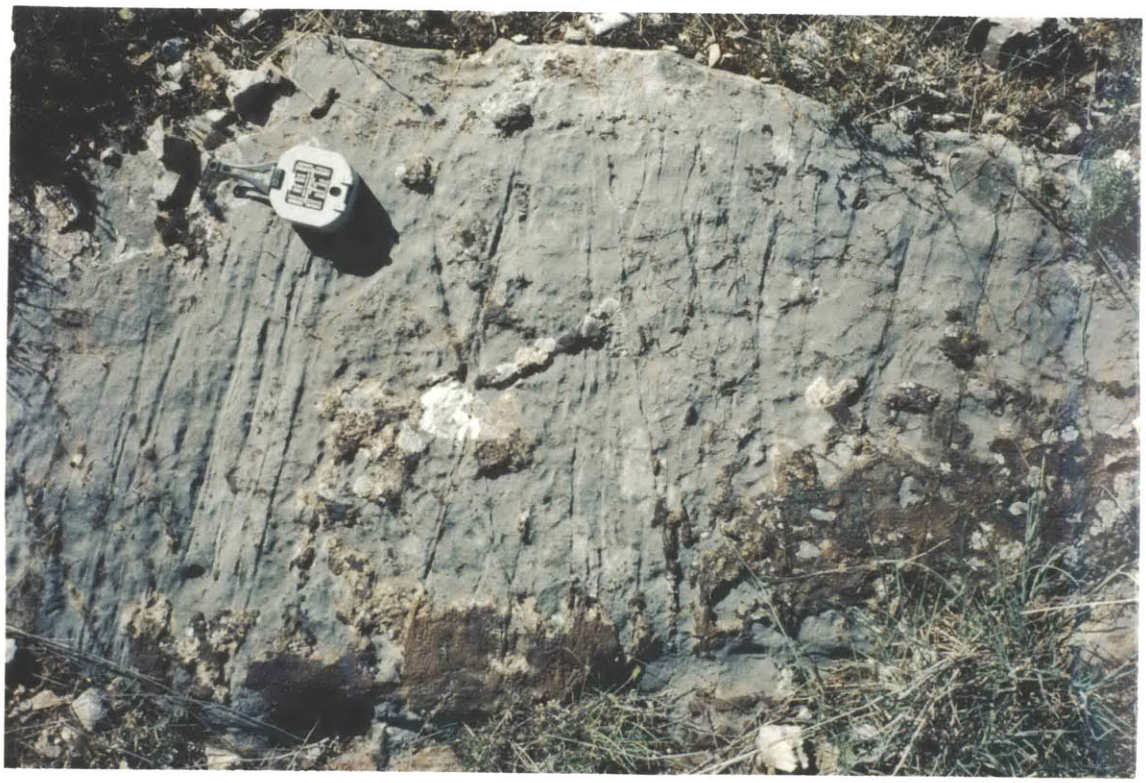

Plate 13. Plan view showing two generations of closed or "fused" tensional cracks oriented subperpendicular to calcite stretching lineations in Falakron series marbles in the Menoikion Mountains. Older set, best developed in the center of this outcrop, is associated with ~S35°W-trending lineations, inferred to be D_1 shear elements. Younger set (left and right sides of outcrop) is associated with ~S53°W-trending lineations (parallel to siting arm of Brunton compass in photograph), presumed to represent D_3 shearing in the Strymon Valley detachment system. Where the third dimension is visible, such cracks typically dip steeply in the inferred direction of upper plate transport, top-to-the-southwest for both D_1 and D_3. The cracks locally displace metamorphic foliations a few mm in a normal sense, down-to-the-southwest for both D_1 and D_3 deformation. Dark brown material at base of photograph is D_3 chloritic microbreccia.

Plate 14. Oblique view of small duplex structure on the Strymon Valley detachment surface, constructed of marble slivers 1 - 4 cm thick thrust successively into a nested stack 5 - 15 cm high and 1 - 2 m wide. Such structures uniformly verge to the southwest, indicating a top-to-the-southwest sense of D_3 shearing. Siting arm of Brunton compass points S53°W.

Plate 15. Plan view of marble-sliver duplex on the Strymon Valley detachment, showing terminations of duplex slivers at a lunate fractures facing in the D_3 displacement direction (Siting arm of Brunton compass points S53°W). Accumulations of chloritic microbreccia are common in structural shadows of the stacked slivers (e.g., at left of compass).

Plate 16. Steep, N80°W-striking normal fault associated with a prominent scarp and near-vertical slickenside grooves has modified the southwest margin of the Drama basin and displaces the Strymon Valley detachment up to ~50 m vertically. Such faults are interpreted here as secondary extensional structures in an active (late-D_4) tectonic regime dominated by distributed dextral shear on northeast-striking strike-slip faults.

Plate 17. Steep, disjunctive J_4 joints spaced at regular intervals of 0.3 - 3.0 m in Falakron marbles in the Angitis Gorge south of Mt. Menoikion (Fig. 3). J_4 joints strike N15°-45°E and are tentatively considered to represent the plane of principal flattening during late D_4 deformation, because flattening on such planes is consistent within the northeast-striking dextral strike-slip system inferred to dominate the late D_4 kinematic enviroment.

Plate 18. J_4 joints exposed in a quarry wall on the north rim of the Angitis Gorge. In this area, two sets of steep joints nearly parallel in strike and intersecting at angles ≤ 20° are developed, neither set displacing the other (see right side of photograph). Metamorphic foliations are not significantly offset by J_4 joints, but display some disjuncture across them owing to the origin of the joints as pressure solution surfaces. Gentle corrugations of joint surfaces about subhorizontal axes are common.

Table 1. $^{40}Ar/^{39}Ar$ dates and sample characteristics, Symvolon granodiorite, Rhodope metamorphic core complex, NE Greece

Sample	Mineral	Size fraction	J*	Heating method	Steps†	Age (Ma)	Correlation method
M90-K5	K-feldspar	80 – 100	0.00567	furnace step-heat	10	15.0 ± 0.1	York 1
"	biotite	80 – 150	0.00576	furnace step-heat	10	15.5 ± 0.3	York 2; MSWD‡ = 0.6
"	"	80 – 150	0.00581	laser fusion	10	15.4 ± 0.3	York 2; MSWD = 1.1
"	hornblende	80 – 150	0.00581	laser fusion	14	21.7 ± 0.4	York 2; MSWD = 1.4
M90-K12	biotite	80 – 100	0.00583	laser fusion	10	11.1 ± 0.2	York 2; MSWD = 1.1
M90-K71	hornblende	80 – 150	0.00574	furnace step-heat	10	20.1 ± 0.3	York 1
"	"	80 – 150	0.00581	laser fusion	11	20.8 ± 0.4	York 2; MSWD = 1.7
M90-K73	K-feldspar	80 – 100	0.00566	furnace step-heat	10	13.8 ± 0.3	York 2; MSWD = 0.5
"	biotite	60 – 80	0.00576	furnace step-heat	10	14.1 ± 0.5	York 1
"	"	60 – 80	0.00581	laser fusion	10	12.8 ± 0.3	York 2; MSWD = 1.6
"	"	80 – 150	0.00573	furnace step-heat	10	13.9 ± 0.3	York 2; MSWD = 2.2
"	hornblende	80 – 100	0.00583	laser fusion	10	21.4 ± 0.4	York 2; MSWD = 0.3
M90-K79	K-feldspar	60 – 80	0.00576	furnace step-heat	10	13.4 ± 1.7	York 1
"	biotite	60 – 80	0.00573	furnace step-heat	10	13.4 ± 0.3	York 2; MSWD = 0.4
"	"	60 – 80	0.00584	laser fusion	10	13.7 ± 0.3	York 2; MSWD = 2.1
"	hornblende	60 – 80	0.00576	furnace step-heat	12	20.1 ± 0.4	York 2; MSWD = 0.9
"	"	60 – 80	0.00584	laser fusion	20	21.3 ± 3.1	York 1

* ±0.00005

† Number of heating increments for furnace step-heat analyses; number of 1- to 5-grain subsamples for laser-fusion analyses.

‡ Mean squared weighted deviation.

Table 2. U-Pb dates and sample characteristics, Symvolon granodiorite, Rhodope metamorphic core complex, NE Greece

Sample	Mineral	Pick	Size	Color	# grains	weight (mg)	$^{206}Pb^*/^{238}U$ age†	$^{207}Pb^*/^{235}U$ age†	$^{207}Pb^*/^{206}Pb^*$ age†
M90-K71	titanite	1	80-100	honey	>400	2.1641	19.7 ± 0.3	22.6 ± 2.3	345.4 ± 35.7
M90-K73	"	1	100-140	amber	>400	3.4380	20.0 ± 0.5	28.4 ± 2.5	808.3 ± 69.4
"	"	2	80-100	"	>400	1.9940	21.1 ± 0.8	27.9 ± 7.3	663.3 ± 174.6
M90-K73	zircon	1	140-200	none	44	0.0756	42.5 ± 0.1	43.8 ± 0.2	116.3 ± 0.5
	"	2	100-140	"	22	0.0790	64.7 ± 0.1	67.9 ± 0.2	185.6 ± 0.4
	"	3	100-140	"	31	0.1440	82.6 ± 0.04	87.9 ± 0.1	233.1 ± 0.3
	"	4	140-200	"	57	0.1290	63.1 ± 0.1	68.6 ± 0.1	265.4 ± 0.3
	"	5	100-140	hyacinth	30	0.1560	96.9 ± 0.1	101.9 ± 1.0	221.0 ± 2.1
	"	6	140-200	"	26	0.0624	77.1 ± 0.1	80.4 ± 0.3	177.2 ± 0.5
	"	7	80-100	"	1	0.0147	24.4 ± 0.7	27.2 ± 1.3	281.8 ± 9.3

* Denotes radiogenic isotope.

† Ma

TABLE 3. PUBLISHED RADIOMETRIC AGES, IGNEOUS ROCKS IN THE SOUTHERN RHODOPE PROVINCE*

Intrusive rocks

Rhodope metamorphic core complex

Rock unit and type	Method	Mineral	Age (Ma)	Reference	Sample
Vrondou quartz monzonite	K-Ar	hornblende	29.0 ± 1.0	1	
Vrondou quartz monzonite	K-Ar	hornblende	29.0 ± 1.0	1	
Vrondou quartz monzonite	K-Ar	hornblende	30.0 ± 1.0	1	
Vrondou quartz monzonite	K-Ar	hornblende	30.0 ± 2.0	1	
Vrondou quartz monzonite	K-Ar	hornblende	31.0 ± 1.0	1	
Vrondou diorite	K-Ar	hornblende	33.0 ± 2.0	1	
Vrondou granodiorite	K-Ar	biotite	30.0 ± 3.0	2	
Panorama granodiorite	K-Ar	biotite	26.8 ± 0.5	3	
Granitis granodiorite	K-Ar	biotite	28.2 ± 0.5	3	
Krinides granite	K-Ar	biotite	26.0 ± 0.5	3	
Xanthi granodiorite	K-Ar	biotite	27.1 ± 0.4	3	
Xanthi granodiorite	K-Ar	biotite	27.9 ± 0.5	3	
Xanthi granodiorite	K-Ar	biotite	28.8 ± 0.3	4	XAN 10
Xanthi granodiorite	K-Ar	hornblende	30.4 ± 0.6	4	XAN 10

South central Thrace

Rock unit and type	Method	Mineral	Age (Ma)	Reference	Sample
Tris Vrisses calc-alkaline granitoid	Rb-Sr	biotite	34.9 ± 1.5	5	CK 56 T
Halasmata calc-alkaline granitoid	Rb-Sr	biotite	32.0 ± 0.8	5	SA 61 H
Leptokaria calc-alkaline granitoid	Rb-Sr	biotite	31.4 ± 0.7	5	SA 68 L
Leptokaria calc-alkaline granitoid	Rb-Sr	biotite	31.9 ± 0.5	5	CK 22 L
Kirki calc-alkaline granitoid	Rb-Sr	biotite	31.8 ± 0.6	5	CK 23 Ki
Kassitera calc-alkaline granitoid	Rb-Sr	biotite	31.9 ± 0.5	5	CK 49 Ka
Maronia calc-alkaline granitoid	Rb-Sr	biotite	28.4 ± 0.9	5	SA 32 M
Maronia calc-alkaline granitoid	Rb-Sr	biotite	29.3 ± 0.9	5	CK 15 M
Maronia calc-alkaline granitoid	Rb-Sr	biotite	28.9 ± 0.9	5	CK 19 M

TABLE 3 (cont.). PUBLISHED RADIOMETRIC AGES, IGNEOUS ROCKS IN THE SOUTHERN RHODOPE PROVINCE

Volcanic rocks

Overlying West Thracian gneiss complex in Nestos River vicinity

Rock unit and type	Method	Material	Age (Ma)	Reference	Sample
Paranestion liparite	K-Ar	sanidine	28.7 ± 1.1	6	E-Dim-S
"	K-Ar	biotite	30.6 ± 1.1	6	E-Dim-B
"	K-Ar	sanidine	30.8 ± 1.0	6	E-Zar-S
"	K-Ar	biotite	30.0 ± 1.0	6	E-Zar-B
"	K-Ar	sanidine	30.6 ± 1.1	6	E-50-S
"	K-Ar	biotite	30.6 ± 1.1	6	E-50-B
Paranestion trachy-andesite	K-Ar	sanidine	28.7 ± 1.0	6	E-66-S
Paranestion dolerite	K-Ar	orthoclase	29.2 ± 1.0	6	E-53-Or
Paranestion andesite	K-Ar	whole rock	23.7 ± 1.7	6	E-61-G
"	K-Ar	pyroxene	25.5 ± 15.0	6	E-61-P
"	K-Ar	whole rock	33.6 ± 0.8	6	E-70-G
"	K-Ar	whole rock	35.0 ± 1.2	6	E-57-G
"	K-Ar	whole rock	34.7 ± 0.7	6	E-57-G
basaltic andesite dike east of Xanthi pluton	K-Ar	hbl phenocrysts	33.5 ± 1.2	7	

South central Thrace

Rock unit and type	Method	Material	Age (Ma)	Reference	Sample
Chaitou-Kotili basalt	K-Ar	groundmass	30.3 ± 0.7	8	P333
Kaloticho basalt	K-Ar	whole rock	24.4 ± 0.6	8	P357
Kaloticho basaltic andesite	K-Ar	whole rock	33.0 ± 1.2	8	P360
Maronia basaltic andesite	K-Ar	whole rock	32.1 ± 0.7	8	P72
"	K-Ar	whole rock	33.1 ± 0.7	8	P73
"	K-Ar	whole rock	30.0 ± 0.7	8	P93
Kirki-Essemi basaltic andesite	K-Ar	groundmass	30.0 ± 0.8	8	P57
Fere-Dadia basaltic andesite	K-Ar	groundmass	29.7 ± 0.4	8	P32
"	K-Ar	groundmass	28.4 ± 0.3	8	P37
"	K-Ar	groundmass	30.6 ± 0.3	8	P41
"	K-Ar	groundmass	29.2 ± 0.3	8	P44

TABLE 3 (cont.). PUBLISHED RADIOMETRIC AGES, IGNEOUS ROCKS IN THE SOUTHERN RHODOPE PROVINCE

Volcanic rocks (continued)

South central Thrace (continued)

Rock unit and type	Method	Material	Age (Ma)	Reference	Sample
Fere-Dadia basaltic andesite	K-Ar	groundmass	27.4 ± 0.3	8	P223
"	K-Ar	groundmass	26.8 ± 0.6	8	P226
"	K-Ar	groundmass	25.6 ± 0.3	8	P228
"	K-Ar	groundmass	26.0 ± 0.3	8	P237
"	K-Ar	groundmass	23.6 ± 0.4	8	P239
"	K-Ar	groundmass	28.5 ± 0.3	8	P242

* Excludes data from the Symvolon and Mesolakkia granodiorite plutons and mylonitic cover rocks in the Marmara Valley area. See Table 4.
References: (1) Marakis, 1969; (2) Dürr et al., 1978; (3) Meyer, 1968; (4) Liati, 1986; (5) Del Moro et al., 1988; (6) Eleftheriadis & Lippolt,1984; (7) Eleftheriadis et al.,1984; (8) Innocenti et al., 1984.

TABLE 4. PUBLISHED RADIOMETRIC AGES, SYMVOLON AND MESOLAKKIA PLUTONS AND METAMORPHIC COVER ROCKS

Rock unit and type	Method	Mineral	Age (Ma)	Reference	Sample (frac.)
Mesolakkia granodiorite	K-Ar	bio	15.0 ± 0.3	1	302 (600-400μ)
"	K-Ar	bio	13.8 ± 0.2	1	302 (400-200μ)
Symvolon granodiorite	K-Ar	biotite	15.5 ± 0.5	2	81
Symvolon granodiorite	K-Ar	biotite	17.8 ± 0.8	2	23
"	$^{206}Pb/^{238}U$	zircon	95 ± 5*	2	23
"	$^{207}Pb/^{235}U$	zircon	101 ± 8*	2	"
"	$^{208}Pb/^{232}Th$	zircon	63 ± 10*	2	"
"	$^{207}Pb/^{206}Pb$	zircon	335 ± 40†	2	"
Marmara Valley paragneiss§	Rb-Sr	muscovite	18.3 ± 0.6	3	K-8
Marmara Valley paragneiss§	Rb-Sr	muscovite	22.6 ± 0.7	3	K-38
Marmara Valley paragneiss§	Rb-Sr	muscovite	22.3 ± 0.7	3	CK-42
"	Rb-Sr	biotite	12.2 ± 0.4	3	CK-42
Marmara Valley paragneiss	Rb-Sr	biotite	12.6 ± 0.4	3	CK-90a

* Discounted by Kokkinakis (1980b); interpreted in this study as mixing ages.

† Considered by Kokkinakis (1980b) to represent a Carboniferous or earlier emplacement age for the Symvolon pluton; interpreted in this study as a result of inherited lead composition.

§ Mapped in part by Kokkinakis (1980a) and in this study as granitic mylonites marginal to the Symvolon pluton.

References: (1) Harre et al., 1968; (2) Kokkinakis, 1980b; (3) Del Moro et al., 1990.

TABLE 5. PUBLISHED GEOCHRONOLOGIC DATA, SERBO-MACEDONIAN GNEISS COMPLEX

Vertiskos series

Rock type	Method	Mineral	Age (Ma)	Reference	Sample # (size)	Location
schistose pegmatite	K-Ar	muscovite	191 ± 3	1	305(600-400μ)	N. of L. Langadas
schistose pegmatite	K-Ar	muscovite	135 ± 2	1	305(400-200μ)	"
Lachanas granite	K-Ar	biotite	139 ± 3	2		"
Lachanas granite	K-Ar	biotite	140 ± 3	2		"
Arnea granite	$^{40}Ar/^{39}Ar$	phlogopite	136.8 ± 1.5	3	AD134	S. of Lake Volvi
"	Rb-Sr	whole rock	155 ± 11	3	AD134	"
garnet-staurolite schist	K-Ar	white mica	91 ± 4.5	4	RA 1	N. of Lake Volvi
"	K-Ar	white mica	90 ± 5.0	4	RA 1	"
garnet-mica schist	K-Ar	white mica	116.2 ± 5.3	4	RA 2	"
mus-bio-chl schist	K-Ar	white mica	123 ± 5.5	4	RA 5	"
"	K-Ar	biotite	114.6 ± 5.4	4	RA 5	"
quartz-rich paragneiss	K-Ar	white mica	120 ± 5	4	RA 7	"
biotite-rich orthogneiss	K-Ar	white mica	110 ± 4.6	4	RA 10	"
"	K-Ar	biotite	87.8 ± 4.2	4	RA 10	"
"	Rb-Sr	white mica	145.7 ± 15	4	RA 10	"
"	Rb-Sr	biotite	78.2 ± 10	4	RA 10	"
mus-plag gneiss	K-Ar	white mica	125 ± 5.6	4	RA 13	"
"	Rb-Sr	white mica	172.7 ± 31	4	RA 13	"
2-mica gneiss	K-Ar	white mica	116.2 ± 4.8	4	RA 14	"
orthogneiss	K-Ar	white mica	114 ± 5.5	4	RA 12	"
amphibolite	K-Ar	hornblende	93.0 ± 5.3	4	RA 8	"
amphibolite	K-Ar	hornblende	122.8 ± 8	4	RA 11	"
amphibolite	K-Ar	hornblende	111 ± 3	1	208 (300-200μ)	"
"	K-Ar	hornblende	110 ± 2	1	208 (200-100μ)	"
amphibolite	K-Ar	hornblende	109 ± 3	1	209 (600-300μ)	"
"	K-Ar	hornblende	114 ± 3	1	209 (300-200μ)	"
"	K-Ar	hornblende	108 ± 3	1	209 (200-100μ)	"
schistose pegmatite	K-Ar	muscovite	104 ± 1.6	1	116 (600-300μ)	"
"	Rb-Sr	muscovite	21.8 ± 6.2	1	116 (600-300μ)	"

TABLE 5 (continued). PUBLISHED GEOCHRONOLOGIC DATA, SERBO-MACEDONIAN GNEISS COMPLEX

Vertiskos series (continued)

Rock type	Method	Mineral	Age (Ma)	Reference	Sample # (size)	Location
schistose pegmatite	K-Ar	biotite	124 ± 5.2	4	RA 4	N. of Lake Volvi
"	Rb-Sr	white mica	131 ± 10	4	RA 4	"
"	Rb-Sr	biotite	102 ± 10	4	RA 4	"
gabbro-amphibolite	K-Ar	hornblende	1370 ± 76	4	B 35	"

Kerdilion series

Rock type	Method	Mineral	Age (Ma)	Reference	Sample # (size)	Location
granite	K-Ar	biotite	36 ± 1	2		E. of Lake Volvi
pegmatite	K-Ar	muscovite	41 ± 2	2		"
pegmatite	K-Ar	muscovite	42 ± 1	2		"
plag-microcline-gneiss	K-Ar	muscovite	41.8 ± 0.8	1	113 (600-200μ)	W. of Strymon R.
"	Rb-Sr	muscovite	55.8 ± 4.0	1	113 (600-200μ)	"
"	K-Ar	biotite	37.7 ± 0.6	1	113 (600-300μ)	"
granodiorite	K-Ar	biotite	39.0 ± 0.8	1	114 (600-200μ)	"
	Rb-Sr	biotite	43.2 ± 3.1	1	114 (600-200μ)	"
pegmatite	K-Ar	biotite	32.9 ± 0.6	1	115 (600-300μ)	"
"	Rb-Sr	biotite	39.0 ± 2.8	1	115 (600-300μ)	"
"	K-Ar	biotite	31.3 ± 0.6	1	115 (300-200μ)	"
biotite gneiss	K-Ar	biotite	32.8 ± 0.5	1	303 (600-400μ)	"
"	K-Ar	biotite	33.6 ± 0.4	1	303 (400-200μ)	"
amphibolite	K-Ar	hornblende	78 ± 2	1	304 (400-200μ)	"
schistose pegmatite	K-Ar	muscovite	36.8 ± 0.6	1	117 (600-300μ)	"
"	Rb-Sr	muscovite	48.0 ± 2.0	1	117 (600-300μ)	"
Stratoni granite	K-Ar	biotite	29.6 ± 1.4	5		"
plag-microcline-gneiss	K-Ar	muscovite	35.0 ±0.5	1	112 (600-200μ)	E. of Strymon R.
"	K-Ar	biotite	33.9 ± 0.7	1	112 (300-200μ)	"
"	Rb-Sr	biotite	39.3 ± 2.4	1	112 (300-200μ)	"

References: (1) Harre et al., 1968; (2) Marakis, 1969; (3) De Wet et al., 1989; (4) Papadopoulos & Kilias, 1985; (5) Papadakis, 1971.

TABLE 5 (continued). PUBLISHED GEOCHRONOLOGIC DATA, SERBO-MACEDONIAN GNEISS COMPLEX
Sithonia and Athos Peninsulas

Rock type	Method	Mineral	Age (Ma)	Reference	Sample #	Location
granitoid	Ar-Ar	muscovite	47.2 ± 0.7	De Wet et al., 1989	AD314	Ouranopolis
"	Ar-Ar	biotite	44.5 ± 1.1	"	"	Ouranopolis
granitoid	Ar-Ar	muscovite	50.5 ± 1.0	"	AD167	Sithonia
granitoid	Ar-Ar	muscovite	50.0 ± 0.9	"	AD172	Sithonia
granitoid	Ar-Ar	biotite	42.6 ± 0.4	"	AD189	Sithonia
granitoid	K-Ar	biotite	40 ± 1.5	Kondopoulou et al, 1984	SA	Sithonia (Sarti
granitoid	Rb-Sr	whole rock	c. 40	Vergely, 1984		Sithonia
granitoid	Rb-Sr	whole rock	50.9 ± 0.5	Christofides et al., 1986		Sithonia
2-mica granites	Rb-Sr	muscovites	54.5 ± 3.1 to 45.6 ± 1.3	"		Sithonia
"	Rb-Sr	biotites	47.7 ± 0.8 to 28.9 ± 1.1	"		"
granodiorite	Rb-Sr	biotites	46.5 ± 0.9 to 41.3 ± 0.7	"		"

TABLE 6. SUMMARY OF TERIARY TECTONIC AND MAGMATIC EVENTS IN THE STRYMON VALLEY REGION

Event	Age (Ma)	Associated deformation	Correlations w/ Schermer (1990, 1993)
D_1 (southwest-vergent Nestos thrust accommodates A-type subduction of Falakron carbonate platform beneath Serbo-Macedonian-West Thracian gneiss complex)	47-36*	N35°-50°E-trending, gently northeast-plunging major open or sheath (?) folds, small tight to isoclinal folds, and mineral stretching lineations in the Falakron marble series and lower Serbo-Macedonian-West Thracian gneiss complex.	D_3 (southwest-vergent Olympos thrust; high-P metamorphism of Olympos carbonate unit)
Mid-Oligocene magmatism	33-28†	Intrusion of Vrondou, Xanthi, and several smaller granodiorite plutons in the Rhodope metamorphic core complex; extrusion of Paranestion andesites above West Thracian gneiss complex.	
D_2 (emplacement and synintrusional mylonitization of Symvolon pluton within a coaxial shear at southwest margin of Rhodope core complex)	23-16	Intrusion of Symvolon pluton ~21 - 22 Ma.§ Gently northeast-plunging minor tight to isoclinal folds and mineral stretching lineations in Symvolon pluton and southwestern Falakron marble series. Mean lineation attitude = 18°, N58°E.	D_5 (top-to-the-northeast low-angle normal faults on north and south flanks of Mt. Olympos)
D_3 (gently southwest-dipping Strymon Valley detachment; Serbo-Macedonian gneiss complex moves 3°, S53°W in hanging wall; Rhodope metamorphic core complex emerges in footwall)	16-3.5**	N45°-60°E-trending, gently southwest-plunging minor tight to isoclinal folds and mineral stretching lineations in southwestern Symvolon and Vrondou plutons and southwestern Falakron marble series; deposition and tilting of syndetachment basin complex in hanging wall (northwest-trending normal faults soling into detachment).	
D_4 (top-to-the-northeast? North Aegean detachment bounded to the southeast by the North Aegean trough)	3.5**-present	Northwest-trending normal faults accommodate subsidence of modern Strymon and Drama basins, possibly above a mid-crustal detachment.	D_7 (northeast-dipping high-angle normal faults at southwest margin of modern Vardar-Thermaikos basin)
late D_4 (strike-slip and related faulting)	?-present	Northeast-trending, mainly dextral strike-slip faulting; secondary extension on seismogenic? N70°-85°W-striking normal faults.	

* Ages based on K-Ar hornblende dates at base of West Thracian gneiss complex (Liati, 1986) and K-Ar muscovite and biotite dates at base of Serbo-Macedonian gneiss complex (Harre et al., 1968; Marakis, 1969). See Tables 5 and 7.

† Ages based on K-Ar hornblende dates from Vrondou pluton (Marakis, 1969) and Xanthi pluton (Liati, 1986). See Table 3.

§ Ages based on $^{40}Ar/^{39}Ar$ hornblende dates and U-Pb titanite and zircon dates from the Symvolon pluton obtained in this study (Tables 1 and 2).

** Based on fossil ages in syndetachment basin complex [MN3-MN6 *Micromeryx flourensianus* Lartet in the Struma basin (Kojumdgieva et al., 1982); MN15 rodent fauna in the Serres basin (Armour-Brown et al., 1979)], on K-Ar biotite dates from the Mesolakkia (Harre et al., 1968) and Symvolon (Kokkinakis, 1980b) plutons, and on $^{40}Ar/^{39}Ar$ biotite and K-feldspar dates from the Symvolon pluton obtained in this study (Table 3).

TABLE 7. PUBLISHED RADIOMETRIC AGES, WEST THRACIAN GNEISS COMPLEX

Metamorphic rocks

Rock type	Method	Mineral	Age (Ma)	Ref.	Sample	Location
common amphibolite*	K-Ar	hbl	46.9 ± 0.7	1	GOR 34†	~300 m above Nestos thrust (N.of Xanthi)
common amphibolite*	"	hbl	46.7 ± 0.9	1	GOR 82†	~325 m above Nestos thrust (N.of Xanthi)
common amphibolite*	"	hbl	45.7 ± 0.8	1	GOR 35†	~350 m above Nestos thrust (N.of Xanthi)
common amphibolite*	"	hbl	45.4 ± 0.5	1	SIR 5†	~700 m above Nestos thrust (N.of Xanthi)
common amphibolite*	"	hbl	34.0 ± 0.5§	1	KIM 100†	~700 m above Nestos thrust (N.of Xanthi)
common amphibolite*	"	hbl	39.8 ± 0.6	1	GOR 18†	~900 m above Nestos thrust (N.of Xanthi)
common amphibolite*	"	hbl	41.4 ± 0.6	1	GOR 54†	~1000 m above Nestos thrust (N.of Xanthi)
common amphibolite*	"	hbl	37.3 ± 0.6	1	GOR 55†	~1000 m above Nestos thrust (N.of Xanthi)
common amphibolite*	"	hbl	40.5 ± 0.6	1	ECH 6	Upper "Echinos unit"†† (N.of Xanthi)
common amphibolite*	"	hbl	39.2 ± 0.6	1	RH 3	~3000 m above Nestos thrust (N.of Drama)
common amphibolite*	"	hbl	45.6 ± 0.7	1	RH23	~3000 m above Nestos thrust (N.of Drama)
common amphibolite*	"	hbl	49.0 ± 0.6	1	RH 24	~3000 m above Nestos thrust (N.of Drama)
common amphibolite*	"	hbl	50.5 ± 0.7	1	RH 26	~3000 m above Nestos thrust (N.of Drama)
eclogitic amphibolite**	"	hbl	78.9 ± 0.6	1	GOR 13†	~500 m above Nestos thrust (N.of Xanthi)
eclogitic amphibolite**	"	hbl	57.4 ± 0.6	1	SIR 25†	~600 m above Nestos thrust (N.of Xanthi)
eclogitic amphibolite**	"	hbl	95.1 ± 1.1	1	SIR 12†	~650 m above Nestos thrust (N.of Xanthi)
eclogitic amphibolite**	"	hbl	76.0 ± 1.1	1	RH 25	~3000 m above Nestos thrust (N.of Drama)
eclogitic amphibolite**	"	hbl	81.0 ± 1.5	1	RH 28	~3000 m above Nestos thrust (N.of Drama)
2-mica schist	"	bio	36.6 ± 0.4	1	GOR 14†	~500 m above Nestos thrust (N.of Xanthi)
"	"	mus	36.1 ± 0.4	1	GOR 14†	~500 m above Nestos thrust (N.of Xanthi)
schist	"	mus	35.3 ± 0.3	1	GOR 15†	~500 m above Nestos thrust (N.of Xanthi)

TABLE 7 (continued). PUBLISHED RADIOMETRIC AGES, WEST THRACIAN GNEISS COMPLEX

Metamorphic rocks (continued)

Rock type	Method	Mineral	Age (Ma)	Ref.	Sample	Location
augen gneiss, migmatite	"	bio	34.8 ± 0.3	1	GOR 17A	Near base of "Echinos unit"††
augen gneiss, migmatite	"	bio	35.8 ± 0.3	1	ECH 2	Central part of "Echinos unit"††
biotite gneiss	"	bio	32.8 ± 0.3	1	RH 1	~3000 m above Nestos thrust (N.of Drama)
biotite gneiss	"	bio	32.5 ± 0.3	1	RH 2	~3000 m above Nestos thrust (N.of Drama)

Intrusive rocks

Rock type	Method	Mineral	Age (Ma)	Ref.	Sample	Location
Kentavros diorite	K-Ar	hbl	38.0 ± 0.4	1	KEN 85	~1.5 km above base of "Echinos" unit
migmatitic granite	K-Ar	bio	29.1 ± 1.2	2		Elataia-Skalote batholith
granite	"	bio	35.6 ± 1.4	2		Elataia-Skalote batholith (Pefki)
granite	"	bio	38.5 ± 1.5	3		Elataia-Skalote batholith (Tholos)
pegmatite dyke	"	mus	38.3 ± 1.1	3		Elataia-Skalote batholith (Tholos)
granodiorite	Rb-Sr	w.r.§§	87.7 ± 27	4		Elataia-Skalote batholith
gabbro	?	?	~157	5		E. of Xanthi pluton

* "Common amphibolites" in the West Thracian gneiss complex are considered by Liati (1986) to be derived from eclogites of basaltic composition that completely recrystallized under amphibolite-grade conditions subsequent to early high-P metamorphism.

† These samples lie within the "Siroko nappe" of Koukouvelas and Doutsos (1990), the structurally lowest tectonostratigraphic unit in the West Thracian gneiss complex, referred to in this study as the "Siroko unit".

§ Lies within the contact aureole of the ~31 Ma Xanthi pluton (Liati, 1986).

** "Eclogitogenic amphibolites" of Liati (1986), considered to represent incompletely recrystallized eclogites of basaltic composition based on the presence of sodic augite, plagioclase-clinopyroxene symplectites, rutile, kelyphitic garnet, and high pyrope content of garnet.

†† The "Echinos nappe" of Koukouvelas and Doutsos (1990), referred to in this study as the "Echinos unit" overlies the "Siroko unit at a strongly cataclasized, gently northeast-dipping shear contact north of Xanthi.

§§ Rb-Sr whole-rock isochron.

References: (1) Liati, 1986; (2) Sklavounos, 1981, unpub. Univ. of Thessaloniki Ph.D. thesis: dates reported in Kotopouli and Pe-Piper, 1991; (3) Meyer, 1968; (4) Soldatos, 1985; (5) Christophidis, pers. commun., 1988, reported in Koukouvelas and Pe-Piper, 1991.

CHAPTER 5

STRATIGRAPHY AND STRUCTURE OF THE STRYMON VALLEY REGION, NORTHEASTERN GREECE

David A. Dinter
Department of Earth, Atmospheric and Planetary Sciences
Massachusetts Institute of Technology
Cambridge, MA 02139

INTRODUCTION

Convergence between the African and European plates is accommodated in the eastern Mediterranean region by northeastward subduction of Ionian and Adriatic lithosphere beneath mainland Greece, the Aegean Sea, and southwestern Turkey (Fig. 1). The Hellenic subduction system appears to have been established in roughly its present setting by 13 Ma (Le Pichon and Angelier, 1979). Prior to that time major shortening occurred in more easterly positions within the Hellenic Alps, where southwest-vergent thrusting migrated westward throughout much of Tertiary time (e.g., Burchfiel, 1980).

In the hinterland of the Hellenides, the overriding plate of the Hellenic subduction system is greatly extended. Crustal thickness beneath the Aegean Sea varies from about 22 to 32 km, compared with 40 to 50 km beneath mainland Greece and Turkey (Jongsma et al., 1977; Makris, 1976; Makris and Vees, 1977). Based on these values, derived from seismic refraction and gravity studies, the Aegean region may have widened by more than 100%. The modern Aegean extensional province lies in the back-arc of the Hellenic subduction system and is characterized by numerous, large, elongate sedimentary basins. High-angle normal faults bounding these basins are nearly parallel and subequally spaced over broad sectors, and it has been suggested that each set of such faults and basins may be the surface expression of a distinct extensional system that soles into a ductile detachment zone in the middle crust (Jackson and McKenzie, 1983; Dinter and Royden, 1993).

A key structural element in the extensional evolution of the north Aegean region and a principal focus of the present study is the Strymon Valley detachment, a southwest-dipping, Neogene, low-angle normal fault that forms the southwestern boundary of the Rhodope metamorphic province for more than 200 km along strike in southwestern Bulgaria, northeastern Greece, and on the island of Thasos (Figs. 2 and 3; Dinter, 1991). Southwestward transport of the hanging wall in this detachment system from ~16 to 3.5 Ma resulted in the unroofing of the Rhodope metamorphic core complex, which is exposed northeast of the Strymon River beneath a strongly disrupted veneer of unmetamorphosed syndetachment basinal deposits. Regional geologic relations suggest a minimum displacement of 25 km on the detachment in northern Greece (Dinter and Royden, 1993).

The large-magnitude lateral displacement of major tectonostratigraphic units in the Strymon Valley detachment system redefines the kinematic environment of extension in the north Aegean region and has important implications for the origin and deformation of Cenozoic basins. Moreover, fundamentally new information bearing on earlier tectonic events is gained by palinspastically restoring the displaced units to their preextensional positions. This simple reconstruction necessitates a reevaluation of several long-accepted tenets of the regional geology and serves as the underpinning to a fundamentally new model for the tectonic evolution of southwestern Rhodope and Serbo-Macedonia.

GEOLOGIC SETTING OF THE STRYMON VALLEY REGION

The geographical designation "Rhodope" has been applied in several tectonic contexts. The *Rhodope continental fragment* subsumes the entire region between the Vardar zone and the Carpathian-Balkan branch of the Alpine chain (Fig. 1), whereas the *Rhodope massif* or *metamorphic complex* includes only the mountainous central portion of

this fragment, bounded by the Struma-Strymon and Maritsa Basins (Figs. 1 and 2). This region will be referred to here simply as the *Rhodope metamorphic province*, because it does not exemplify the tectonic stability implied by the term "massif" (see below). *The Rhodope metamorphic core complex* comprises only the southwestern segment of the Rhodope province, approximately bounded by the Strymon and Nestos Rivers, and corresponds to the tectonically unroofed footwall of the Strymon Valley detachment system (Dinter and Royden, 1993).

The Rhodope continental fragment has been interpreted as a piece of western Tethyan lithosphere that was isolated by rifting during the early Mesozoic breakup of Pangaea (Burchfiel, 1980). Its southern remnant is exposed on the southeastern Balkan peninsula, where it comprises three major crystalline domains – the Serbo-Macedonian and Rhodope metamorphic provinces, and the north-vergent thrust nappes of the Balkan Mountains (Fig. 1). During Alpine convergence between Africa and Europe, the northern (Balkan) margin of the Rhodope fragment was underthrust by the Moesian continental platform, and its southwestern (Vardar) margin was a locus of northeast-directed subduction. The last of the "Vardar ocean" was probably consumed by latest Cretaceous or Paleocene time, resulting in a collision between southwestern Rhodope and "Apulia", another Tethyan continental fragment, which comprises much of Italy, western former Yugoslavia, Albania and western mainland Greece (e.g., Smith, 1971; Burchfiel, 1980). Convergence continued within and immediately west of the Vardar zone after the collision throughout most of Eocene time, accommodated by northeastward A-type subduction of the eastern Apulian continental margin (Schermer, 1990, 1993). Subsequently, the locus of shortening migrated incrementally westward across the Hellenic and Dinaric Alps to its present position at the eastern margin of the Adriatic Sea.

Serbo-Macedonia and the Balkans, the marginal crystalline provinces of the southern Rhodope fragment, were clearly deformed during Alpine orogenesis because they are disrupted by thrust faults involving late Mesozoic sediments (e.g. Kockel et al., 1971; Kauffmann et al.; 1976; Jacobshagen et al., 1978). By contrast, the Rhodope province, which forms the central portion of the fragment, was long considered to represent a Precambrian or Hercynian "massif" or "Zwischengebirge" that remained essentially stable during Alpine deformation around its margins (e.g., Kober, 1931; Schwan, 1962; Georgiev, 1963; Boncev, 1971). Detailed structural mapping and geochronologic studies have shown to the contrary that both in Greece (Kronberg, 1969; Meyer, 1969; Birk et al., 1970) and in Bulgaria (Ivanov, 1981; Burg et al., 1990), the Rhodope province was strongly folded, sheared, and metamorphosed in the course of Alpine orogenic events. It has been suggested that this deformation represents intracratonic shortening of the Rhodope continental fragment owing to stresses transmitted inward from the convergent zones at its boundaries (Burchfiel, 1980); however, major aspects of the regional structure have been poorly resolved and the tectonic setting of the Rhodope province during Alpine orogenesis has remained largely an open question (cf. Jacobshagen, 1978).

In the southwestern Rhodope province the gross structural geometry is quite simple (Figs. 3 and 4): An enormously thick, strongly deformed marble unit of unknown age exposed between the Strymon and Nestos Rivers, referred to in this study as the "Falakron marble series", is overlain at its southwestern margin on a brittle, low-angle, southwest-dipping fault by the Serbo-Macedonian gneiss complex, and at its northeastern margin on a ductile, northeast-dipping shear zone by a unit designated here the "West Thracian gneiss complex", which corresponds exactly to the "Glimmerschiefer-Serie G" of Osswald (1938), the "Obere Schiefergneis-Folge" of Meyer and Pilger (1963), the "upper tectonic unit" of Papanikolaou and Panagopoulos (1981), and the "Xanthe-Echinos gneiss complex" of Kotopouli et al. (1991). The Falakron marble series bears upper greenschist-

facies mineral assemblages (Schenk, 1970; Kronberg et al., 1970), whereas the overlying Serbo-Macedonian and West Thracian gneiss complexes were both regionally metamorphosed under upper amphibolite-facies conditions with local anatectic melting (Kockel et al., 1977; Kronberg and Raith, 1977, respectively).

The cataclasized, low-angle, southwest-dipping contact between the Serbo-Macedonian gneiss complex and the underlying Falakron marble series is exposed in several short segments at the northeast margin of the Strymon Valley. Kockel and Walther (1965) interpreted this contact as a northeast-vergent thrust, the "Strimonüberschiebung", which purportedly accommodated the emplacement of Serbo-Macedonia over the southwest margin of the Rhodope province. Schenk (1970) concluded that the latest displacement on this fault must have been Tertiary or later because unmetamorphosed sediments of indefinite Tertiary age are locally sheared in the fault zone. He also noted that the fault cuts ductile strain fabrics preserved in the footwall marbles and schists, and argued that as these fabrics are also present in the Messolakia pluton, which yielded Miocene K-Ar biotite dates (Meyer, 1968), the fault cannot be older Miocene. The 'Tertiary thrust' identity of this structure is generally accepted and widely cited as an expression of mid-Tertiary compression in the Strymon Valley area (e.g., Jacobshagen et al., 1978). Recently, however, the supposed thrust exposures have been remapped as segments of the extensional Strymon Valley detachment (Dinter and Royden, 1993). The reinterpretation of the "Strimonüberschiebung" as a low-angle normal fault negates the principal evidence for a mid-Tertiary compressional event in the north Aegean region. Furthermore, the top-to-the-southwest sense of shear on the detachment implies that the Serbo-Macedonian gneiss complex occupied a predetachment position overlying the Falakron marble, and thus lay roughly adjacent to the West Thracian gneiss complex prior to ~16 Ma.

The moderately northeast-dipping mylonitic contact between the West Thracian gneiss complex and the underlying Falakron marble, exposed in the Nestos River vicinity, is referred to here as the "Nestos thrust". Metamorphic foliations in the juxtaposed units dip northeast within several kilometers of the contact zone (Fig. 3; Kronberg and Eltgen, 1973), and northeast-plunging minor fold axes and stretching lineations are also common to the marble (Meyer, 1968) and the gneiss complex (Koukouvelas and Doutsos, 1990). While acknowledging that the contact is strongly sheared, early workers presumed that it preserved essentially primary stratigraphy (e.g., Kronberg, 1969; Kronberg and Raith, 1977). Based on the contrast in metamorphic grade between the two units, however, Papanikolaou and Panogopoulos (1981) suggested that the contact might be a thrust fault, and Zachos and Dimadis (1983) openly favored a thrust origin on this basis. The minimum age of the Nestos thrust is constrained by the emplacement of the Xanthi granodiorite, whose undeformed, intrusive northern margin cuts the thrust and associated ductile shear structures and fabrics in its footwall northwest of Xanthi (Kronberg and Eltgen, 1973). Radiometric age data obtained from the Xanthi pluton include K-Ar biotite dates of 27.1 ± 0.4 Ma, 27.9 ± 0.9 Ma (Meyer, 1968) and 28.8 ± 0.3 Ma (Liati, 1986), and a single K-Ar hornblende date of 30.4 ± 0.6 Ma (Liati, 1986), which may be taken as a minimum emplacement age. At its eastern margin the Xanthi body intrudes andesitic dykes from which hornblende phenocrysts yielded a K-Ar date of 33.5 ± 1.2 Ma (Eleftheriadis et al.,1984). This date provides a maximum emplacement age providing that the Ar system of the extrusive hornblendes was not partially reset as a result of the intrusion. This assumption is probably valid because a large tract of andesitic volcanics that overlies the West Thracian gneiss complex 20 km to the northwest has yielded K-Ar dates clustering in the range of 28.7 Ma to 35.0 Ma (Eleftheriadis and Lippolt, 1984). Thus, the Nestos thrust and associated structural elements must be older than 30.4 - 33.5 Ma.

Between the Serbo-Macedonian and West Thracian gneiss complexes, roughly coincident with the surface exposure of the underlying Falakron marble series, lies the Rhodope metamorphic core complex, which emerged to the northeast from beneath Serbo-Macedonia in the footwall of the Strymon Valley detachment system from middle Miocene through early Pliocene time (Dinter and Royden, 1993). As noted above, the crystalline portion of the hanging wall in the Strymon Valley detachment system is metamorphosed to a much higher grade than the footwall, a situation inherited from an initial juxtaposition of the gneiss and marble units in an Alpine thrust setting. Thus, Neogene extension on the Strymon Valley detachment opened a tectonic window into an Alpine thrust zone. Deformational elements related to these distinct shear events are commonly difficult to tell apart in the Rhodope core complex because ductile shearing in both cases occurred on northeast-southwest axes at relatively low angles and with southwest vergence.

TECTONOSTRATIGRAPHY

Rocks exposed northeast of the Strymon River in northeastern Greece may be divided into three broad tectonostratigraphic sequences based on their structural positions with respect to the Strymon Valley detachment. They either lie in its footwall, and therefore belong to the Rhodope metamorphic core complex, in its hanging wall, or are part of the "overlap sequence", composed of late Pliocene and Quaternary sediments deposited after detachment motion ceased. Hanging-wall rocks are further subdivided into crystalline rocks that existed prior to the origin of the detachment system, that is, metamorphic rocks of the Serbo-Macedonian province, and syndetachment sediments, deposited in a basin overlying the up-dip limit of the detachment system and penecontemporaneously incorporated into its hanging wall (Fig. 4).

The quality of exposure in the Strymon Valley region varies greatly as a function of rock type. Carbonates both above and below the detachment and evaporites and lacustrine siltstones in supradetachment basin deposits generally support only sparse foliage and are well-exposed. Coarse-grained silicic rocks, by contrast, tend to be poorly exposed. Most parts of the Symvolon and Vrondou plutons, gneiss layers within the Falakron marble series, and Neogene sandstones and conglomerates within the syndetachment basin complex are strongly sheared, deeply weathered, and covered with dense brush. Good exposures are limited to quarries, stream incisions, roadcuts, and coastal bluffs, which allows for detailed examinations of these units in isolated areas but generally precludes the tracing of stratigraphic horizons and faults for more than a few hundred meters.

Footwall rocks: the Rhodope metamorphic core complex

Three major tectonostratigraphic units were mapped in the footwall of the Strymon Valley detachment: the Falakron marble series, of unknown pre-mid-Oligocene age, the Vrondou pluton, one of a chain of calc-alkaline intrusives inferred to have been emplaced ~31 - 33 Ma in the southern Rhodope province, and the Symvolon granodiorite, determined in this study to have been emplaced ~21 - 22 Ma (Chapter 3). The Falakron marble series is highly strained and bedding is not generally discernible. Intercalations of gneiss, schist, and amphibolite, and shear-bounded layers within the marble can be traced over significant areas, however, and were mapped where they are thick enough (at least 10 m, typically) to appear at the local map scale. Plutons were not subdivided.

Falakron marble series

The Falakron marble series crops out over an area covering > 4000 km^2 between the Strymon and Nestos Rivers and on the island of Thasos (Fig. 3; Zachos, 1982;

Bornovas and Rondogianni-Tsiambaou, 1983; Vavelidis et al., 1987). The marbles increase dramatically in structural thickness northeastward in the Rhodope core complex, from < 200 m in southwestern Mount Pangaion and the Menoikion Mountains to > 5000 m in the central Falakron and Lekanis Mountains (Kronberg, 1969; Schenk, 1970; de Boer, 1970). The dominant lithology is a massive, white to light gray, granular marble so strongly sheared and recrystallized that virtually all primary sedimentary features have been obliterated. Impure banded marbles bearing varying proportions of quartz and phengite, and lesser plagioclase and clinozoisite with accessory graphite and pyrite are also common (Kronberg, 1969). Intercalations of micaceous gneiss, two-mica schist, and actinolite schist appear locally in lenses and layers < 1 m to > 400 m thick. The age of the Falakron series is poorly constrained. Meyer and Pilger (1963) reported a single colonial (?) coral find from the central part of the unit, constraining the marbles to be post-Cambrian; however, preservation proved too poor for the specimen to be identified (Kronberg et al., 1970). Based on structural arguments presented in a later section, the marbles must be pre-middle Eocene in age.

Mineral compositions and assemblages observed in metapelites and impure marbles throughout the mainland exposure area of the Falakron series are typical of greenschist-facies (quartz-albite-epidote-biotite subfacies) regional metamorphism (Kronberg et al., 1970). On the island of Thasos, greenschist assemblages also predominate (Vavelidis et al., 1987); however, relict kyanite and sillimanite are locally present in gneiss and schist layers, providing evidence of an earlier higher-grade metamorphism (Atzori et al., 1990). According to Kronberg (1969), the massive marbles represent reefs and reef debris, while the mica schists and gneisses are metapelites and metagraywackes or arkosic graywackes, respectively. Metamorphic foliations are ubiquitous in the Falakron series, commonly defining recumbent, tight to isoclinal folds with wavelengths and amplitudes from several centimeters to several meters, and axes showing strongly preferred orientations in the range

N40°-60°E (Meyer, 1969). Kronberg et al. (1970) characterize the major structures affecting the Falakron marble as upright, km-scale, gently northeast-plunging, open anticlines and synclines, and interpret all ductile deformational elements in this unit as products of a single, early Tertiary, Alpine compressional event.

The Falakron marble series of this study corresponds exactly to the "lower tectonic unit" of the Greek Rhodope province as defined by Papanikolaou and Panagopoulos (1981). Earlier workers divided this unit into an upper sequence dominated by massive marbles, the "Marmorserie F" of Osswald (1938) or "Marmor-Folge" of Meyer and Pilger (1963), and a lower sequence of gneiss and schist with sparse marble intercalations, the "Gneis-Serie E" of Osswald (1938) or "Untere Schiefergneis-Folge" of Meyer and Pilger (1963). According to Kronberg (1969; 1973) and Schenk (1970), the gneiss and schist sequence crops out primarily beneath massive marbles on the southeast flank of Mount Pangaion and as a country-rock carapace overlying the northwest flank of the Symvolon pluton. However, Kokkinakis (1980a) remapped the Symvolon exposures as a marginal blastomylonitic phase of the Symvolon granodiorite, and based on my own observations, many of the Pangaion exposures also appear to be strongly mylonitized plutonic rocks rather than paragneisses. Although muscovite and two-mica schists and gneisses representing country rock do crop out locally in both areas, their thickness and tectonic position within the footwall is presently uncertain. As they are petrographically indistinguishable from schist and paragneiss intercalated within marbles elsewhere in the core complex (Kronberg et al., 1970), the Pangaion and Symvolon metasediments are assigned here to the Falakron series. Radiometric ages obtained from these rocks in the Marmara Valley south of Mt. Pangaion include Rb-Sr muscovite dates of 18.3 ± 0.6 Ma, 22.3 ± 0.7 Ma, and 22.6 ± 0.7 Ma, and Rb-Sr biotite dates of 12.2 ± 0.4 Ma and 12.6 ± 0.4 Ma (Del Moro et al., 1990). These values are similar to K-Ar ages from the Symvolon

pluton and also from the Mesolakkia pluton, which intrudes the Falakron marble beneath Mount Pangaion and is probably continous with the Symvolon pluton in the subsurface.

Tertiary calc-alkaline magmatites

Tertiary intrusives ranging in composition from gabbro to granite crop out in scattered locations throughout the Rhodope metamorphic core complex, but occur in especially great volumes beneath its southwestern margin, corresponding to the thinnest part of the Falakron series (Meyer, 1968; de Boer, 1970; Schenk, 1970). With the addition of new $^{40}Ar/^{39}Ar$ and U-Pb dates (Chapter 3), there are now sufficient radiometric data from the major intrusive bodies in the southern Rhodope province to facilitate their division into groups representing two distinct magmatic episodes. The Xanthi and Vrondou plutons and a number of smaller intrusives were emplaced in mid-Oligocene time, a period also characterized by widespread andesitic volcanism in southwestern Bulgaria. The Symvolon granodiorite is an early Miocene intrusive.

Oligocene intrusive and volcanic rocks

The Vrondou pluton, composed dominantly of quartz monzonite, crops out as a N55°E-elongate dome approximately 35 km long and 10 - 15 km wide at the southwestern margin of the Rhodope metamorphic core complex just south of the Bulgarian border (Fig. 3). Its northeastern margin is an undeformed intrusive contact that cuts across northeast-trending structural and fabric elements in the Falakron series and is associated with a narrow contact aureole. Its southern margin, by contrast, is strongly mylonitized and bears uniformly southwest-plunging stretching lineations (Kolocotroni and Dixon, 1991; Dinter and Royden, 1993). K-Ar hornblende dates from Vrondou quartz monzonites range from 29 ± 1 Ma to 33 ± 2 Ma (Marakis, 1969), and a biotite separate from the Vrondou pluton

yielded a K-Ar date of 30.0 ± 3.0 Ma (Dürr et al., 1978), documenting a rapid cooling of the Vrondou body in mid-Oligocene time from > 500°C to < 300°C, the approximate Ar closure temperatures of hornblende and biotite, respectively (Harrison, 1981; Harrison et al., 1985). These data must be interpreted *sensu strictu* to indicate a minimum emplacement age in the range 31 - 33 Ma. However, the Vrondou body is similar in composition and radiometric age characteristics to the Xanthi pluton (Kotopouli and Pe-Piper, 1989a), which is known to have been emplaced in the range 30.4 - 33.5 Ma based on crosscutting relationships with andesitic volcanics (e.g., Liati, 1986). Moreover, the Xanthi pluton and the eastern margin of the Vrondou pluton crosscut structures that formed as late as 36 Ma within the Falakron marble series (see below). It is likely, therefore, that the eastern part, at least, of the Vrondou body was emplaced during the same mid-Oligocene intrusive event as is represented by the Xanthi pluton. The Elaion pluton appears to be continuous with the Vrondou pluton to the south in the Menoikion Mountains and is inferred to have been emplaced at about the same time (cf. de Boer, 1970).

Intrusive bodies with compositions, radiometric ages, and structural settings similar to those of the Vrondou and Xanthi plutons are scattered throughout the southern Rhodope province. The small Granitis and Krinides (or Philippi) granites, which intrude the Falakron series between the Vrondou and Xanthi bodies, yielded 28.2 ± 0.5 Ma and 26.0 ± 0.5 Ma K-Ar biotite dates, respectively (Meyer, 1968). Del Moro et al. (1988) interpret Rb-Sr biotite-whole rock isochron ages in the 28 - 32 Ma range obtained from several small granodiorite and quartz monzonite bodies in eastern Thrace as emplacement ages. These granitoids define a belt of mid-Oligocene calc-alkaline plutonism that trends roughly east-southeast for more than 200 km across the southern Rhodope province (Figs. 2 and 3). This belt is closely related spacially, temporally, and compositionally to the Paranestion volcanic series, a calc-alkaline arc suite composed of andesites, rhyolites, and dacites that overlies the West Thracian gneiss complex along the Greek-Bulgarian border (Fig. 2;

Fytikas et al., 1984). The Xanthi granodiorite and rhyolitic Paranestion tuffs are nearly identical in composition, and are interpreted by Kotopouli and Pe-Piper (1991) as magmatic equivalents. Biotite and sanidine separates from the Paranestion volcanics yielded K-Ar dates ranging from 28.7 ± 1.1 Ma to 30.6 ± 1.1 Ma (Eleftheriadis and Lippolt, 1984).

Given the association with arc volcanics and a geochemical character consistent with a fractionated mantle source contaminated by crustal constituents, the Vrondou and Xanthi plutons are considered by Kotopouli and Pe-Piper (1989a), Kolocotroni and Dixon (1991), and Koukouvelas and Pe-Piper (1991) to be products of subduction-related magmatism. A similar origin is inferred for the mid-Oligocene granitoids and volcanics of eastern Thrace by Innocenti et al. (1984) and Del Moro et al. (1988). Thus the east-southeast-trending Vrondou-Xanthi-Thracian intrusive belt appears to have been emplaced above a mid-Oligocene subduction zone.

Early Miocene Symvolon pluton

The Symvolon granodiorite crops out from the port of Kavala southwest along the north Aegean coastline for 40 km as a N50°-55°E-elongate dome 10 to 15 km wide. Its margins are pervasively mylonitized and contacts with country rocks are, in general, ductile shear zones concordant with the mylonitic foliation planes. No contact aureole is preserved. The interior of the pluton is also mylonitic, and characterized by gently-dipping, northeast-trending stretching lineations and outcrop-scale folds (Kokkinakis, 1980a). Compositions typically range from 20 - 30% quartz, 30 - 50% plagioclase, 15 - 25% potassium feldspar, 5 - 25% biotite, and 0 - 5% hornblende, with trace amounts of chlorite and epidote, and accessory zircon, apatite, and titanite (Kokkinakis, 1980b), and K-feldspar phenocrysts as long as 4 cm are common.

The emplacement age of the Symvolon (or "Kavala") granodiorite is a subject of some debate. Meyer (1968) proposed a pre-middle Eocene age for the pluton because he believed that its penetrative shear fabric must have formed during a supposed single episode of ductile shear in the southwestern Rhodope province, interpreted to be pre-middle Eocene based on stratigraphic relationships in eastern Thrace. From the results of a single U-Pb zircon analysis that gave discordant $^{206}Pb/^{238}U$ and $^{207}Pb/^{235}U$ model ages of 95 ± 5 Ma and 101 ± 8 Ma, respectively, and a $^{207}Pb/^{206}Pb$ age of 335 ± 40 Ma, Kokkinakis (1980c) interpreted a Carboniferous emplacement age.

New radiometric data acquired from the Symvolon pluton in this study include K-feldspar, biotite, and hornblende $^{40}Ar/^{39}Ar$ dates, and titanite and zircon U-Pb dates (Chapter 3). Middle Miocene biotite and K-feldspar model ages are discussed below in the context of the Strymon Valley detachment system. $^{40}Ar/^{39}Ar$ hornblende and $^{206}Pb/^{238}U$ titanite dates fall in the range 19.7 ± 0.3 Ma to 21.4 ± 0.4 Ma. Based on thin-section observations, hornblende appears to have crystallized in the shear environment that produced S-C mylonitic fabrics throughout the pluton, whereas titanite represents a euhedral to subhedral, early or pre-mylonitic phase that was passively rotated into alignment with C- and particularly with S-planes during shear deformation. Zircons commonly appear as inclusions in K-feldspar phenocrysts. The minimum $^{206}Pb/^{238}U$ zircon date obtained in this study is 24.4 ± 0.7 Ma; however, all of the zircons analyzed showed a strong component of inheritance in their isotopic compositions. The radiometric ages of these phases record cooling through closure temperatures of approximately 500°C for hornblende (Harrison, 1981), 600°C for titanite, and >750°C for zircon (Ghent et al., 1988). Their convergence in earliest Miocene time records an abrupt cooling event interpreted here as the emplacement of the pluton. Rb-Sr muscovite dates of 22.3 ± 0.7 Ma and 22.6 ± 0.7 Ma obtained by Del Moro et al.(1990) from gneisses intruded by the Symvolon pluton in the Marmara Valley area are consistent with this interpretation.

Hanging-wall units

The crystalline portion of the hanging wall in the Strymon Valley detachment system is the petrologically heterogeneous, upper amphibolite-facies Serbo-Macedonian gneiss complex (Figs. 2 and 3). Outcrops of Serbo-Macedonian rocks in direct fault contact with the underlying upper greenschist-grade Rhodope metamorphic complex are rare, because the Strymon basin is superposed on the contact region at the trailing edge of the hanging wall (Dinter and Royden, 1993). However, two small exposures of the Serbo-Macedonian "Kerdilion series" crop out above the Falakron marble unit northeast of the Strymon Valley on short segments of the Strymon Valley detachment that were previously mapped as outcrops of the "Strimonüberschiebung" (Kockel and Walther, 1965; Schenk, 1970; Koukouzas, 1972). Along the remainder of its exposed length, the detachment is immediately overlain by strongly faulted deposits of the Struma, Siderokastro, Serres, Angitis, Akropotamos, and South Symvolon basins (Fig. 3; Dinter and Royden, 1993).

Serbo-Macedonian gneiss complex

The Serbo-Macedonian gneiss complex in northern Greece is divided by Kockel et al. (1971) into a western "Vertiskos" series, composed largely of amphibolite-facies gneiss and schist and several strongly sheared felsic, basic, and ultrabasic intrusives, and an underlying eastern "Kerdilion" series, dominantly biotite gneiss and migmatitic gneiss intercalated with marble and minor amphibolite. The contact between the two series is a cataclastic southwest-dipping shear zone (Kockel et al., 1977). K-Ar and $^{40}Ar/^{39}Ar$ dates on metamorphic biotites and muscovites from the Vertiskos series range from 87.8 ± 4.2 Ma to 136.8 ± 1.5 Ma (Harre et al., 1968; Marakis; 1969; Papadopoulos and Kilias, 1985; De Wet et al., 1989), contrasting strongly with K-Ar dates in the range 32 - 38.5 Ma on

biotites and 36 - 43 Ma on muscovites from migmatitic Kerdilion gneisses (Harre et al., 1968). The small Kerdilion exposure overlying the Strymon Valley detachment at the southwest margin of Mt. Pangaion is composed of mylonitic, micaceous, plagioclase-microcline-gneiss that yielded K-Ar dates of 35.0 ± 0.5 Ma and 33.9 ± 0.7 Ma from muscovite and biotite, respectively, and a Rb-Sr biotite model age of 39.3 ± 2.4 Ma (Harre et al., 1968). The Serbo-Macedonian gneiss complex is conventionally regarded as the deformed western margin of the Tethyan "Rhodope fragment". Dixon and Dimitriadis (1984) suggest instead that significant portions of the Vertiskos series represent a Mesozoic subduction complex.

Syndetachment basin complex

Tilted, poorly consolidated Neogene clastic deposits mantling the southwest margin of the Rhodope metamorphic core complex are exposed onshore in fully or partially distinct lobes that have conventionally been regarded as discrete basins, including the Struma basin in western Bulgaria, and the Siderokastro, Serres, Angitis, and Akropotamos and South Symvolon basins at the northeastern margin of the Strymon Valley in Greece (Fig. 3). The Prinos-Kavala basin and possibly the Thasos-Samothraki basin in the northeast Aegean Sea are offshore representatives of this series. These 'basins' define a N35°W-trending belt of roughly coeval deposits that persists for more than 200 km along strike and coincides with the outcrop area of the Strymon Valley detachment. Dinter and Royden (1993) recognized this belt as the remnant of a basin complex that accumulated in the region evacuated by Serbo-Macedonian rocks in the breakaway zone of the Strymon Valley detachment system (cf. Fedo and Miller, 1992). Penecontemporaneously with its deposition the basin complex was incorporated and deformed in the hanging wall of the detachment as it moved in a southwesterly direction over the emerging Rhodope core complex. The width of the syndetachment basin complex in the direction of hanging-wall transport increases

southward from less than 5 km in western Bulgaria to about 40 km at the north Aegean coastline. Even greater widths may be attained offshore. Thicknesses of syndetachment deposits increase southward from ~850 m in western Bulgaria (Zagorcev, 1992) to > 3500 m in the offshore Prinos-Kavala basin (Pollak, 1979; Proedrou, 1979). The width of the Rhodope metamorphic core complex also increases southward, from which Dinter and Royden (1993) inferred a possible southerly increase in the magnitude of extension on the Strymon Valley detachment system.

Syndetachment basin deposits have been widely sampled for fossils and their ages and depositional environments are fairly well characterized locally as a result. The faunal suites lack reliable stratigraphic and structural contexts because the strata which bear them are pervasively disrupted by poorly-exposed faults. Nonetheless, the range of ages represented provides a primary constraint on the timing of Strymon Valley detachment activity. The oldest specimen presently known from the syndetachment basin complex is a tooth of *Micromeryx flourensianus* Lartet recovered in a borehole from , the Delcevo Formation of the Struma basin (Kojumdgieva et al., 1982). This is an early Miocene species on the Balkan Peninsula (MN3 - MN6), probably 15 - 18 Ma in age (R. Bernor, personal commun., 1992). The youngest known syndetachment deposits are nonmarine sandstones of the Spilia formation in the Serres basin, which bear MN15 rodent fauna that may be as young as 3.5 Ma (Armour-Brown et al., 1977; Steininger and Rögl, 1984).

The Struma basin in Bulgaria and the Siderokastro basin in northernmost Greece contain only terrigenous deposits (Kojumdgieva et al., 1982; Zagorcev, 1992), whereas the Serres basin (von Freyberg, 1951; Armour-Brown et al., 1977), and syndetachment deposits at the southern margin of Strymon Valley (Gramann and Kockel, 1969; Dermitzakis et al., 1985), preserve a lower Pliocene shallow marine interval separating two nonmarine sequences. The Akropotamos, South Symvolon, and Prinos-Kavala basins

preserve both Messinian evaporites and lower Pliocene marine beds between predominantly nonmarine sequences (Psilovikos and Syrides, 1983; Dermitzakis et al., 1985; Pollak, 1979; Proedrou, 1979).

Stratigraphic units in the syndetachment basin complex are described only from areas where they were mapped in the present study, including sections of the Angitis, Akropotamos, and South Symvolon basins. Geographic unit designations are informal.

Northeast Angitis basin

The Angitis River bisects an area of some 400 km^2 between the modern Strymon and Drama basins where syndetachment sediments mantle a structurally low section of the Strymon Valley detachment in thicknesses up to ~1200 m. This region, bounded to the southeast by Mt. Pangaion and to the northwest by Mt. Menoikion, is referred to here as the Angitis basin (Fig. 3). Elements of the Strymon Valley detachment system are well-exposed in the northeastern part of the Angitis basin, which was mapped in sufficient detail to establish a tentative stratigraphic section of hanging-wall basinal deposits preserved there. Polymictic basal conglomerates and sandstones interfinger with and are conformably overlain by lacustrine siltstones, which are gradationally succeeded by alluvial sandstones and conglomerates. These clastic beds dip uniformly to the southwest, and are overlain at an angular unconformity by a thick succession of limestones representing several depositional environments. Informal names applied here to these units are the Angitis conglomerate, Lefkothea siltstone, Angitis sandstone, and Menoikion carbonate breccia.

Angitis conglomerate

The Angitis conglomerate unit comprises the earliest known syndetachment deposits in the northeast Angitis basin, a sequence of strongly sheared, crudely bedded, poorly sorted, polymictic pebble and cobble conglomerates interbedded with silty sandstones and sandy siltstones. Conglomerate clasts include 60 - 80% mylonitic granite, 10 - 30% foliated marble, and 10% quartz, schist, gneiss, rare amphibolite, and minor unmetamorphosed sedimentary constituents. Sorting is generally poor, and angular and rounded clasts 1 - 40 cm in diameter are commonly mixed in single, matrix-supported layers. Angular blocks of mafic metamorphic rock with dimensions as large as 5 meters are present locally. Matrix material ranges from poorly-sorted, immature, variably calcareous sand to gritty silt. Interbeds up to 5 m thick of sandstone, siltstone, and lignite compose up to 25% of the unit. The sandstones are moderately sorted, medium- to coarse-grained, locally laminated, calcareous arkoses. Silty beds tend to be poorly indurated, poorly sorted, and highly sheared. Widespread faulting, rapid lateral facies variations, and poor exposure impede accurate section measurements of the Angitis unit; however, a composite of several profiles suggests a minimum preserved thickness of 200 - 300 meters. The original thickness may have been considerably greater because the base of the Angitis conglomerate coincides with the Strymon Valley detachment, where sustained shearing may have resulted in substantial tectonic erosion.

Bedding characteristics and sedimentary textures preserved in the Angitis conglomerate are consistent with an origin in a high-gradient alluvial fan setting dominated by debris flow processes, but characterized by intermittent tractional transport as well. The mixing of angular and rounded clasts in single debris flow layers suggests reworking of associated talus and alluvial deposits. Finer grained beds are probably products of streams and intermittent lakes that occupied areas between active fan lobes. Local concentrations of

soft, rounded, white cataclasite pebbles up to 3 cm in diameter must have been eroded from subaerial exposures of the Strymon Valley detachment, and provide direct evidence that a primary provenance of the conglomerates was the uplifted footwall of the detachment system. The top of the Angitis conglomerate is poorly exposed, but as bedding orientations are consistent with those in the overlying siltstones and there is no obvious evidence of faulting, this contact is tentatively interpreted as conformable.

Lefkothea siltstone

Calcareous, well-indurated, homogeneous, muddy siltstones assigned to the Lefkothea unit weather medium gray and crop out in a distinctive badlands topography. Fine biotite and muscovite flakes are commonly concentrated on bedding planes, and some beds contain up to 5% fine, angular, arkosic sand dispersed in the matrix. As in the Angitis conglomerate, internal shearing precludes an accurate section measure, but aggregate thickness is on the order of 300 - 400 m. Sparse interbeds of fine- to medium-grained, angular, poorly-sorted, silty, arkosic sandstone are present near the base of the unit, largely absent from its central portion, and reappear in the upper ~100 m, increasing upwards in grain size, thickness, and abundance towards a gradational contact with the overlying Angitis sandstone. At their first appearance in the upper part of the section, sandstone interbeds are fine grained, 2 - 8 cm thick, and compose only 5 - 10% of the total volume. Near the top of the unit they are medium- to coarse-grained and occur in beds as thick as 2 - 3 m that account for ~50% of the volume. A typical sand composition is 80% feldspar, 15% quartz, and 5% biotite, with minor carbonaceous fragments. Siltstone beds near the top of the unit tend to be sandier and more commonly fossiliferous than those below, and mudcracks are preserved locally. Rare interbeds of lignite and paper shale up to 5 cm thick bear wood fragments and imprints of large leaves. Faunal remains present in the Lefkothea siltstone include fish scales and tests of ostracodes, gastropods, and the

bivalve *L. Limnocardium* (F. Steininger, written commun., 1991). This species attests to a lacustrine environment (Hutchinson, 1967), and is known from the latest middle Miocene (Sarmatian) to the late Pliocene (Romanian) in eastern Europe (Cox et al., 1969). The Lefkothea siltstone also crops out in the southeastern part of the Angitis basin at the foot of Mt. Pangaion near the town of Kormista (Gramann and Kockel, 1969).

Angitis sandstone

Interbedded siltstone and sandstone at the top of the Lefkothea unit yield gradationally upwards to poorly consolidated, poorly sorted, angular, fine to medium grained, buff-weathering, silty arkose at the base of the Angitis sandstone. Within a few meters upsection the average grain size increases, and well-bedded, intermittently laminated, medium to coarse grained sandstones and gritstones are interbedded with polymictic pebble conglomerates containing clasts of foliated granite, gneiss, quartz, and marble. Sparse siltstone, mudstone, and lignite beds a few centimeters thick are also present. Some 25 m above the base of the unit, a 5-m thick, gray-weathering, cliff-forming, rounded marble cobble conglomerate mappable over several square kilometers signals an increasing abundance of marble in the source terrain. Above this level, alternating sandstone and conglomerate beds appear more oxidized than those below, typically weathering tan to light orange. The Angitis sandstone is mainly alluvial in origin, representing a generally less energetic environment than the Angitis conglomerate, as evidenced by smaller clast and grain sizes. Relatively uniform bedding and laminations indicate a predominance of traction transport over debris flow. On these grounds the Angitis sandstone unit is interpreted as a product of moderate-gradient alluvial fans that spread across the plain of the former lake basin represented by the Lefkothea siltstone. The preserved thickness of the Angitis sandstone is ~40 - 50 meters; its top is not exposed.

Menoikion carbonate megabreccia

The Menoikion carbonate breccia, which forms a sheet as thick as 500 - 600 m covering ~50 km^2 at elevations of 250 to nearly 1500 m on the southeast flank of Mt. Menoikion. It overlies augen gneiss and marble of the Rhodope metamorphic core complex at the Strymon Valley detachment and must have been emplaced relatively late in the detachment episode because it also overlies the southwest-tilted clastic units described above at an abrupt angular discontinuity. In places this discontinuity is strongly sheared and associated with brown, chloritic microbreccia or powdery, white, calcareous ultracataclasite; elsewhere it appears erosional. The carbonate sheet consists of relatively intact blocks as wide as ~100 m separated by indurated breccia zones up to 25 m wide. Within the intact blocks, laminated limestone and dolomite, homogeneous, unlaminated micritic limestone, and well-rounded, virtually monomictic marble pebble conglomerate with micritic matrix material alternate in beds 0.1 - 3.0 m thick. The laminated intervals display an orbicular texture in some places and commonly contain storm rip-up breccias in layers 2 - 5 cm thick. Slightly impure, unlaminated micrites locally bear fish scales and poorly preserved ostracode tests (de Boer, 1970). Pebble conglomerates tend to be well-sorted by bed, with clast diameters ranging up to 20 cm, but averaging only 1 - 3 cm. Clasts are at least 99% foliated marble, but gneiss and granite are locally present both as conglomeratic clasts and as angular breccia blocks within shear zones.

Laminated limestones and dolomites in the Menoikion carbonate unit are supratidal algal flat deposits, and unlaminated micrites bearing aquatic faunal remains probably represent bioturbated intratidal or lagoonal environments. The low-lying coastal region in which these carbonates accumulated was periodically blanketed by marble pebble conglomerates derived from the Falakron marble series in nearby uplands. Rounding and sorting of clasts attest to their abrasion and transport in an alluvial environment. Some of

the conglomerates are channelized and probably represent distributary channels crossing the tidal flat. Others form thin, laterally persistent sheets displaying negligible erosion at the base, and may be products of sheet flow during intermittent periods of heavy rainfall and flooding. The relatively great thickness of these deposits is suggestive of fairly rapid rates of subsidence and sedimentation, as might be anticipated in the region evacuated by the receding hanging wall in a detachment system. Subsequent to their initial deposition the Menoikion carbonates were uplifted and shed as a breccia sheet over previously tilted, subaerially exposed, syndetachment clastic deposits. The dimensions and internal disruption of the breccia sheet, the variably developed shearing at its base, and the local disruption of underlying clastic sediments are all features characteristic of large-rock avalanche deposits formed in arid environments (Yarnold and Lombard, 1989). As the persistent deposition of supratidal algal dolomites and the paucity of plant material in alluvial conglomerates are also suggestive of arid climatic conditions, I tentatively regard the Menoikion carbonate breccia as a product of Messinian deposition and tectonism in the Strymon Valley detachment system, because the Messinian is known to be a period of prolonged aridity in the eastern Mediterranean region (e.g., Meulenkamp, 1977).

Akropotamos basin

The syndetachment sedimentary lobe occupying the mouth of the Marmara River Valley below the village of Akropotamos, bounded to the northwest by Mt. Pangaion and to the southeast by Mt. Symvolon, is referred to here as the "Akropotamos basin". Strong tectonic disruption and poor exposure in this area permit the construction of only a highly generalized stratigraphic section. Alluvial deposits in the lower part of the Akropotamos exposure include at least 40 meters of fine- to coarse-grained arkosic sandstone, siltstone, and well-rounded pebble and cobble conglomerate in beds 0.2 - 1.5 m thick. Conglomerate clasts range from 1 - 50 cm in diameter, tend to be moderately well-sorted in

any given bed, and are composed of 50 - 100% foliated granite and 0 - 50% marble, with proportions of marble generally increasing upsection. Above the alluvial interval, ~15 m of gypsum, siltstone, fine-grained sandstone and paper shale in alternating beds up to 10 cm thick, bearing faunal suites of Messinian age (Dermitzakis et al., 1985), are conformably overlain by at least 3 m of laminated algal limestone and dolomite. This sequence is overlain at a regionally developed low-angle shear surface localized in siltstone and mudstone deposits by a widely distributed limestone unit as thick as ~100 m composed primarily of carbonate sand and micrite.

South Symvolon basin

Syndetachment clastic sediments and evaporites that mantle the Strymon Valley detachment in thicknesses up to ~300 m on the southern flank of Mt. Symvolon are overlain on a low-angle shear surface at the western margin of their exposure by a limestone unit ~50 - 150 m thick that is also displaced by the main detachment. All of these deposits are tilted, mainly to the northeast, suggesting rotation on southwest-dipping, syndetachment normal faults. As in the Akropotamos basin, pervasive faulting and poor exposure preclude the construction of a comprehensive stratigraphic section. Generalized descriptions of hanging-wall lithologies are therefore provided by geographic area.

A massive, highly sheared, monomictic granite breccia sheet 10 - 15 m thick, composed of unsorted, angular blocks as large as 0.7 m in diameter floating in a matrix of poorly sorted granitic grit and sand, overlies the easternmost coastal outcrops of the main detachment surface. This deposit probably corresponds to the "matrix-rich zone" at the base of a large rock-avalanche deposit (Yarnold and Lombard, 1989). A second type of monomictic granite breccia, composed of 15 - 60% angular to subangular clasts 0.5 - 10 cm in diameter, floating in a coarse, angular, unsorted sand matrix, crops outs to the west

in well-defined beds 5 - 25 cm thick, inferred to be debris- or sheet-flow deposits, possibly derived from the coarser landslide breccia.

The central part of the South Symvolon hanging wall is dominated by at least 50 meters of nonmarine sandstone and conglomerate in beds 5 - 100 cm thick, with common intercalations of siltstone and rare lignite. A transgressive sequence appears to be preserved in this area, with alluvial beds in the lower part of the section yielding upwards to either beach or deltaic deposits. Alluvial environments are represented by up to 40 meters of sandstone, siltstone, pebble and cobble conglomerate, and redbeds. Conglomerate clasts are typically well-rounded and moderately well-sorted, consisting of 50 - 95% foliated granite, 5 - 50% marble, and minor schist, amphibolite, and reworked granite pebble conglomerate. Overlying the alluvial sediments in some places are up to 18 meters of alternating gray, sandy, laminated silt, and clean, white, laminated sand in beds 1 - 5 m thick, which are tentatively regarded as backbeach-forebeach cycles. Elsewhere, the alluvial beds are succeeded by more than 15 meters of angular to subrounded, fine- to medium-grained arkosic sandstone containing abundant woody fragments and charcoal, and mollusk tests up to ~0.5 cm in diameter concentrated in storm layers with laminated rip-up clasts of siltstone and fine sandstone. Beds are typically planar, 5 - 20 m thick, and rarely display climbing ripples. These sandstones are inferred to represent a deltaic environment.

Near the western margin of the Symvolon hanging-wall exposure, 5 - 10 m of bedded gypsum are overlain by 4 m of fine grained sandstone and siltstone, paper shale, and 2 - 5 cm interbeds of laminated algal limestone. These deposits are interpreted as Messinian in age because that is the only period during which evaporites are known to have been deposited in the north Aegean region (Meulenkamp, 1977), and because up to 800 m of Messinian evaporites are present just offshore in the Prinos-Kavala basin (Lalechos and

Savoyat, 1977; Pollak, 1979; Proedrou, 1979). Thick, syndetachment limestones overlying the evaporitic sequence on a low-angle shear surface are unlaminated carbonate sands and impure micrites in beds 0.5 - 1.2 m thick, locally bearing ostracodes. These might either be late Messinian freshwater deposits or early Pliocene marine beds.

Postdetachment overlap deposits

Post-Strymon Valley detachment sediments preserved near the southern margin of the Rhodope metamorphic core complex include (1) marine and nonmarine deposits generally not exceeding ~150 m in thickness that unconformably overlie Rhodope bedrock, tilted supradetachment strata, or the detachment itself between the Strymon and Drama basins, (2) up to ~1000 m of basin fill within the Strymon and Drama basins, and (3) clastic and carbonate sections up to several hundred meters thick that lie in fault contact with either Rhodope bedrock or supradetachment strata owing to postdetachment tectonism. In many of the latter cases the tectonic affinity of the faulted sediments is uncertain, but one fault block or the other is tentatively regarded as postdetachment in origin either because it is less tectonically disrupted than typical syndetachment strata, or because it contains lithologic sequences atypical of supradetachment basin. As the youngest known syndetachment deposits are ~3.5 Ma in age (Armour-Brown et al., 1979), all late Pliocene and younger sediments in the Strymon Valley area are considered to belong to the postdetachment overlap sequence.

Where the Strymon Valley detachment coincides with the base of a marble mountain front as at Mts. Pangaion and Menoikion, it is commonly covered at least in part by 2 - 10 m of highly consolidated marble talus breccia. In some places this material is actively accumulating. Over much of the Angitis basin, however, coalescing sheets of marble talus breccia appear to define a planation surface graded to a base level at least 200 m higher than

at present. The breccia is not commonly observed *below* elevations of ~200 m, and is deeply eroded by modern gullies and streams.

On the southern flank of Mt. Pangaion above the village of Galypsos at an elevation of ~290 m, a wave-cut platform pierced by distinctive *Lithodomus* borings marks the top of a 4-m thick, horizontally bedded, well-consolidated, nearshore marine gritstone that depositionally overlaps the Strymon Valley detachment. From this unit and an underlying 30-m thick section of unconsolidated shallow marine sand and silt, Psilovikos and Syrides (1983) collected a suite of 59 molluscan and brachiopod fauna. Six of the species are restricted to the Pliocene; however, owing to the possibility of reworking, a Quaternary age for these strata cannot be excluded. Erosional remnants of similar marine deposits overlie syndetachment strata at an angular unconformity throughout much of the Angitis basin at elevations lower than ~260 m (e.g. Xidas, 1984), and flat-lying beach and shallow marine strata are exposed at elevations of ~200 m within basin fill at the eastern margin of the Drama basin. These deposits are inferred to represent a late Pliocene or Quaternary highstand of sea level that probably defined the base level for the subaerial planation surface described above. Given that glacioeustatic fluctuations cannot account for highstands greater than ~60 m above present sea level subsequent to 3.5 Ma (e.g., Dinter et al., 1990), the present elevations of late Pliocene marine deposits between the Strymon and Drama basins attest to at least 200 m of post-depositional uplift. Several small marine terraces that were probably deposited during one or more Quaternary transgressions crop out at lower elevations surrounding the lower Strymon River.

The stratigraphy of the Strymon basin is known principally from the Strymon 1 and Strymon 2 boreholes approximately 12 km south-southeast of Serres. Summary logs in Erki et al. (1984) show ~900 m of Quaternary, 900 m of Pliocene, and 1800 m of Miocene sand, silt, marl, conglomerate, and sedimentary breccia overlying schist of probable Serbo-

Macedonian affinity in the central part of the basin. Although the entire sedimentary section is conventionally regarded as Strymon basin fill, the geometry and timing of the Strymon Valley detachment system require that all lower Pliocene and older deposits in these cores actually belong to the syndetachment hanging-wall basin complex, and are overlapped unconformably by at most 1000 - 1500 m of post-detachment Strymon basin fill (Dinter and Royden, 1993). A similar situation probably prevails in the Drama basin, and the postulated syndetachment-postdetachment unconformity in both basins has presumably gone unrecognized in boreholes and seismic sections.

Clastic and carbonate sequences tentatively interpreted as postdetachment in origin crop out southwest of the Akropotamos and south Symvolon syndetachment basin lobes in the hanging walls of several north- to northwest-trending high-angle faults, and southeast of the northeast-trending "Tower Bluff fault" along the north Aegean coastline (Fig. 3). From bottom to top the section exposed west of the Akropotamos lobe includes: 40 - 50 m of poorly-sorted, angular to subrounded cobble conglomerate with 95% foliated granite and 5% marble clasts up to 30 cm in diameter in crudely defined beds 0.2 - 1.5 m thick; 12 - 15 m of carbonate sand with thin interbeds of rip-up breccia; and 50 - 60 m of white-weathering, moderately sorted pebble conglomerates with clast compositions of 50 - 90% foliated granite and 10 - 50% marble, overlain by a second carbonate sand interval at least 15 m thick. All contacts within this sequence are depositional and conformable. The lower cobble conglomerates are interpreted as a mixture of fanglomerate and talus breccia, and the upper pebble conglomerates as a product of braided streams. No fossils were collected from the limestone intervals and it is unclear whether they are marine or nonmarine.

The earliest deposits exposed in the Tower Bluff sequence are 15 m of laminated algal limestone and pebble conglomerate interbeds 0.1 - 1.0 m thick. Pebbles are 90% marble and 10% foliated granite up to 2 cm in diameter. This interval is succeeded in turn

by 3 m of angular, highly consolidated marble talus breccia, 4 m of algal limestone, and 4 m of massive cobble and breccia conglomerate consisting of ~65% poorly sorted clasts up to 40 cm in diameter and 35% calcareous, coarse sand matrix, interpreted as a debris-flow deposit. The clasts are 90% well-rounded, foliated, granite cobbles and 10% angular blocks derived from the underlying beds, including both algal limestone and pebble conglomerate. Overlying this layer are 4 m more of algal limestone and unlaminated micrite. The overall depositional character of the Tower Bluff sequence is similar to that of the Menoikion unit in the Angitis basin, representing a supratidal-intratidal carbonate flat intermittently blanketed by coarse clastic material shed from adjacent highlands.

STRUCTURAL OBSERVATIONS

During three field seasons from 1989 to 1991, the Strymon Valley detachment and adjacent hanging-wall and footwall rocks were mapped by the author from the north Aegean coastline southwest of Kavala around the southwestern margins of Mts. Symvolon and Pangaion, and north and south of the Angitis River between the modern Strymon and Drama Basins at a scale of 1:25,000 using topographic and SPOT satellite image bases. Parts of the northeastern Angitis basin were mapped at 1:6000 on stereographic air photos. In addition, short segments of the detachment and adjacent rocks were examined in reconnaissance fashion at the base of the Serres and Siderokastro syndetachment basin lobes, south and north of Mt. Vrondou, respectively, to verify the continuity of the detachment north of the study area. Footwall rocks at structural levels considerably deeper than the Strymon Valley detachment were mapped in small areas north and east of the Vrondou pluton and at the northeast margin of the Drama basin. Limited observations of crystalline hanging-wall rocks belonging to the Serbo-Macedonian province were made at the southwest margin of Mt. Pangaion and in the Kerkini Range, which bounds the modern Strymon basin to the north. The results of this mapping (1) establish the existence,

kinematic character, and regional significance of the Strymon Valley detachment as a Neogene low-angle normal fault, (2) identify the southwestern Rhodope province, roughly coincident with the outcrop area of the Falakron marble series, as a metamorphic core complex that emerged from beneath Serbo-Macedonia in the footwall of the Strymon Valley detachment, (3) imply that the present geologic character of the Rhodope metamorphic core complex may be understood as the result of four successive Cenozoic deformational events, and (4) identify the Neogene Siderokastro, Serres, Angitis, Akropotamos, and South Symvolon "basins" as lobes of a syndetachment basin complex that predates and is structurally unrelated to the modern Strymon and Drama basins.

Strymon Valley detachment

The southwest margin of the Rhodope metamorphic province is a southwest-dipping low-angle normal fault, the Strymon Valley detachment, which persists for more than 200 km in a northwest-striking outcrop zone as wide as 25 km northeast of the Struma/Strymon River and on the island of Thasos (Dinter and Royden, 1993). The crystalline portion of the hanging wall, the Serbo-Macedonian gneiss complex, lies mainly southwest of the Strymon River. Strongly deformed syndetachment basin deposits overlie the detachment along most of its exposed length and are observed to be rotated and truncated from below by the detachment over its entire down-dip width, providing a minimum estimate of 25 km of displacement on the main detachment in northern Greece.

Although the regional dip of the Strymon Valley detachment is gently southwestward, southwest-dipping detachment outcrops are rarely observed in the field because the fault surface is strongly corrugated about an axis that plunges gently to the southwest. The largest corrugations, with 10 - 35 km wavelengths and amplitudes as great as 1 km control the gross regional structural geometry and strongly influence modern

topography. Ridges in the fault surface correspond to northeast-elongate domal exposures of footwall rocks that appear in map view as a series of southwest-facing scallops at the southwest margin of the Rhodope metamorphic province (Fig. 3). Intervening depressions are occupied by strongly tectonized, southwest-thickening lobes of the syndetachment basin complex that were transported to their present positions in the hanging wall of the detachment system. Smaller scale corrugations of the detachment are also characteristic, ranging from undulations with 50 - 300 m wavelengths and 10 - 50 m amplitudes superimposed on the limbs of the principal corrugations, to outcrop-scale fluting with 1 - 5 m wavelengths and 0.2 - 1.0 m amplitudes. The regional corrugation axis is consistent in orientation with outcrop-scale fluting axes, plunging roughly 3° to S53°W. There is no evidence to suggest that corrugations at any scale are folds. They appear rather to be primary "fault mullions" or cylindrical undulations of the detachment surface (cf. John, 1987). Locations of major ridges and depressions in the detachment may be related to contrasting material properties in the footwall. The Vrondou and Symvolon granodiorite plutons correspond to prominent footwall domes, whereas Falakron marble or gneiss lithologies tend to underlie major depressions (Fig. 3).

Strymon Valley detachment exposures are of two general types, the type developed in any given area being primarily dependent on the nature of the overlying hanging-wall material. Discrete, well-polished detachment surfaces, typically streaked with chloritic microbreccia parallel to the slip direction, occur where the hanging wall consists of poorly consolidated syndetachment clastic deposits. By contrast, breccia zones as thick as 40 - 50 m occur where the hanging-wall material is limestone or crystalline metamorphic rock.

Discrete detachment surfaces

Along most of its sinuous outcrop length the Strymon Valley detachment coincides with the top of the Falakron marble series. Tertiary granodiorite is the dominant footwall lithology beneath Mts. Vrondou and Symvolon, but even in those areas a highly tectonized marble carapace up to several meters thick is commonly observed immediately beneath the detachment surface. Cross-sectional exposures of discrete detachment planes on marble or granite preserve 2 - 5 cm, rarely as much as one meter, of polished, resistant, dark brown chloritic microbreccia, which contains angular fragments up to 5 mm in diameter of the underlying footwall material. Flat-iron exposures typically preserve only a few mm of this microbreccia arrayed in diffuse streaks that trend within a few degrees of S53°W, subparallel to outcrop-scale fluting of the detachment. Rare slickenside grooves have similar orientations. Marble weathers faintly pink for several cm immediately below the microbreccia layer; granitic rocks weather to a rust color.

Where the footwall beneath poorly consolidated clastic hanging-wall deposits is marble, the detachment plane locally bears small duplex structures consisting of marble slivers 1 - 4 cm thick thrust successively into a nested stack 5 - 15 cm high and 1 - 2 m wide. The duplexes uniformly verge to the southwest and typically terminate at a roughly lunate, southwest-facing fracture that may have an accumulation of chloritic microbreccia at its base, in the structural shadow of the stacked slivers (Fig. 5). The vergence of these structures, combined with the regional consistency in orientation of corrugation axes, microbreccia streaks, and slickensides, provide conclusive evidence that the hanging wall of the Strymon Valley detachment moved in a S53°W direction with respect to the footwall.

The main detachment is commonly overlain by a white-weathering, calcareous, fine-grained, moderately consolidated cataclasite layer 1 - 5 m thick. In most exposures

this material is unfoliated and contains 5 - 30% angular to subrounded fragments derived from both footwall and hanging-wall rocks dispersed with random orientations in the white, fine-grained matrix. Marble and gneissic quartz augen are common footwall-derived clasts; weathered, foliated granite or gneiss cobbles and sheared, angular clasts of dark gray laminated mudstone represent the hanging wall. The matrix consists of 50 - 90% cryptocrystalline calcite, locally recrystallized, presumably derived from marble in the footwall, and up to 50% angular to subrounded feldspar and quartz grains ≤ 1 mm in diameter. Minor constituents include up to 3% coarse, detrital muscovite, typically crimped and folded on a microscopic scale, 1% fine- to medium-grained biotite, and 1% subhedral red garnet ≤ 0.5 mm in diameter. The muscovite, which occurs in flakes as large as 1 cm in diameter, appears to be derived from cobbles of pegmatite and two-mica gneiss that appear in basal conglomerates of the supradetachment basin complex. Cretaceous to Eocene $^{40}Ar/^{39}Ar$ dates obtained from the muscovites (Dinter, in prep.) are considerably older than radiometric dates obtained from crystalline rocks anywhere in the in the Rhodope core complex, suggesting that the hanging-wall conglomerates are not locally derived.

Weak foliations present locally in the cataclasite are defined by an alignment of detrital muscovite and biotite grains and, in some places, by recrystallized calcite. Such foliations typically dip gently northeast and intersect the southwest-dipping detachment at a low angle, defining an outcrop-scale shear fabric that resembles a top-to-the-SW mylonitic S-C fabric. If the sense-of-shear implications of the two fabrics are similar, then the orientations of the cataclasite foliations provide additional evidence that the hanging wall of the detachment system moved southwest with respect to its footwall.

The cataclasite layer is commonly overlain by up to 5 m of highly sheared, laminated, gray mudstone, siltstone, and lignite mottled with pods of the cataclasite, and also containing small shear-bounded lenses of strongly weathered, highly fractured,

sandstone and conglomerate. Anastamosing shears both subparallel to and discordant with the main detachment are pervasive in this interval, which appears to serve with the underlying cataclasite as a basal accommodation zone for bookshelf-style block rotations of hanging-wall strata. Intermittent zones of intense shearing and brecciation, typically localized in fine-grained clastic beds, persist for up to ~100 m above the main detachment.

Immediately beneath the main detachment, marble is commonly highly fractured within an allochthonous slab as thick as 10 m bounded below by a microbrecciated intrafootwall detachment, and granite and gneiss are divided by anastamosing, microbrecciated shear surfaces into axe-blade shaped lenses 2 - 3 m wide and up to 1 m thick, elongate in the direction of detachment displacement. Angular blocks of marble, gneiss, or granite up to 10 m thick that were probably incised from this zone occur sporadically at the base of the hanging wall.

Diffuse low-angle fault zones

Where the hanging wall consists of well-consolidated marl, algal limestone, or marble breccia, a distinct detachment surface is rarely developed. Rather, shear strain is distributed in a breccia zone as thick as 40 - 50 m containing angular hanging-wall and footwall clasts ranging from boulder-size down to fine grit. The lower third of a typical breccia zone contains clasts derived primarily from the footwall, the upper third is dominated by hanging-wall clasts, and the central section contains a mixture of clasts from above and below. Where the hanging-wall material is limestone, the portion of the breccia zone dominated by limestone clasts weathers deep tuscan red. Matrix material in diffuse shear zones is gritty, angular, poorly-sorted sand derived at least in part by tectonic abrasion of larger clasts. Such zones are plausible sources of nearly monolithologic landslide and debris flow breccias that occur intermittently in the supradetachment basin.

Timing and rate constraints

The Strymon Valley detachment truncates the early Miocene Symvolon pluton at its southwestern margin and is itself displaced by normal faults bounding the Strymon and Drama basins, the age of which is presently constrained only by the minimum age of rodent fossils in the Serres basin, estimated as ~3.5 Ma by Armour-Brown et al. (1979). This value also provides the best available upper limit on Strymon Valley detachment activity. The oldest known syndetachment deposits are at most 18 Ma in age (see above).

K-Ar biotite dates of 13.8 ± 0.2 Ma and 15.0 ± 0.3 Ma from the Mesolakkia pluton, which intrudes the Falakron series beneath Mt. Pangaion (Harre et al., 1968), and 15.5 ± 0.5 Ma and 17.8 ± 0.8 Ma from the Symvolon pluton (Kokkinakis, 1980c) were interpreted by Dinter and Royden (1993) as cooling ages related to the unroofing of the Rhdope core complex in the footwall of the Strymon Valley detachment. New $^{40}Ar/^{39}Ar$ biotite dates from the central part of the Symvolon pluton ranging from 12.8 ± 0.3 Ma to 15.5 ± 0.3 Ma and K-feldspar dates from 13.4 ± 0.3 Ma to 15.0 ± 0.1 Ma are consistent with this interpretation, implying that the pluton cooled below ~150°C - 300°C during a post-intrusive cooling episode that began no later than ~15.5 Ma (Chap. 3).

These ages weakly define a trend of more youthful cooling to the southwest over an approximate 12-km down-dip cross section of the Strymon Valley footwall. Assuming *a priori* that this cooling gradient is linearly related to the progressive unroofing of more southwesterly segments of the core complex from beneath Serbo-Macedonia, an estimate of ~6.0 mm/yr may be calculated for the average middle Miocene horizontal displacement rate on the Strymon Valley detachment, using a biotite date of 15.4 Ma for sample M90-K5 at the northeast margin of the study area and an average value of 13.4 Ma representing a

group of samples collected ~12 km to the southwest in the line of displacement (Fig. 6). An independent estimate of the average horizontal displacement rate may be calculated by dividing the width of the core complex in any displacement-parallel cross section by the total duration of detachment activity, ~12.0 - 14.5 m.y. At the latitude of the Symvolon pluton the core complex is ~80 km wide, corresponding to displacement rates in the range 5.5 - 6.7 mm/yr, which compare favorably with the value provided by the cooling ages.

Rhodope metamorphic core complex

Ductile deformation (events D_1 - D_{3a})

During the 1960's, members of the German "Clausthal group" measured thousands of metamorphic foliations, mineral lineations, and minor fold axes in the Falakron marble series in northeastern Greece (Jordan, 1969; Meyer, 1969; Kronberg, 1969; Birk et al., 1970). Similar measurements from the Symvolon granodiorite pluton are reported in Kokkinakis (1980a). These studies demonstrated that lineations and minor fold axes are remarkably uniform in morphology and orientation throughout the Rhodope metamorphic core complex, typically plunging 0° - 25° northeast or southwest. Northeasterly plunges commonest, varying in trend from about N35°-55°E, but clustering strongly in the range N40°-50°E (Meyer, 1969; Kokkinakis, 1980a). Kronberg (1969) interpreted outcrop-scale folds and lineations in the Falakron series as products of intralimb shear on km-scale, upright, northeast-trending folds – defined by metamorphic foliations rather than bedding – that appear to dominate the regional structure. All such ductile structural elements in the southwestern Rhodope province were thought to have formed during a single Alpine convergent event (e.g., Meyer, 1969). The Symvolon pluton was considered syntectonic to this Alpine deformation it appeared to share the regional shear fabric and the Xanthi pluton was interpreted as post-tectonic because its margins cut this fabric (Meyer, 1968).

The uniformity of mineral-lineation and minor fold-axis orientations in the Falakron marble series is misleading. Geologic relationships in the Mt. Vrondou and Mt. Symvolon regions demonstrate that gently plunging, northeast-trending folds and lineations within the Rhodope metamorphic core complex represent three distinct episodes of ductile shear. The Vrondou pluton was emplaced ~31 - 33 Ma (see above). Its undeformed eastern margin cuts northeast-trending folds and lineations in the Falakron marble series that must, therefore, predate the emplacement of the pluton. By contrast, its western margin is strongly imprinted by northeast-trending folds and mylonitic stretching lineations. The shearing event that produced these later structural elements appears to have been associated with minor renewed magmatism (Kolocotroni and Dixon, 1991), but clearly postdates the emplacement of the main body of the pluton. The pre-Vrondou ductile shearing of the Falakron series corresponds to the Alpine convergent episode recognized by earlier workers (e.g., Jordan, 1969; Kronberg, 1969; Meyer, 1969) and is designated here as deformational event D_1. The post-emplacement mylonitization of the western Vrondou pluton and related deformation at the southwestern margin of the Rhodope province occurred within the Strymon Valley detachment zone (Dinter and Royden, 1993).

Yet another ductile-fabric-forming event intervened between the mid-Oligocene emplacement of the Vrondou pluton and the middle Miocene initiation of the Strymon Valley detachment system: The Symvolon pluton appears to have been emplaced in early Miocene time *within* a northeast-dipping coaxial shear zone. Its interior and all of its margins are strongly mylonitized and bear uniformly northeast-plunging stretching lineations (Fig. 6; Kokkinakis, 1980a). Contacts with Falakron-series country rocks are zones of concentrated ductile shear up to 100 m wide within which mylonitic granitoid, marble, and calc-silicate schist layers and sheets ranging from 20 m down to a few mm in thickness are pervasively interlaminated. These structural elements are cut by Strymon

Valley mylonitic fabrics and by the detachment itself at the southwest margin of the pluton. The northeast-dipping "Symvolon shear zone" is therefore ascribed to a D_2 deformational event in the southern Rhodope province, and the Strymon Valley detachment system defines event D_3. Gently plunging, northeast-trending minor folds and stretching lineations that originated during these successive events are commonly so similar in morphology and orientation that their tectonic affinities are difficult to determine in many cases. Nonetheless, discriminating D_1, D_2, and D_3 structural elements on a regional basis is a crucial factor in resolving the tectonic evolution of the Rhodope core complex.

Falakron marble series

Ductile structural elements measured in marbles of the Falakron series include metamorphic foliations, mineral lineations, minor tight to isoclinal fold axes, and tectonic joints. Foliations are defined by grain size contrasts, color banding, or the alignment of flattened calcite crystals in pure marble, and by compositional banding in impure marble. Lineations coincide with very low-angle intersections of isoclinally folded, coarse-grained marble foliations with axial planar foliations to those folds. The coarse calcite grains that define these intersection lineations are strongly elongated parallel to them, and so also represent mineral stretching lineations. Tectonic joints in the Falakron marble are rough to smooth disjunctive solution surfaces, commonly mineralized with aragonite.

Foliations, stretching lineations, and minor folds in Falakron marbles are confidently attributed to D_1 deformation where they are cut by undeformed intrusive margins of mid-Oligocene plutons, as at Xanthi and eastern Mt. Vrondou, and in areas distant from the influence of the D_2 and D_3 shear zones, including most of the region north and east of the Drama basin, where the structural thickness of the Falakron series reaches 5000 - 7000 m (Fig. 3; Jordan, 1969; Kronberg, 1969). In general, D_1 stretching

lineations and fold axes in the Falakron and Lekanis Mountains and eastern Mt. Pangaion trend N35°-45°E and plunge gently northeast (Birk, 1970; Jordan, 1969; Kronberg, 1969; Kronberg et al., 1970; Meyer and Pilger, 1963; Meyer, 1969). Southwesterly plunges typical of L_1 lineations at the eastern margin of the Drama basin (Fig. 7) may record Quaternary tilting above an active northeast-dipping detachment (see below).

D_2 and D_3 structural elements appear to be strongly developed only southwest of the Drama basin, where the Falakron series is only 200 - 500 m thick (Kronberg, 1969; de Boer, 1970; Schenk, 1970). Foliations and stretching lineations in the Vrondou, Menoikion, west Pangaion, and Symvolon areas, all of which lie along the southwest margin of the Rhodope core complex, appear in Kolocotroni and Dixon (1991), de Boer (1970), Schenk (1970), and Kokkinakis (1980a), respectively. Data measured in this study in the Menoikion Mountains and southwest Mt. Pangaion are found in Chapter 4. Foliations in these areas commonly strike northeast and dip at low to moderate angles. Stretching lineations vary in trend from N45°-65°E, but cluster strongly in the range N50° - 60°E, typically plunging gently southwest beneath the Strymon Valley detachment, where they appear to represent ductile D_3 shearing, and gently to moderately northeast elsewhere. Northeast-plunging stretching lineations and minor folds are clearly D_2 elements in the Symvolon pluton and on the southeast flank of Mt. Pangaion, but may represent a mixture of D_1 and D_2 features in other areas. An average 10° - 15° difference in trend between L_1 and later stretching lineations is probably diagnostic of slightly differing shear azimuths during convergent D_1 deformation and the later events. A general association of northeasterly fold-axis and lineation plunges with events D_1 and D_2, and of southwesterly plunges with event D_3 appears to be valid regionally and is consistent with the inferred orientations of the Nestos, Symvolon, and Strymon Valley shear zones, respectively.

Closed or "fused" tensional cracks commonly define eroded grooves subperpendicular to calcite stretching lineations on metamorphic foliation planes. Locally, two generations of tensional cracks are discernible. In the Menoikion Mtns. the younger set is associated with ~S53°W-trending lineations, presumed to represent Strymon Valley detachment deformation, and the older set with ~S35°W-trending lineations, inferred to be products of D_1 shear. Where the third dimension is visible, such cracks are observed to dip steeply toward the inferred direction of upper plate transport, top-to-the-southwest for both D_1 and D_3. In some places the cracks offset metamorphic foliations a few mm in a normal sense, down-to-the-southwest for both D_1 and D_3 deformation.

Foliations defined by the alignment of either mica or augen in Falakron-series gneisses most commonly dip northeast, (Chapter 4; additional data in de Boer, 1970). The age of the gneiss foliations is unknown and may vary from place to place; however, their apparent uniformity in orientation over large areas may indicate a common D_1 origin, because only D_1 deformation is pervasive in the core complex.

Symvolon pluton

The Symvolon or "Kavala" granodiorite intruded Falakron marbles at the southwest margin of the Rhodope core complex ~21 - 22 Ma (see above). Its interior and margins are uniformly mylonitized, bearing stretching lineations that characteristically plunge gently to moderately northeast. Tails and truncations of K-feldspar phenocrysts and zones of strongly sheared biotite and recrystallized quartz spaced a few mm apart define C-planes in S-C mylonites, and the pronounced elongation and streaking of these elements on C-planes define mineral stretching lineations that have a pasty appearance in the field. C-planes in the central part of the pluton typically dip gently northeast and associated stretching lineations have orientations in the range 10° - 25°, N50°-70°E, with a well-defined mean of

18°, N58°E (Fig. 6). Similar results obtain for the remainder of the pluton (Kokkinakis, 1980a) except in regions immediately underlying the Strymon Valley detachment, where northeast-dipping D_2 mylonitic fabrics appear to be overprinted by southwest-dipping D_3 mylonitic fabrics (Dinter and Royden, 1993).

S-planes in S-C mylonites are defined by the orientations of hornblende and biotite that crystallized in the D_2 shear zone, and by asymmetric, strain-insensitive, recrystallized quartz fabrics (Chap. 3). S-C fabrics in 10 thin sections are equally divided between top-to-the-southwest and top-to-the-northeast shear asymmetries. Field determinations of shear sense in 62 locations show an approximate 5:3 bias toward southwest vergence, which I consider to be statistically insignificant owing to the possibility of mistaking S- and C-foliations in the field (Fig. 6). The nonuniformity of shear-sense indicators in the Symvolon shear zone contrasts markedly with the uniform southwest vergence associated with the Strymon Valley detachment zone (Kolocotroni and Dixon, 1991; Dinter, 1991; Dinter and Royden, 1993) and may indicate a strong component of flattening (pure shear) during the intrusion of the Symvolon pluton.

As noted above, the Falakron series is an order of magnitude thinner at the southwest margin of the Rhodope province than it is to the northeast in the Falakron and Lekanis Mountains. Given the areal coincidence of the attenuated marble section with the Symvolon and Mesolakkia plutons and the strong evidence of congruent, synintrusional stretching and shearing in the plutons and their host rocks, I propose that the Symvolon shear zone represents an extensional space that was created by the stretching, thinning, and near rupturing of the Falakron marble unit in early Miocene time along the southwestern margin of the Rhodope metamorphic core complex.

Detachment-related brittle structures

The Rhodope metamorphic core complex passed upward through the ductile-brittle transition during its tectonic unroofing in the footwall of the Strymon Valley detachment, resulting in the overprinting of early Strymon Valley mylonitic fabrics (D_{3a}) by increasingly brittle structures (D_{3b}). The emergence of the core complex progressed from northeast to southwest such that at any given time, brittle deformation at upper levels of the detachment system proceeded contemporaneously with ductile shear at mid-crustal levels down dip to the southwest. D_{3b} structures within the Strymon Valley footwall include microbrecciated detachment surfaces subparallel to the main detachment and, possibly, northwesterly-trending high-angle normal faults.

Intrafootwall detachments spaced at intervals of 5 - 20 m in the upper 80 - 100 m of the Rhodope core complex are particularly common in marbles, where they dip several degrees more steeply than the main detachment and are truncated by it up-dip. Given the destruction of stratigraphic horizons in the Falakron series, it is difficult to determine whether these detachments omit section. They are assumed to be extensional because of their clear spatial and geometric affinities to the Strymon Valley detachment.

Minor moderate- to high-angle normal faults with offsets of 0.1 - 3.0 cm, spaced at 0.1 - 3.0 m intervals in the Symvolon granodiorite, strike in the range N55°-85°W (Chaper 4). Although these structures are subparallel to normal faults bounding the Strymon and Drama basins, they are not brecciated and so probably represent deeper and, therefore, somewhat older deformation. I tentatively regard these and similar faults in the Falakron series as D_{3b} structures that facilitated the isostatic uplift of emergent sections of the Rhodope core complex relative to yet-to-be-unroofed sections to the southwest.

Pre- and syndetachment hanging-wall deformation

A D_3 syndetachment basin complex, represented in the area of the present study by the Angitis, Akropotamos, and South Symvolon basin lobes, was strongly disrupted by high- and low-angle normal faults as it moved southwestward in the hanging wall of the Strymon Valley detachment. Shear zones in the basin deposits are exposed only in short segments and tend to be localized in mudstone or siltstone beds highly susceptible to weathering, so that their presence must commonly be inferred exclusively from contrasts in lithology and bedding orientation across zones covered by foliage or modern alluvium. White, calcareous cataclasite concentrated above the main detachment is highly mobile, and appears in lenses along shear zones throughout the D_3 basin complex.

Bedding in clastic strata of the northeast Angitis basin characteristically dips 10° - 40° southwest, with a well-defined mean attitude of N38°W, 28°SW. The tilting of these beds was facilitated by northeast-dipping normal faults antithetic to the Strymon Valley detachment (Chapter 4). As these faults locally sole into or are truncated by the main detachment surface, they must be syndetachment structures (D_{3b}). Tilted blocks are internally extended on minor normal faults striking subparallel to their bounding structures and spaced ≤ 2 m apart with offsets ranging up to ~0.5 m. Southwest-dipping shear zones that did not cause significant tilting in the Angitis basin are tentatively interpreted as structures related to the formation of the Strymon and Drama basins. Bedding in the Menoikion carbonate breccia is less regular than in the underlying clastic deposits. Northwest-striking shear zones in this unit are inferred to be syndetachment structures (D_{3b}), because the Menoikion breccia is clearly truncated by the Strymon Valley detachment and is likely, therefore, to have been deformed in its hanging wall (Chapter 4).

Bedding in the Akropotamos and South Symvolon lobes of the supradetachment basin complex typically dips 10° - 45° northeast, with a mean attitude of N50°W, 32°NE, and was tilted northeastward on southwest-dipping normal faults synthetic to the Strymon Valley detachment (Chapter 4). Northeast-*striking* beds are common on the south flank of Mt. Symvolon, where they appear to have been rotated subparallel to the corrugated main detachment in strongly sheared zones at the base of the hanging wall. As in the Angitis basin, shear zones that dip oppositely to the D_{3b} structures responsible for observed bedding inclinations are tentatively regarded as post-detachment structures.

Low-angle shear zones, characteristically microbrecciated and suffused with distorted pods of white cataclasiste, persist over areas as large as several km^2 within the syndetachment basin complex. In many instances these structures are younger than D_{3b} high-angle normal faults and represent splays of the main detachment. They aretypically localized in fissile mudstone and siltstone beds, but also occur as bedding-parallel shears in algal carbonates and evaporites. Elsewhere, the low-angle shear zones are not tectonic faults, but surfaces that facilitated the emplacement of deformed breccia sheets interpreted as landslide deposits (e.g., the Menoikion carbonate breccia). The occurrence of such deposits at numerous stratigraphic levels in the hanging-wall basin complex is indicative of an active tectonic environment during its accumulation.

The crystalline portion of the Strymon Valley hanging wall, the Serbo-Macedonian gneiss complex, was not examined in detail because it rarely crops out northeast of the Strymon River. A small tract of Serbo-Macedonian gneiss exposed immediately above the Strymon Valley detachment at the southwest margin of Mt. Pangaion bears northeast-trending stretching lineations of uncertain tectonic affinity (Schenk, 1970). Steep, mainly southwest-dipping breccia zones observed in Serbo-Macedonian schist and paragneiss west

of the Strymon River possibly represent D_{3b} normal faults; however, their geometric relationship to the underlying Strymon Valley detachment was not observed.

Post-detachment deformation

Northwest-striking, high-angle normal faults that bound the Strymon and Drama basins displace the Strymon Valley detachment by as much as 3.5 km vertically based on the structural depth to the base of syndetachment deposits in the Strymon 1 borehole (Erki et al., 1984). These appear to be among the earliest structures that originated after the cessation of Strymon Valley detachment activity, and are considered to represent the initiation of a D_4 deformational event. D_4 range-front faults are commonly covered by consolidated marble talus breccia; however, rare stream cuts reveal unconsolidated fault zones as wide as 15 m in which breccia blocks up to a meter in diameter are surrounded by sandy, dark-red weathering, porous matrix material.

Subsidence in the Strymon and Drama basins was accompanied by significant uplift of the region between them. The Menoikion carbonate breccia, inferred to have been deposited at or near sea level in Messinian time, now appears at elevations of nearly 1500 m in the footwall of normal faults bounding the southwest margin of the Drama basin. Assuming that all of this uplift occurred after Strymon Valley detachment activity ceased ~3.5 Ma, the average uplift rate since that time is ~0.4 mm/yr. A second sea level datum is provided by undeformed beach deposits that lie at elevations between 290 and 300 m above the village of Galypsos at the southwest margin of Mt. Pangaion. These deposits clearly overlap tilted syndetachment strata and must, therefore, be late Pliocene or younger. Unconsolidated marine sediments that probably represent the same transgression overlie syndetachment deposits at elevations up to about 260 m in much of the area between the Strymon and Drama basins. Given that glacioeustatic variations can only account for sea

levels up to ~60 m higher than at present from late Pliocene through Quaternary time (e.g., Dinter et al., 1990), the Galypsos beach deposits must have been elevated by at least 230 m since their deposition during a late Pliocene or Quaternary high stand.

The Strymon and Drama basins continue as modern depocenters and their northwest-trending bounding faults are locally associated with fault scarps. In several areas, however, the basin boundaries have been modified by younger faults of several orientations considered here to represent late D_4 deformation. Steep faults striking in the range N40°-50°E appear to be mainly dextral(?) strike-slip structures, although they may accommodate some normal displacement as well. Three major faults of this type were recognized in the Strymon Valley area. The "Tower Bluff fault" parallels the North Aegean coastline southeast of Mt. Symvolon, juxtaposing a carbonate conglomerate of unknown age against poorly consolidated syn- and postdetachment sediments. It may be a segment of the regionally developed Kavala-Xanthi-Komotini strike-slip fault (Fig. 3; Lybéris, 1984; Koukouvelas and Doutsos, 1990). The "Achladochorian fault" forms the southeast boundary of the small Achladochorian basin near the Bulgarian border, and juxtaposes the Falakron marble laterally against the strongly sheared northwest margin of the Vrondou pluton. A third fault of this type is identified solely on morphologic grounds. The N50°E-trending Angitis Gorge, which cuts deeply into the Falakron marble between the Strymon and Drama basins, is offset by several right steps of ~100 m. Each such offset is associated with an apparent dextral rhombochasm defined by the gorge walls. On this basis the Angitis River is tentatively inferred to follow the trace of a N50°E-trending dextral strike-slip structure with relatively minor cumulative offset, the "Angitis fault".

Steep, young normal faults striking in the range N75°-85°W and bearing slickenside grooves indicative of nearly pure dip-slip displacement displace the Strymon Valley detachment up to ~50 m, modify the boundaries of the Drama and Strymon basins, and are

commonly associated with dramatic scarps. I propose that such faults are secondary extensional structures in a tectonic regime dominated by dextral shear on the northeast-trending faults described above. Relatively minor, steep faults trending N25°-40°E that appear to offset range-front faults by as much as 10 - 15 m in a normal and/or strike-slip sense may represent splays within this system (e.g., Twiss and Moores, 1992).

Widely developed disjunctive joint surfaces spaced at regular intervals of 0.3 - 3.0 m in the Falakron marble on the south flank of Mt. Menoikion within about 30 m beneath the Strymon Valley detachment tend to be steep, with strikes clustered strongly in the range N15°-45°E (Chapter 4). Gentle corrugations of the joint surfaces about subhorizontal axes are common. In some places two sets of steep joints nearly parallel in strike and intersecting at angles $\leq 20°$ are developed, neither set displacing the other. Metamorphic foliations are not significantly offset by the joints, but display some disjuncture across them owing to the origin of the joints as pressure solution features.

The joints must be middle Miocene or younger, because D_1, D_2, and D_{3a} deformation in the Rhodope core complex occurred within the ductile regime, and the Falakron series presumably did not rise to crustal levels high enough that joints could form and be preserved until it was unroofed in the footwall of the Strymon Valley detachment. Beyond this constraint, however, the relative age of the joints is unclear because cross-cutting relationships with other brittle structures are ambiguous. Disjunctive joints probably coincide with the plane of principal flattening at the time they form (e.g., Twiss and Moores, 1992). I speculate that the joints are late D_4 in origin, because flattening on high-angle planes striking N15°-45°E is dynamically consistent in a tectonic setting dominated by dextral strike-slip displacement on high-angle faults trending ~N50° E.

SYNTHESIS: CENOZOIC DEFORMATION IN THE STRYMON VALLEY REGION

The present juxtaposition of tectonostratigraphic units in the Strymon Valley region may be rationalized as the result of four successive Cenozoic deformational events (Table 1). D_1 deformation produced gently northeast-plunging folds and stretching lineations throughout the Falakron marble series in an Alpine compressional setting. The Vrondou and Xanthi granodiorite plutons, emplaced ~31 - 33 Ma crosscut D_1 structural elements. D_2 - D_4 designate phases in the quasi-continuous Neogene extension of the north Aegean region. D_2 is principally expressed by the ~21 - 22 Ma emplacement of the Symvolon and Mesolakkia plutons in a northeast-dipping extensional rupture, the coaxial Symvolon shear zone. D_3 corresponds to the evolution of the Strymon Valley detachment system from ~16 to 3.5 Ma and the unroofing of the Rhodope core complex in its footwall. D_4 is identified with the late Pliocene(?) - Quaternary subsidence of the Strymon and Drama basins, two modern depocenters whose northwest-striking bounding structures displace the Strymon Valley detachment. A poorly defined system of active faults, possibly forming within a N60°E-trending strike-slip setting, has modified the boundaries of the Strymon and Drama basins and is probably responsible for modern seismicity in the north Aegean region.

D_1: Early Tertiary Alpine convergence

D_1 was the first of three Tertiary deformational periods during which gently plunging, northeast-trending stretching lineations and minor folds formed within the Falakron series. By contrast with the later D_2 and D_{3a} ductile-fabric-forming events, which affected only areas south and west of the Drama Basin, D_1 deformation pervasively and penetratively disrupted the entire exposure area of the Falakron series, destroying all but crude compositional expressions of stratigraphic layering. Open folds with 10- to 20-km wavelengths and gently-plunging, northeast-trending axes persisting for up to 70 km,

modified in some places by northwest-trending folds, were defined by earlier workers as the major structures associated with D_1 deformation (Jordan, 1969; Kronberg, 1969; Meyer, 1969; Schenk, 1970; de Boer, 1970). A major, northeast-plunging D_1 anticline expressed by metamorphic foliations in the Falakron marble at the northeastern margin of the Rhodope metamorphic core complex is truncated by the intrusive margin of the ~31 - 33 Ma Xanthi pluton east of the Nestos River (Kronberg and Eltgen, 1973). The tectonic affinities of similar folds in the southwestern part of the core complex are more difficult to establish because of the congruency of D_1, D_2 and D_{3a} defomation there.

Important minor structures and fabrics associated with D_1 deformation in the Falakron series include uniformly northeast-trending, gently plunging, calcite stretching lineations and outcrop-scale folds. A northeast-plunging axis of D_1 shear transport is indicated by the orientation of L_1 stretching lineations. Major and minor F_1 fold axes are oriented subparallel to the direction of shear transport, which, by analogy with other regions displaying this attribute, implies that the Falakron marble accommodated very large magnitudes of ductile shear strain during D_1 deformation (e.g., Hansen, 1971). A comparison of fabric elements proximal to and well beneath the Strymon Valley detachment suggests that there may be a systematic difference in average trend of ~10° - 15° between L_1 and later stretching lineations, with L_1 lineations clustering principally in the range N35°-50°E, and L_2 and L_{3a} lineations in the range N45°-65°E. Steep, closed, extensional fractures subperpendicular to L_1 lineations commonly offset S_1 foliations a few mm down-to-the-SW, and are interpreted as evidence of a top-to-the-SW sense of D_1 shear.

Given the paucity of stratigraphic horizons in the Falakron series, it is difficult to ascertain whether D_1 shear accommodated contraction or extension solely on the basis of structural relationships *within* the Rhodope core complex. The gross tectonic significance of the D_1 event becomes clear, however, when the Serbo-Macedonian gneiss complex is

restored to its pre-D_3 position overlying the Falakron marble. Middle - upper amphibolite-facies conditions persisted in eastern Serbo-Macedonia until at least early Eocene time based on hornblende K-Ar ages (Harre et al., 1968), whereas metamorphic assemblages in the underlying Falakron marble are uniformly upper greenschist-facies. The contrast in metamorphic grade across a sheared contact, with higher grade rocks lying *above* the shear zone, implies strongly that the two units were originally juxtaposed by thrusting. On this basis, the D_1 deformational event is identified with the underthrusting of the Falakron marble series beneath the Serbo-Macedonian and West Thracian gneiss complexes.

Assuming that Serbo-Macedonian rocks residing at amphibolite-facies conditions cooled fairly rapidly upon being underplated by relatively cold Falakron marbles, early Eocene K-Ar cooling ages of Serbo-Macedonian minerals with moderately high closure temperatures (e.g., hornblende, ~500°C) are unlikely to greatly postdate the underplating event, although they might significantly predate it. On this basis, D_1 convergence probably began in early Eocene time and, based on crosscutting relationships with the Xanthi and Vrondou plutons, ended no later than 31 Ma. Regional evidence that provides further constraints on the age and tectonic significance of D_1 deformation is discussed below.

Mid-Oligocene magmatism

The Vrondou pluton provides a crucial chronological datum in the evolution of the Rhodope metamorphic core complex because its emplacement postdates D_1 compressional deformation and predates D_2 and D_{3a} extensional deformation. Its northern and eastern boundaries are relatively undeformed intrusive contacts that cut D_1 structures in Falakron-series marble and gneiss. Along its southern margin, the Vrondou pluton has been strongly mylonitized in a gently southwest-dipping shear zone. Kolocotroni and Dixon (1991) argue that the mylonitization was synintrusional because the mylonites are intruded

by "later melts" that are also somewhat mylonitized. An alternative interpretation, that the mylonitization occurred within the Strymon Valley detachment zone some 15 to 18 m.y. after the pluton was emplaced, and that the "later melts" represent synextensional magmatism unrelated to the original emplacement episode, is preferred here because the Vrondou mylonites (1) are restricted principally to the southwest margin of the pluton, underlying the Strymon Valley detachment, and (2) bear gently southwest-plunging stretching lineations subparallel to the transport direction on the Strymon Valley detachment and S-C fabrics indicative of top-to-the-southwest shear. The age of the "later melts" is crucial to resolving this issue; unfortunately, these materials have not yet been dated.

The Vrondou pluton, composed predominantly of granodiorite and quartz monzonite, was emplaced within the Falakron series ~31 - 33 Ma based on K-Ar hornblende ages (Marakis, 1969) and on compositional and structural analogies with the well-dated Xanthi pluton (Liati, 1986). Granitoids of similar composition and age to the Vrondou and Xanthi plutons in northeastern Greece include the Elaion pluton in the Menoikion Mts. (de Boer, 1970), the Granitis, Krinides, and Potami bodies in the Falakron Mts. (Meyer, 1968), and several intrusives in eastern Thrace (Del Moro et al., 1988). These intrusives define a belt of granodioritic magmatism up to 35 km wide that trends ~N80°W for > 200 km across the southern Rhodope province (Fig. 2). The trend of this belt is probably related to the geometry of mid-Oligocene subduction of the African plate beneath southern Greece and Anatolia.

D_2: Early Miocene extension and intrusion (Symvolon shear zone)

Pervasive mylonitization of the Symvolon pluton and the correlative Mesolakkia pluton underlying Mt. Pangaion to the north, concordant and coeval mylonitization of adjacent Falakron-series host rocks, and the absence of contact aureoles suggest strongly

that these plutons were emplaced in a ductile shear zone. Uniform northeast plunges of stretching lineations and minor folds, northwest-trending boudinage of aplite dikes (Kokkinakis, 1980a), and the gross northeast-plunging dome structure of the pluton imply, in the absence of evidence that these structures have been significantly rotated, that the "Symvolon shear zone" dipped gently to moderately northeast, oppositely to the later Strymon Valley detachment zone. The *sense* of shear in the Symvolon shear zone is indeterminate based on presently available fabric data, with asymmetric S-C mylonite fabrics observed in thin sections about equally divided between northeast and southwest vergence, possibly indicative of significant flattening subparallel to C-planes during shearing (i.e., coaxial shear). Field measurements of such fabrics, considered generally less reliable owing to the possibility of mistaking S- and C-foliations in relatively fine-grained rocks, show a statistically insignificant bias toward southwest-vergent shear. The Falakron series is only 200 - 500 m thick at the southwestern margin of the Rhodope core complex, but exceeds 5000 m in thickness north and east of the Drama Basin. I propose that the Symvolon shear zone represents an early Miocene extensional rupture of the Falakron series within which the Symvolon and Mesolakkia plutons were intruded.

The Symvolon shear zone was definitely active ~21 - 22 Ma during the emplacement of the Symvolon pluton, and became inactive no later than 15.5 Ma, when it was transected at the southwest margin of the Rhodope core complex by the nascent Strymon Valley detachment system. N50°-70°E-trending fabrics and structures associated with the Symvolon shear zone are evident thoughout Mt. Symvolon and along the southeastern flank of Mt. Pangaion, where they are distinguishable from younger, similarly oriented D_3 structural elements, even in the absence of cross-cutting relationships, owing to their intimate association with syntectonic intrusive material. It is not clear how far north of Mt. Pangaion the effects of the coaxial Symvolon shear zone persist because of the paucity

of syntectonic magmatites north of the Angitis River. The marked westward thinning of the Falakron series, however, is evident at least as far north as the Bulgarian border.

D_3: Middle Miocene - early Pliocene extension (Strymon Valley detachment system)

The Symvolon shear zone was succeeded in middle Miocene time by the Strymon Valley detachment system, which comprises a regionally southwest-dipping low-angle normal fault and related structures in its footwall and hanging wall. The main detachment defines the southwestern margin of the Rhodope metamorphic core complex for > 200 km along strike, and is strongly corrugated – not folded – about an axis plunging 3°, S53°W, with wavelengths ranging from ~35 km down to a few m. Sense-of-shear indicators preserved on the detachment plane imply that the hanging wall, including Serbo-Macedonian metamorphic rocks and a deformed, Neogene syndetachment basin complex, moved in a southwesterly direction with respect to the footwall. The down-dip width over which syndetachment deposits are truncated by the detachment provides a minimum displacement estimate of 25 km. If the Falakron marble unit was unexposed prior to its unroofing in the footwall of the Strymon Valley detachment, then its exposed width at the Aegean coastline provides an independent minimum displacement estimate of ~80 km.

The duration of activity on the Strymon Valley detachment system, constrained by fossils contained in supradetachment basinal deposits and by K-Ar and $^{40}Ar/^{39}Ar$ biotite and K-feldspar dates from the Symvolon pluton, is ~12.5 m.y., from ~16 Ma to 3.5 Ma. The average horizontal displacement rate on the Strymon Valley detachment at the latitude of the Symvolon pluton is estimated at 5.5 - 6.7 mm/yr.

D_{3a}: Ductile deformation

The Strymon Valley detachment coincides approximately with the top of the Falakron marble series and may represent a reactivation of the Nestos thrust as a low-angle normal fault. General criteria were proposed above for distinguishing D_1, D_2, and D_{3a} ductile shear elements based on a 10° - 15° difference in the azimuth of shear transport direction between D_1 and the later events, and on the observation that D_2 and D_3 fabrics are strongly developed only in the southwestern part of the core complex, whereas D_1 features are pervasive. Distinguishing D_2 from D_{3a} shear elements is more difficult because stretching lineations associated with both events trend N45°-65°E. On a regional basis, northeast-plunging stretching lineations and minor folds within and adjacent to the Symvolon and Mesolakkia plutons are identified with the D_2 event, and mylonitic fabrics in marbles or granitoids are confidently interpreted as D_{3a} features only where they uniformly plunge southwestward and lie within a few meters beneath the Strymon Valley detachment.

D_{3b}: Brittle deformation

Gently southwest-dipping, microbrecciated, intrafootwall detachments disrupt the Falakron marble within ~100 m beneath the main detachment. As many as three such surfaces in a vertical section divide the marble into tabular masses 5 - 20 m thick. They are usually subparallel to foliations in the adjacent marble, and must have developed earlier than the main detachment because they are commonly truncated by it up dip at very low angles. These intrafootwall detachments are regarded as D_{3b} structures because of their unambiguous spatial affinity to the main detachment.

Brittle shear elements developed on the Strymon Valley detachment surface include primary corrugations, microbreccia streaks, and sparse slickenside grooves, all of which

define an average displacement direction of 3°, S53°W. Small duplexes composed of marble slivers a few cm thick are uniformly southwest-vergent, indicating a top-to-the-southwest sense of shear on the detachment system. Immediately below the main detachment, marble is typically fractured to varying degrees in a zone 2 - 10 m thick bounded below by an intrafootwall detachment, and granite is broken into lenses 2 - 3 m wide, ≤ 1 m thick, bounded by anastamosing shear surfaces subparallel to the main detachment. Immediately above the main detachment, syndetachment clastic deposits and footwall marbles are ground to a white, calcareous cataclasite that forms a layer 2 - 5 m thick, overlain by several m of highly brecciated sediment. Shear deformation at the base of the hanging wall is concentrated in weakly consolidated siltstone and cohesive mudstone layers. Bedding in a strongly sheared zone as thick as 30 m at the base of the hanging wall is commonly, though not uniformly, rotated into subparallelism with the detachment plane.

N55°-85°W-striking, predominantly southwest-dipping normal faults with offsets of 0.1 - 3.0 cm, spaced at 0.1 - 3.0 m intervals, are widely developed in the Symvolon pluton. These and similar faults in the Falakron series are tentatively interpreted as structures that accommodated the isostatic uplift of the Rhodope core complex as it was unroofed in the footwall of the Strymon Valley detachment. Narrow, consolidated breccia zones with similar orientations may also be components of this distributed shear system.

The Struma basin in western Bulgaria, the Siderokastro, Serres, Angitis, Akropotamos, and South Symvolon basins at the northeastern margin of the Strymon Valley, and the mostly offshore Prinos - Kavala basin are lobes of a syndetachment basin complex that straddled the trailing edge of the hanging wall in the Strymon Valley detachment system. Both high- and low-angle normal faults deformed the accumulating basin strata as they were transported southwestward over the emerging Rhodope core complex. Poorly exposed N20°-70°W-striking normal faults sole into or are truncated by

the main detachment. In the northeastern Angitis basin such faults dip northeast, antithetic to the main detachment, and affected beds dip to the southwest. In the Akropotamos and South Symvolon basins, these faults dip predominantly southwest and bedding dips northeast. Angular unconformities within the basin section indicate that deformation proceeded concurrently with deposition. Low-angle normal faults, typically localized in fine-grained sediments, are also common within syndetachment basinal deposits, and many represent splays of the main detachment. In some places these intrahanging-wall detachments truncate the steep, northwest-striking normal faults.

D_{3b} structures in the eastern Serbo-Macedonian metamorphic province, which constitutes the crystalline portion of the hanging wall in the Strymon Valley detachment system, were not mapped in this study. However, reconnaissance observations in quarry exposures of Serbo-Macedonian rocks in the Kerkini Mtns. at the northern boundary of the Strymon basin reveal a population of steep, N15°-55°W-striking, southwest-dipping faults that may be D_{3b} structures similar to those in the supradetachment basin complex.

D_4: Late Pliocene - Quaternary extension (Strymon and Drama Basins)

The Strymon Valley detachment and the supradetachment basin complex are displaced up to 3.5 km vertically by northwest-striking, high-angle normal faults that bound the Strymon and Drama basins. A key implication of this relationship is that poorly consolidated sediments in the Strymon Valley region represent two distinct basin systems. Highly tectonized deposits that accrued in the hanging-wall basin complex are presently exposed only as a thin carapace overlying the detachment, but must also be present in thicknesses as great as 2600 m beneath ~1000 m of relatively undeformed fill in the Strymon and Drama basins. The transition from D_3 to D_4 deformation is presently constrained only by the age of the youngest known fossils in the supradetachment basin

complex, ~3.5 Ma (Armour-Brown et al., 1977). An angular(?) unconformity corresponding to this tectonic transition has presumably gone unrecognized in two boreholes in the Strymon basin (e.g., Erki et al., 1984). Subsidence in the Strymon and Drama basins must have been accompanied by as much as 1500 m of uplift in the region between them based on the present elevations of carbonate deposits inferred to have been deposited near sea level during the waning phases of Strymon Valley detachment activity.

The southwest margins of the Strymon and Drama basins are steep contacts between bedrock and modern basin fill, whereas their northeast margins slope more gently toward the basin axes. This asymmetry is suggestive of a half-graben morphology, and is shared by the Vardar-Thermaikos basin west of Thessaloniki (Bornovas and Rondogianni-Tsiambaou, 1983) and by several offshore basins in the north Aegean Sea (e.g., Lybéris, 1984). Dinter and Royden (1993) suggest that these basins may be subsiding above an active northeast-dipping "North Aegean detachment zone" that succeeded the Strymon Valley detachment as the major structure accommodating back-arc extension in the north Aegean region. The North Aegean detachment system is inferred to terminate southward at a N45°E-trending transfer structure, the North Aegean Trough, which represents the offshore continuation of the dextral North Anatolian strike-slip fault (Fig. 2).

Late D_4: Late Quaternary wrenching and extension

Relatively steep faults of at least three general orientations have modified the margins of the Strymon and Drama basins and may also be responsible for modern erosional patterns and seismicity in the Strymon Valley region. High-angle faults striking N40°-50°E, subparallel to the North Aegean Trough, are apparently dextral strike-slip structures, although they may accommodate some normal displacement as well. Steep, young normal faults striking N75°-85°W displace the Strymon Valley detachment as much

as 50 m vertically at the southwest margin of the Drama basin, and relatively minor, steep faults trending N25°-40°E appear to offset range-front faults up to 15 m in a normal and/or strike-slip sense. I propose that the northeast-trending strike-slip faults may be acting as transfer structures within the extending hanging wall of the North Aegean detachment system posited by Dinter and Royden (1993), and that the N75°-85°W-striking normal faults represent secondary extensional structures within this regime of distributed dextral shear. Minor N25°-40°E-striking faults have orientations consistent with an origin as splays or "P-shears" in such a system.

Focal plane mechanisms of large earthquakes in the north Aegean region suggest that major faults similar in orientation and sense of displacement to those described above are seismogenic. Events centered in the North Aegean Trough have yielded dextral strike-slip mechanisms on vertical, northeast-striking planes, and the Thessaloniki (1978) and Volos (1980) earthquakes involved normal slip on high-angle surfaces trending ~N80°W (e.g., Jackson and McKenzie, 1983). A chain of Plio-Quaternary trachyte-rhyolite fissure eruptions that trends N75°W across the northern part of the Greek Serbo-Macedonian province (Panagos et al., 1978) may also coincide with a major zone of secondary normal faulting within an active northeast-trending wrenching regime.

IMPLICATIONS FOR THE ALPINE TECTONIC EVOLUTION OF NORTHEASTERN GREECE

The Serbo-Macedonian and West Thracian gneiss complexes: A proposed correlation

The Falakron marble series emerged to the northeast from beneath the Serbo-Macedonian gneiss complex in the footwall of the Strymon Valley detachment. Upon

restoring the displaced units to their pre-detachment positions, it becomes apparent that prior to ~16 Ma the Serbo-Macedonian and West Thracian gneiss complexes lay in adjacent positions in the Nestos River vicinity, and it is tempting on geometric grounds to suggest that they may be correlative. The lithologic, geochemical, and structural characteristics of the two gneiss complexes are compared briefly below in an effort to determine whether they are sufficiently similar to warrant such a correlation on geologic grounds.

Serbo-Macedonian gneiss complex

The Serbo-Macedonian province is a 30- to 40-km-wide, strongly deformed, high-grade metamorphic complex that strikes ~N45°W from the Chalkidiki Peninsula in northern Greece into eastern rump Yugoslavia and western Bulgaria. It is commonly interpreted as the western margin of the pre-Alpine "Rhodope fragment", which was intermittently underthrust in Jurassic through Eocene time first by oceanic lithosphere and subsequently by the "Apulian continental fragment" at the northeast-dipping Vardar subduction zone. Serbo-Macedonia is considered to owe much of its preserved geologic character to deformation and metamorphism at or within the leading edge of the overriding plate in this subduction system (e.g. Kockel et al., 1977; Jacobshagen et al., 1978; Burchfiel, 1980). Kockel et al. (1971) divide the Greek portion of the Serbo-Macedonian province into two tectonostratigraphic series. The western "Vertiskos" series, composed of amphibolite-facies gneiss and schist and several strongly sheared basic to ultrabasic intrusives, overlies the eastern "Kerdilion" series, dominantly biotite gneisses and migmatitic gneisses intercalated with marbles and minor amphibolites, at a cataclasized, southwest-dipping shear contact of uncertain tectonic significance east of Lake Volvi (Fig. 2; Kockel et al., 1977). The Stratoni granite, which cuts metamorphic fabrics in the Kerdilion series but appears to be truncated by this shear zone (Kockel et al., 1978), yielded a K-Ar biotite age of 29.6±1.4 Ma (Papadakis, 1971).

Gneiss, schist, and amphibolite assigned to the Vertiskos series constitute the bulk of the Serbo-Macedonian gneiss complex in Greece (Kockel et al., 1971). The dominant foliations in this unit dip southwest, and formed during a regional metamorphic event that reached upper amphibolite-facies conditions (Kockel et al., 1977). The southwest-dipping fabrics are cut by northeast-dipping shear zones at the southwestern margin of the Vertiskos series, where it is underthrust by weakly metamorphosed Triassic to Lower Jurassic(?) sediments of the circum-Rhodope belt (Kauffmann et al., 1976). This underplating by relatively cool continental material may be related to the Early to Late Cretaceous cooling of Vertiskos rocks below the Ar closure temperatures of biotite and white micas (about 310° - 420°C; Robbins, 1972; Giletti, 1974; Harrison et al., 1985). K-Ar and $^{40}Ar/^{39}Ar$ dates on biotites and muscovites from the Vertiskos series range from 136.8 ± 1.5 Ma to 87.8 ± 4.2 Ma (Harre et al., 1968; Marakis; 1969; Papadopoulos and Kilias, 1985; De Wet et al., 1989), contrasting strongly with Tertiary cooling ages characteristic of adjacent regions, including the underlying Kerdilion province (Harre et al., 1968). Several basic and ultrabasic bodies crop out within the Vertiskos series at or near its structural base near the eastern margin of Serbo-Macedonia (Kockel et al., 1971). The largest of these, the Volvi complex, is interpreted by Dixon and Dimitriadis (1984) as a Mesozoic intracontinental rift complex. Amphibolites from the northeast margin of the Volvi complex yielded hornblende K-Ar dates in the range 116 - 113 Ma, consistent with cooling ages for the rest of the Vertiskos series (Harre et al., 1968).

The Kerdilion series, which has a structural thickness exceeding 3000 m, consists primarily of high-grade biotite gneiss and plagioclase-microcline gneiss that locally attained conditions of anatexis, but also includes near its top two prominent coarse-grained marble layers, each with a maximum thickness of ~500 m (Kockel et al., 1971; Kockel et al., 1977). The upper layer immediately underlies the shear contact with the overlying

Vertiskos series along much of its length; the lower parallels that contact ~1 km below. Harre et al. (1968) obtained K-Ar dates in the range 36 - 43 Ma on muscovites from migmatitic Kerdilion gneisses, 32 - 38.5 Ma on biotites, and 79.5±1 Ma from a single amphibolitic hornblende analysis. The tract of Kerdilion gneiss that overlies the Strymon Valley detachment surface on the southwest flank of Mt. Pangaion yielded K-Ar dates of 35.0 ± 0.5 Ma and 33.9 ± 0.7 Ma from muscovite and biotite, respectively, and a Rb/Sr biotite model age of 39.3 ± 2.4 Ma (Harre et al., 1968).

West Thracian gneiss complex

The West Thracian gneiss complex overlies the Falakron marble series at the mylonitic, northeast-dipping Nestos thrust zone and is estimated to exceed 3500 m in structural thickness (Kronberg, 1969; Kronberg and Eltgen, 1973; Zachos and Dimadis, 1983; Liati, 1986; Mposkos et al., 1988). It crops out from the Nestos River vicinity northward into Bulgaria and eastward into Turkey. Quartzo-feldspathic and pelitic gneisses, migmatites, amphibolites, and partially amphibolitized eclogites are the primary lithologies, with ultramafic bodies including large tracts of serpentinite becoming increasingly common to the east (Kronberg, 1969; Liati, 1986, 1988; Mposkos, 1989). Approximately 2 - 3 km above the Nestos thrust, migmatitic augen gneiss, amphibolite and minor calc-silicates and mica schists are tectonically intercalated with two marble layers, each up to 500 m thick, that define a gently northeast-plunging anticline (Kronberg, 1969; Kronberg and Eltgen, 1973). The top of the upper marble layer roughly coincides with the base of a strongly cataclasized, northeast-dipping shear zone interpreted by Koukouvelas and Doutsos (1990) and Kotopouli et al. (1991) as an intraformational thrust . In the "Siroko nappe" below this shear zone, metamorphic conditions increase upward from upper greenschist facies near the thrust contact with the Falakron marble to upper amphibolite facies, with local anatexis of paragneisses, < 2 km structurally above

(Kronberg and Raith, 1977; Liati, 1986, 1988; Kotopouli et al., 1991). The "Echinos nappe" above the shear zone is intruded near the Greek-Bulgarian border by the Elataia-Skalote pluton, which is thought to have been derived from the West Thracian gneiss complex by partial melting because the compositions of the two units are similar and the contacts between them are gradational (Kotopouli and Pe-Piper, 1989a). The pluton and the gneiss complex are reported to be unconformably overlain by up to 50 m of conglomerate, sandstone, and lignite-bearing siltstone and 400 m of welded, crystalline tuffs belonging to the Paranestion or Dipotama volcanic sequence (Kotopouli and Pe-Piper, 1991; Baker and Liati, 1991), which has yielded K-Ar dates ranging from 28.7 ± 1.1 Ma to 35.0 ± 1.2 Ma (Eleftheriadis and Lippolt, 1984).

Three successive metamorphic episodes have affected the West Thracian gneiss complex: (1) a high-P event that produced eclogites from tholeiitic basalt protoliths with compositions corresponding to MORB, (2) a regional amphibolite-facies event during which the eclogites were almost completely converted to amphibolites, and gneissic rocks were partially melted to form the Elataia-Skalote pluton, and (3) a retrograde greenschist-facies metamorphism that strongly affected only the lower parts of the gneiss complex (Liati, 1986, 1988; Mposkos, 1987, 1988, 1989, Mposkos and Perdikatsis, 1987; Mposkos et al., 1988; Liati and Mposkos, 1990; Kotopouli and Pe-Piper, 1989b; Koutopouli et al., 1991). Pressures of at least 14 - 15 kbar and temperatures of 550° - 600°C for the eclogite-forming event are indicated by the occurrence of primary rutile and absence of primary titanite (Liati, 1986), by jadeite contents in clinopyroxene, and by the garnet-clinopyroxene geothermometer (Liati and Mposkos, 1990). P-T conditions of 7 - 9 kbar at 550° - 650°C were regionally attained in the gneiss complex during the subsequent amphibolite-facies event, with temperatures locally reaching 728° - 746°C in associated migmatites (Liati, 1986; Koutopouli et al., 1991).

Liati (1986) reports a suite of K-Ar hornblende model ages from completely and partially amphibolitized eclogites within the "Siroko nappe" of the West Thracian gneiss complex north of Xanthi. Seven dates ranging from 37.3 ± 0.6 Ma to 46.9 ± 0.7 Ma yielded by the completely recrystallized samples were interpreted as evidence that the regional amphibolite-facies metamorphism was of Eocene age (Liati, 1986; Koukouvelas and Doutsos, 1990; Kotopouli et al., 1991). However, as K-Ar dates represent *cooling* ages, and temperatures attained during the high-grade event were considerably higher than the ~500°C Ar closure temperature of hornblende (Harrison, 1981), these dates must be considered minimum metamorphic ages. A Rb-Sr whole rock isochron of 87.7 ± 27 Ma (initial $^{87}Sr/^{86}Sr = 0.706 \pm 0.0002$) reported for the Elataia granodiorite by Soldatos (1985) may approximate more closely the time of peak amphibolite-facies metamorphic conditions. Three K-Ar hornblende dates of 57.4 ± 0.6 Ma, 78.9 ± 0.6 Ma, and 95.1 ± 1.1 Ma yielded by partially recrystallized eclogites are considered by Liati (1986) to result from excess Ar. Alternatively, if these dates represent partially reset ages acquired during the initial crystallization of the eclogitic amphiboles, then a minimum Albian - Cenomanian age is indicated for the early high-P metamorphic event.

Correlations and tectonic significance

The Serbo-Macedonian and West Thracian gneiss complexes, which overlie the Falakron marble series at its southwestern and northeastern margins, respectively, are markedly similar in lithology, thickness, tectonic position, deformational style, metamorphic grade, and radiometric age characteristics, and I propose here that they formed a single, continuous tectonostratigraphic unit prior to their separation by Neogene low-angle normal displacement on the Strymon Valley detachment. This correlation has not previously been imagined, because it is generally accepted that the two gneiss complexes were thrust over the marble unit from opposite directions (e.g., Kockel and

Walther, 1965; Koukouvelas and Doutsos, 1990), a view that must be abandoned in light of the reinterpretation of the supposed northeast-vergent "Strymon thrust" as a southwest-vergent low-angle normal fault (Dinter and Royden, 1993).

The "Kerdilion series" and the "Siroko nappe", the structurally lowest tectonostratigraphic subunits in the Serbo-Macedonian and West Thracian gneiss complexes, respectively, lie adjacent to one another when ~80 km of displacement on the Strymon Valley detachment are restored, and they are similar in lithology, thickness, metamorphic grade, and radiometric age characteristics. Distinctive double marble horizons occur near the tops of both units, and both are bounded above by cataclastic shear zones. Based on these similarities, a correlation between the two subunits (and the two shear zones) seems highly probable. Koukouvelas and Doutsos (1990) interpret the shear zone at the top of the "Siroko nappe" as a southwest-vergent thrust that formed during a late brittle stage of the same deformational phase represented by the ductile Nestos thrust. I consider this interpretation to be questionable because (1) there is no obvious repetition of tectonostratigraphic section in the supposed thrust nappes identified in the West Thracian gneiss complex, and (2) the probably correlative shear zone at the top of the Kerdilion series appears to be younger than ~29.6 Ma based on a cross-cutting relationship with the small Stratoni pluton, which may be a member of the mid-Oligocene Vrondou-Xanthi-Thracian plutonic belt, and is thus considerably younger than the Nestos thrust (see below). For these reasons, the tectonic significance of brittle low-angle shear zones within the Serbo-Macedonian and West Thracian gneiss complexes should probably be considered unresolved until more detailed structural data become available.

The composite Serbo-Macedonian-West Thracian gneiss complex, composed of tectonically intercalated metasediments, metabasites, metaeclogites, serpentinites, ophiolitic remnants, and syndeformational intrusives that were first metamorphosed in an extremely

high-P environment and later subjected to regional high-T conditions (Liati, 1986), must surely represent a B-type (oceanic) accretionary subduction complex that was subducted and then transferred, perhaps by underplating, to a position within a thickening orogen at the leading edge of the overriding plate (cf. Platt, 1986). Early Cretaceous K-Ar cooling ages are common in amphibolite-facies rocks of the Serbo-Macedonian Vertiskos series, whereas the oldest such ages known from comparable stratigraphic levels in the West Thracian complex are Cenomanian, which may imply that the unroofing of the marginal orogen progressed from southwest to northeast. I suggest that the Serbo-Macedonian-West Thracian gneiss complex represents, in large part, a pre-Cretaceous subduction complex. It may have formed in connection with the eastward subduction of the Vardar ocean beneath the western margin of the Rhodope province (cf. Jacobshagen et al., 1978; Burchfiel, 1980; Dixon and Dimitriadis, 1984).

The Nestos thrust: Middle-late Eocene continental subduction

The D_1 shear event in the Rhodope metamorphic core complex corresponds to the thrust emplacement of the upper greenschist-facies Falakron marble series beneath the composite upper amphibolite-facies Serbo-Macedonian-West Thracian gneiss complex. The mylonitic, northeast-dipping Nestos shear zone appears to preserve the original deep-level D_1 thrust contact between the Falakron series and the overlying West Thracian gneiss complex in the Nestos River vicinity. The Strymon Valley detachment may represent a reactivation of a segment of the Nestos thrust as a low-angle normal fault during D_3 extension. Northeast-plunging D_1 stretching lineations in the Falakron series and the West Thracian gneiss complex constrain the azimuth of D_1 shear to be in the range N40°-50°E (Meyer, 1969; Kronberg and Eltgen, 1973; Kronberg and Raith, 1977). Koukouvelas and Doutsos (1990) argue that the northeast dip of the Nestos thrust implies southwest vergence, citing minor associated southwest-vergent folds as corroborating evidence.

Asymmetric mylonitic fabrics within the thrust zone indicate a uniform top-to-the-southwest sense of shear (Kilias and Mountrakis, 1990).

Undeformed intrusive boundaries of the Vrondou and Xanthi granodiorite plutons cut D_1 structural elements near the southwest and northeast margins, respectively, of the Rhodope core complex, constraining the D_1 shear event to be pre-mid-Oligocene. Radiometric data from the West Thracian gneiss complex reported in Liati (1986) may provide more precise constraints on the age of the Nestos thrust. K-Ar hornblende dates in the range 45.5 - 46.9 Ma from mafic rocks bearing well-preserved upper amphibolite-facies mineral assemblages within the "Siroko nappe" less than 1 km above the Nestos thrust zone, and somewhat younger dates of 37.3 - 41.4 Ma from similar rocks 1 - 3 km structurally higher in the gneiss complex, were interpreted by Liati (1986), Koukouvelas and Doutsos (1990), and Kotopouli et al. (1991) as peak amphibolite-facies metamorphic ages (see above). I propose instead that these dates record the abrupt cooling of amphibolites near the base of the West Thracian gneiss complex to temperatures below ~500°C as a result of being underthrust beginning ~47 Ma by the Falakron marble series, and that the inverted metamorphic and cooling gradients observed in the "Siroko nappe" immediately above the Nestos thrust (Kronberg and Raith, 1977; Liati, 1986) reflect the thermal equilibration of the West Thracian gneiss complex to this event. I suggest further that the upward-progressive cooling of West Thracian gneisses above the Nestos thrust zone through 37.3 Ma implies continued underthrusting of the Falakron marble series until at least that date, because thermal models of the subduction process show that sustained underthrusting of cool material is required to maintain low-T conditions at depth (e.g., Oxburgh and Turcotte, 1974; Draper and Bone, 1981; England and Thompson, 1984; Rubie, 1984; Peacock, 1987). This interpretation is consistent with K-Ar muscovite ages ranging from 36.8 ± 0.6 Ma to 42.0 ± 1.0 Ma that record the cooling of the Serbo-Macedonian Kerdilion series west of the Strymon River to below ~420°C (Harre et al.,

1968; Robbins, 1972), and also with the presence of relict high-P metamorphic assemblages in the Falakron marble series on the island of Thasos (Atzori et al., 1990).

The Apulian Olympos-Ossa carbonate unit and the Falakron marble series: Another proposed correlation

An intriguing possibility regarding the tectonic affinity of the Falakron marble series arises in considering its thrust emplacement beneath the Serbo-Macedonian-West Thracian gneiss complex in the larger context of the middle to late Eocene structural environment in northern Greece and rump Yugoslavia. A central tectonic element in this region is the Vardar zone, a northwest-trending ophiolitic belt ~60 km wide that separates the Hellenides of western mainland Greece, Albania, Croatia, and Bosnia-Herzogovina from the Serbo-Macedonian province, and is commonly regarded as a suture between the Apulian and Rhodope continental fragments (e.g., Mercier et al., 1975; Jacobshagen et al., 1978; Burchfiel, 1980). The Vardar ocean, which separated these fragments subsequent to the early Mesozoic breakup of western Tethys, was completely consumed by northeast-dipping B-type (oceanic) subduction beneath Serbo-Macedonia by latest Cretaceous time (e.g., Burchfiel, 1980). Continued northeast-southwest convergence after the collision with Apulia was accommodated in part by shortening within the Apulian fragment, but also by A-type (continental) subduction of the eastern Apulian margin to the northeast (Schermer, 1990, 1993; Schermer et al., 1990), presumably beneath Serbo-Macedonia. The Olympos-Ossa unit, comprising more than 4000 m of Triassic to Eocene Apulian platform carbonates exposed beneath the "Olympos thrust" in a window just west of the Vardar suture (Fig. 2; Godfriaux, 1968; Schmitt, 1983), had been subducted by 42 Ma and continued to experience lower blueschist-facies metamorphism as late as 36 Ma based on $^{40}Ar/^{39}Ar$ ages of blueschist-facies minerals (Schermer, 1990; Schermer et al., 1990). Thus, the Olympos-Ossa unit and the Falakron marble series, two carbonate sequences of comparable

thickness, lithology, and metamorphic grade, were simultaneously emplaced by A-type subduction northeastward beneath the Serbo-Macedonian-West Thracian gneiss complex in middle to late Eocene time. I propose on that basis that they are correlative, representing the up- and down-dip segments, respectively, of a previously continuous carbonate slab. If this hypothesis is correct, then the principal tectonostratigraphic unit exposed in the Rhodope metamorphic core complex, the Falakron marble series, is not ancestrally a part of a "Rhodope fragment", but represents, as does the Olympos-Ossa unit, the subducted continental margin of Apulia, and its exposure in the footwall of the Strymon Valley detachment provides a window into the deeper levels of an A-type subduction zone. Moreover, if the Olympos-Ossa and Falakron carbonates are correlative, then the Olympos and Nestos thrusts must also be equivalent, implying that the suture between Apulia and Rhodope is not localized within the Vardar zone, but crops outs over a region as wide as 200 km between Mt. Olympos and western Thrace.

The coaxial Symvolon shear zone: Linked to an early Miocene detachment?

After being subducted to the northeast beneath Serbo-Macedonia from at least 47 to 36 Ma, the Olympos-Ossa carbonate unit reemerged to the southwest from ~23 to 16 Ma in the footwall of a northeast-dipping low-angle normal fault system exposed on the northwest and southeast flanks of Mt. Olympos (the "Lizadiko Ridge" and "Kallipevki" low-angle normal faults; Fig. 2; Schermer, 1990, 1993). Assuming that the Olympos-Ossa and Falakron carbonate units formed a continous slab during middle to late Eocene A-type subduction as suggested above, then the fact that the Nestos thrust was *not* reactivated as a normal fault implies strongly that this slab must have been greatly extended somewhere beneath the Serbo-Macedonian gneiss complex from ~23 to 16 Ma to accommodate the observed normal faulting in the Mt. Olympos area. As determined in this study, the Symvolon pluton was emplaced and mylonitized in a northeast-dipping shear zone of

indeterminate vergence ~21 - 22 Ma at the southwest margin of the Rhodope core complex, where the Falakron series is an order of magnitude thinner than it is to the east. I propose that the early Miocene Symvolon shear zone represents an extensional pull-apart or rupture of the Olympos-Falakron carbonate slab at mid-crustal depths, and that this zone was physically linked to the Mt. Olympos low-angle normal fault system by a northeast-dipping "Olympos-Symvolon detachment" that facilitated the unroofing of the Olympos-Ossa unit by reactivating the segment of the Olympos-Nestos thrust that lay up-dip of the Symvolon pluton as a top-to-the-northeast, extensional detachment. A corollary to this hypothesis is that Olympos-Symvolon detachment may not have penetrated the entire lithosphere; it may have terminated at an extensional rupture within the middle crust (cf. Wernicke, 1985). Alternatively, the Symvolon shear zone may represent a ramp space that facilitated the descent of the Olympos-Symvolon detachment to a deeper structural level.

The Symvolon pluton is not an isolated early Miocene magmatite. It occurs at the northern end of an enormous tract of andesitic volcanics dated at 22.7 - 15.5 Ma that crops out in a northwest-trending belt on numerous northeast Aegean islands and covers much of the northwest corner of Turkey (Fytikas et al., 1984). If this belt coincides with a pull-apart rupture at the down-dip culmination of an early Miocene detachment system as envisioned here, then the up-dip breakaway zone of that detachment system, mapped by Schermer (1989) in the Mt. Olympos vicinity, may persist southeastward for more than 200 km and coincide approximately with the Aegean coast of mainland Greece.

CONCLUDING REMARKS

The Rhodope metamorphic province has previously been regarded as the interior of a Tethyan continental fragment that was deformed in the hinterland of a Mesozoic to early Tertiary subduction zone, remnants of which are preserved in the ophiolitic Vardar suture

in northern Greece and rump Yugoslavia (e.g., Jacobshagen et al., 1978; Burchfiel, 1980). The results of the present study imply a fundamentally different origin for the Rhodope province, in Greece at least, as an Alpine collisional orogen that accommodated enormous magnitudes of shortening through the end of Eocene time and was subsequently greatly extended on a series of low-angle extensional detachments in the back arc of the Hellenic subduction system. I recognize only two major tectonostratigraphic sequences in the Greek Rhodope province, neither of which represents a "Rhodope continental fragment". The composite, upper amphibolite-facies Serbo-Macedonian-West Thracian gneiss complex, which bears metaeclogites, serpentinites, and other ophiolitic remnants, is interpreted as a predominantly an oceanic accretionary subduction complex (cf. Dixon and Dimitriadis, 1984), that was first subducted with the Vardar ocean and later incorporated at the base of a thickening collisional orogen. The composite, lower blueschist- to upper greenschist-facies, Triassic to early Eocene Olympos-Falakron carbonate platform, inferred to be ancestrally a part of the Apulian continental fragment, underthrust this gneiss complex in a northeast-dipping, middle to late Eocene continental subduction zone, which is now a continental suture represented by the (correlative) Olympos and Nestos thrusts. An inverted metamorphic gradient was produced in the lower part of the overriding gneiss complex during the Eocene subduction event, and upon the cessation of subduction, high-P metamorphic assemblages in the subducted slab were almost completely converted to upper greenschist-facies assemblages as predicted by thermal models of the subduction process. The Falakron marble series accommodated large magnitudes of shear strain as it was being subducted, evidenced by the virtually complete destruction of original stratigraphy and the pervasive development of shear-related D_1 structural elements, including major sheath(?) folds, minor shear folds, and mineral stretching lineations, all of which typically plunge northeast, subparallel to the inferred axis of shear displacement within the subduction zone.

$^{40}Ar/^{39}Ar$ cooling ages of blueschist-facies minerals in the Olympos-Ossa unit (Schermer et al., 1990) and of hornblende and muscovite in the lower parts of the Serbo-Macedonian and West Thracian gneiss complexes (Harre et al., 1968; Liati, 1986) are interpreted here as evidence that A-type subduction of the Apulian Olympos-Falakron slab continued until ~36 - 37 Ma (cf. Schermer, 1990, 1993), whereas significant extension in northern Greece apparently did not begin until ~23 Ma with the development of the Olympos-Symvolon detachment system. Thus the Oligocene epoch appears to have been a period of relative tectonic quiescence in the Rhodope metamorphic core complex, punctuated by the emplacement of a N80°W-trending belt of plutons with undeformed intrusive margins 30 - 33 Ma. The chemistry of this intrusive belt and its association with a large tract of andesitic volcanics are consistent with an origin as a subduction-related magmatic arc (Innocenti et al., 1984; Del Moro et al., 1988; Kotopouli and Pe-Piper, 1989a; Kolocotroni and Dixon, 1991; Koukouvelas and Pe-Piper, 1991).

Early Miocene to Recent northeast-southwest extension of the north Aegean region appears to have been accommodated by a succession of three low-angle detachment zones that alternate in polarity. Top-to-the-northeast displacement from ~23 - 16 Ma on the Olympos-Symvolon detachment (D_2) may have amounted to approximately 40 km based on the width of the Symvolon pluton, which I interpret to have been emplaced in an extensional rupture that may coincide with the down-dip termination of the detachment at mid-crustal depths. The Strymon Valley detachment (D_3), which accommodated top-to-the-southwest extensional displacement locally exceeding 80 km from ~16 Ma to ~3.5 Ma, may have been succeeded by a presently active, top-to-the-northeast "North Aegean detachment system" (D_4) postulated by Dinter and Royden (1993), above which the Thermaikos, Strymon, and Drama basins are subsiding. I tentatively regard active wrenching on northeasterly trends and associated extension on N75°-85°W-trending normal faults to result from a transfer of dextral strike-slip motion from the North Aegean Trough,

the northerly offshore branch of the North Anatolian dextral strike-slip fault, northwestward into the hanging wall of the North Aegean detachment system.

D_1, D_2, and early D_3 structural elements in the Rhodope metamorphic core complex formed within the ductile regime beneath the composite Serbo-Macedonian-West Thracian gneiss complex. A reactivation of the upper section of the southwest-vergent Nestos thrust as a northeast-vergent low-angle normal fault, the Olympos-Symvolon detachment, may have resulted in the stretching and rupturing in early Miocene time of a previously continuous Olympos-Falakron marble unit at mid-crustal depths and the intrusion of the Symvolon pluton in the coaxial rupture zone. The Serbo-Macedonian-West Thracian gneiss complex was split beginning in middle Miocene time as the Strymon Valley detachment reactivated a second (deeper) section of the Nestos thrust as a southwest-vergent low-angle normal fault and the Serbo-Macedonian province was displaced in a S53°W direction in its hanging wall, carrying with it a syndetachment basin complex represented in western Bulgaria by the Struma basin, in northeastern Greece by the Siderokastro, Serres, Angitis, Akropotamos, and South Symvolon "basins", which are actually lobes of a single basin that correspond to structurally low sections of the strongly corrugated detachment surface, and in the north Aegean Sea by the Prinos-Kavala basin. The detachment and a thin cover of Neogene syndetachment deposits also crop out on the southwest corner of the island of Thasos, and the detachment system may persist offshore southeast of Thasos, as well. The Rhodope core complex emerged northeastward in the footwall of the Strymon Valley detachment, exposing the effects of earlier ductile deformation and igneous activity in the "Falakron window" between the Strymon and Nestos Rivers. Assuming the Serbo-Macedonian-West Thracian and Olympos-Falakron tectonostratigraphic correlations proposed above to be correct, the cumulative extension between Mt. Olympos and the Nestos River since early Miocene time as a result of normal displacement on the Olympos-Symvolon, Strymon Valley, and North Aegean detachment

systems is on the order of 200 - 300%, a factor that must be taken into account in reconstructions of Alpine and earlier tectonic events in the southern Balkan region.

REFERENCES

Armour-Brown, A., de Bruijn, H., Maniati, C., Siatos, G. and Neisen, P., 1977, The geology of the Neogene sediments north of Serrai and the use of rodent faunas for biostratigraphic control, in Kallergis, G., ed., VI Colloquium on the Geology of the Aegean Region, Proceedings, II, Athens, Institute of Geological and Mining Research, p. 615-622.

Armstrong, R. L., 1982, Cordilleran metamorphic core complexes — From Arizona to southern Canada: Annual Reviews of Earth and Planetary Science, v. 10, p. 129-154.

Atzori, P., Lo Giudice, A., Kokkinakis, A., Kyriakopoulos, K., Magganas, A., Pezzino, A. and Sideris, K., 1990, Petrological and geochemical study of crystalline rocks from Thassos Island, northern Greece: Proceedings of the 2nd Hellenic-Bulgarian Symposium, Thessaloniki, 1989, Geologica Rhodopica, v. 2, p. 157-165.

Baker, J. H. and Liati, A., 1991, The Oligocene volcano-sedimentary sequence of the Dipotama Basin, N. Greece: temporal relationships between Tertiary granites and volcanics, and implications for the regional tectonic evolution: Geologie en Mijnbouw, v. 70, p. 75-83.

Bernoulli, D. and Laubscher, H., 1972, The palinspastic problem of the Hellenides: Ecologae geologicae Helvetiae, v. 65, 107-118.

Birk, F., de Boer, H. U., Kronberg, P., Meyer, W., Pilger, A. and Schenck, P., 1970, Zur Geologie des Rhodopen-Kristallins im Gebiet zwischen Strimon und Nestos (Griechisch-Ostmazedonien): Beihefte zum Geologischen Jahrbuch, v. Heft 88, p. 179.

Birk, F., 1970, Zur Geologie und Petrographie des östlichen Bos-Dag-Massivs bei Drama in Griechisch-Mazedonien, in Birk, F., de Boer, H. U., Kronberg, P., Meyer, W., Pilger, A. and Schenck, P., ed., Zur Geologie des Rhodopen-Kristallins im Gebiet zwischen Strimon und Nestos (Griechisch-Ostmazedonien), Beihefte zum Geologischen Jahrbuch, Heft 88, Hannover, p. 5-42.

Boncev, E., 1971, Problems of Bulgarian Geotectonics, Sofia, Technika, 204 p.

Bornovas, J., and Rondogianni-Tsiambaou, T., 1983, Geological map of Greece, second edition: Athens, Institute of Geology and Mineral Exploration, scale 1:500,000.

Burchfiel, B. C., 1980, Eastern European Alpine system and the Carpathian orocline as an example of collision tectonics: Tectonophysics, v. 63, p. 31-61.

Burg, J.-P., Ivanov, Z., Ricou, L.-E., Dimor, D. and Klain, L., 1990, Implications of shear-sense criteria for the tectonic evolution of the Central Rhodope massif, southern Bulgaria: Geology, v. 18, p. 451-454.

Cheshitev, G., and Kancev, I., 1989, Geological Map of the People's Republic of Bulgaria: Sofia, Committee of Geology, Department of Geophysical Prospecting and Geological Mapping, scale 1:500,000.

Cox, L. R., Newell, N. D. and 23 others, 1969, Bivalvia, Part N, Molluska 6, in Moore, R. C., ed., Treatise on Invertebrate Paleontology, v. 2, Boulder, CO, Geological Society of America, p. N491-N952.

Crittenden, M. D., Coney, P. J. and Davis, G. H., 1980, Cordilleran Metamorphic Core Complexes: Boulder, CO, Geological Society of America Memoir 153, 490 p.

Davis, G. A. and Lister, G. S., 1988, Detachment faulting in continental extension; Perspectives from the Southwestern U.S. Cordillera, in S.P. Clark, B. C. B., and J. Suppe, ed., Processes in Continental Lithospheric Deformation, 218, Boulder, CO, Geological Society of America Memoir 218, p. 133-159.

de Boer, H. U., 1970, Geologisch-petrographische Untersuchungen im Rhodope-Massiv Griechisch-Ostmazedoniens: Der Menikion-Bergzug nordöstlich Serrai, in Birk, F., de Boer, H. U., Kronberg, P., Meyer, W., Pilger, A. and Schenck, P., ed., Zur Geologie des Rhodopen-Kristallins im Gebiet zwischen Strimon und Nestos (Griechisch-Ostmazedonien), Beihefte zum Geologischen Jahrbuch, Heft 88, Hannover, p. 43-79.

Del Moro, A., Innocenti, F., Kyriakopoulos, C., Manetti, P. and Papadopoulos, P., 1988, Tertiary granitoids from Thrace (northern Greece): Sr isotopic and petrochemical data: Neues Jahrbuch für Mineralogie, Abhandlungen, v. 159, p. 113-135.

Del Moro, A., Kyriakopoulos, K., Pezzino, A., Atzori, P. and Lo Giudice, A., 1990, The metamorphic complex associated to the Kavala plutonites: an Rb-Sr geochronological, petrological and structural study: Proceedings of the 2nd Hellenic-Bulgarian Symposium, Thessaloniki, 1989, Geologica Rhodopica, v. 2, p. 143-152.

Dermitzakis, M. D., Georgiades-Dikeoulia, E. and Velitzelos, E., 1985, Ecostratigraphic observations on the Messinian deposits of Akropotamos area (Kavala, N. Greece): Annales Géologiques des pays Helléniques, v. 33, p. 367-376.

De Wet, A. P., Miller, J. A., Bickle, M. J. and Chapman, H. J., 1989, Geology and geochronology of the Arnea, Sithonia, and Ouranopolis intrusions, Chalkidiki Peninsula, northern Greece: Tectonophysics, v. 161, p. 65-79.

Dinter, D. A., 1991, Neogene detachment faulting and the Rhodope metamorphic core complexes, northern Greece [abs.]: Eos, Transactions, American Geophysical Union, v. 72, p. 460.

Dinter, D. A., Carter, L. D. and Brigham-Grette, J., 1990, Late Cenozoic geologic evolution of the Alaskan North Slope and adjacent continental shelves, in Grantz, A., Johnson, L. and Sweeney, J. F., ed., The Arctic Ocean region, L, The Geology of North America, Boulder, Colorado, Geological Society of America, p. 459-490.

Dinter, D. A. and Royden, L., 1993, Late Cenozoic extension in northeastern Greece: Strymon Valley detachment and Rhodope metammorphic core complex: Geology, v. 21, p. 45-48.

Dixon, J. E. and Dimitriades, S., 1984, Metamorphosed ophiolitic rocks from the Serbo-Macedonian Massif, near Lake Volvi, North-east Greece, in Dixon, J. E. and Robertson, A. H. F., ed., The Geological Evolution of the Eastern Mediterranean, Geological Society Special Publication No. 17, Oxford, Blackwell Scientific Publications, p. 603-618.

Draper, G. and Bone, R., 1981, Denudation rates, thermal evolution, and preservation of blueschist terrains: Journal of Geology, v. 89, p. 601-613.

Dürr, S., Altherr, R., Keller, J., Okrusch, M. and Seidel, E., 1978, The median Aegean crystalline belt: stratigraphy, structure, metamorphism, magmatism, in Closs, H., Roeder, D. and Schmidt, K., ed., Alps, Apennines, Hellenides, Inter-Union Commission on Geodynamics Scientific Report No. 38, Stuttgart, E. Schweizerbart'sche Verlagsbuchhandlung, p. 455-477.

Eleftheriadis, G., Christofides, G. and Kassoli-Fournaraki, A., 1984, Geochemistry of the high-K calc-alkaline basaltic sills and dykes in the south Rhodope massif (N. Greece): Bulletin Volcanologique, v. 47, p. 569-579.

Eleftheriadis, G. and Lippolt, H. J., 1984, Altersbestimmungen zum oligozänen vulkanismus der Süd-Rhodopen/Nord Griechenland: Neues Jahrbuch für Geologie und Paläontologie, Monatshefte, v. 3, p. 179-191.

England, P. C. and Thompson, A. B., 1984, Pressure-temperature-time paths of regional metamorphism, Part I: Heat transfer during the evolution of regions of thickened continental crust: Journal of Petrology, v. 25, p. 894-928.

Erki, I., Kolios, N. and Stegena, L., 1984, Heat flow density determination in the Strymon basin, NE Greece: Journal of Geophysics, v. 54, p. 106-109.

Fedo, C. M. and Miller, J. M. G., 1992, Evolution of a Miocene half-graben basin, Colorado River extensional corridor, southeastern California: Geological Society of America Bulletin, v. 104, p. 481-493.

Freyberg, v. B., 1951, Geologie und Lagerstättenkunde des Braunkohlenrevier von Serrae (Makedonien): Annales géologiques des pays Hélleniques, v. 3, p. 87-154.

Fytikas, M., Innocenti, F., Manetti, P., Mazzuoli, R., Peccerillo, A. and Villari, L., 1984, Tertiary to Quaternary evolution of volcanism in the Aegean region, in Dixon, J. E. and Robertson, A. H. F., ed., The Geological Evolution of the Eastern Mediterranean, Blackwell Scientific Publications, p. 687-699.

Georgiev, G., 1963, Petrographie der metamorphen Gesteine, Sofia, Verlag Technika, 272 p.

Ghent, E. D., Stout, M. Z. and Parrish, R. R., 1988, Determination of metamorphic pressure-temperature-time (PTt) paths., in Nisbet, E. G. and Fowler, C. M. R., ed., Short Course on Heat, Metamorphism, and Tectonics, Saint John's, Mineralogical Association of Canada, p. 155-188.

Giletti, B. J., 1974, Studies in diffusion I: argon in phlogopite mica, in Hofmann, A. W., Giletti, B. J., Yoder, H. S. and Yund, R. A., ed., Geochemical Transport and Kinetics, Washington, D.C., Carnegie Institute, p. 107-115.

Godfriaux, I., 1968, Etude géologique de la région de l'Olympe (Grèce): Annales Géologiques des Pays Helléniques, v. 19, p. 1-271.

Gramann, H. and Kockel, F., 1969, Das Neogen im Strymon-becken (Griechisch-Ostmazedonien), Teil 1, Lithologie, stratigraphie und paläogeographie: Geologisches Jahrbuch, v. 87, p. 445-484.

Hansen, E., 1971, Strain Facies, Berlin, Springer-Verlag, 207 p.

Harre, W., Kockel, F., Kreuzer, H., Lenz, H., Müller, P. and Walther, H. W., 1968, Über Rejuvenationen im Serbo-Madzedonischen Massiv (Deutung radiometrischer Altersbestimmungen) [abs.]: Proceedings of the 23rd International Geological Congress, Prague, p. 223-236.

Harrison, T. M., 1981, Diffusion of ^{40}Ar in hornblende: Contributions in Mineralogy and Petrology, v. 78, p. 324-331.

Harrison, T. M., Duncan, I. and McDougall, I., 1985, Diffusion of ^{40}Ar in biotite: temperature, pressure, and compositional effects: Geochimica Cosmochimica Acta, v. 49, p. 2461-2468.

Hutchinson, G. E., 1967, Treatise on Limnology, New York, John Wiley and Sons, 1115 p.

Innocenti, F., Kolios, N., Manetti, P., Mazzuoli, R., Peccerillo, G., Rita, F. and Villari, L., 1984, Evolution and geodynamic significance of the Tertiary orogenic volcanism in northeastern Greece: Bulletin Volcanologique, v. 47, p. 25-37.

Ivanov, R., 1981, The deep-seated central Rhodope nappe and interference tectonics of the Rhodope crystalline basement: Geologica Balcanica, v. 11, p. 47-66.

Jackson, J. A. and McKenzie, D. P., 1983, The geometrical evolution of normal fault systems: Journal of Structural Geology, v. 5, p. 471-482.

Jacobshagen, V., Dürr, S., Kockel, F., Kopp, K.-O., Kowalczyk, G., Berckhemer, H. and Büttner, D., 1978, Structure and geodynamic evolution of the Aegean region, in Closs, H., Roeder, D. and Schmidt, K., ed., Alps, Apennines, Hellenides, Inter-Union Commission on Geodynamics Scientific Report No. 38, Stuttgart, E. Schweizerbart'sche Verlagsbuchhandlung, p. 537-564.

John, B. E., 1987, Geometry and evolution of a mid-crustal extensional fault system: Chemehuevi Mountains, southeastern California, in Coward, M. P., Dewey, J. F. and Hancock, P. L., eds., Continental Extensional Tectonics, Geological Society Special Publication No. 28, Oxford, Blackwell Scientific Publications, p. 313-335.

Jongsma, D., Wissman, G., Hinz, K., and Garde, S., 1977. Seismic studies in the Cretan Sea, 2, The southern Aegean Sea: an extensional marginal basin without seafloor spreading?, "Meteor" Forschungsergeb. Reihe C, p. 27.

Jordan, H., 1969, Geologie und Petrographie im Zentralteil des Bos Dag (Drama, Griechisch-Makedonien): Geotectonische Forschungen, v. 31, p. 50-85.

Kauffmann, G., Kockel, F. and Mollat, H., 1976, Notes on the stratigraphic and palaeogeographic position of the Svoula formation in the innermost zone of the Hellenides (northern Greece): v. 18, p. 225-230.

Kilias, A. and Mountrakis, D., 1990, Kinematics of the crystalline sequences in the western Rhodope massif, in Konstantinos, S., ed., Geologica Rhodopica, Proceedings of the 2nd Hellenic-Bulgarian Symposium, Thessaloniki, 1989, v. 2, Thessaloniki, Aritstotle University Press, p. 100-116

Kober, L., 1931, Das alpine Europa un sein Rahment, Berlin, Borntraeger, 310 p.

Kockel, F. and Walther, H. W., 1965, Die Strimonlinie als Grenze zwischen Serbo-Mazedonischem und Ril-Rhodope-Massiv in Ost-Mazedonien: Geologisches Jahrbuch, v. 83, p. 575-602.

Kockel, F., Mollat, H. and Walther, H. W., 1971, Geologie des Serbo-Mazedonischen Massivs und seines mesozoischen Rahmens (Nordgriechenland): Geologisches Jahrbuch, v. 89, p. 529-551.

Kockel, F., Mollat, H. and Walther, H. W., 1977, Erläuterungen zur Geologischen Karte der Chalkidhiki und angrenzender Gebiete 1:100,000 (Nord-Griechenland), Hannover, Bundesanstalt für Geowissenschaften und Rohstoffe, 119 p.

Kockel, F., Mollat, H., Walther, H. W., Antoniades, P. and Ioannides, K., 1978, Geological Map of Greece, Stratoniki Sheet: Athens, Institute of Geology and Mineral Exploration, 1:50,000.

Kockel, F. and Walther, H. W., 1965, Die Strimonlinie als Grenze zwischen Serbo-Mazedonischem und Ril-Rhodope-Massiv in Ost-Mazedonien: Geologisches Jahrbuch, v. 83, p. 575-602.

Kojumdgieva, E., Nikolov, I., Nedjalkov, P. and Busev, A., 1982, Stratigraphy of the Neogene in Sandanski graben: Geologica Balcanica, v. 12, p. 69-81.

Kokkinakis, A., 1980a, Zum faltenbau des Symvolongebirges und des gebietes von Kavala (Griechisch-Ostmakedonien): Annales Géologiques des Pays Helléniques, v. 30, p. 398-420.

Kokkinakis, A., 1980b, Geologie und petrographie des Kavala-Gebietes und des Symvolon-gebirges in Griechisch-Ostmakedonien: Zeitschrift der Deutschen Geologischen Gesellschaft, v. 131, p. 903-925.

Kokkinakis, A., 1980c, Altersbeziehungen zwischen Metamorphosen, mechanischen Deformationen und Intrusionen am Südrand des Rhodope-Massivs (Makedonien, Grieschenland): Geologische Rundschau, v. 69, p. 726-744.

Kolocotroni, C. and Dixon, J. E., 1991, The origin and emplacement of the Vrondou granite, Serres, N.E. Greece: Bulletin of the Geological Society of Greece, v. 25, p. 469-483.

Kotopouli, C. N. and Pe-Piper, G., 1989a, Geochemical characteristics of felsic intrusive rocks within the Hellenic Rhodope: A comparative study and petrogenetic implications: Neues Jahrbuch für Mineralogie, Abhandlungen, v. 161, p. 141-169.

Kotopouli, C. N. and Pe-Piper, G., 1989b, Chemical composition of pargasite and hornblende in low to high grade metamorphic rocks of the Rhodope zone, Xanthi, Greece: Mineralogy and Petrology, v. 40, p. 275-288.

Kotopouli, C. N. and Pe-Piper, G., 1991, Geochemistry of the Paranestion volcanic rocks, Hellenic Rhodope, Greece: Chemie der Erde, v. 51, p. 13-22.

Kotopouli, C. N., Pe-Piper, G. and Katagas, C. G., 1991, The metamorphism and migmatization of the Xanthe-Echinos metamorphic complex, Central Rhodope, Greece: Lithos, v. 27, p. 79-93.

Koukouvelas, I. and Doutsos, T., 1990, Tectonic stages along a traverse cross cutting the Rhodopian zone (Greece): Geologische Rundschau, v. 79, p. 753-776.

Koukouvelas, I. and Pe-Piper, G., 1991, The Oligocene Xanthi pluton, northern Greece: a granodiorite emplaced during regional extension: Journal of the Geological Society, London, v. 148, p. 749-758.

Koukouzas, C., 1972, Le chévauchement de Strymon dans la région Strymon dans la région de la frontiére Gréco-Bulgare: Zeitung der deutsche geologische Gesellschaft, v. 123, p. 343-347.

Kronberg, P., 1969, Gliederung, Petrographie und Tectogenese des Rhodopen-Kristallins im Tsal-Dag, Simvolon und Ost-Pangäon (Griechisch-Makedonien): Geotektonische Forschungen, v. 31, p. 1-49.

Kronberg, P., 1973, Geological Map of Greece, Kavala sheet: Athens, Institute of Geology and Mineral Exploration, scale 1:50,000.

Kronberg, P. and Eltgen, H., 1973, Geological Map of Greece, Xanthi sheet: Athens, Institute of Geology and Mineral Exploration, scale 1:50,000.

Kronberg, P., Meyer, W. and Pilger, A., 1970, Geologie der Rila-Rhodope-Masse zwischen Strimon und Nestos (Nordgriechenland), in Birk, F., de Boer, H. U., Kronberg, P., Meyer, W., Pilger, A. and Schenck, P., eds., Zur Geologie des Rhodopen-Kristallins im Gebiet zwischen Strimon und Nestos (Griechisch-Ostmazedonien), Beihefte zum Geologischen Jahrbuch, Heft 88, Hannover, p. 133-180.

Kronberg, P. and Raith, M., 1977, Tectonics and metamorphism of the Rhodope crystalline complex in Eastern Greek Macedonia and parts of Western Thrace: Neues Jahrbuch für Geologie und Paläontologie, Monatshefte, v. 11, p. 697-704.

Lalechos, N. and Savoyat, E., 1977, La sédimentation Néogène dans le Fossé Nord Egéen, in Kallergis, G., ed., VI Colloquium on the Geology of the Aegean Region, Proceedings, II, Athens, Institute of Geological and Mining Research, p. 591-603.

Le Pichon, X. and Angelier, J., 1979, The Hellenic Arc and Trench system: A key to the neotectonic evolution of the eastern Mediterranean area: Tectonophysics, v. 60, p. 1-42.

Liati, A., 1986, Regional metamorphism and overprinting contact metamorphism of the Rhodope zone, near Xanthi (N. Greece). Petrology, geochemistry, geochronology [Ph.D. thesis]: Techn. Univ. Braunschweig, 186 p.

Liati, A., 1988, Amphibolitized eclogites in the Rhodope crystalline complex, near Xanthi (N. Greece): Neues Jahrbuch für Mineralogie, Monatshefte, v. H. 1, p. 1-8.

Liati, A. and Mposkos, E., 1990, Evolution of the eclogites in the Rhodope zone of northern Greece: Lithos, v. 25, p. 89-99.

Lybéris, N., 1984, Tectonic evolution of the North Aegean trough, in Dixon, J. E. and Robertson, A. H. F., ed., The Geological Evolution of the Eastern Mediterranean, Geological Society Special Publication No. 17, Oxford, Blackwell Scientific Publications, p. 709-725.

Makris, J., 1976. Crustal structure of the Aegean Sea and the Hellenides obtained from geophysical surveys: Journal of Geophysics, v. 41, 441.

Makris, J., and Vees, R., 1977. Crustal structure of the central Aegean Sea and the islands of Evvia and Crete, Greece, obtained by refraction seismic experiments: Journal of Geophysics, v. 42, p. 329.

Marakis, G. I., 1969, Geochronologic studies of some granites from Macedonia: Annales Géologiques des Pays Helléniques, v. 21, p. 121-152.

Mercier, J., Vergely, P. and Bebein, J., 1975, Les ophiolites helléniques "obductés" au Jurassique supérior sont-elles les vestiges d'un océan tethysien ou d'une mer marginale périeuropéene?: Compte rendu sommaire des Sciences de la Societe géologique de France, v. 17, p. 108-112.

Meulenkamp, J. E., 1977, The Aegean and the Messinian salinity crisis, in Kallergis, G., ed., VI Colloquium on the Geology of the Aegean Region, Proceedings, III, Athens, Institute of Geological and Mining Research, p. 1253-1263.

Meyer, W., 1968, Zur Alterstellung des Plutonismus im Südteil der Rila-Rhodope-Masse (Nordgriechenland): Geologica et Paleontologica, v. 2, p. 173-192.

Meyer, W., 1969, Die Faltenachsen im Rhodopen-Kristallin östlich des Strimon (Nordost-Griechenland): Geotektonische Forschungen, v. 31, p. 86-96.

Meyer, W. and Pilger, A., 1963, Zur Geologie des Gebietes zwischen Strimon und Nestos (Rhodopen-Massiv) in Griechisch-Makedonien: Neues Jahrbuch für Geologie und Paläontologie, Abhandlungen, v. 118, p. 272-280.

Mposkos, E., 1987, Polymetamorphism in central and east Rhodope Massif.: Proceedings of the First Bulgarian-Greek Symposium on the Geology and Physical Geography of the Rhodope Massif, Geologica Rhodopica, v. 1, p. 153-159.

Mposkos, E., 1988, The chloritoid-staurolite schists of the lower tectonic unit in east Rhodope: Bulletin of the Geological Society of Greece, v. 22, p. 393-411.

Mposkos, E., 1989, High-pressure metamorphism in gneisses and pelitic schists in the east Rhodope zone (N. Greece): Mineralogy and Petrology, v. 41, p. 25-39.

Mposkos, E. and Perdikatsis, V., 1987, High-pressure metamorphism in east Rhodope Massif (Greece): Fortschrift Mineralogie, v. 65, p. 140.

Mposkos, E., Perdikatsis, V. and Liati, A., 1988, Geochemical investigation of amphibolites from eastern and central Rhodope: Bulletin of the Geological Society of Greece, v. 22, p. 413-427.

Osswald, K., 1938, Geologische Geschichte von Griechisch-Nordmazedonien: Denkschrift der Geologische Landesantalt von Griechenland, v. Heft 3, p. 142 p.

Oxburgh, E. R. and Turcotte, D. L., 1974, Thermal and regional metamorphism in overthrust terrains with special reference to the Eastern Alps: Schweizerische Mineralogische und Petrographische Mitteilungen, v. 54, p. 641-662.

Panagos, A. G., Pe, G. G. and Varnavas, S. P., 1978, The volcanic rocks of Strymonikon-Metamorphosis, central Macedonia, Greece: Chemie der Erde, v. 37, p. 50-61.

Papadakis, A., 1971, On the age of the granitic intrusion near Stratonion, Chalkidiki (Greece): Annales Géologiques des Pays Helléniques, v. 23, p. 297-300.

Papadopoulos, V. C. and Kilias, A., 1985, Altersbeziehungen zwischen Metamorphose und Deformation im zentralen Teil des Serbomazedonischen Massivs (Vertiskos Gebirge, Nord-Griechenland): Geologische Rundschau, v. 74, p. 77-85.

Papanikolaou, D. and Panagopoulos, A., 1981, On the structural style of Southern Rhodope, Greece: Geologica Balcanica, v. 11, p. 13-22.

Peacock, S. M., 1987, Creation and preservation of subduction-related inverted metamorphic gradients: Journal of Geophysical Research, v. 92, p. 12,793-12,781.

Platt, J. P., 1986, Dynamics of orgenic wedges and the uplift of high-pressure metamorphic rocks: Geological Society of America Bulletin, v. 97, p. 1037-1053.

Pollak, W. H., 1979, Structural and lithological development of the Prinos-Kavala basin, Sea of Thrace, Greece: Annales Géologiques des pays Helléniques, tome hors série, v. fasc. II, p. 1003-1011.

Proedrou, P., 1979, The evaporites formation in the Nestos-Prinos graben in the northern Aegean Sea: Annales Géologiques des pays Helléniques, tome hors série, v. fasc. II, p. 1013-1020.

Psilovikos, A. and Syrides, G., 1983, Stratigraphy, sedimentation and palaeogeography of the Strymon Basin, eastern Macedonia/northern Aegean Sea, Greece: Clausthaler Geologische Abhandlungen, v. 44, p. 55-87.

Robbins, G. A., 1972, Radiogenic argon diffusion in muscovite under hydrothermal conditions [M.S. thesis]: Brown University, Providence, R.I.

Royden, L. H., 1988, Late Cenozoic tectonics of the Pannonian basin system, in Royden, L. H. and Horvath, F., ed., Pannonian Basin: A Study in Basin Evolution, AAPG Memoir 45, p. 27-48.

Rubie, D. C., 1984, A thermal-tectonic model for high-pressure metamorphism and deformation in the Sesia Zone, Western Alps: Journal of Geology, v. 92, p. 21-36.

Schenk, P.-F., 1970, Geologie des westlichen Pangaion in Griechisch-Ostmakedonien, in Birk, F., de Boer, H. U., Kronberg, P., Meyer, W., Pilger, A. and Schenck, P., ed., Zur Geologie des Rhodopen-Kristallins im Gebiet zwischen Strimon und Nestos (Griechisch-Ostmazedonien), Beihefte zum Geologischen Jahrbuch, Heft 88, Hannover, p. 81-132.

Schermer, E. R., 1989, Tectonic Evolution of the Mt. Olympos Region, Greece [Ph.D. Thesis]: Cambridge, Massachusetts Institute of Technology, 272 p.

Schermer, E. R., 1990, Mechanisms of blueschist creation and preservation in an A-type subduction zone, Mount Olympos region, Greece: Geology, v. 18, p. 1130-1133.

Schermer, E. R., 1993, Geometry and kinematics of continental basement deformation during the Alpine orogeny, Mt. Olympos region, Greece: Journal of Structural Geology, v. 15, p. 571-591.

Schermer, E. R., Lux, D. R. and Burchfiel, B. C., 1990, Temerature-time history of subducted continental crust, Mount Olympos region, Greece: Tectonics, v. 9, p. 1165-1195.

Schmitt, A., 1983, Nouvelles contributions a l'étude géologique des Pieria, de l'Olympe, et de l'Ossa (Grèce du Nord) [Ph.D. thesis]: Faculte Polytechnique de Mons (Belgium), 215 p.

Schwan, W., 1962, Deckenfragen im Balkan—Mit einer Einführung in die geotektonischen Verhältnisse Bulgariens: Geologische Rundschau, v. 51, H. 1, p. 181-218.

Smith, A. G., 1971, Alpine deformation and the oceanic areas of the Tethys, Mediterranean and Atlantic: Geological Society of America Bulletin, v. 82, p. 2039-2070.

Steininger, F. F. and Rögl, F., 1984, Paleogeography and palinspastic reconstruction of the Neogene of the Mediterranean and Paratethys, in Dixon, J. E. and Robertson, A. H. F., ed., The Geological Evolution of the Eastern Mediterranean, Geological Society Special Publication No. 17, Oxford, Blackwell Scientific Publications, p. 659-668.

Twiss, R. J. and Moores, E. M., 1992, Structural Geology, New York, W.H. Freeman and Company, 532 p.

Vavelidis, M., Eleftheriadis, G. and Kassoli-Fournaraki, A., 1987, A petrological study of the crystalline complex in the island Thasos: Annales Géologiques des pays Helléniques, v. 33, p. 203-216.

Wernicke, B. P., 1981, Low-angle faults in the Basin and Range Province—Nappe tectonics in an extending orogen: Nature, v. 291, p. 645-648.

Wernicke, B. P., 1985, Uniform-sense normal simple shear of the continental lithosphere: Canadian Journal of Earth Sciences, v. p. 108-125.

Xidas, S., 1984, Geological Map of Greece, Rodholivos sheet: Athens, Institute of Geology and Mineral Exploration, scale 1:50,000.

Yarnold, J. C. and Lombard, J. P., 1989, A facies model for large rock-avalanche deposits formed in dry climates, in Colburn, I. P., Abbott, P. L. and Minch, J., eds., Conglomerates in Basin Analysis: A Symposium Dedicated to A.O. Woodward, 62, Pacific Section, Society of Economic Paleontologists and Mineralogists, p. 9-31.

Zachos, S., 1982, Geological Map of Greece, Thasos sheet: Athens, Institute of Geology and Mineral Exploration, scale 1:50,000.

Zachos, S. and Dimadis, E., 1983, The geotectonic position of the Skaloti-Echinos granite and its relationship to the metamorphic formations of Greek Western and Central Rhodope: Geologica Balcanica, v. 13, p. 17-24.

Zagorcev, I. S., 1992, Neotectonic development of the Struma (Kraistid) Lineament, southwest Bulgaria and northern Greece: Geological Magazine, v. 128, p. 197-222.

Zimmerman, J., Jr., 1972, Emplacement of the Vourinos ophiolitic complex, northern Greece, in Shagam, R. et al., eds., Studies in Earth and Space Sciences: Geological Society of America Memoir 132, p. 225-239.

FIGURE CAPTIONS

Figure 1. Sketch map of major tectonic elements in southeastern Europe and the northeastern Mediterranean region. RCF – Rhodope continental fragment (horizontal lines), RMP – Rhodope metamorphic province (vertical lines), RMCC – Rhodope metamorphic core complex (gray pattern). NAT – North Aegean trough. Modified from Burchfiel (1980), Royden (1988), and Dinter and Royden (1993).

Figure 2. Tectonic map of the north Aegean region. See text for discussion, Fig. 3 for explanation of contact symbols. Data compiled from Bornovas and Rondogianni-Tsiambaou (1983), Cheshitev and Kancev (1989), Schermer (1993), Dinter and Royden (1993), and unpublished mapping by the author.

Figure 3. Generalized geology of the Strymon Valley region. Heavy lines are faults, dashed where inferred: with barbs – thrust fault (barbs on hanging wall), with boxes – low-angle normal fault (boxes on hanging wall), with balls – high-angle normal fault (balls on hanging wall), with arrows parallel to fault trace – strike-slip fault, unadorned – fault of uncertain tectonic identity. Attitude symbols: open triangles – metamorphic foliations, solid boxes – fault planes, short lines – bedding. Light solid lines – depositional or intrusive contacts. Light dashed line in West Thracian gneiss complex – contact between migmatic granite and host rock. See Fig. 2 for location, Fig. 4 for explanation of tectonostratigraphic units.

Figure 4. Generalized tectonostratigraphy, Tertiary deformational sequence, and schematic structural relationships in the southern Rhodope province, northeastern Greece. Unit patterns keyed to Fig. 3. See text and Table 1 for explanation of deformational sequence.

Figure 5. Diagrammatic representation of detachment-plane duplex structure, commonly developed on marble substrate underlying poorly consolidated, clastic, supradetachment basin deposits (see Plates 14 and 15). (a) Plane view. (b) Cross section.

Figure 6. Structural and geochronological data, central Symvolon pluton. Attitudes with boxes are on brittle shear surfaces (D_{3b}); attitudes with triangles are on mylonitic C-planes (S_2). Arrows represent L_2 stretching lineations. Single barb or outer barb of double-barbed arrows gives plunge of lineation. Inner barb gives sense of shear based on mylonitic fabric indicators. (Barb points in transport direction of material *above* shear plane.) In data boxes, (f) indicates furnace step-heating analysis, (l) indicates laser-fusion analysis. Inset: L_2 stretching lineations plotted with mylonitic sense of shear on equal area net. (Arrows point in transport direction of material *above* shear plane.) Bar graph tabulates top-to-the-southwest vs. top-to-the-northeast sense-of-shear based on field determinations of S-C asymmetries. See Fig. 3 for location.

Figure 7. Minor fold-axis and stretching lineation axes in the Falakron marble series between the Strymon and Nestos Rivers in northeastern Greece from Meyer (1969).

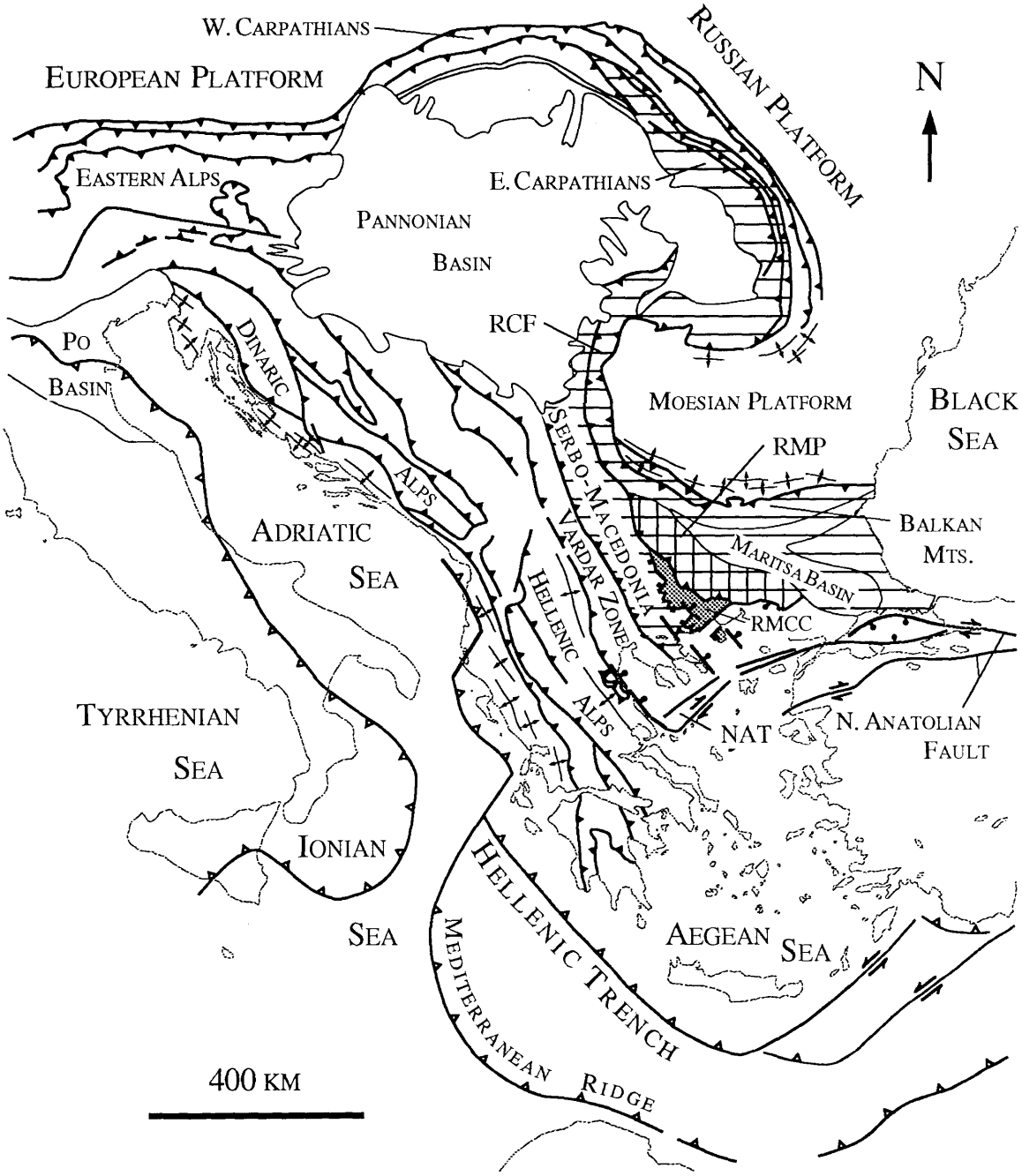

Figure 1. Sketch map of major tectonic elements in southeastern Europe and the northeastern Mediterranean region. RCF – Rhodope continental fragment (horizontal lines), RMP – Rhodope metamorphic province (vertical lines), RMCC – Rhodope metamorphic core complex (gray pattern). NAT – North Aegean Trough. Modified from Burchfiel (1980), Royden (1988), and Dinter and Royden (1993).

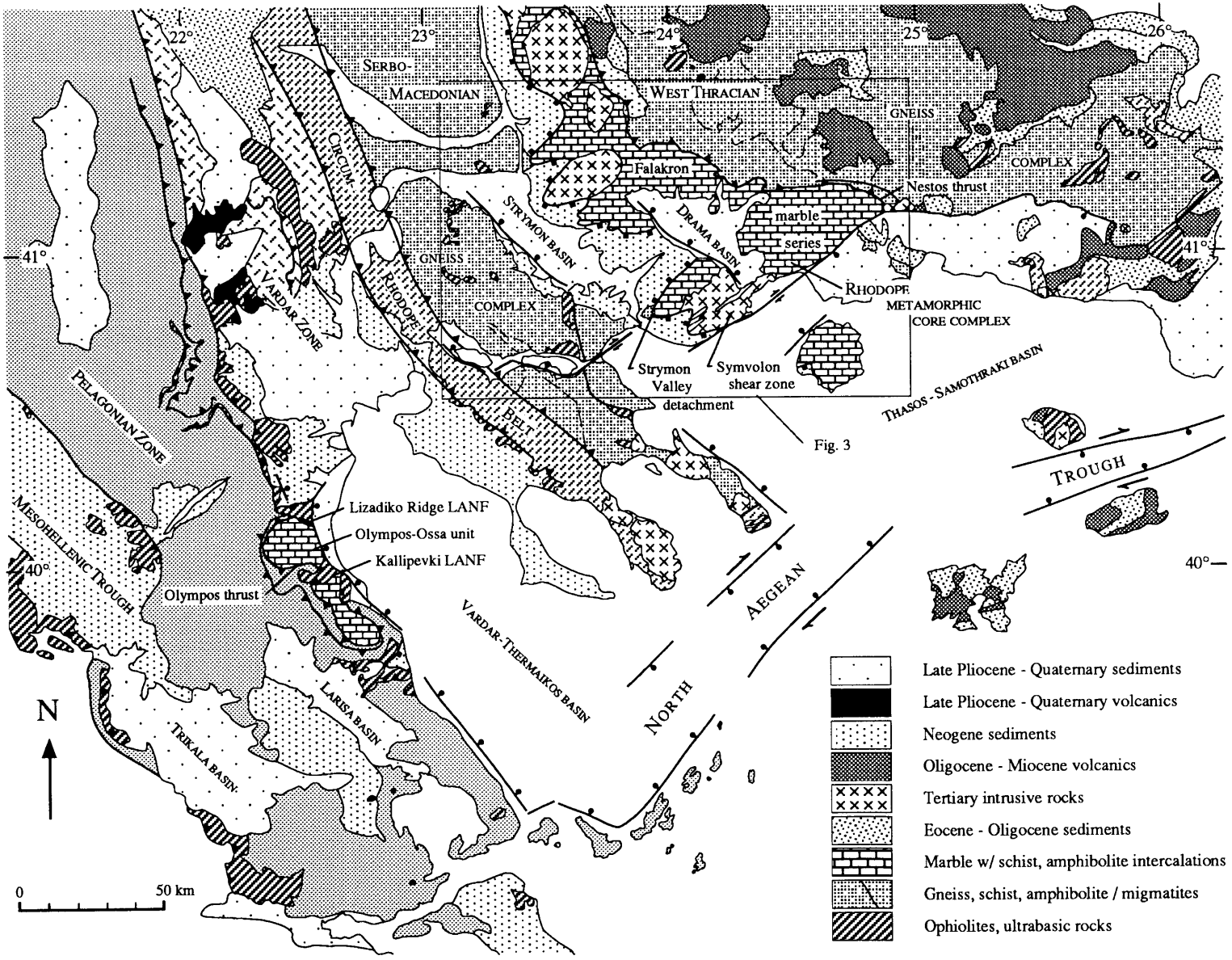

Figure 2. Generalized tectonic map of the north Aegean region. See Fig. 3 for explanation of contact symbols.

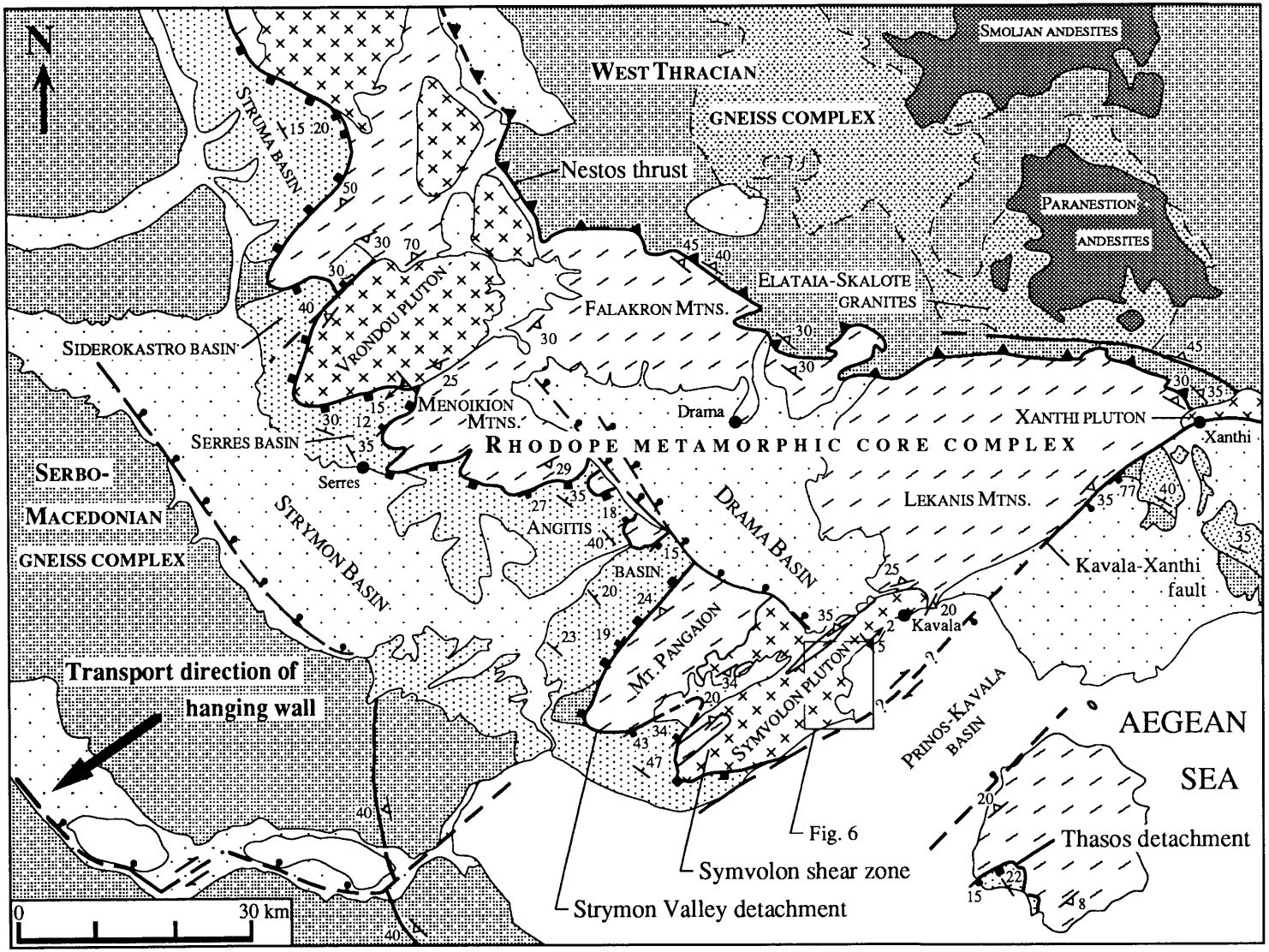

Figure 3. Generalized geology of the Strymon Valley region. See Fig. 2 for location, Fig. 4 for explanation of tectonostratigraphic units.

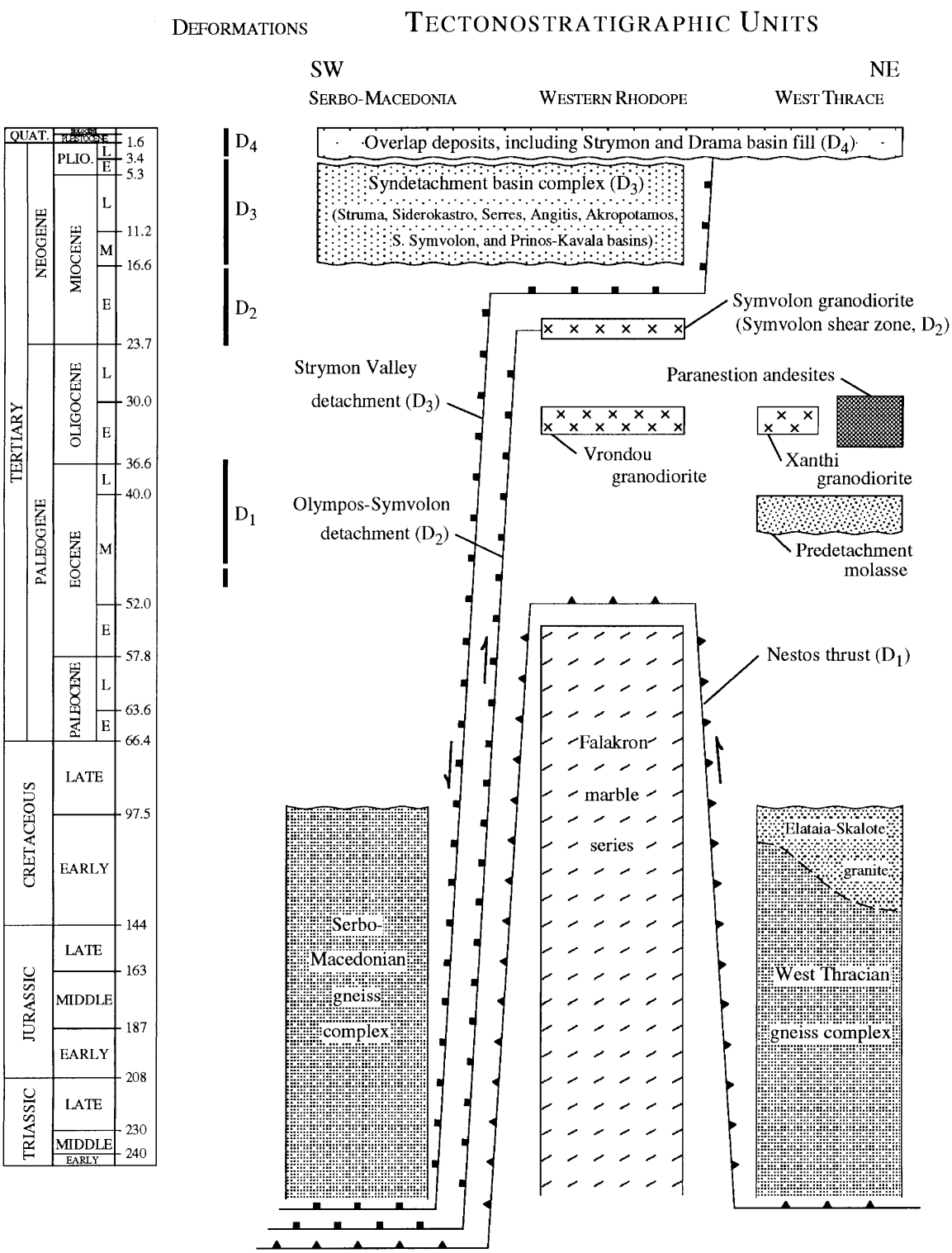

Fig. 4. Tertiary deformational-intrusive sequence, generalized tectonostratigraphy, and schematic structural relationships in the Strymon-Nestos region, northeastern Greece.

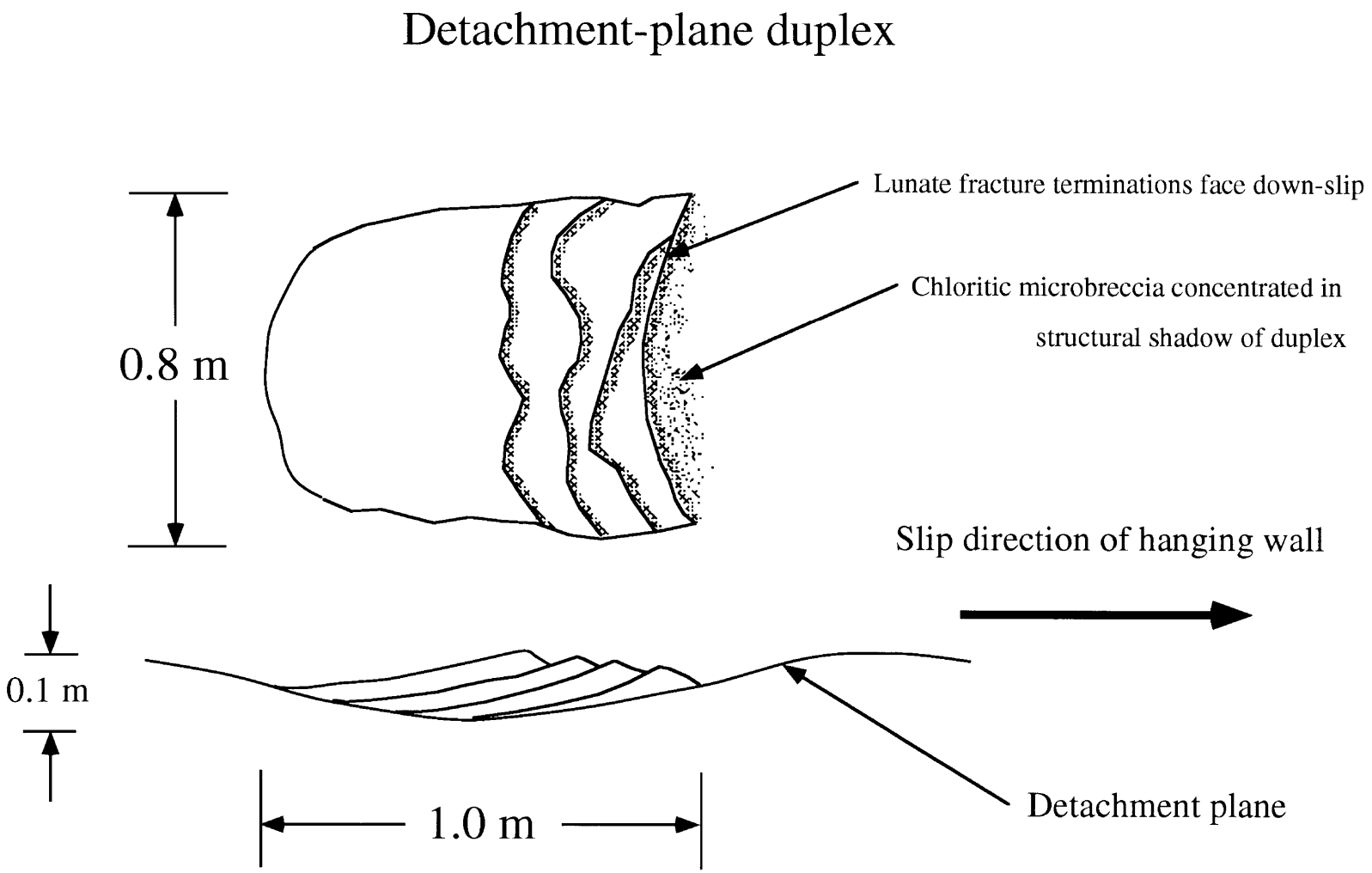

Figure 5. Diagrammatic representation of a detachment-plane duplex structure. (a) Plan view. (b) Cross section.

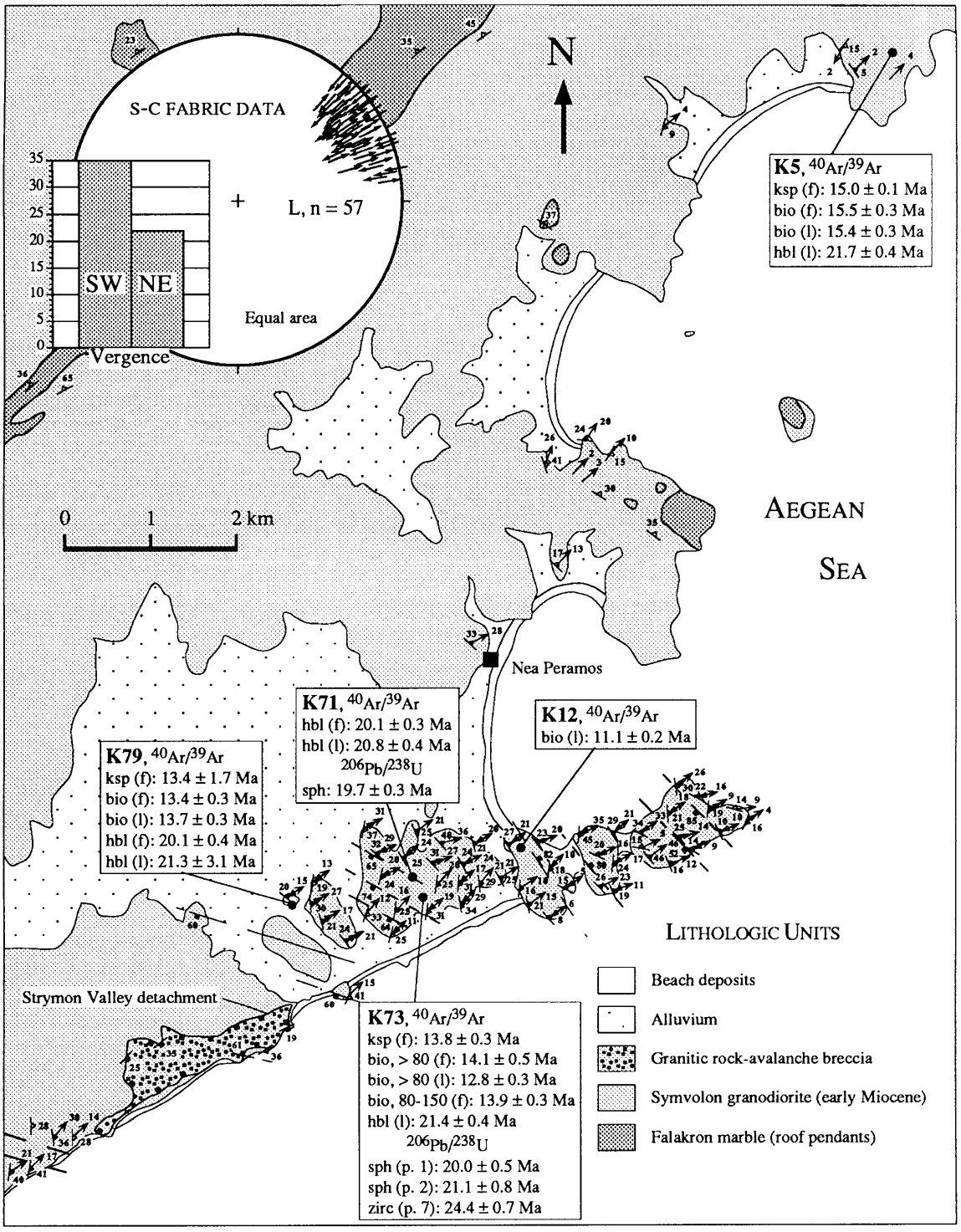

Figure 6. Structural and geochronological data, central Symvolon pluton. Attitudes with boxes are on brittle shear surfaces; attitudes with triangles are on mylonitic C-planes. Arrows represent stretching lineations. Single barb or outer barb of double-barbed arrows gives plunge of lineation. Inner barb gives sense of shear based on mylonitic fabric indicators. (Barb points in transport direction of material above shear plane). In data boxes, (f) indicates furnace step-heating analysis, (l) indicates laser-fusion analysis. Inset: Stretching lineations plotted with mylonitic sense of shear on equal area net. (Arrows point in transport direction of material above shear plane.) Bar graph tabulates SW vs. NE sense-of-shear indicators based on field determinations of S-C asymmetries. See Fig. 3 for location.

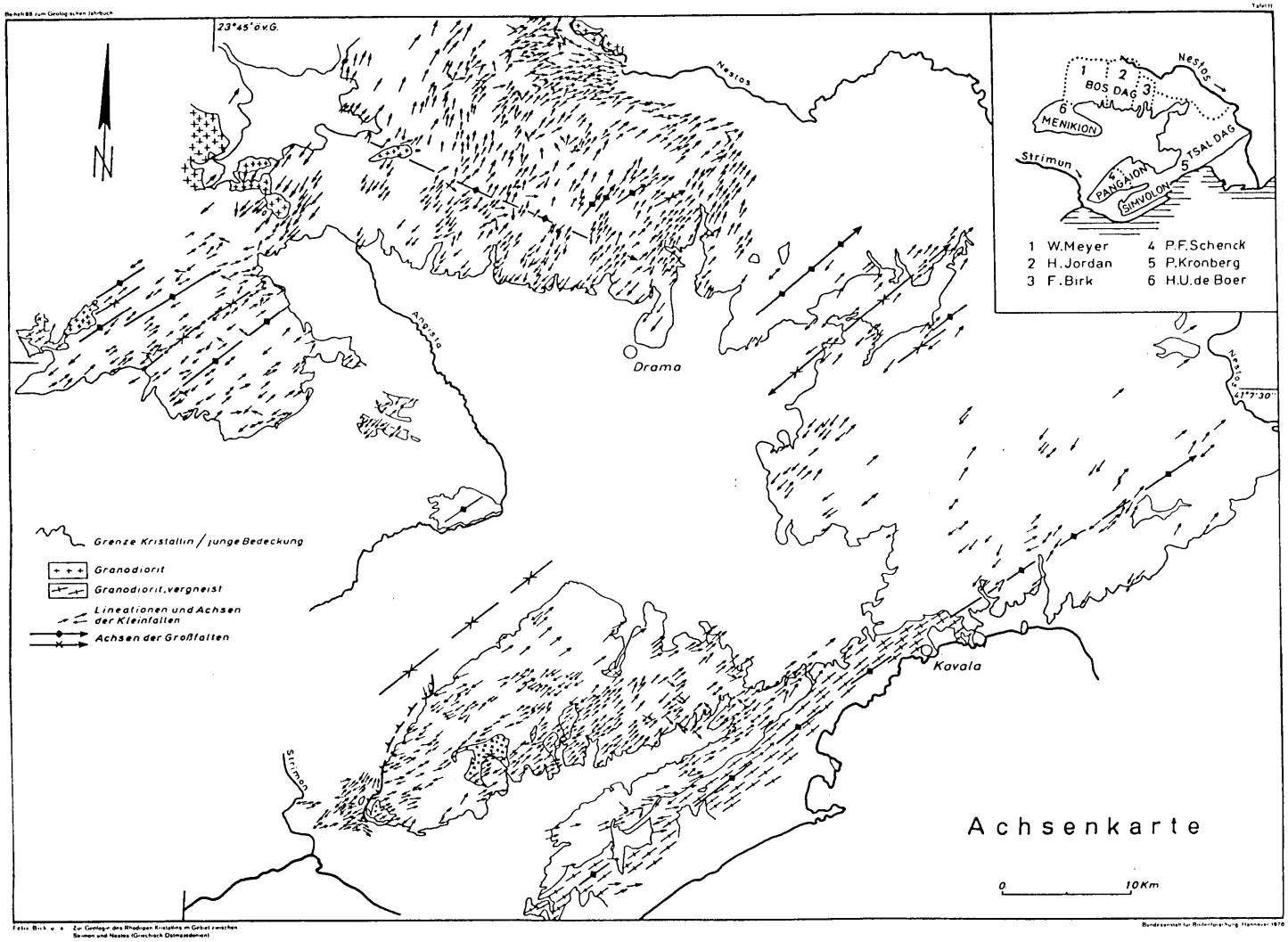

Figure 7. Minor fold-axis and stretching lineation axes in the Falakron marble series between the Strymon and Nestos Rivers in northeastern Greece from Meyer (1969).

TABLE 1. SUMMARY OF TERIARY TECTONIC AND MAGMATIC EVENTS IN THE STRYMON VALLEY REGION

Event	Age (Ma)	Associated deformation	Correlations w/ Schermer (1990, 1993)
D_1 (southwest-vergent Nestos thrust accommodates A-type subduction of Falakron carbonate platform beneath Serbo-Macedonian-West Thracian gneiss complex)	47-36*	N35°-50°E-trending, gently northeast-plunging major open or sheath (?) folds, small tight to isoclinal folds, and mineral stretching lineations in the Falakron marble series and lower Serbo-Macedonian-West Thracian gneiss complex.	D_3 (southwest-vergent Olympos thrust; high-P metamorphism of Olympos carbonate unit)
Mid-Oligocene magmatism	33-28†	Intrusion of Vrondou, Xanthi, and several smaller granodiorite plutons in the Rhodope metamorphic core complex; extrusion of Paranestion andesites above West Thracian gneiss complex.	
D_2 (emplacement and synintrusional mylonitization of Symvolon pluton within a coaxial shear at southwest margin of Rhodope core complex)	23-16	Intrusion of Symvolon pluton ~21 - 22 Ma.§ Gently northeast-plunging minor tight to isoclinal folds and mineral stretching lineations in Symvolon pluton and southwestern Falakron marble series. Mean lineation attitude = 18°, N58°E.	D_5 (top-to-the-northeast low-angle normal faults on north and south flanks of Mt. Olympos)
D_3 (gently southwest-dipping Strymon Valley detachment; Serbo-Macedonian gneiss complex moves 3°, S53°W in hanging wall; Rhodope metamorphic core complex emerges in footwall)	16-3.5**	N45°-60°E-trending, gently southwest-plunging minor tight to isoclinal folds and mineral stretching lineations in southwestern Symvolon and Vrondou plutons and southwestern Falakron marble series; deposition and tilting of syndetachment basin complex in hanging wall (northwest-trending normal faults soling into detachment).	
D_4 (top-to-the-northeast? North Aegean detachment bounded to the southeast by the North Aegean trough)	3.5**-present	Northwest-trending normal faults accommodate subsidence of modern Strymon and Drama basins, possibly above a mid-crustal detachment.	D_7 (northeast-dipping high-angle normal faults at southwest margin of modern Vardar-Thermaikos basin)
late D_4 (strike-slip and related faulting)	?-present	Northeast-trending, mainly dextral strike-slip faulting; secondary extension on seismogenic? N70°-85°W-striking normal faults.	

* Ages based on K-Ar hornblende dates at base of West Thracian gneiss complex (Liati, 1986) and K-Ar muscovite and biotite dates at base of Serbo-Macedonian gneiss complex (Harre et al., 1968; Marakis, 1969). See Tables 5 and 7.

† Ages based on K-Ar hornblende dates from Vrondou pluton (Marakis, 1969) and Xanthi pluton (Liati, 1986). See Table 3.

§ Ages based on $^{40}Ar/^{39}Ar$ hornblende dates and U-Pb titanite and zircon dates from the Symvolon pluton obtained in this study (Tables 1 and 2).

** Based on fossil ages in syndetachment basin complex [MN3-MN6 *Micromeryx flourensianus* Lartet in the Struma basin (Kojumdgieva et al., 1982); MN15 rodent fauna in the Serres basin (Armour-Brown et al., 1979)], on K-Ar biotite dates from the Mesolakkia (Harre et al., 1968) and Symvolon (Kokkinakis, 1980b) plutons, and on $^{40}Ar/^{39}Ar$ biotite and K-feldspar dates from the Symvolon pluton obtained in this study (Table 3).

Geologic Map of the Southwestern Rhodope Province, Northeastern Greece

by David A. Dinter

1:100,000

Contour interval = 20 m.

0 5 10 km

Correlations of Map Units

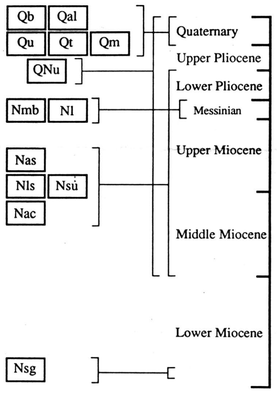

Descriptions of Map Units

Qb **Beach deposits [Holocene]:** Unconsolidated, arkosic, modern beach sand, principally derived from the Symvolon granodiorite.

Qal **Alluvium [Holocene]:** Unconsolidated sand, silt, and gravel in modern stream beds.

Qu **Talus [Quaternary]:** Highly consolidated talus and coalescing fanglomerate sheets overlapping tilted Neogene supradetachment deposits, the Strymon Valley detachment, and Quaternary range front faults. Clasts predominantly foliated marble.

Qt **Talus [Quaternary]:** Highly consolidated talus and coalescing fanglomerate sheets overlapping tilted Neogene supradetachment deposits, the Strymon Valley detachment, and Quaternary range-front faults. Clasts predominantly foliated marble.

Qm **Marine terrace deposits [Quaternary]:** Poorly consolidated beach and nearshore marine terraces overlapping tilted supra-detachment strata in Akropotamos basin. Probably Quaternary.

QNu **Undifferentiated clastic sediments [Neogene - Quaternary]:** Tilted, Neogene, supradetachment strata and Quaternary overlap deposits as thick as ~300 m (fanglomerate, talus breccia) in the southern Angitis basin.

Nmb **Menoikion carbonate breccia [latest Miocene - early Pliocene(?)]:** Highly consolidated large-rock avalanche breccia 500-600 m thick, ~50 km2 in area, overlies tilted clastic strata on a sheared, angular discontinuity at elevations of ~250-1500 m in the northern Angitis basin. Intact blocks as wide as ~100 m consist of 0.1- to 3.0-m thick interbeds of unlaminated micritic limestone, laminated algal limestone and dolomite, storm rip-up breccia, and well-rounded, marble pebble conglomerate with micritic matrix material. Pebbles up to 20 cm in diameter are ~99% foliated marble, 1% gneiss and granite. Probable Messinian age.

Nl **Limestone [latest Miocene - early Pliocene(?)]:** Nearshore, algal, and, possibly, nonmarine limestone beds overlying supra-detachment clastic deposits in the South Symvolon, Akropotamos, and southern Angitis basins.

Nas **Angitis sandstone [late Miocene(?)]:** Medium- to coarse-grained, buff-weathering, silty, arkosic, alluvial sandstone and gritstone interbedded with polymictic pebble conglomerate containing clasts of foliated granite, gneiss, quartz, and marble. Thickness ~40 - 50 meters in northern Angitis basin; top not exposed.

Nls **Lefkothea siltstone [late Miocene(?)]:** Calcareous, gray-weathering, muddy siltstone ~300-400 m thick crops out in "badlands" topography in the northern Angitis basin; mudcracks preserved locally. Sparse interbeds of fine-grained, angular, poorly-sorted, micaceous, silty, arkosic sandstone present near base, absent from central part of unit, abundant in upper ~100 m. Grain size, thickness, and abundance of sand beds increase upwards towards gradational contact with Angitis sandstone. Lignite and paper shale interbeds up to 5 cm thick bear wood fragments and imprints of large leaves. Siltstone contains fish scales, ostracodes, gastropods, and the lacustrine bivalve *L. Limnocardium*, known from the latest middle Miocene (Sarmatian) to the late Pliocene (Romanian) in eastern Europe (Cox et al., 1969).

Nac **Angitis conglomerate [middle(?) - late Miocene]:** Crudely bedded, poorly sorted, polymictic pebble and cobble conglomerate interbedded with silty sandstone and sandy siltstones in the northern Angitis basin. Conglomerate clasts are 60-80% mylonitic granite or gneiss, 10-30% foliated marble, 10% quartz, schist, amphibolite. Matrix material ranges from poorly-sorted, calcareous sand to gritty silt. Contains ~25% interbeds up to 5 m thick of sandstone, siltstone, and lignite.

Nsu **Undifferentiated supradetachment basin deposits [middle(?) - late Miocene]:** Tilted, poorly consolidated Neogene deposits in the hanging wall of the Strymon Valley detachment in the South Symvolon, Akropotamos, and southern Angitis basins. Predominantly sandstone, conglomerate, and siltstone; minor lignite, gypsum, limestone, and monomictic granite breccia.

Nsg **Symvolon granodiorite [early Miocene]:** Pervasively mylonitized granodiorite characterized by gently northeast-plunging stretching lineations and outcrop-scale folds. 20-30% quartz, 30-50% plagioclase, 15-25% potassium feldspar, 5-25% biotite, 0-5% hornblende, minor chlorite and epidote, accessory zircon, apatite, and titanite. Common K-feldspar porphyroclasts as long as 4 cm. No discrete contact aureole; marginal mylonitic shear zones contain diopside, tremolite, other calc-silicates. $^{206}Pb/^{238}U$ zircon and titanite dates and $^{40}Ar/^{39}Ar$ hornblende dates indicate an early Miocene (21-22 Ma) emplacement age (Dinter, 1994).

Nmg **Mesolakkia granodiorite [early Miocene]:** Pervasively mylonitized granodiorite probably correlative with the Symvolon granodiorite. Exposed beneath Falakron marbles at the southwest margin of Mt. Pangaion.

fs/fg **Falakron marble series [Mesozoic(?) - early Eocene(?)]:** Highly strained, white to light gray, granular marble and darker, impure, banded marble bearing quartz and phengite, lesser plagioclase and clinozoisite, accessory graphite and pyrite. Primary sedimentary features mostly obliterated. Thickness as great as 5000-7000 m northeast of Drama Basin in the Falakron and Lekanis Mountains, but ≤500 m southwest of Drama Basin. Contains intercalations <1 m to >400 m thick of micaceous gneiss, two-mica schist, and actinolite schist bearing upper greenschist-facies assemblages. Age poorly constrained. A single, unidentifiable coral constrains a post-Cambrian age (Meyer and Pilger, 1963). Regional structural relationships contrain a pre-middle Eocene age.

Mzsm **Serbo-Macedonian gneiss complex [Mesozoic]:** Mylonitic, amphibolite-facies, micaceous, plagioclase-microcline-gneiss and biotite gneiss of the Serbo-Macedonian "Kerdilion series" overlying the Strymon Valley detachment at the southwest margin of Mt. Pangaion.

Map Symbols

- Intrusive or depositional contact
- High-angle normal fault (ball on downthrown side)
- Low-angle normal fault (tick on hanging wall)
- Strymon Valley detachment (box on hanging wall)
- Strike-slip fault
- 40 — Bedding attitude
- 22 15 — Foliation attitude (with stretching lineation)
- 79 42 — Fault or shear zone attitude (with slickenside lineation)